The petrogenesis of the older (> 3.0 Ga) potassic granitoids of eastern Mpumalanga (South Africa) and Swaziland: An investigation of crustal formation processes in the early Earth

by

Cynthia J. M. G. Sanchez-Garrido

Dissertation presented for the degree of Doctor of Geology
at the
University of Stellenbosch (South Africa)

Promoters: Prof. Gary Stevens
Prof. Hervé Martin
Dr. Régis Doucelance
Prof. Jean-François Moyen

Faculty of Science
Department of Earth Sciences

March 2012

DECLARATION

By submitting this dissertation electronically, I declare that the entirety of the work contained therein is my own, original work, that I am the sole author thereof (save to the extent explicitly otherwise stated), that reproduction and publication thereof by Stellenbosch University will not infringe any third party rights and that I have not previously in its entirety or in part submitted it for obtaining any qualification.

Signed . . . . . .
(Cynthia Sanchez-Garrido)

ABSTRACT

Earth's oldest preserved granitoid crust dates back to the Paleoarchean and consists predominantly of sodic tonalite-trondhjemite-granodiorite (TTG) granitoids that arose through the partial melting of hydrated metabasalts. In contrast, granites (sensu stricto) typically postdate the TTG and appear late in the plutonic record of the old cratons.

However, the existence of Hadean zircons with mineral inclusion suites that are consistent with crystallization from peraluminous granitic magmas indicates that granitic rocks formed part of the earliest felsic crust; although we have direct evidence, this earliest felsic crust is not preserved.

In this PhD I present an unusual variety of markedly CaO-poor, K_2O-rich, rutile-bearing, peraluminous granite and rhyolite that are located in the basal conglomerate of the Moodies Group (South Africa). These rocks challenge the common view of the Archean craton evolution as they were produced concurrently with TTG magmas during three magmatic cycles in the Barberton Greenstone Belt (BGB) and were later emplaced, as clasts, in a younger conglomerate.

The study of mineral inclusions located in the zircons present within the granites and rhyolites, shows that alkali feldspar inclusions are abundant relative to plagioclase inclusions and demonstrates that the main characteristics of these granites, i.e. they are K-rich and Ca-poor, are a magmatic signature. The oxygen isotope signature of these zircon grains reveals that the zircons have preserved the $\delta^{18}O$ value of the magma from which the granites originated and that the source of the granites had a magmatic oxygen isotope value close to the one of the regional coeval TTG. Further study of the zircons shows that their Lu-Hf isotopic system reflects the crustal signature of the magma into which they grew. Sm-Nd study of the granites and rhyolites whole rock indicates that the minimum age of the source's protolith of the granites and rhyolites is close to 3.9 billion years, which is in agreement with the zircons' Lu-Hf signature. Additionally I show in this thesis that the peraluminous character of the granites and rhyolites, along with their high Sr and low Ca content associated to their Eu/Eu* ~ 1 is a consequence of phengite melting in a metagreywacke source at pressures in excess of plagioclase stability.

My work therefore illustrates that K-rich, Ca-poor peraluminous granites were generated in the Paleo and Meso Archean, alongside with the sodic TTG, through partial melting of sediments at high pressures. Not only has this process demonstrated the ability of the early Earth to recycle relatively young material since 3.9 billions years ago, but it has also contributed to each episode of continental crustal growth through the Paleoarchean to Mesoarchean in the BGB, despite leaving no plutonic record at the typical mid-crustal level of exposure that the TTG plutons around the belt represent.

Keywords: *Paleoarchean granites, peraluminous, LU-Hf, Sm-Nd, $\delta^{18}O$.*

OPSOMMING

Die aarde se oudste bewaarde granitoïed kors dateer terug na die Paleo Argeïkum en bestaan hoofsaaklik uit natrium-ryke tonaliet-trondhjemiet-granodioriet (TTG) granitoïede wat ontstaan het deur die gedeeltelike smelting van gehidreerde metabasalte. In teenstelling hiermee is graniete (sensu stricto) tipies jonger as die TTG's en verskyn laat in die plutoniese rekord van die ou kratons.

Die bestaan van Hadeaanse zirkone met mineraal insluitsels wat ooreenstem met die kristallisasie van peralumineuse granietiese magma dui egter daarop dat granietiese gesteentes deel gevorm het van die vroegste felsiese kors. Alhoewel daar direkte getuienis is hiervoor het hierdie vroegste felsiese kors nie behoue gebly nie. In hierdie dissertasie toon ek 'n ongewone verskeidenheid van merkbaar CaO-arm, K2O-ryk, rutiel-draende, peralumineuse graniet en rioliet wat in die basale konglomeraat van die Moodies Groep (Suid-Afrika) voorkom. Hierdie gesteentes daag die algemene siening van Argeïkum kraton evolusie uit omdat hulle gelyktydig met TTG magma geproduseer is tydens drie TTG magmatiese siklusse in die Baberton-groensteenstrook en later ingeplaas is as klaste in 'n jonger konglomeraat. Die studie op minerale insluitsels in zirkone binne die graniete en rioliete toon dat alkaliveldspaat insluitsels volop is relatief tot plagioklaas insluitsels. Dit toon ook dat die hoof eienskap van hierdie graniete, hulle K-ryke en Ca-arme samestelling, 'n onderskeidende magmatiese kenmerk is. Die suurstof-isotoop samestelling van hierdie zirkoon minerale onthul dat die zirkone die δ18O waarde van die magma waaruit die graniet gevorm is behou het en dat die bronnemateriaal van die graniete 'n magmatiese suurstofisotoop waarde gehad het nader aan dié van die plaaslike sinchroniese TTG waardes. Verdere studie van die zirkone dui daarop dat hul Lu-HF isotoopstelsel die aardkorseienskappe weerspieël van die oorspronklike magma waarin hulle gegroei het. Sm-Nd studie van die graniete en rioliete heelgesteente dui daarop dat die minimum ouderdom van die protoliet van graniete en rioliete ongeveer 3,9 biljoen jaar is, wat ooreenstem met die zirkone se Lu-HF eienskappe. Daarbenewens het hierdie dissertasie bewys dat die peralumineuse karakter van die graniete en rioliete, tesame met hulle hoë Sr- en lae Ca-inhoud geassosieer tot hul Eu/Eu * ~ 1, 'n gevolg is van "phengite" smelting in' n metagrouwak bron by drukking hoër as plagioklaas stabiliteit.

Hierdie studie illustreer dus dat K-ryke, Ca-arme peralumineuse graniete gegenereer is in die Paleo en Meso Argeïkum, saam met die natrium-ryke TTG's, deur middel van parsiële smelting van sedimente teen 'n hoë druk. Hierdie proses het nie slegs getoon dat die vroeë aarde sedert 3,9 biljoen jaar gelede die vermoë gehad het om relatief jong materiaal te herwin nie; dit het ook bygedra tot elke episode van kontinentale korsgroei deur die Paleo en Meso Argeïkum in die Barberton groensteenstrook, ten spyte daarvan dat geen plutoniese rekord gelaat is teen die tipiese mid-kors vlak van blootstelling wat die TTG plutone in die strook verteenwoordig nie.

Keywords: *Paleoarchean granites, peraluminous, LU-Hf, Sm-Nd, $\delta^{18}O$.*

RESUMÉ

La croûte de granitoïdes de la Terre Primitive la plus ancienne qui ait été préservée remonte au Paleoarchéen et se compose principalement de granitoïdes sodiques tonalite-trondhjémite-granodiorite (TTG) qui se sont formés par la fusion partielle de métabasaltes hydratés. En revanche, les granites (stricto sensu) sont en général postérieurs aux TTG et apparaissent tardivement dans les cratons anciens.

Cependant, l'existence de zircons Hadéens préservant des suites d'inclusions minérales qui sont compatibles avec la cristallisation à partir d'un magma granitique peralumineu, indique que les roches granitiques faisaient aussi partie de la croûte felsique de la Terre Primitibe; même si nous n'avons pas de preuves directes et que cette dernière n'ait pas été conservée.

Dans cette thèse, je présente une variété inhabituelle de granites et rhyolites peralumineux qui sont marquée par une forte teneur en K_2O et une faible teneur en CaO et qui possèdent du rutile. Ces roches sont situées dans le conglomérat basal du Groupe du Moodies (Afrique du Sud). Elles défient la vision commune que l'on a de l'évolution des cratons Archéens puisqu'elles ont été produites en même temps que des magmas TTG, pendant trois cycles magmatiques qui ont affecté la ceinture de roches vertes de Barberton (CRVB). Ces roches ont été par la suite mises en place, comme galets, dans un conglomérat plus jeune.

L'étude des inclusions minérales localisées dans des zircons présents dans les granites et les rhyolites qui font le sujet de cette étude, montre que les inclusions de feldspaths alcalins sont plus abondantes que les inclusions de plagioclases et démontre que les principales caractéristiques de ces granites, c'est à dire qu'ils sont riches en K et pauvres en Ca, sont une signature magmatique. La signature isotopique de l'oxygène de ces zircons révèle que ceux-ci ont conservé la valeurdu $\delta^{18}O$ du magma à partir duquel les granites se sont formés. De plus ceci montre que la valeur du $\delta^{18}O$ de la source des granites était proche de celle de TTG contemporains. La poursuite de l'étude des zircons montre que leur système isotopique Lu-Hf reflète la signature crustale du magma dans lequel ils ont cru. L'étude Sm-Nd des granites et rhyolites indique que l'âge minimum du protolithe de leur source est de près de 3,9 milliards d'années, ce qui est en accord avec la signature Lu-Hf des zircons. De plus, je montre dans cette thèse que le caractère peralumineux des granites et des rhyolites, avec leurs forte teneur an Sr et basse teneur en Ca associé à leur Eu / Eu * ~ 1, est une conséquence de la fusion partielle de phengite dans une source métagrauwacke à des pressions supérieures a celle de la stabilité du plagioclase.

Mon travail montre donc que des granites peralumineux riche en K et pauvre en Ca ont été générés durant le Paléo et Méso-Archéen, aux côtés des TTG sodiques, par la fusion partielle de sédiments, à

haute pression. Non seulement ce processus a démontré la capacité de la Terre Primitive à recycler du matériel relativement jeune et ce, dès 3,9 milliards d'années; mais il a également contribué à chaque épisode de croissance crustale à travers le Paleo- et Méso-Archéen dans la CRVB, malgré l'absence de pluton mis en place profondeur à des profondeurs identiques à celles des TTG.

Keywords: *Paleoarchean granites, peraluminous, LU-Hf, Sm-Nd, $\delta^{18}O$.*

ACKOWLEDGEMENTS

Le chêne et le Roseau

Le Chêne un jour dit au Roseau :
“Vous avez bien sujet d’accuser la Nature ;
Un Roitelet pour vous est un pesant fardeau.
Le moindre vent, qui d’aventure
Fait rider la face de l’eau,
Vous oblige à baisser la tête :
Cependant que mon front, au Caucase pareil,
Non content d’arrêter les rayons du soleil,
Brave l’effort de la tempête.
Tout vous est Aquilon, tout me semble Zéphyr.
Encor si vous naissiez à l’abri du feuillage
Dont je couvre le voisinage,
Vous n’auriez pas tant à souffrir :
Je vous défendrais de l’orage ;
Mais vous naissez le plus souvent
Sur les humides bords des Royaumes du vent.
La nature envers vous me semble bien injuste.
- Votre compassion, lui répondit l’Arbuste,
Part d’un bon naturel ; mais quittez ce souci.
Les vents me sont moins qu’à vous redoutables.
Je plie, et ne romps pas. Vous avez jusqu’ici
Contre leurs coups épouvantables
Résisté sans courber le dos ;
Mais attendons la fin. “Comme il disait ces mots,
Du bout de l’horizon accourt avec furie
Le plus terrible des enfants
Que le Nord eût portés jusque-là dans ses flancs.
L’Arbre tient bon ; le Roseau plie.
Le vent redouble ses efforts,
Et fait si bien qu’il déracine
Celui de qui la tête au Ciel était voisine
Et dont les pieds touchaient à l’Empire des Morts.

Jean de La Fontaine, Les fables de La Fontaine, Livre 1, Fable 22

Le Lion et le Rat

Il faut, autant qu'on peut, obliger tout le monde :
On a souvent besoin d'un plus petit que soi.
De cette vérité deux Fables feront foi,
Tant la chose en preuves abonde.
Entre les pattes d'un Lion
Un Rat sortit de terre assez à l'étourdie.
Le Roi des animaux, en cette occasion,
Montra ce qu'il était, et lui donna la vie.
Ce bienfait ne fut pas perdu.
Quelqu'un aurait-il jamais cru
Qu'un Lion d'un Rat eût affaire ?
Cependant il advint qu'au sortir des forêts
Ce Lion fut pris dans des rets,
Dont ses rugissements ne le purent défaire.
Sire Rat accourut, et fit tant par ses dents
Qu'une maille rongée emporta tout l'ouvrage.
Patience et longueur de temps
Font plus que force ni que rage.

Jean de La Fontaine, Les fables de La Fontaine, Livre 2, Fable 11

For my family, for those who are still here and those who have gone too quickly. I love you.

I have started thinking about writing the acknowledgments of this thesis almost in my first day in South Africa. Along my journey here I have met incredible persons, I have met people I have laugh with, people I have cried with, people I have shared everything with, people I have argued

with, but most of all people I have learn from. So I will begin here, by thanking my supervisor Professor Gary Stevens. He taught me geology in a way I had never been taught before. I learned to take the problem that was coming to me as a challenge and I felt excited to overcome them. I have learned to challenge previous scientific hypothesis with no fear (almost). My brain was sometimes boiling of ideas, most of the time all wrong, but it felt good to see Science in that way again, as I've been taught in school with a problem to solve and hypothesis to test. Professor Gary Stevens also introduced me to a brand new world of granite and amongst it, the petrogenesis of granite. He spends endless hours explaining me how granites formed. This does not have a single straight answer as I have learnt now. He showed me how to write scientific papers, to be critical about everything I write, I read, I hear and I think I know. Criticism is a powerful tool if you know how to use it. But Professor Gary Stevens you are not only a brilliant professor I admire for your work, you are also a kind men. So Garry, thank you for your help during these last 5 years. Thank you for putting up with my mood during professional or personal crisis. Thank you for the time you spend helping me in anyway you can, and for everything I learnt thanks to you. I wish everybody to have a supervisor like you. To you, THANK YOU !!

I would also like to thank my other supervisors, Professor Jean-Francois Moyen, Professor Hervé Martin and Doctor Regis Doucelance who have all helped me in many difference way. Jeff and Hervé were my Guru of geochemistry whereas Regis was the one in radiogenic isotopes. I also have learnt a lot from them. I have learned how difficult it could be to work with 4 supervisors at the same time, but I also how to prepare and acquire good data, how to be confident my data. They teach me to be independent too. Jeff showed me many times who to use Adobe Illustrator or GCDkit for example. Hervé and him re-introduced me chemical modeling, which I had barely touch before. I must say it was sometimes a challenge to do geochemical modeling with geochemist and petrograph advisors, but we got there. Thank you to you three and your warm welcome every time I was coming to Clermont-Ferrand, and for helping me with the administrative aspect of my visits.

During these 5 yeard of PhD I have met people who have done nothing else but help me, so these are who I want to thank: to Chantal Bosq, the Queen of the white room. The showed me her way of cleaning and preparing the samples, and thanks to her teaching and help I have enjoyed my time in the lab a lot, and became aware of the amount of work that sometimes need to be produced before an analysis. Thanks to her way of making sure the lab was spotless which made your "chance" of getting good results at the analysis greatly improve. Than you very much for everything you taught me and for you kindness. I would like to thank Richard Armstrong who welcomed me nicely in

Canberra but who teaching me and showing me the lab. Learning how to acquire data with the SHRIMP was not always easy, but he was there to make sure our stay in Australia was going well. Thank you Richard for the data you send me. I also want to thank Chris Harris for showing me around his isotope laboratory and for producing great data for me, thank you. Thank you to Madelein for teaching me how to use the SEM, and for being there when it needed fixing. Thank you very much for Riana for teaching me how to use the La-ICP-MS for my whole rock traces and rare Earth elements. I would like to thank Dr. Cristiano Lana for showing me how to use the LA-ICP-MS for zircons analysis, but also for having been a great friend and teaching me how to improve my English during our recurrent tea time. I also would like to thanks Hershel and Mat for their help and for preparing my samples for trace and REE analysis many times.

I now wish to thank some people I have met fewer times but who their help was precious: Thank you Loxie for helping me dealing with all the administration aspect of the PhD. Many tanks to George who did the same, who made sure everything (copier paper, access to the microscope room on your student card….) were OK. Thanks to Archille for is great help during the second preparation of my samples. Archill is not only a nice person to be around, he also works in great and clean way. Thank you to Matthew who allowed me to use his lab and the agate ball mill in the department

Thanks to my first flat mate Gwen for the warm welcoming she gave me when I arrived in South Africa. Thanks to my former officemate Arnaud for our laughter, arguments and for showing me the interesting places to go in Stellenbosch and who introduced me to his friends. I also would like to wish particularly Cristiano Lana that I consider as a great friend. He took 40 min everyday with me, for months, to teach me English and correct my English. So thank you Cristiano, it is thanks to you that I give an entire talk in English. I wish to thank .Myriam Moyen and her 3 kidds, as well as Jeff Moyen. You have taking well care of me hear. Myriam you have been a great friend by listening to me when I needed. Having diner with your family was always lovely. And you kids are great, I can not believe they re growing so fast though. I wish to thanks Dorothy Stevens for being the first person I saw at my first registration at the University. After that we saw each other in different circumstances and thank to you to opening your house to crazy geologist for diner.

This private part of my acknowledgement is one I have been waiting to write. I would like to first thank my friends: Virginie (you have supported me all the way even though you went through hell. You gave me the most amazing present when you ask me to be the goddaughter of Lena), lena,

Enzo, Jean-Mi, Sophie and Vincent (mes miraculeux decoupeurs de petits rond vert et faiseurs d'époxie jusque tres tot dans la matinee, out res tard le soir), merci les amoureux d'avoir fait le voyage, c'est un gest qui restera graver dans ma memoirs) thank you for your support and for visiting me often during my stay back in France; Yan, Anais, Adeline, Sebastien, Bikett, Julia, Kimmy, Marion, Blaise, Dr. Nick, Isa, Nico and their cute family, Lyderic, Lydie, Sarah, Toff, Mathieu, Soizic, Miki, Maud, Mat', Vincent and Jojo. My friends you have been their all along, welcoming me in your house, throwing my 1st surprise party, encouraging me all this time. You never let me down, ever in the worst time and for that you very much. You made my time in France awesome, extremely fun and sometimes very emotional. Thank you for everything we shared and experienced. And a special thanks to Anais and Bikett whose support and kindness helped me go through tough times (merci ma morue preferee). Justine, Capucine, Oscar and Sophie-Charlotte you came here, little frenchies and brought me a piece of French and great laughers, thanks. And thank you to all the teachers/professors/lecturers I had in all my years of study: a part of me is here thanks to you.

I also wish to give a huge thank my officemate Dr. Jeanne Taylor, brilliant mind, good writer, awesome flute player and best friend. Jeanne you have been there with me and for me, trough hell and back. Your advice are always been proved useful. You took care of me even in your extremely busy times, like a sister. I can share everything with you. You give me strength to overcome tough times and happiness to enjoy the nice moments. I discover in you a true friend. Thank you for everything you have done for me. Before you I did not know how to care, help and listen to people the way you do. You are my new definition of kindness as it is what you taught me, kindness and believing that there is always a solution to my problem.

A Big thanks to my others colleagues: Angelique Laurie your smile and enthusiasm about your work always putt me in a great mood and I have found your passion for your field inspiring. I am glad you are in the team. Thank you very much for Federico and the international Italian culture he is bringing to the group. B, how can I not thank you? Byron you are genuinely kind and don't hesitate to help. I like that side of you as well as the fun. You took me out of my office cocoon and made me more social, thanks B and to your acolyte, Theo.

Thanks to Dr. McKerron: your advice and support helped me get through my work when I needed it the most.

A thank I had never thought I will give is to you Johann. Even in my best dreams I had never imagine I would be so lucky to have you in my life. Thank you my smarty for our almost strictly

un-professional relationship and everything it brings me.

It is also very important to me to thanks Anita and Nadina who are my South African aunts. They took very good care of me during all these years and made sure my life outside the department was enjoyable and that everything was running OK into my little flat. This was the perfect place to live and it staying with you brought me a lot of joy.

These will be my last thanks but not least and go to my family:

Mom, Dad, Romain, Nelly and Samantha (my brother and sisters), Mamy, Papy, Marraine, Parrain, Meme, tata Cathy, Allan and Fred. You have always been there into tough and easy times. I don't know to express my gratefulness to you. Communication were difficult at the beginning but got easier and free towards the end, and for that I can be grateful to our internet provider □. Your presence and love gives me so much strength. I missed you everyday but not a day went by without me thinking of you and sending you all the love I have for you. Your un-conditional love and support is what kept me together during all these years. I know me leaving was not easy for you: the second time I decide to leave home is to go on the other side of the Earth. And leaving in n amazing country as South Africa is, is challenging but great, which it make it easy to not miss France, but it is still impossible to not miss HOME, where you are. Thank you for your love. Thank you for your support, for the letters and delicious French treats you sent me. I love you and this PhD is dedicated to you and to Pepe, Meme and Papy who, as you, I kept in my heart.

REMERCIEMENTS

J'ai commencé à réfléchir à mes remerciements presque des le premier jour de ma thèse en Afrique du Sud. Durant mon séjour ici j'ai rencontré des personnes incroyables ; j'ai rencontré des personnes avec qui j'ai ri, d'autres avec qui j'ai pleuré, et ceux avec qui j'ai tout partagé, j'ai rencontré des personnes avec qui je me suis disputée mais tous m'ont apporté quelque chose. Je vais donc commencer par remercier mon superviseur Professeur Gary Stevens. Il m'a appris beaucoup de choses, enseigné la géologie d'une façon qui m'était jusqu'alors inconnu. Grâce à lui j'ai appris à appréhender chaque problème comme un challenge que j'étais excitée de résoudre. J'ai appris à challenger certaines hypothèses scientifiques et à garder l'esprit ouvert, sans être apeurée (enfin presque). Mon cerveau bouillonnait parfois d'idées, la plupart du temps toutes fausses, mais cela était satisfaisant de revoir la SCIENCE de nouveau sous cet angle, de la revoir de la même manière dont celle qui m'avait été enseigné à l'école, avec un problème à résoudre et des hypothèses à tester. Professeur Gary Stevens a aussi réussit à me présenter à un tout nouveau monde : celui des granites et de leur pétrogenèse. Il passa d'innombrables heures à m'expliquer la formation des granites. Cela n'ayant pas de réponses claires comme je l'avais appris il est facile d'imaginer le temps passé autour de cette discussion. Professeur Stevens m'a aussi éduqué à la rédaction d'articles scientifiques à avoir un esprit critique sur tout ce que je lis, j'entends, et sur ce que je pense savoir. La critique devient alors, lorsqu'on la comprend mieux, un outil fabuleux à utiliser. Cher Gary, vous n'êtes pas seulement un professeur brillant que je respecte et admire pour vos travaux de recherches, vous êtes aussi un homme admirable. Je souhaite donc vous remercier pour votre aide durant ces 5 dernières années. Merci d'avoir gérer mes humeurs et crises professionnelles comme personnelles. Merci d'avoir toujours su trouver du temps pour m'aider. Je souhaite à bien des personnes d'avoir un superviseur tel que vous. Merci !!

Je souhaiterai aussi et bien entendu remercier mes autres superviseurs sans qui une grande partie de mon travail n'aurait pas pu être réalisé. Merci aux Professeurs Jean-François Moyen, Professeur Hervé Martin et Docteur Régis Doucelance qui m'ont tous aidé de manières bien différentes. Jeff et Hervé ont été mes Gourous de la géochimie alors que Régis a été celui des isotopes.

J'ai aussi beaucoup appris de vous. Travailler sous la codirection de 4 grands chercheurs n'a pas été une mince affaire, mais cela m'a montré ce que c'était de travailler en groupe avec plusieurs disciplines. J'ai appris à préparer des échantillons de manière a obtenir les meilleurs résultats lors des analyses. J'ai appris à être confiante envers mes résultats et analyses Vous m'avez tous les trois

enseignés à être plus indépendante. Jeff m'a montré maintes fois comment utiliser Adobe Illustrator ou GCDkit par exemple. Hervé et lui-même m'ont enseigné la modélisation géochimique, chose délicate à laquelle je n'avais presque jamais touché avant cela. Je dois dire que c'était un challenge de parfois faire à distance de la modélisation géochimique lorsque l'on est à distance et entouré d'un superviseur pétrographe, mais nous y sommes arrivés. Merci à vous trois pour les innombrables fois ou je vous ai demandé des corrections. Merci pour votre accueil toujours chaleureux lors de mes visites à Clermont.

Durant ces 5 ans de thèse j'ai rencontré des gens formidables qui n'ont fait que m'aider, donc les voici, ceux qui ont eux aussi toute ma gratitude : à Chantal Bosq, la Reine de la salle blanche. Merci de m'avoir montré comment préparer mes échantillons, merci pour m'avoir enseigné et aidé lors de mes séjours en salle blanche. J'ai beaucoup aimé le temps passé au labo, et je suis devenue consciente de la quantité de travail que représente une bonne préparation d'échantillons et du temps que cela prends avant de pouvoir analyser. Merci de toujours faire en sorte que la salle blanche soit impeccablement propre, ce qui augmente exponentiellement la « chance » d'avoir de bonnes analyses. Merci pour votre gentillesse et tout ce que vous m'avez appris. Je souhaiterai aussi remercier Richard Armstrong qui nous a accueilli moi et ma collègue chaudement à Canberra, en plein mois d'hiver. Merci de nous avoir fait visiter le labo de Canberra et là aussi, de nous avoir montré comment préparer les échantillons. Apprendre comment acquérir des données sur la SHRIMP n'a pas toujours été facile, mais ce fut une expérience incroyable d'avoir eu la chance de travailler sur cet instrument de renommée mondiale. Merci d'avoir fait en sorte que tout se passe bien lors de notre séjour en Australie, et merci pour les données que vous m'avez envoyé. Je souhaiterai aussi remercier Chris Harris pour m'avoir fait visiter et expliquer comment fonctionne le laboratoire d'isotopes stables. Merci d'avoir produit les données de l'oxygène en si peu de temps et de si bonne qualité. Merci aussi à Madelein pour m'avoir enseigné comment utiliser le MEB et pour avoir été là lorsqu'il y en avait besoin. Merci beaucoup à Riana pour m'avoir appris comment le LA-ICP MS fonctionne et pour m'avoir appris à acquérir mes données d'élément trace pour roche totale ou pour mes zircons. Je souhaiterai remercier chaudement Dr. Cristiano Lana qui m'a aussi montré comment acquérir les données d'élément trace sur zircons et qui m'a apprit à dater des zircons en utilisant le LA-ICP MS. Mais surtout merci Cristiano pour avoir été un ami et pour m'avoir aidé à améliorer grandement mon anglais lors de nos cessions quotidiennes de « the ». Je souhaite aussi remercier Herschel et Mat pour m'avoir aidé et avoir préparé avec moi de nombreuses fois mes échantillons pour XRF et LA ICP MS.

Je souhaiterai maintenant remercier quelques personnes avec qui j'ai eu moins de contact quotidien mais qui m'ont là aussi toujours aidé avec un sourire et dont l'aide fut précieuse. Merci a Loxie pour m'avoir aidé avec le côté administratif de ma thèse ; merci a George qui de même a fait en sorte que tout fonctionne dans le département (de l'accès à la salle des microscopes jusqu'à la photocopieuse) ; merci a Herschel qui fut d'une grande aide lors de la seconde préparation de mes échantillons. Herschel n'est pas seulement amical, il est aussi doué dans ce qu'il fait et j'ai eu toute confiance en lui.

Merci à ma première colloc, Gwen pour l'accueil chaleureux qu'elle m'a fait lors de mon arrivée en Afrique du Sud. Merci à Arnaud, mon premier collègue de bureau pour son humour, nos coups de gueule et pour m'avoir fait découvrir les coins sympas de Stellenbosch ainsi que ses amis. Merci encore à Cristiano que je considère comme un ami cher, qui a passé 40 min, pendant des mois à me réapprendre l'anglais et à corriger mon anglais. C'est grâce à lui que mon accent est potable et que j'arrive a donner une présentation en anglais. Je souhaiterai remercier très chaleureusement Myriam Moyen, Jeff et leurs trois adorables enfants. Vous avez pris grand soin de moi ici. Myriam est une amie formidable qui a su m'écouter lorsque j'en avais besoin. Merci pour les dîners en famille, cela fut très agréable, merci à vos bambins qui grandissent trop vite ! Je souhaiterai au même titre remercier Dorothy Stevens qui fut la première sud africaine que j'ai rencontré à mon arrivée et qui s'est occupée de moi lors de ma première inscription à la fac. Nous nous sommes revues par la suite en d'autres circonstances, notamment lors de dîner entre géologues chez vous. Merci de nous avoir ouvert votre foyer pour ces repas un peu fou.

Ceci est la partie privée de mes remerciements, celle que j'ai eue envie d'écrire tout de suite. Je souhaite ici remercier les amis qui sont très chers à mon cœur : Virginie (tu as toujours été la dans les coups durs comme dans la joie. Tu m'as toujours épaulé même lorsque tu vivais un enfer. Tu m'as fait l'un des cadeaux les plus incroyables en me demandant d'être la marraine de Lena), Lena, Enzo et Jean-Mi ; Sophie et Vincent (mes miraculeux découpeurs de petits ronds verts et faiseurs d'époxie jusque très tôt dans la matinée, où voir très tard le soir), merci les amoureux d'avoir fait le voyage, deux fois ! C'est un geste qui restera graver dans ma mémoire); Yan ; Adeline et Sébastien ; Anaïs et Bikett, Julia, Kimmy, Marion, Blaise, Dr. Nick ; Isa et Nico et leur famille adorable ; Lyderic, Lydie, Sarah, Toff ; Mathieu, Soizic, Miki, Maud, Mat', Vincent et Jojo. Mes amis vous avez toujours été là pour moi, vous m'avez accueilli chez vous et vous m'avez toujours encouragé.

Vous ne m'avez jamais laissé tomber dans les meilleurs comme dans les pires moments, et pour cela je vous en suis très très reconnaissante. Vous avez fait de mes voyages en France des moments exceptionnels, tellement drôles et parfois très émotionnels. Merci pour tout ce que nous avons partagé. Un énorme merci très spécial pour Anaïs et Bikett : merci pour votre soutien, pour votre gentillesse sans fin et pour m'avoir toujours aidé d'une façon toute particulière et très touchante (merci ma morue préférée). Justine, Capucine, Oscar et Sophie-Charlotte vous avez fait un petit tour en Afrique du Sud et vous m'avez apporté un petit morceau de France à chaque fois, et passé de très bons moments avec de franches rigolades, merci.

Merci aussi à tous mes enseignants/professeurs que j'ai eu au cours de ma vie, si j'en suis là c'est aussi en partie grâce à vous.

Je souhaiterai aussi remercier énormément et très chaleureusement ma collègue Jeanne : esprit brillant, brillante joueuse de flute traversière et meilleure amie. Jeanne tu as toujours été là avec moi, et pour moi, from hell and back. Tes conseils m'ont toujours été précieux et se sont toujours révélés très utiles. Tu as toujours pris le temps de prendre soin de moi, même dans les moments les plus fous et les plus intenses, comme une sœur. Je peux tout partager avec toi. Tu m'as donné du courage pour surmonter des épreuves et de la joie pour profiter des très bons moments. J'ai découvert en toi une vraie amie. Merci pour tout ce que tu as fait pour moi. Avant de te rencontrer je ne savais pas ce qu'était vraiment de prendre soin de quelqu'un, d'écouter et d'aider. Tu es ma nouvelle définition du mot « gentillesse » car tu m'as appris ce que cela voulait vraiment dire et tu m'as appris qu'il y avait toujours une solution à un problème.

Un autre grand grand merci à mes autres collègues très proches : Angélique Laurie tes sourires et ton enthousiasme pour le boulot et la vie en général m'ont toujours mise de bonne humeur. J'ai trouvé ta passion pour la géologie très inspirante. Je suis très heureuse que tu fasses partie du groupe. Merci beaucoup à Federico Farina et la culture italienne qu'il apporte au group. B (Byron) comment ne pourrais-je pas te dire merci. B tu es honnêtement gentil et n'hésite pas à aider quand tu le peux. Tu m'as aidé à sortir de mon cocon et hors de mon bureau, donc merci B et merci à ton acolyte de toujours Theo !

Merci au Dr. McKerron: vos conseils et votre aide m'ont été précieux et m'ont aidé dans mon travail lorsque j'en avais le plus besoin.

Un merci que je n'aurai jamais cru pouvoir donner est à Johan. Je n'aurai jamais pu penser que j'aurai la joie de t'avoir dans ma vie. Merci mon Smartie pour notre relation strictement non-professionnel et tout ce que tu m'as apporté.

Il est aussi pour moi très important de remercier Anita et Nadina, mes tatas sud africaines Elles ont toujours pris grand soin de moi pendant toutes ces années et ont fait en sorte que ma vie hors du département soit toujours fun et agréable. Elles ont aussi toujours fait en sorte que tout fonctionne proprement dans mon petit appart. Cet appart fut le parfait endroit pour vivre et j'ai été très heureuse là-bas.

Ceci est mon dernier remerciement, mais pas le moindre :

Maman, Papa, Romain, Nelly et Samantha (mon frère et mes sœurs), Mamy, Papy, Marraine, Parrain, Mémé, tata Cathy, Allan et Fred. Vous avez TOUJOURS été là, dans les moments agréables comme dans les moments les plus difficiles. Je ne sais pas comment vous exprimer ma gratitude !? Votre présence, votre amour m'ont donné une force incroyable. Vous m'avez manqué chaque jour et il ne s'est pas passé un jour sans que je ne pense à vous et à tout l'amour que j'ai pour vous. Votre amour inconditionnel et votre soutien sont ce qui m'a permis de tenir le coup pendant tout ce temps loin de vous. Je sais que mon départ ne fut pas facile pour vous non plus : pour la seconde fois que je décide de partir de la maison c'est pour vivre de l'autre côté du monde. Habiter en Afrique du Sud a ses challenges mais c'est un pays formidable, ce qui m'a permis de ne pas trop regretter la France, mais ce fut pour moi impossible de ne pas manqué d'être a la maison, là ou vous êtes. Merci pour votre amour, pour toutes vos lettres et les petits encas français délicieux que vous m'avez fait parvenir. Je vous aime et je vous dédicace cette thèse, ainsi qu'a Pépé, Mémé et Papy que je garde dans mon cœur.

Table of Contents

List of Figures

List of Tables

INTRODUCTION

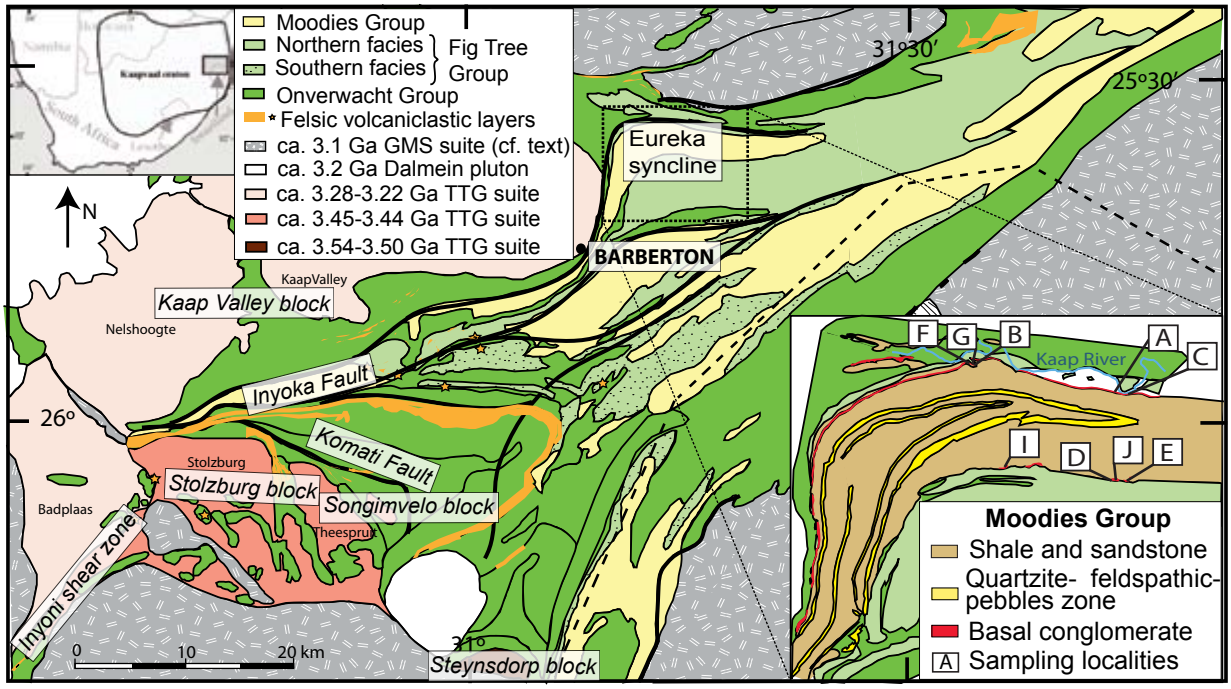

Figure 1: Simplified geological map of the Barberton Greenstone Belt (BGB)

During the last few decades, the Archean rock record has been studied with the aim of developing a better understanding of the evolution of the early Earth, including the formation of Earth's early sialic crust. From a granitoid perspective, the hallmark of this early crust is the Tonalite, Trondhjemite, Granodiorite (TTG) suite of rocks, which form the bulk of the preserved Archean continental crust (e.g. Condie, 1981; Martin, 1994; Windley, 1995) and are uncommon in the post-Archean rock record. This suggests that a fundamental change occurred on Earth towards the end of the Archean Eon, which produced a shift in the products of continental crustal growth (Rapp et al. 2008; Shirey and Hanson, 1984) from sodic leucocratic compositions (TTG) to intermediate compositions (andesites and diorites). It also suggests that other granitoid types might exit that are also unique to the Archean period.

The geochemistry of these TTG granitoids underpins much what we believe we know about the origins of Earth's earliest continental crust. Since the end of the Archean Eon, the dominant continental-crust-forming processes are reasonably well understood. This process is considered to begin with water-saturated partial melting of peridotite in the mantle wedge that is induced by the ascent of slab derived water-rich fluids or melts (Grove et al., 2006). The resultant, initially near water-saturated mantle melts, rise through the wedge, equilibrating with hotter and dryer mantle, to ultimately produce the

basalts and andesites that characterise this setting (Grove et al., 2006). The re-melting of this juvenile crust of intermediate average composition, as well as of volcaniclastic sedimentary material, produces the calc-alkaline series granitoids associated with arcs (e.g. Gill, 1981; Miller and Harris, 1989).

As is the case for the post-Archean granitoids, the generation of Archean TTG magmas is reasonably well understood. The TTGs are characterised by high Na:Ca and Na:K ratios and consequently, they plot near the Na corner of Or:Ab:An ternary plots (Martin, 1994), well off the calc-alkaline trend which characterises most post-Archean felsic granitoids. They are sodic granitoids, rich in silica (>65 wt%), most of them are metaluminous to slightly peraluminous and their Mg# varies mostly between 30 and 40. In contrast to the major element chemistry of the TTG their trace elements are a bit more complex and are considered to reflect the pressure-temperature conditions at which TTG magmas were generated. Consequently, Moyen (2011) divided TTG suite into 3 subgroups according to proposed source depth, namely the low-, medium-, and high-pressure groups. The medium and high pressure group, which broadly constitute the high-Al_2O_3 type TTG as defined by Barker and Arth (1973), dominate the Paleo- to Meso Archean rock record and have thus become the focus for unravelling the genesis of this continental crust. Various processes have been proposed to account for the origin of these granitoids; namely, melts evolved from basaltic magma by fractional crystallization (Arth et al., 1978), the product of the partial melting of a mantle source (Moorbath, 1975) or anatexis of pre-existing tonalites (Johnston and Wyllie, 1988). However, it has been demonstrated that these granitoids generally represent melt compositions from a distinct source and not a significantly evolved magma (Martin et al., 2005) This has also been demonstrated in the specific case of the well preserved Meso-Archean trondhjemites of the Barberton greenstone belt, South Africa (Clemens et al., 2006). Furthermore, this allows for inferences on the petrogenesis and geodynamic setting of these granitoid based on their geochemistry. The medium- and high-pressure TTGs are characterised by highly fractionated REE patterns with strong depletion in HREE, which reflect substantial amounts of garnet in the residuum; Nb-Ta and Ti anomalies, which reflect the presence of rutile in the residuum; and, high Sr and no pronounced Eu anomaly, which reflect the absence of plagioclase in the residuum (Moyen, 2011). Consequently, these magmas are interpreted to arise by the high pressure (>1.5 GPa) partial melting of a hydrated K-poor garnet-bearing amphibolite-facies or eclogite-facies metabasalt (Moyen 2011; Rapp et al., 2003).

The geodynamic setting within which TTG magmas are generated is controversial and remains the subject of debate. One set of models sees TTG magmas as arising through partial melting at the base of an overthickened basaltic plateau in an intra-plate setting (e.g. Smithies, 2000; Zegers and Van Keken, 2001) while other authors suggests that TTGs form by the melting of thick oceanic crust followed by repeated delamination of eclogitised lower crust (Bedard, 2006). However the

most popular model proposes that TTG magmas formed by the anatexis of the upper portions of subducted oceanic crust, in relatively hot subduction setting, with melting occurring via high-pressure hornblende fluid-absent incongruent melting or melting of an eclogitic assemblage, within Archean subduction zones (Condie, 1981; Martin, 1994, 1999; Smithies and Champion, 2000; Smithies et al., 2003; Foley et al., 2002; Rapp et al., 2003). This is proposed to have been a typical feature of Archean subduction zones, as a consequence of higher mantle temperatures, than exist on Earth at present (Rudnick 1995; Albarède 1998; Smithies 2000; Prelevic and Foley 2007; Pollack 1997; Martin, 1986; Martin and Moyen, 2002; Rapp et al., 2003). The chemistry of the medium- and high-pressure type of TTG described above reflects the fact that melting happened at conditions where plagioclase is absent and garnet is stable in the metamafic rock, which require pressures between 15 to 25 kbar, which seem to make the case that TTG formed in a subduction zone.

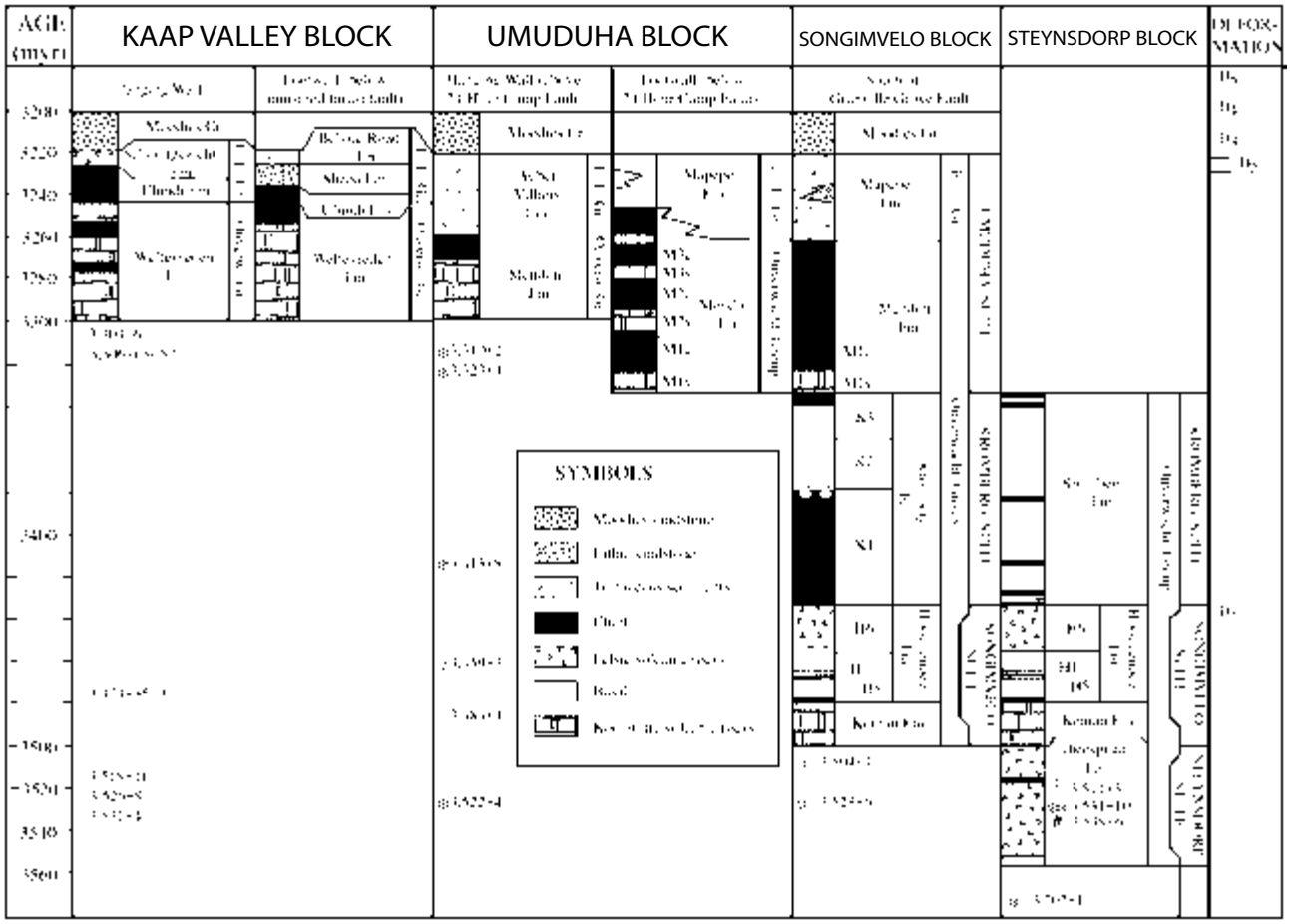

Figure 2: Generalized stratigraphies of the principal tectono-stratigraphic suites in the BGGT (modified from Lowe, 1999).

One of the most extensively studied and well preserved Archean terranes is the Paleo- to Meso-Archean Barberton Granitoid Greenstone Terrane (BGGT), located in South Africa (Figure 1a). Due to its remarkable preservation, the BGGT is regarded as an ideal location to unravel details of the processes which characterised the formation of Earth's early sialic crust. The BGGT is a composite terrane which forms the oldest nucleus to the Kaapvaal craton. It consists of a medium to high-grade metamorphic granitoid-gneiss terrain: the "Ancient Gneiss complex" (AGC) in Swaziland, which contains elements as old as 3.644 ±0.004 Ga (Kröner, 2007); but also the Steynsdorp block (ca.3.55 Ga); the Stolzburg block which contains plutons of ca. 3.45 Ga (Stolzburg pluton, Theespruit pluton …) (Kisters et al, 2003); the Songimvelo block and the KaapValley block that includes the younger plutons located in the western part of the BGGT (Kaap Valley and the Nelshoogte plutons); that are all juxtaposed against the low-grade metamorphic supracrustal sequence of the Swaziland Supergroup (Schoene et al., 2008; Moyen et al., 2007) (Figure 2). The Swaziland Supergroup consists of both volcanic and sedimentary rocks, emplaced between 3.55 and 3.23 Ga (Lowe, 1999) (Figure 2). Late voluminous sheet-like calc-alkaline monzogranitic (s.l.) batholiths, known as the Granodiorite-Monzogranite-Syenite (GMS) suite (Figure 1a), intruded the greenstone belt between 3.2 and 2.6 Ga (Davies, 1971; Hawkesworth et al., 1975; Barton et al., 1983). Although, Archean tectonics, in general, remains the focus of intense debate, the BGGT exhibits perhaps the most convincing evidence supporting Archean subduction. This evidence constitutes the following: 1) The available geochronological data shows that the supracrustal rocks of the Swaziland Supergroup (Figure 1a) in the Northern terrane are ca. 200 Ma younger than the one in the southern terrane (Figure 1a) (Lowe and Byerly, 2007). The boundary between these terranes is the Inyoka fault, a linear structure running the length of the greenstone belt (Figure 1a); 2) the two terranes were juxtaposed at ca. 3.2 Ga (de Ronde and de Wit, 1994), thus this occurred concurrently with high-pressure amphibolite facies metamorphism in the Stolzburg block (Figure 1a) (Moyen et al., 2007; Diener et al., 2005) and moderate-pressure amphibolite facies metamorphism in the AGC (Taylor et al., 2012); 3) the arc-like sedimentary succession of the greenstone belt and 4) the BGGT consists of two different terranes, a southern and northern one, that collided ca 3.23 Ga ago (de Ronde and de Wit, 1994) along the Saddleback-Inyoka fault system (Figure 1a) which represents the collision suture zone.

In the BGGT, the TTGs were emplaced during three distinct magmatic episodes which coincide with the three major tectono-metamorphic episodes that the belt underwent from 3.644 to 3.216 Ga. Recent works showed that, apart from the AGC, the TTG plutons of the BGB (Nelshoogte, KaapValley, Stolzburg, Vlakplaats and Steynsdorp) were emplaced during 3 main chronological events : 3538-3509 Ma, 3470-3443 Ma and 3227-3216 Ma (de Ronde et al., 1994; Kamo and Davis, 1994; Kisters et al., 2010). The ca 3450 Ma plutons have been proposed to have formed syn-orogenically to the

D1 event (De Wit et al., 1992, Schoene et al., 2008) whereas the ca 3230 Ma TTGs were associated with the amalgamation of distinct terranes along the Inyoka-Inyoni fault system during the D2 event. Little is known about the deformation event that happened before 3.45 Ga, and which corresponds to the emplacement of the 3.50-3.55 Ga year's old Steynsdorp pluton which probably formed an early continental nucleus. The Steynsdorp pluton is believed to have formed through partial melting of amphibolite at shallow depth (Moyen et al., 2007).

The period from 3.49-3.45 Ga represent possibly a mid-oceanic ridge like environment. The D1 event, from 3.445 to 3.416 Ga, happened in a compressional context that corresponds to a horizontal shortening. It is described as representing the development of an active margin (oceanic arc) (in either a fore-arc or back-arc environment) (Lowe, 1999; de Ronde and Kamo, 2000; Lowe and Byerly, 2007, and references therein) during which the Stolzburg and Theespruit plutons (located in the Stolzbug block, Figure 1a) were emplaced at shallow depth. This period records the formation of an intra-oceanic supra-subduction-like environment which represents the accretion of the Stolzburg domain. The deep origin of the Stolzburg and Theespruit plutons may indicate that they intruded the supra-subduction which may have occurred along the margin of a pre-existing "proto-continent".

The D2 event is the dominant collisional stage that happened in the BGB between 3.229 to 3.210 Ga (Lowe, 1994; de Ronde and Kamo, 2000). Most of the deformation occurred over a short period of time in response to arc-fore-arc and inter-arc collision, culminating in arc-arc accretion (orogenesis) between two rigid blocks separated by the Saddleback-Inyoka fault system, which is the suture zone of the collision. The accretion itself occurred via under-thrusting where the southern high grade Stolzburg domain represents the lower plate. The 3.29-3.21 Ga years old plutons (Kamo and Davis, 1994) that were emplaced in the BGB are pre- to post-collision TTG magmatism. The 3.29 Ga trondhjemitic magmas of the Badplaas pluton (Figure 1a) are rich in Sr and consequently interpreted to have been generated through partial melting of a plagioclase-free garnet amphibolite or eclogite at high depth (>18 Kbar) and their ages correspond to the accretion phase of the magmatic arc (Kisters et al., 2010). In contrast, the later emplaced 3.21 Ga TTG magmas of the Kaap Valley pluton (Figure 1a) are low in Sr and are interpreted to have formed through partial melting of a plagioclase-bearing amphibolite at shallower depth (10-12 kbars) (Moyen et al., 2007). This transition from deep to shallower condition of partial melting corresponds to an increase in the temperature of the colliding pile observed in modern-day post-orogenic collapse. Consequently these TTGs have been interpreted to formed via the partial melting of over-thickened mafic crust during orogenic collapse and/or slab break-off. The ages of the TTG plutons are progressively younger with movement from the southern terrain to the northern terrane of the BGGT which reflect the change in the nature of the pluton, being syn-subduction (or syn-collision) to syn-orogenic collapse.

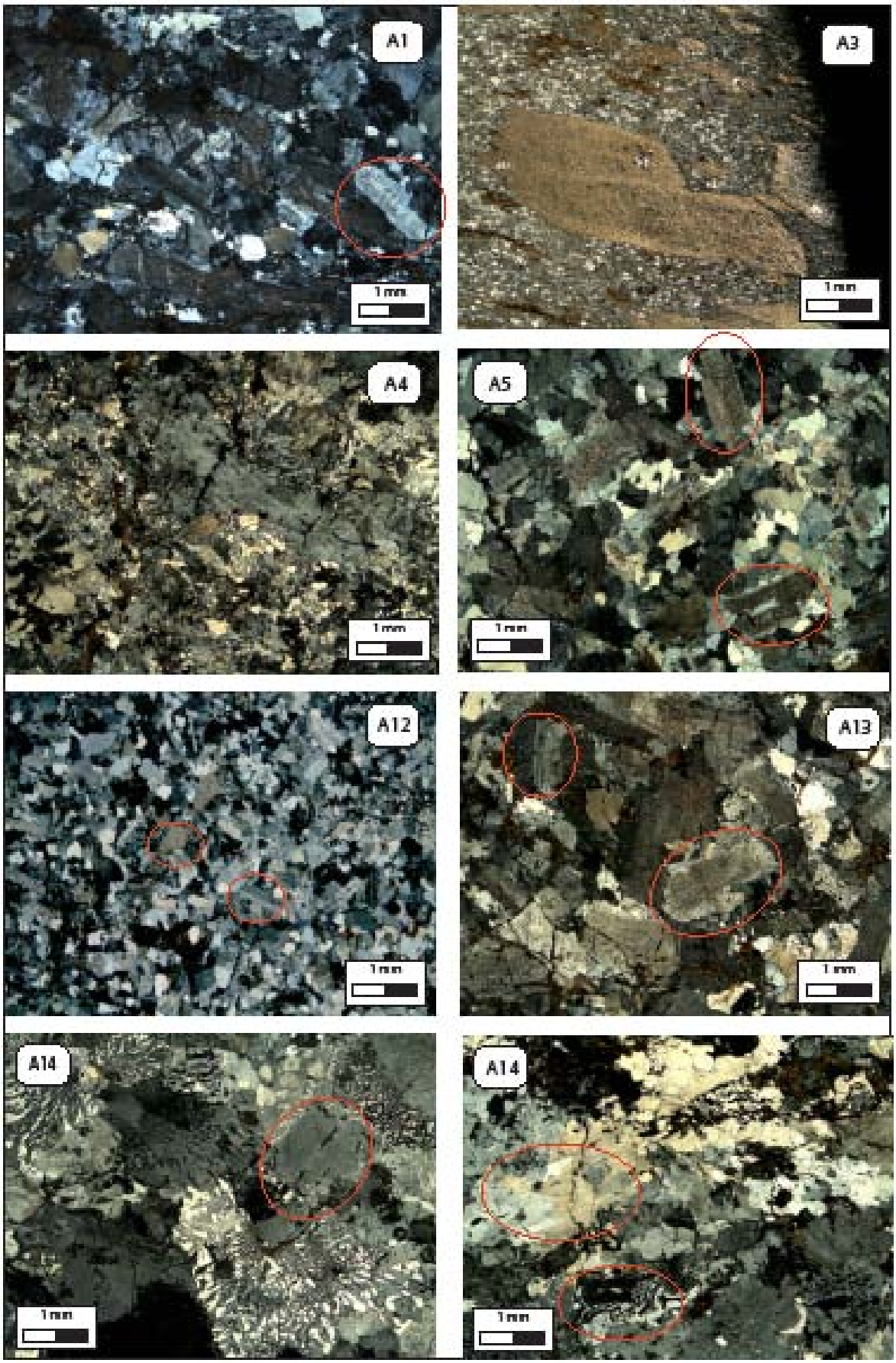

Figure 3: Main petrographic features of some granitic and rhyolitic clasts from the Moodies Group. The highlighted sections in red are example of euhedral alkali feldspar.

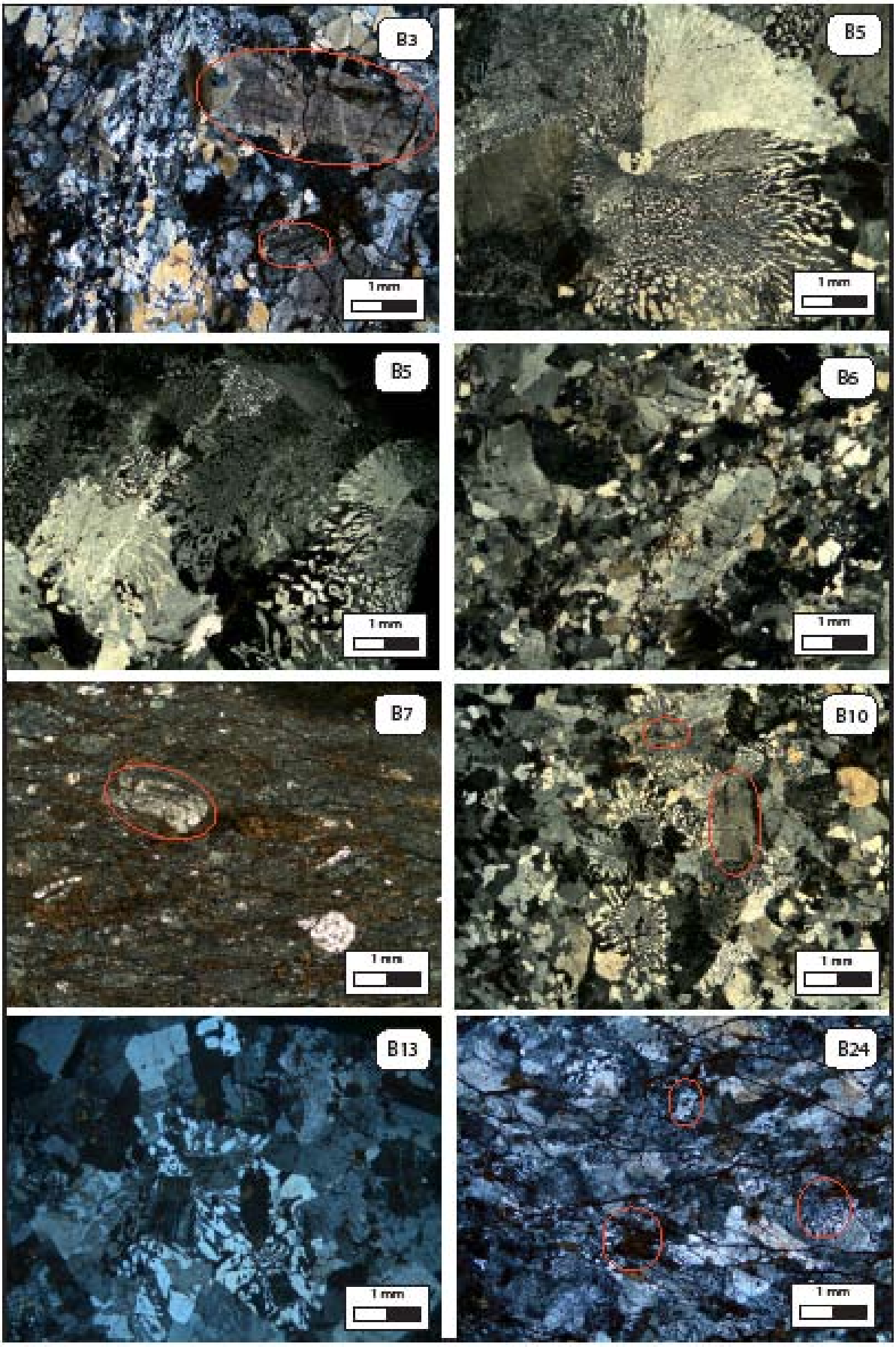

Figure 3 (continued): Main petrographic features of some granitic and rhyolitic clasts from the Moodies Group. The highlighted sections in red are example of euhedral alkali feldspar.

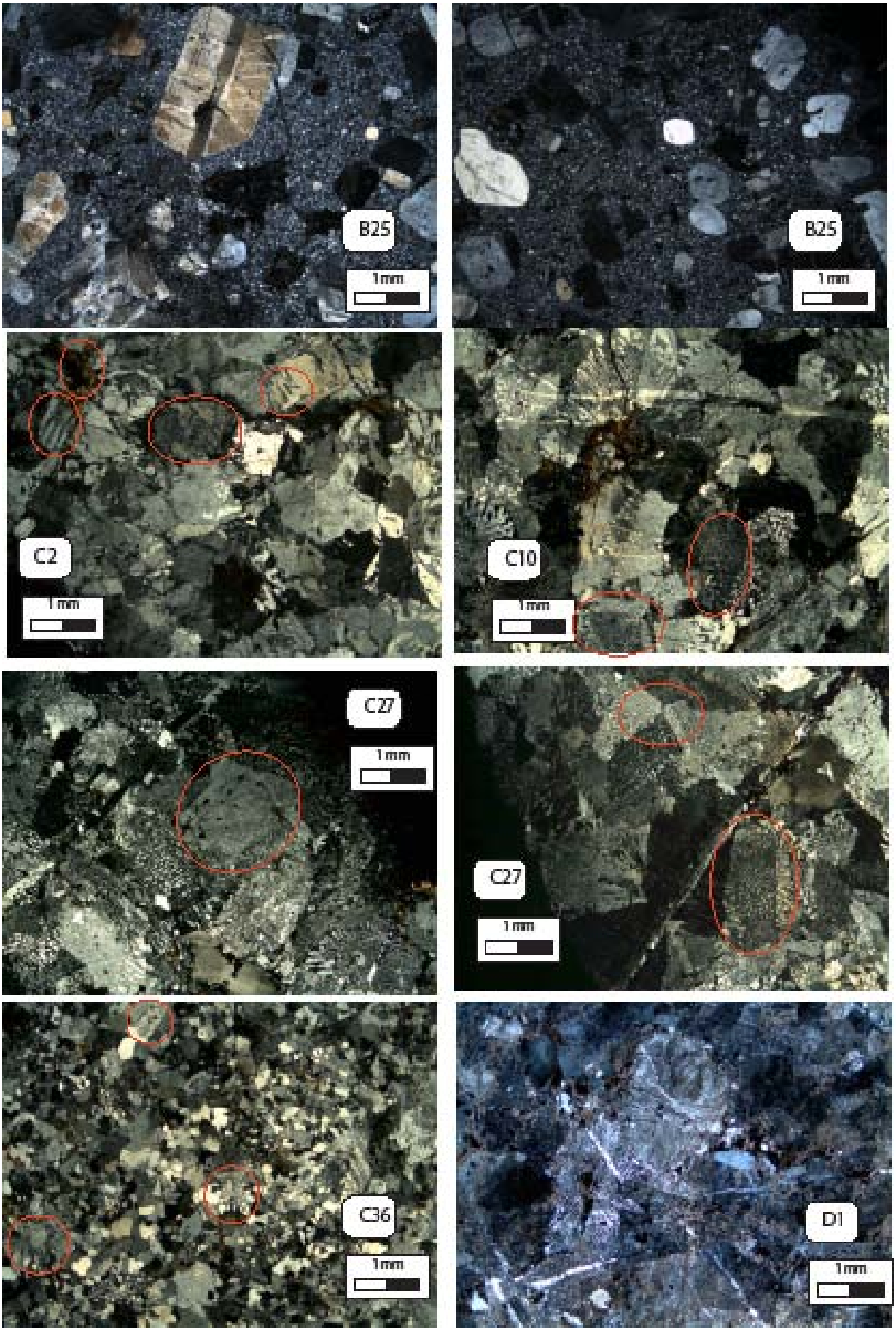

Figure 3 (continued): Main petrographic features of some granitic and rhyolitic clasts from the Moodies Group. The highlighted sections in red are example of euhedral alkali feldspar.

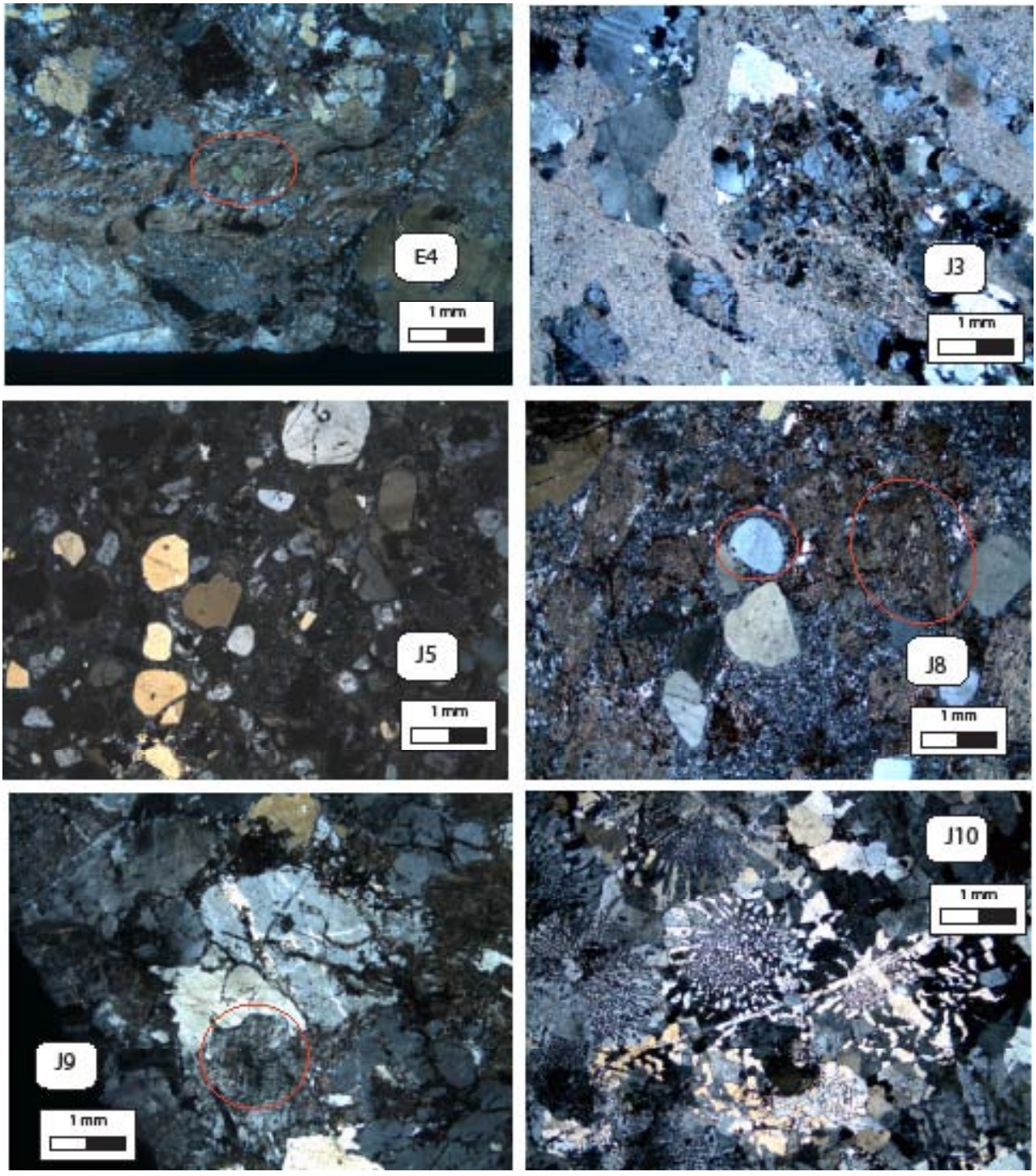

Figure 3 (continued): Main petrographic features of some granitic and rhyolitic clasts from the Moodies Group. The highlighted sections in red are example of euhedral alkali feldspar.

The last main event recorded in the BGGT is the switch from transpressional to transtensional deformation (D3 event). This is mirrored by the presence of the GMS magmatism from 3.126 to 3.084 Ga. These sheet-like batholiths intruded the older TTG basement and grew by batch accretion over several millions of years (Belcher and Kistsers, 2006). Both the intrusive ages and syn-magmatic deformation of the batholiths show that the GMS suite plutonism was concurrent with the last phase of deformation (D3; 3126-3084 Ma, De Ronde et al., 1991) of regional NW-SE shortening and associated folding and thrusting documented in the BGB (De Ronde and De Wit, 1994; Kamo and Davis, 1994). They are relatively rich in potassium. These rocks have been interpreted to be derived from the anatectic recycling of the TTG crust (Glikson, 1976), as has been demonstrated to be the case in other Archean terranes (Champion and Sheraton, 1997; Smith, 2003; Whalen et al., 2004; Jayananda et al., 2006; Nehring et al., 2009; Shang et al., 2007). Various other processes have been proposed to account for the origin of these granitoids in the post-Archean calk-alkaline series around the world such as alkaline metasomatism, interactions involving mantle-derived magmas and TTG or partial melting of pre-existing tonalites. The rocks of the GMS suite are believed to be the first evidence of potassic-rich granitoid in the BGB. Their emplacement helped to stabilize the Kaapvaal craton. Thus the concentration of potassium in the Meso to Proto-Archean granites of the upper crust is seen to be preceded by residency in older TTG crust.

Nevertheless, in addition to the GMS and TTG record, the BGB contains evidence of felsic potassic-rich volcanic and volcaniclastic rocks. These felsic rocks occur as 3.548-3.544 Ga-old (Van Kranendonk et al., 2009) felsic volcaniclastic layers within the Theespruit formation (Kröner et al., 1996); as 3.457-3.416 Ga-old felsic lavas within the H6 layer of the Hooggenoeg formation of the middle-to-upper Onverwacht Group (Kröner et al., 1991; Byerly et al., 1996; Byerly et al., 2002); as 3.298-3.258 Ga-old volcaniclastic and tuffaceous layers within the Mendon formation (Byerly et al., 1996) and as 3.255-3.227 Ga-old felsic volcanic layers of the Mapepe formation in the Fig Tree Group (Kröner et al., 1991; Byerly et al., 1996) (Figure 1a and 2). As these ages correspond with the three episodes of TTG emplacement, some of the felsic layers have been interpreted to represent the K_2O-metasomatised rocks and/or, eruptive equivalents of the TTG plutons (Kröner et al., 1996; de Wit et al., 1987). However, recent work by Diergaardt et al. (2011) has demonstrated the primary magmatic origin of the high K_2O content of feldspar within a substantial fraction of the potassium feldspar phenocrysts in the felsic volcanic/volcaniclastic layers of the H6 layer. The presence of these magmatic potassium-feldspar phenocrysts question the validity of the alteration hypothesis as the source of potassium, as this study demonstrates the magmatic origin of the potassium in these rocks

Additionally to these felsic rocks, the BGB contains evidence of a particular type of old granitic (s.l.) potassic-rich rocks. These high level potassic granites and rhyolites have a low preservation potential

in the typically amphibolite facies basement rocks preserved in association with greenstone belts. These rocks are preserved only as clasts in the basal conglomerate of the Moodies Group (MdB), which is the youngest of the Swaziland Supergroup (Figure 1b). These clasts of granites and rhyolites are the subject of the present thesis. They are described as being older than >3.226 Ga, which is older than any of the GMS suite batholiths, so these rocks offer the opportunity to understand the petrogenesis of K_2O-rich granites that predate the presently preserved plutonic record for such rocks and possibly provide insight into the K_2O-rich igneous activity in the BGB. Their unusually high potassium content has long been described as being a consequence of alteration processes (Lowe, 1999). On contrary, my study demonstrates a magmatic origin for these granitoids' most unusual chemical signatures (i.e. high K_2O and low CaO content). The source of the potassic detritus, within the Moodies Group, has previously been considered to be eroded TTG basement or volcanic TTG input (Reimer, 1985), which has subsequently been metasomatised from the erosion of TTG basement or from a TTG volcanic input. In spite of this and despite the absence of true potassic granites in the plutonic record at the time, these unusual granitic (s.l.) clasts could provide a new path for the accumulation of potassium in volcano-sedimentary depositories. The involvement of these sedimentary rocks in subsequent crustal recycling provides a new model for the generation of the potassic GMS suite rocks. Indeed, the presence of potassic granites is unusual for the Paleo- and Meso- Archean. Therefore, these rocks may be of significant importance to the understanding of early Earth continental crustal formation and may be an important link in the crustal potassium cycle. My study does an inventory of these granitic and rhyolitic clasts present within the layer of the basal conglomerate of the Moodies group and seeks to determine if and how these rocks can be used to understand crustal evolution in the BGGT and in the Kaapvaal craton better. My study also focuses on some felsic layers present in one of the oldest formations of the oldest group of the Barberton greenstone.

The clasts consist mainly of quartz-feldspar bearing crystal tuff, microgranite, medium grained micrographytic granite, and quartz-feldspar-phyric rhyolite; their main petrographic features and mineral textures are shown in figure 3. My work is presented in 3 work portions: one published manuscript in Geology, that defines the ages of the clasts and describe their chemistry; a paper submitted to Journal of Petrology that describes the clasts petrology in detail as well as the petrology of some felsic volcaniclastic rocks from the Theespruit formation; and a paper submitted to Chemical Geology which study the provenance of the clasts as well as the provenance and source of the BGB TTG.

References:

Albarède, F., 1998. The growth of continental crust. Tectonophysics 296, 1–-14.

Arth, J.G. et al., 1978. Geochemistry of the gabbro-diorite-tonalite-trondhjemite suite of southwest Finland and its implications for the origin of tonalite and trondhjemite magmas. Journal of Petrology 19, 289-316.

Barton, J.M. et al., 1983. Geochronological and Sr-isotopic studies of certain units in the Barberton granite-greenstone terrane, South Africa. Special Publication of the Geological Society of South Africa 9, 63–72.

Bédard, J., 2006. A catalytic delamination driven model for coupled genesis of Archaean crust and subcontinental lithospheric mantle. Geochimica and Cosmochimica Acta, 70, 747–771.

Belcher, R.W. and Kisters, A.F.M., 2006. Progressive adjustments of ascent and emplacement controls during the incremental construction of the 3.1 Ga Heerenveen batholith, South Africa. Journal of Structural Geology 28, 1406–1421.

Byerly, G.R. et al., 1996. Prolonged magmatism and time constraints for sediment deposition in the early Archean Barberton greenstone belt: evidence from the upper Onverwacht and Fig Tree groups, Precambrian Research 78, 125–138.

Champion, D.C. and Sheraton, J.W., 1997. Geochemistry and Nd isotope systematics of Archean granites of the Eastern goldfields, Yilgarn craton, Australia: implications for crustal growth processes. Precambrian Research 83, 109-132.

Clemens, J.D., Yearron, L.M. and Stevens, G., 2006. Barberton (South Africa) TTG magmas: Geochemical and experimental constraints on source-rock petrology, pressure of formation and tectonic setting. Precambrian Research 151, 53–78.

Condie, K.C., 1981. Archean greenstone belts, 434 pp., Elsevier, Amsterdam.

Davies, R.D., 1971. Geochronology and isotope evolution of the early Precambrian crustal rocks in Swaziland, Ph.D. Thesis, Univ. Witwatersrand, Johannesburg, p. 135.

de Ronde, C. E. J., de Wit, M. J. and Spooner, E. T. C., 1994. Early Archean (>3.2 Ga) Fe-oxide-rich, hydrothermal discharge veins in the Barberton greenstone belt, South Africa, Geological Society of American Bulletin 106, 86– 104.

de Ronde, C.E.J and Kamo, S.L., 2000. An Archaean arc-arc collisional event: a short-lived (ca 3 Myr) episode, Weltevreden area, Barberton Greenstone Belt, South Africa. Journal of African Earth Sciences 30, 219-248.

de Ronde, C.E.J. and de Wit, M.J., 1994. The tectonothermal evolution of the Barberton greenstone belt, South Africa: 490 million years of crustal evolution. Tectonics 13, 983–1005.

de Ronde, C.E.J. et al., 1991. Field, geochemical and U-Pb isotopic constraints from hypabyssal felsic intrusions within the Barberton greenstone belt, South Africa: Implications for tectonics and the timing of gold mineralization. Precambrian Research 49, 261-280.

de Wit, M. J. et al., 1987. Felsic igneous rocks within the 3.3-to 3.5- Ga Barberton Greenstone Belt: high crustal level equivalents of the surrounding tonalite-trondhjemite terrain, emplaced during thrusting. Tectonic 6 (5), p.529-549.

De Wit, M. J. et al., 1992. Formation of an Archaean continent. Nature 357, 553–562.

Diener, J.F.A. et al., 2005. Metamorphism and exhumation of the basal parts of the Barberton greenstone belt, South Africa: Constraining the rates of Mesoarchaean tectonism. Precambrian Research 143, p.87-112.

Diergaardt, B.N., Stevens, G. and Moyen, J.-F., 2011. 3.45 Ga potassic rhyolites of the Hooggenoeg formation: Barberton Greenstone Belt, 23rd Congress of African Geology, Johannesburg, Janvier 2011.

Foley, S., Tiepolo, M., and Vannucci, R., 2002. Growth of early continental crust controlled by melting of amphibolite in subduction zones. Nature 417, 837-840.

Gill, J., 1981. Orogenic Andesites. New York: Springer-Verlag, 390 pp.

Glikson, A.Y., 1976. Trace element geochemistry and origin of early Precambrian acid igneous series, Barberton Mountain Land, Transvaal. Geochimica et Cosmochimica Acta 40, 1261-1280.

Grove, T.L. et al., 2006. The influence of H2O on mantle wedge melting. Earth and Planetary Science Letters 249, 74–89.

Hawkesworth, C.J. et al., 1975. Age relationships between greenstone belts and “granites” in the Rhodesian Archaean craton. Earth and Planetary Science Lettters 25, 251-262.

Jayananda, M. et al., 2006. 2.61 Ga potassic granites and crustal reworking in the western Dharwar craton, southern India: Tectonic, geochronologic and geochemical constraints. Precambrian Research 150, 1-26.

Johnston, A.D. and Wyllie, P.J., 1988. Constraints on the origin of Archean trondhjemites based on phase relationships of Nfik gneiss with H20 at 15 kbar. Contributions to Mineralogy and Petrology 100, 35-46.

Kamo, S.L. and Davis, D.W., 1994. Reassessment of Archean crustal development in the Barberton Mountain Land, South Africa, based on U-Pb dating. Tectonics 13, 167–192.

Kisters, A.F.M. et al., 2003Extensional detachment faulting and core-complex formation in the southern Barberton granite-greenstone terrain, South Africa: evidence for a 3.2 Ga orogenic collapse. Precambrian Research 127, 355-378.

Kisters, A.F.M et al., 2010. Continental growth and convergence-related arc plutonism in the Mesoarchaean: Evidence from the Barberton granitoid-greenstone terrain, South Africa. Precambrian Research 178, 15–26

Kröner, A. et al., 1996. The oldest part of the Barberton granitoid-greenstone terrain, South Africa: evidence for crust formation between 3.5 and 3.7 Ga. Precambrian Research 78, 105-124.

Kröner, A., 2007. The Ancient Gneiss Complex of Swaziland and Environs: Record of Early Archean Crustal Evolution in Southern Africa. Developments in Precambrian Geology 15, 465-480.

Kröner, A., Byerly, G.R. and Lowe, D.R., 1991. Chronology of early Archaean granite-greenstone evolution in the Barberton Mountain Land, South Africa, based on precise dating by single zircon evaporation. Earth and Planetary Science Letters 193, 41–54.

Lowe D.R., 1999. Geologic evolution of the Barberton Greenstone Belt and vicinity. In Lowe, D.R., Byerly, G.R., Editors, Geologic Evolution of the Barberton Greenstone Belt, Boulder, pp. 287–312 (Geological Society of America Special Paper 329).

Lowe, D.R. and Byerly, G.R., 2007. An Overview of the Geology of the Barberton Greenstone Belt and Vicinity: Implications for Early Crustal Development. Developments in Precambrian Geology 15, 481-526.

Lowe, D.R. and Byerly, G.R., 2007. An Overview of the Geology of the Barberton Greenstone Belt and Vicinity: Implications for Early Crustal Development. Developments in Precambrian Geology 15, 481-528.

Martin, H. and Moyen J.-F., 2002. Secular changes in tonalite-trondhjemite-granodiorite composition as markers of the progressive cooling of the Earth. Geology 30, 319–322.

Martin, H. et al. 2005. An overview of adakite, tonalite–trondhjemite–granodiorite (TTG), and sanukitoid: relationships and some implications for crustal evolution. Lithos 79, 1-24.

Martin, H., 1986. Effect of steeper Archean geothermal gradient on geochemistry of subduction-zone magmas, Geology 14, 753-756.

Martin, H., 1994. The Archean grey gneisses and the genesis of the continental crust, in: Condie, K.C. (Ed.), The Archean Crustal Evolution, Developments in Precambrian Geology. Elsevier, Amsterdam, pp. 205– 259.

Martin, H., 1999. Adakitic magmas: modern analogues of Archaean granitoids. Lithos 46, 411–429.

Miller, N. and. Harris, N., 1989. Evolution of continental crust in the central Andes; constraints from Nd isotope systematics. Geology 17, 615-617.

Moorbath, S., 1975. Evolution of Precambrian crust from strontium isotopic evidence: Nature 254, 395-398.

Moyen, J.-F. and Stevens, G., 2006. Experimental constraints on TTG petrogenesis: implications for Archean geodynamics, in: Benn, K., Mareschal, J.-C., Condie, K.C. (Eds.), Archean geodynamics and environments. AGU monograph 164, 149-178.

Moyen, J.-F. et al., 2007. TTG plutons of the Barberton Granitoid-Greenstone Terrain, South Africa. Developments in Precambrian Geology 15, 607-667.

Moyen, J-F., 2011. The composite Archaean grey gneisses: Petrological significance, and evidence for a non-unique tectonic setting for Archaean crustal growth. Litho 123, 21-36.

Nehring, F. et al., 2009. Internal Differentiation of the Archean Continental Crust: Fluid-Controlled Partial Melting of Granulites and TTG-Amphibolite Associations in Central Finland. Journal of petrology 50, 3-35.

Pollack, H.N., 1997. Thermal characteristics of the Archaean, in De Wit, M.J., and Ashwal, L.D., eds., Greenstone belts: Oxford Monographs on Geology and Geophysics, v. 35, p. 223–232.

Prelevic, D. and Foley, S.F., 2007. Accretion of arc-oceanic lithospheric mantle in the mediterranean: evidence from extremely high-Mg olivines and Cr-rich spinel inclusions in lamproites. Earth and Planetary Science Letters 256, 120–135.

Rapp, R.P., Shimizu, N. and Norman, M.D., 2003. Growth of early continental crust by partial melting of eclogite. Nature 425, 605– 609.

Reimer, O. et al., 1985. Petrography and geochemistry of granitoid and metamorphite pebbles from the early Archaean Moodies Group, Barberton Mountainland/ Southa Africa. Precambrian Research 29, 383-404.

Rudnick, R.L., 1995. Making continental crust. Nature 378, 571–578.

Schoene, B., De Wit, M. J. and Bowring, S. A., 2008. Mesoarchean assembly and stabilization of

the eastern Kaapvaal craton: A structural-thermochronological perspective. Tectonics 27, TC5010; doi:10.1029/2008TC002267.

Shang, C.K. et al., 2007. Archaean high-K granitoids produced by remelting of earlier Tonalite–Trondhjemite–Granodiorite (TTG) in the Sangmelima region of the Ntem complex of the Congo craton, southern Cameroon. International Journal of Earth Sciences (Geol Rundsch) 96: p. 817-841.

Shirey, S. and Hanson, G.N., 1984. Mantle-derived Archaean monzodiorites and trachyandesites. Nature 310, 222-224.

Smith, J.B., 2003. The episodic development of intermediate to silicic volcano-plutonic suites in the Archaean West Pilbara, Australia Chemical Geology 194, 275- 295.

Smithies, R.H. and Champion, D.C., 2000. The Archaean high-Mg diorite suite: links to tonalite-trondhjemite-granodiorite magmatism and implications for early Archaean crustal growth. Journal of Petrology 41, 1653–1671.

Smithies, R.H., 2000. The Archaean tonalite–trondhjemite–granodiorite (TTG) series is not an analogue of Cenozoic adakite. Earth and Planetary Science Letters 182, 115–125.

Smithies, R.H., Champion, D.C. and Cassidy, K.F., 2003. Formation of Earth's early Archaean continental crust. Precambrian Research 127, 89–101.

Van Kranendonk, M.J. et al., 2009. Age, lithology and structural evolution of the c. 3.53 Ga Theespruit Formation in the Tjakastad area, southwestern Barberton Greenstone Belt, South Africa, with implications for Archaean tectonics. Chemical Geology 261, 115–139.

Whalen, J.B. et al., 2004. Geochemical and isotopic (Nd–O) evidence bearing on the origin of late- to post-orogenic high-K granitoid rocks in the Western Superior Province: implications for late Archean tectonomagmatic processes. Precambrian Research 132, 303-326.

Zegers, T.E., and van Keken, P.E., 2001, Middle Archean continental formation by crustal delamination. Geology, v. 29, p. 1083–1086.

Chapter 1: Presentation of the publication

This paper published in Geology, is first-authored by Miss Sanchez-Garrido Cynthia. It describes for the first time in the literature the ranges of ages of Meso- and Paleo-Archean granites located in the Barberton Greenstone belt. This work aims to determine the nature of the relationship between these granites and the contemporaneous Tonalite-Trondhjemite-Granodiorite. It established the primary characteristics of the granites composition and demonstrates that these particular features are not the consequence of alteration of the material but rather are reflecting the magma composition. Finally, this paper evaluates a possible source for the granites and discusses melting conditions at the source. All calculations and data acquisitions were lead by Miss Cynthia Sanchez-Garrido under the supervision of Professor Gary Stevens, Doctor Richard Armstrong, Professor Hervé Martin, Professor Jean-François Moyen and Doctor Régis Doucelance. Doctor Richard Armstrong acquired 40% of the SHRIMP data. All samples preparation (zircons, whole rock XRF, whole rock LA-ICP MS) were done by Miss Sanchez-Garrido. All acquisition of mineral chemistry by SEM was done by Miss Sanchez-Garrido. All heavy mineral separation was done by Miss Sanchez-Garrido. Sampling of the Moodies granites was effectuated by Miss Sanchez-Garrido and Professor Gary Stevens. Sampling of the Barberton TTG was effectuated by Miss Sanchez-Garrido and Professor Jean-Francois Moyen. Acquisition of the trace and REE of the Moodies granites whole rock, done by LA-ICP MS was done equitably between Miss Sanchez-Garrido, Doctor Cristiano Lana and Ms Riana Rossow.

Diversity in Earth's early felsic crust: Paleoarchean peraluminous granites of the Barberton Greenstone Belt

Cynthia J.M.G. Sanchez-Garrido[1,3,4,5], Gary Stevens[1], Richard A. Armstrong[2], Jean-François Moyen[4,5,6], Hervé Martin[3,4,5], and Régis Doucelance[3,4,5]

[1]Center for Crustal Petrology, Department of Earth Sciences, University of Stellenbosch, South Africa Private Bag X-1, Matieland 7602, South Africa

[2]Research School of Earth Sciences, Australian National University, Canberra A.C.T. 0200, Australia

[3]Clermont Université, Université Blaise Pascal, Laboratoire Magmas et Volcans, BP 10448, F-63000 Clermont-Ferrand, France

[4]Centre National de la Recherche Scientifique, UMR 6524, LMV Laboratoire Magmas et Volcans, F-63038 Clermont-Ferrand, France

[5]Institut de Recherche pour le Développement, R 163, LMV (Laboratoire Magmas et Volcans), F-63038 Clermont-Ferrand, France

[6]Université Jean-Monnet, Laboratoire Magmas et Volcans, Département de Géologie 23 rue du Docteur Michelon, 42023 Saint Etienne, France

ABSTRACT

Earth's oldest preserved granitoid crust dates back to the Paleoarchean and consists predominantly of sodic tonalite-trondhjemite-granodiorite (TTG) granitoids that arose through the partial melting of hydrated metabasalts. In contrast, granites (sensu stricto) typically appear relatively late in the plutonic record of the old cratons. However, the existence of Hadean zircons with mineral inclusion suites that are consistent with crystallization from peraluminous granitic magmas indicates that granitic rocks formed part of the earliest felsic crust; although we have direct evidence, this earliest felsic crust is not preserved. Here we present evidence of an unusual variety of markedly low-CaO, K_2O-rich, rutile-bearing, peraluminous granite and rhyolite that was produced concurrently with TTG magmas during three magmatic cycles in the Barberton Greenstone Belt (BGB), southern Africa. This material is not preserved as in situ rock units, but occurs as clasts within a younger conglomerate. Within these rocks, plagioclase feldspar is a rare inclusion in zircon, relative to alkali feldspar, and has low anorthite contents (An < 15%), attesting to the primary nature of the low-Ca signature of the magmas. This, along with Eu/Eu* ~ 1, high K_2O and Sr content, as well as the peraluminous character of the magmas, is a consequence of phengite melting in a metagraywacke source at pressures in excess of those of plagioclase stability. This process contributed to each episode of continental crustal growth through the Paleoarchean to Mesoarchean in the BGB, despite leaving no plutonic record at the typical mid-crustal level of exposure that the TTG plutons around the belt represent.

INTRODUCTION

The most common Archean granitoids, the tonalite-trondhjemite-granodiorites (TTGs), acquire their leucocratic, mildly peraluminous and sodic nature, as well as their characteristically low heavy rare earth element (HREE) contents and steep REE patterns, from the high-pressure melting of hydrous metamafic rocks, either in the garnet-amphibolite (Martin, 1986; Foley et al., 2002) or eclogite facies (Rapp et al., 2003). Archean potassic granites, however, are mostly regarded as the result of remelting of this early felsic sodic crust, forming true potassic granites at a late stage of cratonic evolution. This interpretation is largely supported by the geology of Archean terrains, where granitic plutons tend to be late and postdate early sodic gneisses of TTG composition. This is the case in the well-preserved Paleoarchean–Mesoarchean BGB, southern Africa (Fig. 1A), where continental crust grew during three episodes of TTG magmatism, 3538–3509 Ma, 3470–3443 Ma, and 3290–3216 Ma (Kamo and Davis, 1994; Schoene et al., 2008; de Ronde and de Wit, 1994; Kisters et al., 2010) (Fig. 1B), and where the youngest episode coincides with the amalgamation of distinct northwest and southeast terranes within the greenstone belt (e.g., de Wit et al., 1992). Potassic granitoid plutonism in the BGB occurred between 3236 and ca. 3100 Ma and is represented by the Usutu suite (Schoene and Bowring, 2010), the Dalmein pluton (Lana et al., 2010), and the granodiorite-monzogranite-syenogranite (GMS) batholiths (Schoene et al., 2008; de Ronde and de Wit, 1994). Thus it coincides with or follows the ca. 3210 Ma terrane amalgamation (Fig. 1B) (Lowe, 1994; Moyen et al., 2006). One exception to this is granitic (sensu stricto) clasts that are older than most of the TTG plutons associated with the BGB (Kröner and Compston, 1988). They have been documented within the basal conglomerate of the Moodies Group, a coarse clastic sedimentary succession formed between 3225 and 3215 Ma (Lowe, 1999). In this study, we examined more than 110 granitic clasts from 6 exposures of this basal conglomerate within the Eureka syncline (Fig. 1A), in order to understand their petrogenesis and the significance thereof for early continental crust formation.

RESULTS

The clasts sampled in this study typically display either pristine magmatic textures (Figs. 1C and 1D), ranging from granophyric to porphyric, characterized by quartz and feldspar phenocrysts, or volcaniclastic textures, also with quartz and alkali feldspar as phenocrysts. This demonstrates that the magmas crystallized at shallow depth or erupted at the surface. Most of the clasts have peraluminous granitic compositions (0.97 < A/CNK < 1.83) [A/CNK—molecular Al/(Ca + Na + K)] (Fig. 2D) and display a wide range of SiO_2 content (63.13–76.62 wt%). They are rich in K_2O (3.78–9.02 wt%), poor in CaO (0.02–1.37 wt%), and consequently differ substantially from BGB TTGs (Figs. 2A, 2B), which are peraluminous to metaluminous (A/CNK average ~1.00) (Fig. 2D), have low K_2O (average 1.93 wt%), and relatively high CaO (average 2.85 wt%) contents (Table DR1 in the GSA Data Repository[1]). The granitic (sensu stricto) clasts are relatively Sr rich (12–330 ppm) and Rb poor (32–153 ppm); their light REE patterns are fractionated while their HREE ends are relatively flat with a slightly negative Eu anomaly (Fig. 2E).

Zircons from four of the clasts were analyzed for oxygen isotope compositions by sensitive high-resolution ion microprobe (SHRIMP) at the Research School of Earth Sciences of the Australian National University (ANU). The zircon's $\delta^{18}O$ values range from 4.90‰ to 5.91‰ (standard mean ocean water) (Fig. 1H; Table DR2). The zircons contain inclusions of quartz, alkali feldspar, plagioclase, biotite, monazite, apatite, rutile, and ilmenite that are scattered throughout the magmatic oscillatory

[1]GSA Data Repository item 2011282, Tables DR1–DR4 and Figures DR1 and DR2, is available online at www.geosociety.org/pubs/ft2011.htm, or on request from editing@geosociety.org or Documents Secretary, GSA, P.O. Box 9140, Boulder, CO 80301, USA.

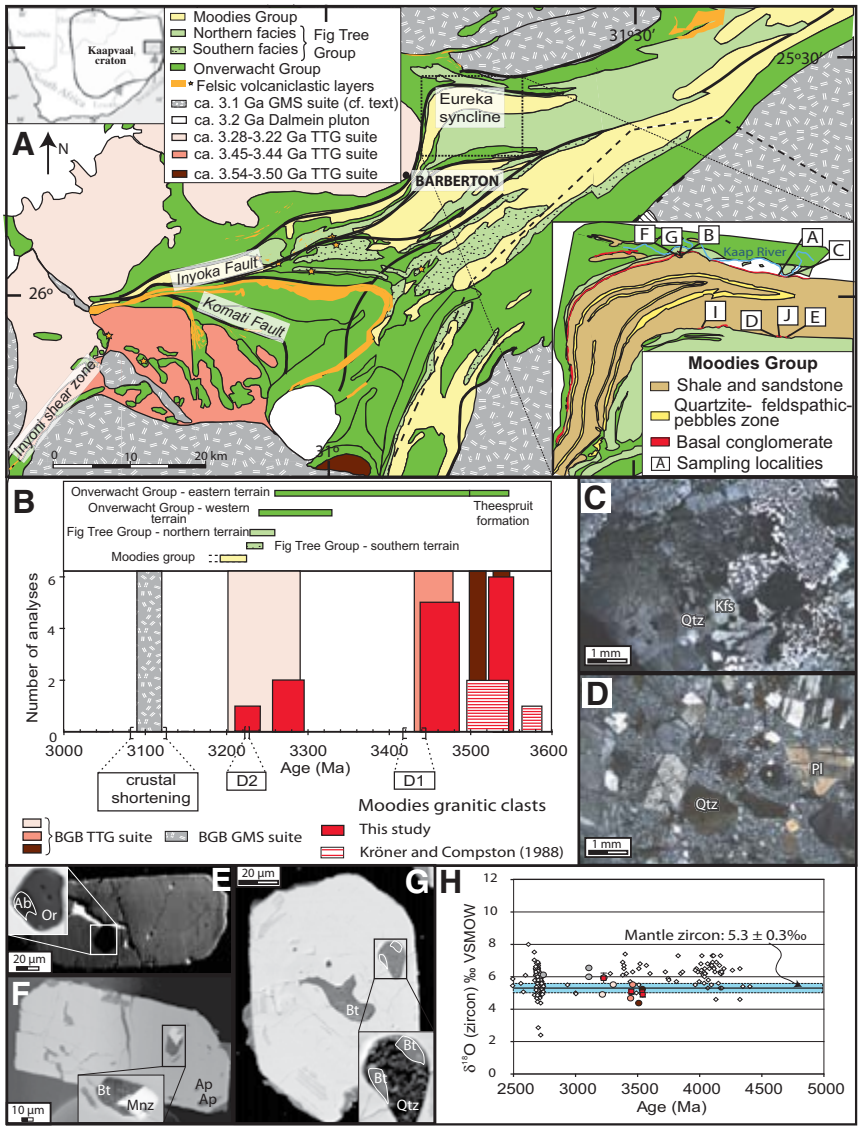

Figure 1. Summary of key geological information relevant to genesis of granitic clasts in Moodies Group basal conglomerate. A: Simplified geological map highlighting stratigraphy of Barberton Greenstone Belt (BGB), southern Africa, and ages of tonalite-trondhjemite-granodiorite (TTG) and younger granitic rocks. Felsic volcaniclastic layers similar to those from which granite clasts were possibly eroded are highlighted in orange. Average compositions for northern and southern facies of Fig Tree Group are provided in Table DR1 (see footnote 1). Inset is geological map of Eureka syncline with sample locations. B: Histogram representing crystallization age frequency in granitic clasts (this study; Kröner and Compston, 1988) (2σ age uncertainty). Only data from clasts where crystallization age is unambiguous have been included. Major tectonic events affecting BGB are represented along age axis. D1 event has been proposed to record processes within an active oceanic arc margin (de Ronde and de Wit, 1994; de Wit et al., 1992; Lowe, 1999); D2 event represents terrain amalgamation during accretionary orogeny. The 3126–3084 Ma event likely represents transcurrent shearing in an intraplate compressional context (de Ronde and de Wit, 1994) accompanied by substantial mantle heat addition to base of crust and widespread granitic magmatism, represented mostly by granodiorite-monzogranite-syenogranite (GMS) suite. C: Crossed-polarized light (CPL) image of typical mineral texture in representative sample of medium-grained micrographic granite (C33). Rock is characterized by micrographic K-feldspar (Kfs) and quartz (Qtz) intergrowths. These are interpreted to represent quench crystallization products. D: Typical mineral textures (in CPL) from representative rhyolitic clast (B25). This rock is quartz–K-feldspar–plagioclase–phyric rhyolite with rounded quartz phenocrysts, abundant large euhedral K-feldspar phenocrysts, and smaller euhedral plagioclase (Pl) phenocrysts. Matrix consists of fine-grained quartz, K-feldspar, and muscovite interpreted to represent recrystallized glass. E: Cathodoluminescence image of zircon (C30-Zr6) with plagioclase (albite, Ab) (An_1-Ab_{94}-Or_5; An—anorthite; Or—orthoclase) and K-feldspar (Or) inclusions (Ab_2-Or_{98}) crosscutting magmatic zoning. F: Scanning electron microscope (SEM) image of zircon (B17-Zr6) with monazite (Mnz), biotite (Bt), and apatite (Ap) inclusions. G: SEM image of zircon (C14-Zr4) with polymineralic quartz-biotite-plagioclase inclusions. H: Evolution of $\delta^{18}O$ (‰; VSMOW—Vienna standard mean ocean water) in zircons from Moodies granites as function of time, compared to those from BGB TTGs (King, 2001) and other Archean granitoids (white diamonds). Legend is identical to that in D.

zoned crystals. (Table DR3; Figs. 1E–1G). The inclusion suite is considered to reflect the assemblage present in the magma during zircon crystallization. Polymineralic quartz-feldspar-mica inclusions are interpreted to represent former melt inclusions.

SHRIMP U/Pb dating of zircons from 22 clasts was undertaken at ANU (Table DR4). No inherited cores were identified in cathodoluminescence images of the zircons (Fig. DR1). The data and ages are plotted on representative concordia diagrams (Fig. DR1); the upper intercept dates are interpreted as crystallization ages. A subset of the ages obtained is consistent with the single-zircon evaporation ages (3570 ± 6 Ma to 3474 ± 35 Ma) of Kröner and Compston (1988). In addition, the ages obtained in this study cluster in three groups that were not identified in previous works: 3519–3554 Ma, 3438–3486 Ma, and 3210–3295 Ma (Fig. 1B). There is no correlation between age group and clast rock type (e.g., crystal tuff, granite, rhyolite); however, these age ranges correlate perfectly with periods of TTG magmatism in the BGB (Fig. 1B).

DISCUSSION

The key characteristic of these granites is their low CaO content, coupled with their high $Na_2O + K_2O$, which could either be a primary magmatic feature or due to postcrystallization alteration. However, several lines of evidence argue in favor of the preservation of the primary magmatic chemical and mineralogical characteristics in the granites. (1) Alkali feldspar and quartz are significantly more abundant than plagioclase as single mineral inclusions within zircon. This is consistent with zircon crystallization from a low CaO magma, as plagioclase would commonly be the first tectosilicate to crystallize in peraluminous magmas with average CaO contents (e.g., Clemens and Wall, 1981). (2) Where plagioclase inclusions in

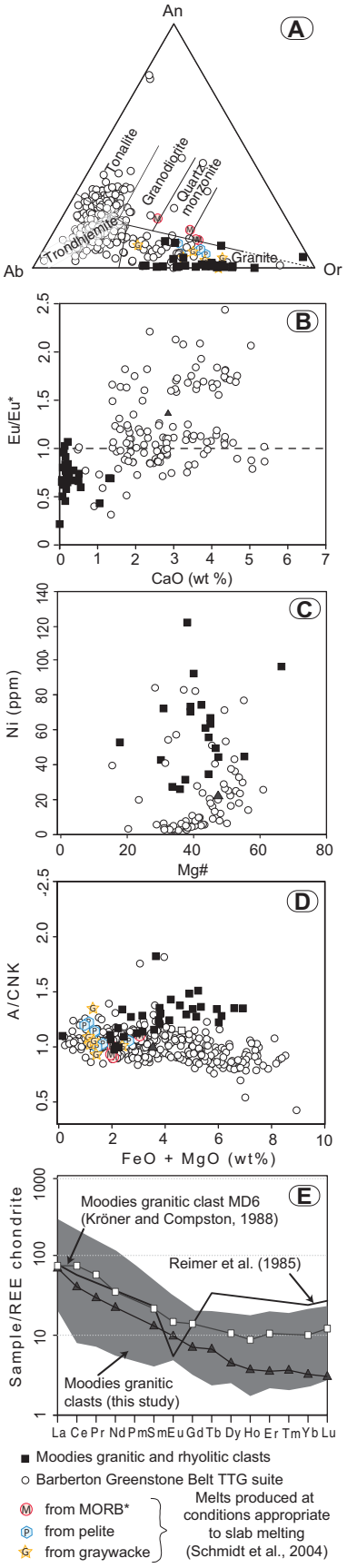

Figure 2. Summary of pertinent geochemical features of granitic clasts compared to Barberton Greenstone Belt (BGB) tonalite-trondhjemite-granodiorite (TTG). Experimental melt compositions from Schmidt et al. (2004) are also plotted for reference. A: Feldspar ternary diagram showing K-rich and CaO-poor nature of clasts compared to dominant TTG suite. B: Eu/Eu* versus CaO (excluding three outliers included in Table DR1; see footnote 1). C: Ni versus Mg# plot highlighting high Ni content of clasts relative to TTG. D: Maficity versus A/CNK [molecular Al/(Ca + Na + K)] plot (excluding two outliers) demonstrating that clasts are peraluminous and that A/CNK is positively correlated with maficity. E: Rare earth element (REE) plot showing that average of BGB TTG (gray triangle) is more depleted in heavy REEs than are the granites of the Moodies Group (gray field). Strong Eu anomaly found in study by Reimer et al. (1985) has proved impossible to duplicate in this study or in study by Kröner and Compston (1988) (as shown by MD6 sample). MORB—mid-oceanic ridge basalt.

zircon do exist (3 have been confirmed in >300 inclusions investigated), their composition is albitic, with An_{15} being the most Ca-rich plagioclase recorded (Table DR3). In contrast, the first plagioclase to crystallize in typical S-type granites would be $An_{40–50}$ (e.g., Clemens and Wall, 1984). (3) The primary magmatic character of the clasts is also supported by the fact that, in the most Ca-rich rocks, plagioclase occasionally displays magmatic oscillatory zoning of Ca content. (4) CaO-poor samples that have the lowest A/CNK values (≤1.1) contain monazite as both a matrix accessory mineral and as inclusions in zircon. Addition of even minor amounts of CaO to these magmas would have resulted in an insufficiently peraluminous composition unable to support monazite stability (Montel, 1993).

All this evidence supports the conclusion that the low CaO character of the clasts is not due to postcrystallization alteration, but is a primary magmatic feature. Consequently, these rocks represent an as-yet undocumented variety of low-CaO peraluminous granite.

The contemporaneous formation of granitic and TTG magmas in the BGB may indicate a petrogenetic link between the two magmas types. In such a scenario, the high K_2O and very low CaO contents of the granitic magma (Fig. 2A) can only be potentially accounted for if they represent either residual liquids from TTG fractional crystallization or liquids produced by low-degree partial melting of a TTG source. Both options would require separation of the magma from essentially all of the plagioclase in the system, which is inconsistent with the lack of significant negative Eu anomaly in the granites (Fig. 2B). Removal of almost all the CaO in the system by Ca-rich ferromagnesian minerals is similarly unlikely, as the Cr and Ni contents of the granites are high (typically as high as the highest TTGs for Cr and as much as four times higher for Ni), and neither clinopyroxene nor amphibole are likely to be stable in the peraluminous and K-rich magma compositions documented here.

Thus, the perfect correlation between the crystallization ages of the TTG plutons and those of these granitic magmas results from the concurrent partial melting of different sources, most likely as a consequence of the same geodynamic process.

The granites documented here share many characteristics with granites generated through anatexis of metasedimentary rocks, including the positive correlation between A/CNK and maficity (Fig. 2D), the K/Na range and variability, the Mg# range, and the close positive correlation between Fe + Mg and Ti. However, they also differ from typical S-types granites by their exceptionally low CaO contents, suggesting that they may represent a uniquely Archean type of magma formed via a unique petrogenetic process. The decoupling between low CaO concentrations and high Sr and Eu values demands a source that contains significant CaO, yet undergoes melting via a mechanism that keeps CaO in the residuum without producing a strong negative Eu anomaly; more specifically, the source has to be an originally plagioclase-rich sediment that melted at a pressure in excess of the plagioclase stability field. High-pressure melting is also supported by their negative Ti anomaly, and their high Zr/Sm and low Nb/Ta ratios, reflecting the presence of residual rutile during melting (John et al., 2010), i.e., at pressures >1.5 GPa at 850 °C (e.g., Patiño Douce and Johnston, 1991). The Ni and Cr contents of the granites are substantially higher than those of S-type granites, indicating the enrichment of these elements in the source. In addition, the average Rb contents of the granites are relatively low but within the range displayed by S-type granites, interpreted to reflect the low Rb content of the source. The $\delta^{18}O$ values of the zircon crystallized from the granites are similar to those of the zircon formed in TTG rocks of the same age (King, 2001). This precludes a significant volume of high $\delta^{18}O$ clay minerals in the source protolith. This is not inconsistent with the peraluminous character of the rocks, as this simply reflects the melting of biotite and does not require a clay-bearing source.

Collectively, this information indicates that the granitic magmas were generated at pressures in excess of plagioclase stability, by low-degree partial melting of an Rb-poor, Ni- and Cr-rich, quartz + mica–bearing source, the protolith of which was plagioclase rich before eclogite facies metamorphism. This leads us to propose an eclogite facies metagraywacke source

derived from relatively unweathered TTG material or from felsic to intermediate volcaniclastic rocks. In both cases, a component of mafic and/or ultramafic greenstone material is required to account for the Ni and Cr values.

Little relevant experimental information exists on the melting of eclogite facies K-rich sources. However, an investigation at 3–5 GPa by Schmidt et al. (2004) showed that, under high-pressure conditions, phengite is the stable K_2O-bearing phase in both mafic and metasedimentary sources. When the experiments are conducted sufficiently close to the phengite solidus (i.e., before significant contributions to the melt from garnet- or clinopyroxene-consuming reactions), the melt compositions produced from the metagraywacke source are similar to those of the granites described in this study (e.g., Table DR1; Fig. 2A), and are consistent with the minimum temperature estimate of magma formation calculated from the zircon saturation temperatures of ~855 °C (Baker et al., 2002) (Table DR1).

CONCLUSIONS

Granitic (sensu stricto) magmatism occurred concurrently with each of the three episodes of TTG magmatism in the BGB. However, the granites and the TTGs are not genetically related, and formed via the synchronous melting of contrasting sources. The same high-pressure conditions of anatexis required by the TTG geochemical characteristics are also required to account for the chemistry of the granites. Consequently, we conclude that the peraluminous granite magmas were generated by high-pressure (in excess of plagioclase stability) anatexis of a phengite-bearing metagraywacke. They thus represent a potentially uniquely Archean variety of S-type granite that formed as a consequence of sedimentary rocks being dragged down the subduction channel and melting at pressures probably >2 GPa. The very low CaO signature documented in this study, in conjunction with the Sr and SiO_2 contents of the rocks, suggests a unique type of magma that has not previously been reported in the Archean rock record. This signature appears to be restricted to the Paleoarchean and Mesoarchean, reflecting the interaction of subducting or foundering crust with a hotter mantle than has existed subsequently on Earth. In essence, these rocks could be an early Earth equivalent of S-type granites. In the BGB this Paleoarchean and Mesoarchean granitic magmatism appears to have produced only eruptive and high-level plutonic rocks; it does not appear to have produced plutons at the mid-crustal levels at which many TTG plutons have intruded. Such superficially emplaced rocks would be vulnerable to erosion, thus accounting for their lack of preservation. The southern facies of the predominantly volcaniclastic Fig Tree Group (Fig. 1A; Table DR1) is characterized by very low average CaO (0.05 wt%) and high K_2O (3.98 wt%) contents. This is much more consistent with this volcano-sedimentary succession having been derived from the granite magmatism described herein than by eruptive TTG magmas. Thus, we suggest that potassic granitic magmatism contributed fundamentally to the development of the BGB rock record. The Moodies Group granitic clasts, by virtue of the fact that only fresh material would have survived to be deposited as clasts, provided us with the opportunity to make these unique insights.

ACKNOWLEDGMENTS

Stevens acknowledges National Research Foundation (NRF, South Africa) funding through the SARChI program. Stevens, Moyen, and Martin acknowledge joint Centre National de la Recherche Scientifique and NRF funding. We thank J. Clemens, M. de Wit, B. Schoene, D. Champion, A. Patiño-Douce, and W. Collins for their very helpful reviews of earlier versions of the manuscript.

REFERENCES CITED

Baker, D.R., Conte, A.M., Freda, C., and Ottolini, L., 2002, The effects of halogens on Zr diffusion and zircon dissolution in hydrous metaluminous granitic melts: Contributions to Mineralogy and Petrology, v. 142, p. 666–678, doi:10.1007/s00410-001-0328-3.

Clemens, J.D., and Wall, V.J., 1981, Crystallization and origin of some peraluminous (S-type) granitic magmas: Canadian Mineralogist, v. 19, p. 111–131.

Clemens, J.D., and Wall, V.J., 1984, Origin and evolution of a peraluminous silicic ignimbrite suite: The Violet Town Volcanics: Contributions to Mineralogy and Petrology, v. 88, p. 354–371, doi:10.1007/BF00376761.

de Ronde, C.E.J., and de Wit, M.J., 1994, Tectonic history of the Barberton greenstone belt, South Africa: 490 million years of Archean crustal evolution: Tectonics, v. 13, p. 983–1005, doi:10.1029/94TC00353.

de Wit, M.J., Roering, C., Hart, R.J., Armstrong, R.A., de Ronde, C.E.J., Green, R.W.E., Tredoux, M., Peberdy, E., and Hart, R.A., 1992, Formation of an Archaean continent: Nature, v. 357, p. 553–562, doi:10.1038/357553a0.

Foley, S., Tiepolo, M., and Vannucci, R., 2002, Growth of early continental crust controlled by melting of amphibolite in subduction zones: Nature, v. 417, p. 837–840, doi:10.1038/nature00799.

John, T., Klemd, R., Klemme, S., Pfänder, J.A., Hoffmann, J.E., and Gao, J., 2010, Nb-Ta fractionation by partial melting at the titanite–rutile transition: Contributions to Mineralogy and Petrology, v. 161, p. 35–45, doi:10.1007/s00410-010-0520-4.

Kamo, S.L., and Davis, D.W., 1994, Reassessment of Archean crustal development in the Barberton Mountain Land, South Africa, based on U-Pb dating: Tectonics, v. 13, p. 167–192, doi:10.1029/93TC02254.

King, E.M., 2001, Oxygen isotope study of magmatic source and alteration of granitic rocks in the western United States and the Superior Province, Canada [Ph.D. thesis]: Madison, University of Wisconsin, 224 p.

Kisters, A.F.M., Belcher, R.W., Poujol, M., and Dziggel, A., 2010, Continental growth and convergence-related arc plutonism in the Mesoarchaean: Evidence from the Barberton granitoid-greenstone terrain, South Africa: Precambrian Research, v. 178, p. 15–26, doi:10.1016/j.precamres.2010.01.002.

Kröner, A., and Compston, W., 1988, Ion microprobe ages of zircons from early Archaean granite pebbles and greywacke, Barberton greenstone belt, southern Africa: Precambrian Research, v. 38, p. 367–380, doi:10.1016/0301-9268(88)90034-4.

Lana, C., Tohver, E., and Cawood, P., 2010, Quantifying rates of dome-and-keel formation in the Barberton granitoid-greenstone belt, South Africa: Precambrian Research, v. 177, p. 199–211, doi:10.1016/j.precamres.2009.12.001.

Lowe, D.R., 1994, Accretionary history of the Archean Barberton Greenstone Belt (3.55–3.22 Ga), southern Africa: Geology, v. 22, p. 1099–1102, doi:10.1130/0091-7613(1994)022<1099:AHOTAB>2.3.CO;2.

Lowe, D.R., 1999, Geologic evolution of the Barberton greenstone belt and vicinity, *in* Lowe, D.R., and Byerly, G.R., eds., Geologic evolution of the Barberton greenstone belt, South Africa: Geological Society of America Special Paper 329, p. 287–213, doi:10.1130/0-8137-2329-9.287.

Martin, H., 1986, Effect of steeper Archean geothermal gradient on geochemistry of subduction-zone magmas: Geology, v. 14, p. 753–756, doi:10.1130/0091-7613(1986)14<753:EOSAGG>2.0.CO;2.

Montel, J.-M., 1993, A model for monazite/melt equilibrium and application to the generation of granitic magmas: Chemical Geology, v. 110, p. 127–146, doi:10.1016/0009-2541(93)90250-M.

Moyen, J.-F., Stevens, G., and Kisters, A., 2006, Record of mid-Archaean subduction from metamorphism in the Barberton terrain, South Africa: Nature, v. 442, p. 559–562, doi:10.1038/nature04972.

Patiño Douce, A.E., and Johnston, A.D., 1991, Phase equilibria and melt productivity in the pelitic system: Implications for the origin of peraluminous granitoids and aluminous granulites: Contributions to Mineralogy and Petrology, v. 107, p. 202–218, doi:10.1007/BF00310707.

Rapp, R.P., Shimizu, N., and Norman, M.D., 2003, Growth of early continental crust by partial melting of eclogite: Nature, v. 425, p. 605–609, doi:10.1038/nature02031.

Reimer, O., Condie, K.C., Schneider, G., and Georgia, A., 1985, Petrography and geochemistry of granitoid and metamorphite pebbles from the early Archaean Moodies Group, Barberton Mountainland/South Africa: Precambrian Research, v. 29, p. 383–404, doi:10.1016/0301-9268(85)90044-0.

Schmidt, M.W., Vielzeuf, D., and Auzanneau, E., 2004, Melting and dissolution of subducting crust at high pressures: The key role of white mica: Earth and Planetary Science Letters, v. 228, p. 65–84, doi:10.1016/j.epsl.2004.09.020.

Schoene, B., and Bowring, S.A., 2010, Rates and mechanisms of Mesoarchean magmatic arc construction, eastern Kaapvaal craton, Swaziland: Geological Society of America Bulletin, v. 122, p. 408–429, doi:10.1130/B26501.1.

Schoene, B., de Wit, M.J., and Bowring, S.A., 2008, Mesoarchean assembly and stabilization of the eastern Kaapvaal craton: A structural-thermochronological perspective: Tectonics, v. 27, TC5010, doi:10.1029/2008TC002267.

Manuscript received 22 February 2011
Revised manuscript received 10 May 2011
Manuscript accepted 16 May 2011

Printed in USA

Chapter 3: Presentation of the publication

This paper submitted to Journal of Petrology, is first-authored by Miss Sanchez-Garrido Cynthia. It describes in greater detail the chemistry and petrography of the Meso- and Paleo-Archean granites (only preserved as clasts in the Moodies group) that were the object of the previous paper in Geology. It also describes the chemistry and petrography of felsic schists located in the Barberton Greenstone Belt. This paper evaluates the possibility of a genetic link between the felsic layers within the Theespruit formation and the granites. This works also aim to constraint in detail the petrogenesis of the studied granites, as well as to determine if the clasts are representative of the whole magmatic system. Finally, this paper discusses the consequences that early Archean potassic rich granitic magmatism had on the Archean sedimentary record and on the genesis of the early Earth continental crust melting conditions at the source. All calculations and data acquisitions (except oxygen isotopic composition and for the Theespruit schists) were lead by Miss Cynthia Sanchez-Garrido under the supervision of Professor Gary Stevens, Professor Hervé Martin, Professor Jean-François Moyen and Doctor Régis Doucelance. Oxygen isotopic composition of the quartz and feldspars grains were analysed by Prof. Chris Harris (UCT). All samples preparations (zircons, whole rock XRF, whole rock LA-ICP MS) were done by Miss Sanchez-Garrido. All acquisition of mineral chemistry of the Moodies granites and their zircons, by SEM, was done by Miss Sanchez-Garrido. Mineral chemistry of the Moodies conglomerate biotite present in the matrix of the conglomerate was done by Miss Justine Jaguin. Sampling of the Moodies granites, of the matrix of the conglomerate of the Moodies Group was effectuated by Miss Sanchez-Garrido and Professor Gary Stevens. Sampling of the Barberton TTG was effectuated by Miss Sanchez-Garrido and Professor Jean-Francois Moyen. Sampling of the felsic schists from the Theespruit formation was done by Professor Jean-Francois Moyen and Lauren K. Andrews. Acquisition of the trace and REE of the Moodies granites whole rock, done by LA-ICP MS was done equitably between Miss Sanchez-Garrido, Doctor Cristiano Lana and Ms. Riana Rossow.

Granitic contributions to the construction of the Paleo-Archean continental crust: Insights from three generations (3.55, 3.45 and 3.23 Ga) of low-Ca rhyolites/granites in the Barberton Granite Greenstone Terrane

Sanchez-Garrido, C.J.M.G[a, b, c, d], Stevens, G.[a], Harris, C.[e], Moyen, J-F.[f, b, c], Martin, H.[b, c, d], Doucelance, R.[b, c, d]

[a] Center for Crustal Petrology, Department of Earth Sciences, University of Stellenbosch, South Africa Private Bag X-1, Matieland 7602, South Africa

[b] Clermont Université, Université Blaise Pascal, Laboratoire Magmas et Volcans, BP 10448, F-63000 Clermont-Ferrand, France

[c] CNRS, UMR 6524, LMV, F-63038 Clermont-Ferrand, France

[d] IRD, R 163, LMV, F-63038 Clermont-Ferrand, France

[e] Department of Geological Sciences, University of Cape Town, Rondebosch 7701, South Africa

[f] Université Jean-Monnet, Laboratoire Magmas et Volcans, Département de Géologie 23 rue du Docteur Michelon, 42023 Saint Etienne, France

Keywords: *Paleo-Archean granites; Kaapvaal Craton, Theespruit felsic schists, oxygen isotope.*

1. Abstract

The preserved Archean felsic crust consists predominantly of sodic granitoids that typically emplaced early in the history of the cratons, within which these rocks have come to constitute part of the continental crust. These rocks are part of the tonalite-trondhjemite-granodiorite (TTG) suite and a significant fraction of these rocks formed via partial melting of hydrated meta-mafic rocks at pressures above the garnet stability field in mafic source rocks. In contrast, (potassic) granites usually appear later and commonly mark the onset of craton stabilisation. These rocks are believed to form by partial melting of pre-existing felsic crust at lower pressure than the TTG magmas. Felsic, potassium-rich volcanic/volcaniclastic rocks present in Archean greenstone sequences are usually viewed as the K-metasomatised volcanic equivalents of the TTG plutons, or as the products of anatectic recycling of TTG crust. In this study, we describe unusual paleo- to Meso-Archean granites present only as clasts in the Barberton Greenstone Belt (BGB), in the Moodies Group, and in-situ felsic potassium-rich schists located in the Theespruit formation (BGB) that both challenge the above statements. Both rock types are characterised by low-CaO and high-K_2O content that we prove are primary magmatic signatures. The granitic clasts presented here were produced during 3 magmatic episodes, concurrently with the formation of TTG magmas. The clasts are relatively unaltered granites and

rhyolites that share many characteristics with S-type granites e.g. they are peraluminous, leucocratic granites with flat heavy rare earth element patterns. Petrogenetic modelling suggests that the unique low-CaO, K_2O-rich and peraluminous character of the granites is a consequence of partial melting of coarse clastic sedimentary source under eclogite facies conditions. Lastly the comparison of the granitic clasts with the concurrent in-situ felsic volcanic layers illustrates that the clasts may have come from similar material which highlights the fact that felsic layers in the Archean are not always genetically linked to the TTG but that they may represent a granitic fraction of the early Archean continental crust which was probably eroded due to intense weathering condition at that time.

2. INTRODUCTION

Most of Earth's Archean felsic crust is TTG-like (Tonalite-Trondhjemite-Granodiorite) in composition (Condie, 1993). Consequently, investigations into the origin of the continental crust have focussed on the processes by which these TTG magmas arose. The acronym "TTG" is now used to describe rocks significantly distinct from the original definition (Jahn et al. 1981; Martin, 1987) which referred to juvenile magmatic rocks. In general TTG are sodic granitoids, they are rich in SiO_2 > 65 wt%, most are metaluminous with some being slightly peraluminous, their Mg# varies mostly between 30 and 40, their LILE content is low and they have relatively high aluminium contents. The recent study by Moyen (2011) shows that TTGs can be divided in 3 subseries that form part of a continuous evolution from a "high" to a "low" pressure group. The most common, high-Al type TTG (also describe as the "high" pressure type, Moyen (2011)) has trace element similarities with typical "arc"-like rocks: the TTG have negative Nb-Ta and Ti anomalies, and positive Pb anomalies. They have high Sr and Eu and low Yb and Y content, with high Sr/Y ratio. These TTG show highly fractionated REE patterns with strong depletion in HREE but no pronounced Eu anomaly. Moyen (2011) showed that these rocks represent several types of magmas, some 20 % of which almost certainly formed via recycling of older TTGs. However, in general, most TTGs are considered to have formed via the partial melting of hydrated metamafic rocks and probably represent magmas generated via partial melting under a range of source P-T conditions (Martin and Moyen, 2002; Moyen, 2011). In these TTGs, strong HREE depletion is accounted for by the presence of residual garnet, typically in excess of 20% during melting of a mafic source (e.g. Barker and Arth, 1976; Tarney et al., 1979; Condie, 1981; Martin, 1986; Rapp et al., 1991; Nair and Chacko, 2008). The latter can only be achieved at pressures in excess of 15 kbar (Martin, 1986, Moyen and Stevens, 2006). This is in support of arguments which suggest that the high Sr and low ($CaO+Na_2O$) content of TTGs reflects

melting of the source at pressures above the plagioclase stability field (Martin and Moyen, 2002) and that their relative Nb depletion (Foley et al., 2002; Rapp et al. 2003), requires pressures of partial melting to be in the rutile stability field. It has also been proposed that, in suitably fertile, hydrated source rocks, such pressures of melting can only be attained in subduction zones (Martin, 1986; Prouteau et al., 1999). In addition, Martin and Moyen (2002) proposed that the resultant TTG magmas may subsequently have reacted with mantle peridotite, in order to account for the relatively high Mg#, Ni and Cr contents of these rocks, implying that the TTG source was overlain by a mantle wedge. Such geometry could easily have been realised in a subduction zone environment. Consequently, there is a reasonably well established framework for understanding the origin of the TTG crust that includes consideration of the possible geodynamic settings of magma production. In contrast, the genesis of a subordinate fraction of granites and granodiorites emplaced within the same pre-cratonization time period, and general environment as the TTGs, has been less studied and consequently is less well understood. However, there may be good reason to consider the production of other granite varieties as a consequence of process similar to that which produced TTG-type magmas. Sanchez-Garrido et al. (2011) recently described K_2O-rich, peraluminous granites from the Barberton Greenstone Belt (BGB) of South Africa that appear to be related, in space and time, with TTG generation. Three episodes of granitic (senso stricto) magmatism took place periodically through the Paleo and Meso-Archean in the BGB, with age clusters at 3.55, 3.45 and 3.23 Ga, which coincided with the ages of TTG emplacement in this area. The granitic rocks occur as clasts of volcaniclastic material, rhyolite and hypabyssal granite from the ca 3.20 Ga-old basal conglomerate of the Moodies group (Figure 1b). Sanchez-Garrido et al. (2011) have argued that the low-CaO content of these magmas, combined with the absence of a significant negative Eu anomaly, high-Ni content and high Mg# of the clasts, preclude their derivation from either recycling of an older TTG-like source, or fractional crystallisation from TTG magma. Consequently, it has been proposed that the temporal and spatial link that exists between these granites and the TTGs resulted from their derivation from different sources within the same general geodynamic setting. Moreover, within the BGB, felsic rocks of volcanic and volcaniclastic origin exist that potentially represent equivalents of the material from which the Moodies granitic clasts were eroded. These felsic rocks occur as 3.548-3.544 Ga-old (Van Kranendonk et al., 2009) felsic volcaniclastic layers within the Theespruit formation (Kröner et al., 1996); as 3.457-3.416 Ga-old felsic lavas within the H6 layer of the Hooggenoeg formation of the middle-to-upper Onverwacht Group (Kröner et al., 1991; Byerly et al., 1996; Byerly et al., 2002); as 3.298-3.258 Ga-old volcaniclastic and tuffaceous layers within the Mendon formation (Byerly et al., 1996) and as 3.255-3.227 Ga-old felsic volcanic layers of the Mapepe formation in the Fig Tree Group (Kröner et al., 1991; Byerly et al., 1996). As these ages correspond with the three episodes of TTG emplacement, some of the felsic layers have been interpreted to represent

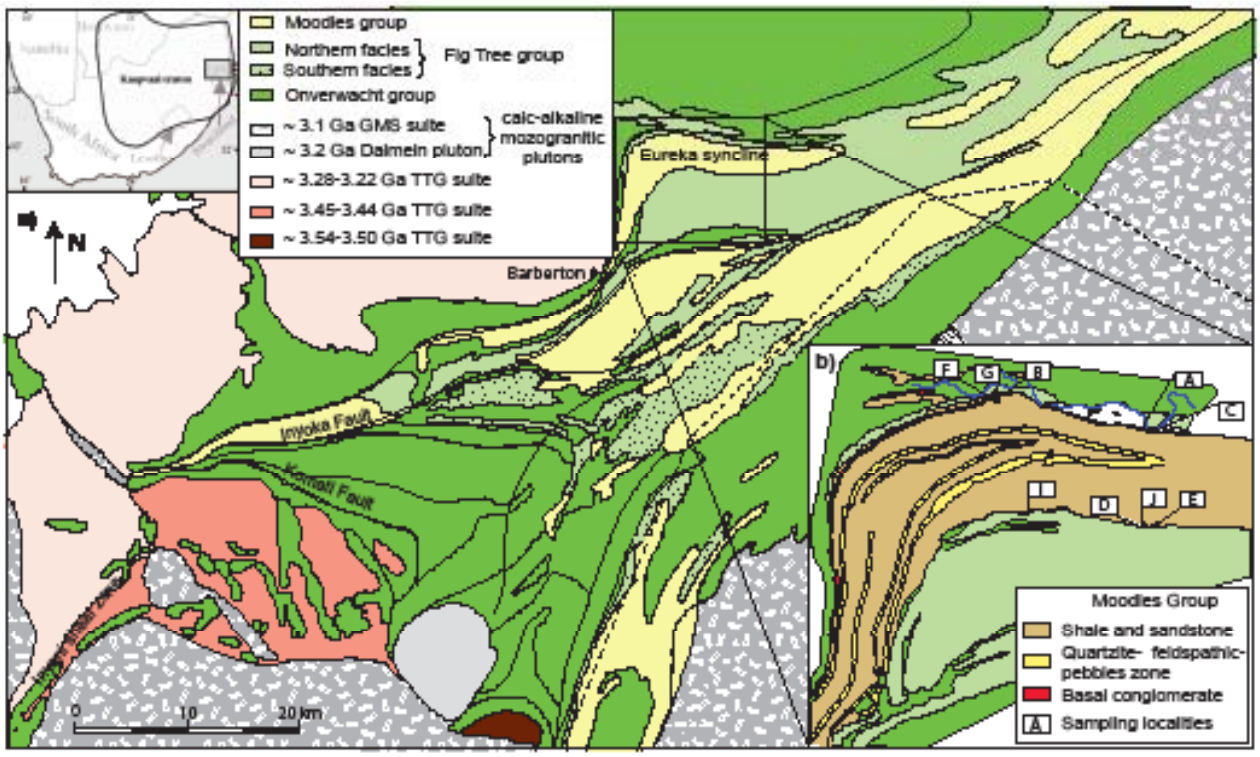

Figure 1. Simplified geological map of the Barberton Greenstone Belt (BGB), highlighting the stratigraphy of the BGB and the ages of the TTGs and younger granitic rocks. The rocks to the south of the Komati Fault have been metamorphosed to amphibolite facies grades as a result of 3230 Ma orogeny, including potassic and felsic volcaniclastic sediments of the Fig Tree Group. The inset represents a detailed geological map of the Eureka Syncline indicating the sample locations of Moodies granites**.**

the K_2O-metasomatised, eruptive equivalents of the TTG plutons (Kröner et al., 1996; de Wit et al., 1987). However, these rocks also generally overlap in age with the granites and rhyolites documented by Sanchez-Garrido et al (2011). Additionally, recent work by Diergaardt et al. (in preparation) has demonstrated the primary magmatic origin of the high K_2O content of feldspar within a substantial fraction of the potassium feldspar phenocrysts in the felsic volcanic/volcaniclastic layers. Thus, the purpose of this paper is to examine in detail the geochemistry and petrogenesis of the low-Ca potassic magmatic rocks (both plutonic and volcanic) described by Sanchez-Garrido et al. (2011), and to understand the implications of their genesis for the development of the Barberton Greenstone Belt. As the studied rocks include only volcanic/granitic clasts from the Moodies conglomerate, it is possible that this reflects a non-representative composition, preserved by virtue of its robustness during weathering and sedimentary transport. The identification of areas within the greenstone belt where rocks of similar composition can be studied in situ would expand the range of material on which conclusions about the origin of early felsic granitic crust in the BGB can be based. Thus, in this study we compare 107 samples of the plutonic and volcanic Moodies clasts (including the samples reported by Sanchez-Garrido et al., 2011) with 36 samples of the ca. 3.55 Ga felsic volcaniclastic layers from the Theespruit Formation (Onverwacht Group) (Figure 1a), in

order to identify a possible genetic link between the two rock types. This work focuses on the detailed mechanism of genesis of the Moodies granites and rhyolite and aims the processes that create the temporal link with the coeval TTG.

3. GEOLOGICAL SETTING

The Barberton Granite Greenstone Terrane (BGGT) is located in the south-eastern domain of the Kaapvaal craton (South Africa), it is comprised of the supracrustal rocks of the Barberton Greenstone Belt (BGB), three generations of TTG plutons which were emplaced at ca. 3.550, ca. 3.445 and ca. 3.225 Ga (Figure 1), and voluminous sheet-like batholiths of younger 3.14-3.10 Ga potassium rich granitoids. Most of these TTG belong to the high Al-TTGs (Moyen, 2011). They have been divided into two sub-series: (1) the high-pressure, relatively low-temperature type, which includes leucocratic trondhjemites with a high Sr content (due to melting above the pressure at which plagioclase is a stable phase); (2) and the lower-pressure, relatively higher-temperature type, which includes a wider range of rock-types with a low Sr content (Moyen et al., 2007). These two types of TTG probably arose in different geodynamic environment. The high-Sr, high-pressure type (emplaced at 3.45 Ga) were presumably generated at depth, possibly in a subduction setting; whereas the low-Sr, hence shallower types of TTG (emplaced at 3.55-3.50 Ga and 3.29-3.24 Ga) suggest formation at the base of a thickened crust (Moyen et al, 2007) or in flatter subduction environment (Martin and Moyen, 2002).

The younger, relatively potassic batholiths that are part of the Granodiorite-Monzogranite and Syenite (GMS) suite, began to intrude the BGB at ca. 3.203 ± 0.007 Ga (Lana et al., 2010) with the emplacement of the Dalmein pluton (Figure 1) in an intra-cratonic compressive tectonic regime (Belcher and Kisters, 2006), and was followed by the continuous emplacement between 3.14-3.10 Ga granitoids (e.g. Schoene and Bowring 2007) which consolidated and stabilised the Kaapvaal Craton.

The supracrustal rocks of the BGB form the Swaziland Supergroup, which ranges in age from ca. 3.550 Ga to ca. 3.210 Ga. This Supergroup is comprised of three stratigraphic units, which are from the bottom to the top: the Onverwacht Group, Fig Tree Group and Moodies Group. The Onverwacht Group is interpreted to have been deposited in a deep to shallow marine environment between 3.550 and 3.250 Ga (Lowe and Byerly, 2007; Lowe, 1982), and consists of metamorphosed ultramafic lavas (e.g. komatiites, komatiitic basalts) and mafic lavas (tholeiites), with minor felsic volcanic (dacitic to rhyolitic calc-alkaline) and sedimentary material. The felsic volcaniclastic schists and breccias of the Onverwacht group are mainly localised in the Theespruit and Hooggenoeg formations (H6 layer), and have yielded ages of 3.548-3.511 Ga (Armstrong et al. 1990, Kröner et al.,1996) and 3.445-3.438 Ga (Lowe and Byerly, 2007) respectively. The Fig Tree Group, dated at 3.260–3.223 Ga (Kröner et al., 1991; Byerly et al., 1996), conformably overlies the Onverwacht Group. This group is rich in felsic volcanic and volcaniclastic material (mostly plagioclase-phyric dacite, located in the Mapepe and Bien Venue formations) as well as greywackes,

shales, minor banded iron formation (BIF), turbidites, cherts and conglomeratic units. The Fig Tree Group is interpreted to have been deposited in a deep (north of the Inyoka fault) to shallow (south of the Inyoka fault) marine environments. The Moodies Group, which represents the youngest stratigraphic unit (3.225-3.109 Ga) (Kamo and Davis, 1994; Lowe, 1999), unconformably overlies the Fig Tree Group. It consists of coarse-grained clastic sediments dominated by interbedded polymict conglomerates, thick arkosic units, lithic and/or quartz-rich sandstones, and minor shales, siltstones, jaspilite and BIF. The Moodies Group is interpreted to represent a range of alluvial, fluvial tidal to shallow marine environments. The basal layer of the Moodies conglomerate is found in the Eureka syncline (Figure 1b), as well as in the central and southern part of the greenstone belt itself. In all cases it is polymict with a quartz-rich sandstone matrix. However, the quantity of pebbles and their composition varies from North to South (Heubeck and Lowe, 1994; Reimer, 1985). This coarse clastic sedimentary succession was deposited between 3.225-3.215 Ga (Kamo and Davis, 1994; Lowe, 1999) as a direct result of the destruction of topographic relief produced during the 3230 Ma collisional event (Heubeck and Lowe, 1994). Paleo-sedimentary studies performed by Heubeck and Lowe (1994, 1999) have described the differences between the northern and southern facies of the Moodies conglomerate. Based on bimodal paleocurrents directions and sedimentary structures representing tidal bedding features, they deduced that the source of the conglomerate was located to the North of the BGB. Hessler and Lowe (2006) reached the same conclusion.

The BGB was assembled during four main tectono-metamorphic events at ca. 3.55-3.49, 3.49-3.42, 3.255-3.225 and 3.203-3.07 Ga (Moyen et al, 2007). The main deformation event (D2) corresponds to the terrane accretion at ca. 3.23-3.21 Ga (de Ronde and de Wit, 1994, Lowe, 1994). The suture of the terrane accretion is localised along the Inyoni-Inyoka fault, which separate the Northern and Southern terranes. These terranes have different ages (for example, the Onverwacht formation in the Southern terrane is on average older (3.55-3.3 Ga) than the Northern one (3.3-3.25) (Lowe and Byerly, 2007).

All rocks in the BGB have been affected by metamorphism, with peak metamorphic conditions generally not exceeding lower greenschist facies conditions in the bulk of the belt (Cloete, 1991; Xie et al., 1997). However, amphibolite facies conditions have been documented along the margins of the BGB, adjacent to the granite-greenstone contacts, as well as in greenstone xenoliths preserved in the surrounding granitoids (Dziggel et al, 2002; Diener et al, 2005; Dziggel et al, 2006). The Moodies conglomerate in the Eureka syncline has been affected by greenschist facies metamorphic conditions, retrogressed to sub-greenschist facies (Dziggel et al., 2006). The metamorphic history of these rocks is therefore important to consider as it has a potential agent that could have modified the primary textures or chemistry of the rocks we are studying here.

In the Southern terrane, most studies have concentrated on the metamorphic history of the Theespruit formation schists. These

rocks underwent heterogeneous deformation and metamorphism during the emplacement of the Theespruit pluton at 3.445 Ga (Kamo and Davis, 1994), overprinted by peak metamorphism during the main D2 accretion event. The Theespruit schists next to the edges of the Theespruit pluton are at amphibolite metamorphic grade (de Wit et al., 2011). The metamorphic grade increases towards the margins of the pluton where contact metamorphism is recorded by andalusite-bearing assemblages (de Wit et al., 1983) and where the schists have been vertically deformed and display L-tectonite fabric (Kisters and Anhaeusser, 1995). The peak metamorphism of the Theespruit formation reached high-pressure amphibolite facies grades, with partial retrogression to greenschist-facies conditions during deformation associated with uplift (Diener et al., 2005; Dziggel et al., 2002). The fabric and peak metamorphism (680°C and 8-11 kbar, e.g. Dziggel et al., 2002) within the kyanite stability field, indicates burial and exhumation of the Steynsdorp terrane relative to the greenstone belt during D2 at ca. 3.229 Ga (Dziggel et al., 2002; Kisters et al., 2004; Diener et al., 2005).

In the Northern part, the terrane amalgamation was followed by the deposition of the Moodies group which was refolded during later stage of the orogeny. The Moodies group and the rest of the greenstone belt were affected by the 3.23 Ga metamorphic event (Stevens and Moyen, 2007). In the Northern margin of the BGB, the Eureka Syncline (which is composed essentially of Moodies rocks, including the granites and rhyolite discussed in this study) was affected by contact metamorphism related to the emplacement of the Stentor pluton. The shear zone which separates the Stentor pluton and the Eureka syncline mark also the separation between the high-grade mid-crustal basement gneiss and the lower grade greenstone belt (Dziggel et al., 2006). The rocks at the hanging wall of this contact are metamorphosed to upper greenschist facies whereas the rocks from the footwall are characterized by amphibolite facies minerals assemblage. The peak metamorphic conditions (600-700 °C and 5±1 kbar) are syntectonic and record the exhumation of the high-grade rocks, during the 3.23 collisional event, relative to the lower-grade rocks (Dziggel et al., 2006). Retrogression of the amphibolite facies into greenschist to sub-greenschist facies (<500 °C and 1-3 kbar) is a consequence of the late collisional orogenic extension that followed the terrane amalgamation (Dziggel et al., 2006).

4. PREVIOUS WORK ON THE MOODIES GRANITIC AND RHYOLITIC CLASTS AND THE FELSIC SCHISTS FROM THE THEESPRUIT FORMATION

Several studies have reported the unusual presence of granitic, metamorphic and volcaniclastic rock pebbles in the basal conglomeratic layer (Md6) of the Moodies Group that outcrops in the Eureka syncline (Reimer, 1985, Van Niekerk and Burger, 1978; Visser, 1956; Bell, 1967; Gay, 1969; Anhaeusser, 1969). Most of these studies have focussed on the age of the granites, although some have given some attention to the origin of their potassium-rich and calcium-poor signature and hypothesised on the nature of their source rocks.

Kröner and Compston (1988), Tegtmeyer and Kröner (1987) and Van Niekerk and Burger (1978) have investigated the U-Pb geochronology of the granitic/rhyolitic clasts. The findings of Tegtmeyer and Kröner (1987) and Van Niekerk and Burger (1978) are not discussed in detail here, as the subsequent study reanalysing the same material but using more accurate analytical tools (e.g. SHRIMP) by Kröner and Compston (1988), failed to confirm the ages published in the two earlier studies. Importantly, the work of Kröner and Compston (1988) indicates that the age of the Moodies granites in the basal conglomerate range between 3.518 and 3.570 Ga. More recently, Sanchez-Garrido et al. (2011) performed extensive SHRIMP U-Pb dating of zircons from the Moodies rhyolites/granites. Their ages cluster in 3 groups, interpreted to represent crystallization at 3.519-3.554, 3.438-3.486 and 3.210-3.295 Ga.

The latter study also demonstrated the magmatic origin of the K-rich and CaO-poor nature of the granites preserved in the Moodies granites, which is in agreement with the findings of the study of Tegtmeyer and Kröner (1987) that pertain to the origin of the chemical characteristics of the rocks. Two main lines of evidence from the Sanchez-Garrido et al (2011) study support this finding: 1. the silicate mineral inclusion suites within magmatic zircon crystals. Most of the silicate inclusions in zircon are alkali feldspar. In the rare instances where plagioclase inclusion occur they have An-poor compositions (the most calcic being An11), which demonstrates that the composition of the melt from which the plagioclase crystallize had an anorthite content lower than An11, therefore the magmas were CaO-poor. 2. K_2O is predominantly accommodated within potassium feldspars which are form a large proportion of the rock (ca. 30%). In most rocks K-feldspar is present as phenocrysts or in quartz-feldspar intergrowths with K-feldspar phenocrysts as their nuclei. The preservation of these delicate magmatic textures of quartz-K-feldspar intergrowths is a sign that the K-feldspar are magmatic and by deduction, because of the large amount of K-feldspar, the potassium-rich nature of the granites is magmatic.

Prior studies (e.g. Reimer, 1985) have proposed that the protolith of the Moodies granites resulted from partial melting of tonalitic to trondhjemitic gneisses similar to the low aluminium gneisses of the Ancient Gneiss Complex (AGC) in Swaziland. In contrast, the study of Sanchez-Garrido et al. (2011), demonstrated that the rhyolitic/granitic magmas cannot be linked to TTG by any magmatic process such as partial melting of a TTG source or fractional crystallisation from a magma of TTG composition. Indeed this study demonstrates that to achieve the very low CaO content of the granites from a magma of TTG composition, removal of a substantial fractionation of plagioclase is required with a strong Eu anomaly produced as a consequence. However, there is no correlation between the very low-CaO content of the granite and their Eu/Eu* nor is their Eu/Eu* significantly deep; this proves that the Moodies granites did not arise from a magma of TTG composition. Moreover, given that the K_2O content of the Moodies granitic/rhyolitic clasts are substantially higher than the TTGs, they would have to represent low proportion melts of a TTG

source, or low proportion residual magmas evolved from a magma of TTG composition. Thus, if clinopyroxene was the main mineral to fractionate instead of plagioclase, considering the highest content of Cr and Ni of the TTG, the fractionated liquid would be poor in Cr and Ni compared to the Moodies granites as Ni and Cr would preferentially partition into the pyroxene bearing residuum. Thus, granites cannot be liquids produced by low-degree partial melting of a TTG-like source. If partially melted at pressure within the plagioclase stability field, the melt produced from the TTG would be CaO-rich and K_2O-poor compared (Singh and Johannes, 1996) to the Moodies granites. Besides, if the melting reaction happened at high pressure, above the plagioclase stability field, garnet would be the main peritectic mineral and the resulting melt from TTG partial melting would have LREE-enriched and HREE-depleted pattern unlike that of the Moodies granites. Based on similar observations, this previous study also excludes mafic rocks as a possible source for the clasts, and consequently these authors concluded that the source of the Moodies granites was immature sediments derived predominantly from felsic crust with a subordinate mafic component.

Similarly to the Moodies granites and rhyolites, few studies have focussed on the origin of the felsic layers present in the BGB. In 1983, de Wit and co-authors concluded that most of the Theespruit formation felsic rocks were in fact reworked felsic tuffs. They described the coarse felsic igneous detritus as being lahars or mudflows rather than pyroclastic rocks. These felsic schists were dated between 3.510 to 3.548 Ga by Kroner et al. in 1996 who demonstrated that the age found most closely reflected the age of igneous crystallization of the original felsic tuff. The K_2O-rich and CaO-poor nature of the felsic, volcanic and volcaniclastic layers within the BGB that appear to be with the same age as with the Moodies granites, has generally been regarded as the result of alteration of coeval TTGs or their volcanic equivalents (Kröner et al., 1996, De Ronde and Kamo, 1994; de Wit et al., 1987). For example, the formation (deposition) age of the Theespruit schist on which part of this study focuses, coincided with the emplacement of the Steynsdorp pluton at 3.548-3.511 Ga (Armstrong et al., 1990, Kröner et al., 1996; Kamo and Davis, 1994), which led to the conclusion that the felsic schists were hypabyssal and volcanic equivalents and/or fractionates of the pluton (de Wit et al., 1987; Kröner et al., 1996).

5. PETROGRAPHY

5.1 The Moodies granites and rhyolites

5.1.1. Petrographic description

In the Eureka syncline, the basal conglomerate displays a variable abundance of granite pebbles, degree of deformation and degree of weathering. The samples that are the subject of this work were extracted from the outcrops labelled from A to J (except H) in the detailed geological map of the Figure 1b. Granites clasts are better preserved in locality A than in localities B and C, which although they contain a higher proportion of granitic pebbles, pebbles are the most weathered. Locality E is a river

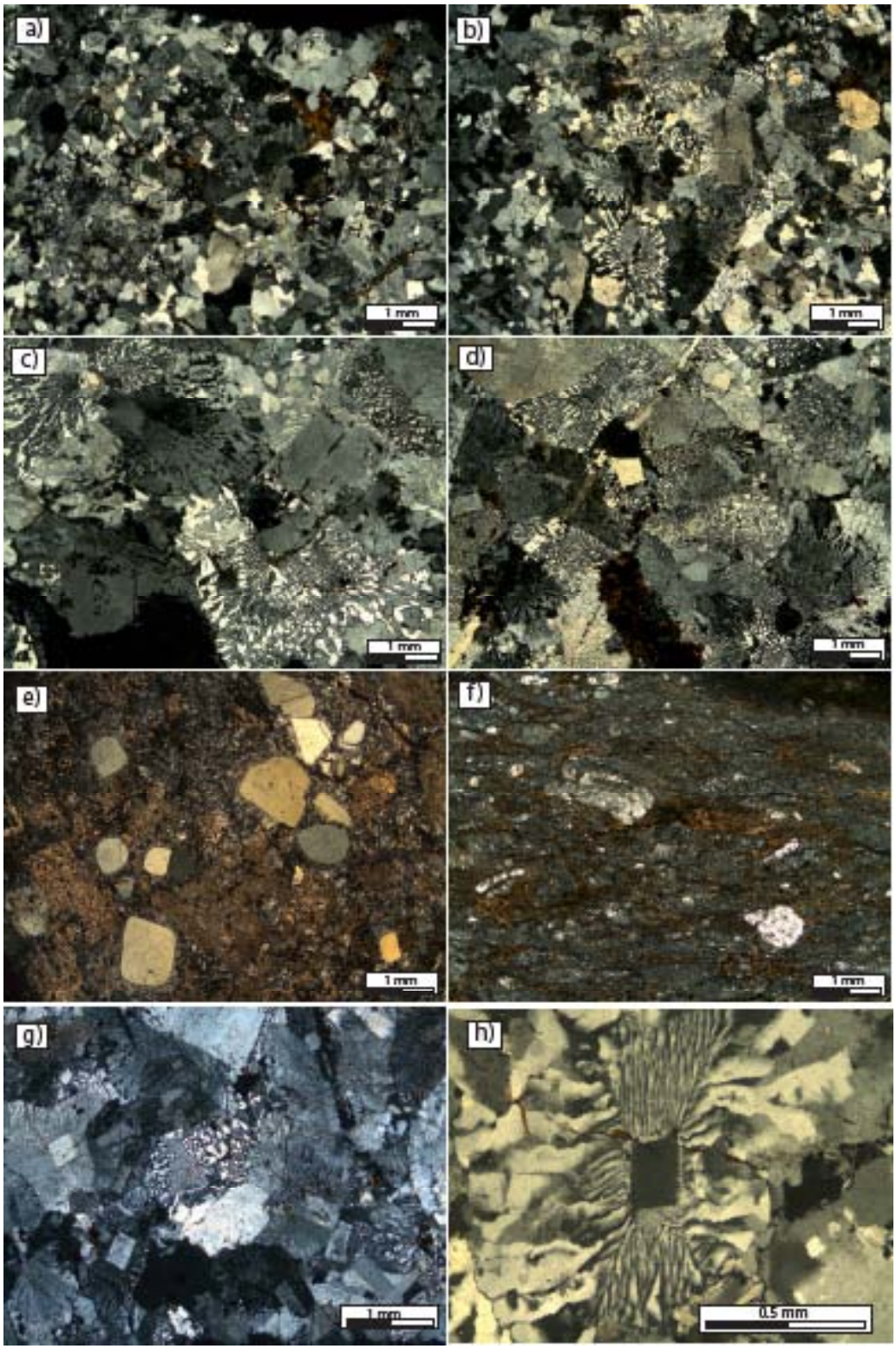

Figure 2. Representative thin section images illustrating the diversity of typical mineral textures displayed by different types of Moodies granites, in crossed polarized light.
a) and b) Image of the typical mineral textures in a representative sample of fine-grained granite (C36 and B10). The original igneous texture is well preserved and is well represented by the micrographic potassium feldspar and quartz intergrowths in some part of the sample. Quartz and Kfs (K-feldspar) represent the main minerals of the rock; Plagioclase (albite) and biotite are present in a smaller amount.

c) and d) Image of the typical mineral textures in a representative sample of medium (A14) and fine grained micrographic granite (C17). The texture is characterized by micrographic feldspar and quartz intergrowths within which an early formed, euhedral feldspar phenocryst is always present as the nucleus. A typical biotite clot can be observed in Figure d), on the bottom part of the picture.
e) An example of the volcanic texture present in several samples (from sample J8), in which quartz and alkali feldspar (here replaced by sericite) represent the main phenocryst minerals. The very finely crystalline groundmass consists mostly of quartz and feldspar (clast of rhyolitic composition).
f) A deformed volcanoclastic sample (B7) in which quartz and subhedral alkali feldspar represent the main phenocrysts present. The fine groundmass contains quartz and feldspar. Biotite marks the main deformation undergone by the rock. This sample is a deformed tuff or ignimbrite.
g) Image of the typical mineral textures in a representative sample of fine grained (C34) micrographic granite. The texture is characterized by perfectly euhedral feldspars as a nucleus in micrographic intergrowths of quartz and feldspar.
h) Picture of a perfectly euhedral feldspars present as a nucleus in micrographic intergrowths of quartz and feldspar in the micrographic granite C45.granite (C33). The texture is characterized by micrographic K-feldspar and quartz intergrowths within which K-feldspar is always present as the nucleus.
d) Fine grain granitic sample (D2). The igneous texture is preserved. Quartz and Kfs represent the main minerals of the rock, Pl (alkali fd) and biotite are present in a smaller amount.

pavement from along the Kaap River bed and represents the freshest outcrop sampled in this study.

The samples can be subdivided into two distinctly different textural varieties: granitic rocks including the sub-categories of microgranite, quartz-porphyries, medium-grained granites and medium-grained micrographic granite; and volcanic/volcaniclastic rocks (ignimbrite, tuff, and rhyolite) including gneissose and schistose examples. The main petrographic categories are described in Supplementary Table 1 and typical textures are illustrated in Figure 2. The mineralogy of the granite and rhyolite clasts is relatively simple, consisting mainly of alkali feldspar, quartz and biotite with zircon, apatite monazite, rutile, ilmenite, pyrite and magnetite constituting the accessory mineral suite.

Granitic pebbles: The degree of weathering of the Moodies granitic pebbles is highly variable. The mineralogy and mineral proportions of the granites, microgranites (Figure 2a and 2b) and granophyres are very similar. The granites and microgranites range from equigranular to fine-grained to medium-grained granites, they contain subhedral to euhedral alkali feldspars (1-0.5 mm) (Figure 2g) and quartz crystals which frequently have recrystallised features: in some samples quartz crystals display undulose extinction and a subgrain texture. Biotite is mostly present in the most altered samples and is either localised along cracks or it often forms clots, possibly representing replacement of anhydrous ferromagnesian minerals. Quartz-feldspar intergrowths are present in several samples of granite, medium grained micrographic granites (Figure 2b, 2c, 2d and 2g) and granophyres. In the best preserved samples the feldspar crystals are mostly euhedral (Figure 2g and 2h) and always form the nuclei of the intergrowth. These grains are very fresh and their size range from 0.5 to 1mm. The most weathered samples of all rock types contain euhedral feldspars with radial sericitisation spreading from the cores of the feldspar to its edge. Relatively rare feldspar crystals show oscillatory zonation that is interpreted to represent magmatic growth zoning. Generally this is observable due to

preferential replacement of alkali-feldspar rich zones by sericite. Minor calcite, chlorite and quartz veins have been found in very few granitic samples (less that 5% of the total samples).

Rhyolitic pebbles: This group of rocks includes lavas and volcaniclastic rocks. The volcanic samples contain rounded phenocrysts in a non-deformed groundmass whereas the volcaniclastic rocks (tuffs, ignimbrite and lahars) mostly have deformed phenocrysts with sharp edges contained in a groundmass that shows evidence of deformation and volcanic flow. In the lavas, phenocrysts consist only of quartz and alkali feldspars. The subhedral to euhedral (Figure 2e) quartz phenocrysts have rounded margins, they are often corroded and embayed. Their size commonly ranges from 0.5 to >1 mm and can reach >1cm. In contrast, the feldspar phenocrysts (0.5 to >1 mm) retain their euhedral shape. Although sericite replacement of feldspar crystals is scarce, in rare samples, the feldspar phenocrysts are almost completely pseudomorphed by sericite (Figure 2e). Biotite and chlorite (when present in some rhyolitic samples) are mostly localised along cracks along which they form clots.

In the quartz-alkali feldspar-phyric volcaniclastic samples the fine-grained groundmass consists essentially of quartz and alkali feldspar, with muscovite and small amounts of biotite and are affected by recrystallization in few samples. In these samples, the phenocrysts are often anhedral to subhedral and are fractured. Some volcaniclastic rocks in this study are characterised by a well developed gneissic texture. In these rocks the foliation is mainly defined by feldspar crystals that were subsequently replaced by sericite, quartz and rare biotite which are deformed. These gneisses are always strongly hydrated, however the previous euhedral shape of some of the phenocrysts remains observable (Figure 2f). The fine-grained matrix of the gneisses consists of quartz and muscovite; it is highly weathered as shown by the almost complete replacement of feldspar by sericite (Figure 2f). Some samples display large (>2 mm), dark and very fine-grained segments of groundmass that have a pointy shape with sharp edges. Biotite and muscovite are abundant and localised along the foliation. Minor calcite, chlorite and quartz veins have been found in very few granitic samples (less that 5% of the whole dataset).

5.1.2. Petrography interpretation

The preservation of euhedral alkali-feldspar and quartz crystals in both volcanic and plutonic samples, even in the most weathered examples, indicates that both these minerals were present as phenocrysts when the magma crystallised. In the gneissic and volcaniclastic samples, the dark portions of groundmass that have sharp edges shape are interpreted to represent highly recrystallised glass shards (Figure 2h). The presence of euhedral phenocrysts minerals held in a fine groundmass indicates that these rocks represent volcaniclastic samples, being deformed post deposition, and the groundmass probably represents former volcanic ash that has undergone recrystallization (Figure 2f and 2e). It is probable that these samples were deformed during the 3.23 Ga collisional event that happened concurrently with the deposition

of the Moodies Group. The presence of the biotite in clots or veins indicates that it formed as a secondary mineral and was not part of the primary magmatic mineral assemblages. The clots of biotite may represent evidence of replacement of a ferromagnesian mineral (garnet or cordierite). All the Moodies granites and rhyolites (sensu stricto) (independently of their degree of alteration) have preserved pristine magmatic textures (Stel, 1992). The volcanic/volcaniclastic samples, by their nature, are more sensitive to deformation. The apparent greater degree of deformation in these types of samples compared to the plutonic examples is biased and reflects the fact that their fine-grained groundmass was less stiff and that the portion of glass is softer.

The common presence of graphic intergrowths of quartz in potassic feldspar in these rocks is important in understanding the setting of crystallization of the granites. The quartz often displays cuneiform textures; these are found predominantly in granitic pegmatites (London, 2008). These textures have been demonstrated to form under feldspar-quartz cotectic conditions. The formation of graphic textures involves substantial liquidus undercooling of an H_2O-undersaturated melt (London, 2008), indeed the tendency to form these textures decreases with increasing H_2O content of the melt (London, 2008; Fenn, 1986). The under-cooling conditions required by this process necessitate that the magma emplaced rapidly into an environment 50 to 200ºC cooler than its solidus. Consequently, these textures are characteristic of magma that emplaced close to the surface (London, 2008). Therefore, the preservation of the graphic textures records shallow depth of emplacement. In this study all the samples that do not have such textures are volcanic rocks.

The presence and characteristics of the volcanic samples also plays an important role in the understanding of the emplacement conditions of the magma, as well as the proximity to the eruptive centres. The variety of pyroclastic fall deposit (tephra) contained within the rhyolitic pebbles studied here is large: it ranges from ashes (tephra size < 4 mm) to lapilli (tephra size between 4 and 32 mm), however, the nature of the volcanic products (predominantly ignimbrite, tuff, …) seem to argue that this material was rapidly cooled, and was “deposited” during an explosive-type eruption, which induced an eruptive column height, most likely, > 5 km (according to the size of the phenocrysts). The tephra size has been determined by the size of the phenocrysts located in 2 of the volcaniclastic samples (E1 and B25). The sample B25 shows well rounded quartz phenocrysts which indicate that in this case the fallout was transported quite far from the vent. Indeed, depending on the size of the phenocrysts in the volcanic fraction of the pebbles (between 0.4 to 1 mm), and the height of the volcanic column, we can roughly estimate that the material was deposited between ca. 0.7 to 27 km from the vent (for a particle or lithic clast size of 1 cm) or between ca. 0.8 and 35 km (for 0.4 cm clast), depending on the volcanic column height (HB=5 or 30 km) (Carey and Sparks, 1986). This is a rough estimate, as the column height varies in term of a number of parameters (wind, eruption velocity, volatile content, viscosity, magma temperature…) that are unknowns and inaccessible to us.

5.2 Felsic schists of the Theespruit formation

Thirty-six samples of rocks described by previous workers as felsic pyroclastic and volcanoclastic rocks (de Wit et al., 1983; de Wit et al., 1987; Van Kranendonk et al., 2009; de Wit et al., 2011) were collected in from the Theespruit formation in the Tjakastad schist belt to the South of the BGB. In this area the Theespruit formation has been subjected to amphibolite facies grades of metamorphism (Diener et al., 2005) and the samples consist of the assemblage quartz + plagioclase + muscovite ± biotite ± chlorite. The foliation is defined by muscovite, biotite and chlorite. Plagioclase and quartz are present in two different textural forms in these samples. They occur as small anhedral grains located within the foliation, in the matrix (Figure 3), and they occur as euhedral phenocrysts within poly-mineral aggregates of plagioclase and quartz

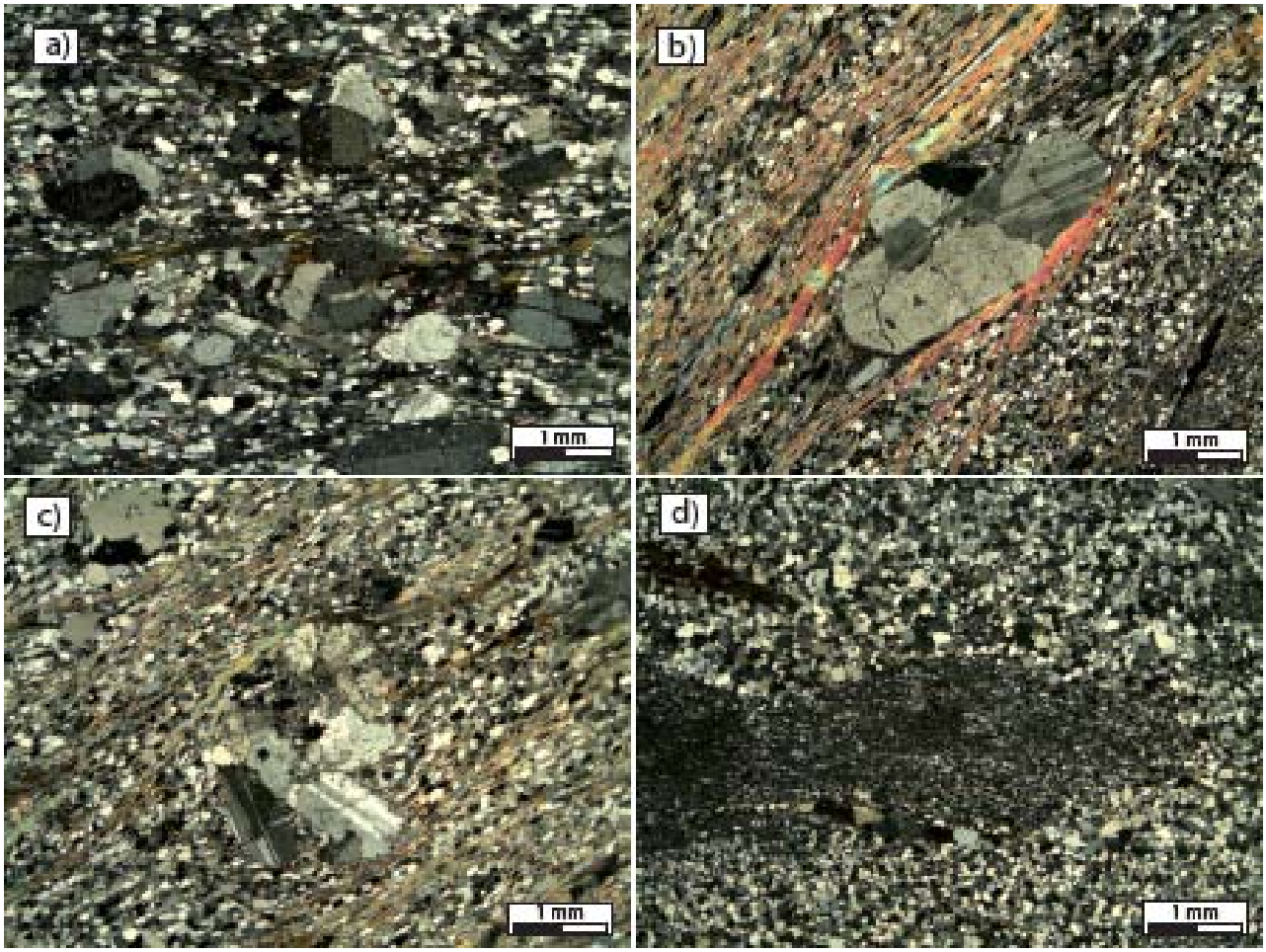

Figure 3. Representative crossed polarized light thin section images and typical mineral textures of the felsic schists of the Theespruit formation
a) Typical textures in a representative sample of schist (TS 02 05).
b) and c) Poly-grain assemblages of euhedral feldspars and quartz forming Moodies granites in a fine grain matrix. The muscovite defining the foliation clearly encircles the aggregates which indicate that they were present prior to metamorphism.
d) Fine grained agglomerate of quartz and plagioclase in a somewhat coarser grained matrix (TS 05 07A). The groundmass contains mostly quartz and plagioclase.

that are characterised by an igneous texture. The foliation wraps around these clasts, which are interpreted to represent lithic fragments (Figure 3a, b and c). The presence of the foliation surrounding these aggregates is evidence that they predate the deformation event which the samples underwent, whilst the conservation of the euhedral shapes of the feldspars is evidence their primary igneous nature (Figure 3b and 3c). The common presence of these clasts within the fine grained matrix suggests that these samples were volcaniclastic prior to the episode of metamorphism they underwent. Several samples also include very fine grained, angular lenses of dark agglomerate which are regarding as representing recrystallised glass shards (Figure 3d). Consequently, as suggested by previous workers, we consider these felsic schists from the Theespruit formation to have a volcaniclastic protolith (tuff) which emplaced in shallow-level crustal depth and at surface. The existence of lithic fragments and glass shards suggest that to some degree, the composition of the schists is likely to reflect the chemistry of the original volcanic system.

6. RESULTS

Henceforth we will use the term "Moodies granites" for the full range of rocks of granitic composition that were sampled as clasts within the Moodies conglomerate, including the volcanic rocks. and the term "Theespruit schists" for the felsic schists of volcaniclastic origin from the Theespruit formation. Moodies granite compositions were previously investigated by Sanchez-Garrido et al 2011; here we present a set of data (>100 samples) more extensive, than in this previous study including some that formed part of the prior study, as well as an entirely new dataset of geochemistry from the Theespruit felsic schists. The major, trace element and REE chemistry of these rocks is presented in Supplementary Table 1. Note that the analytical methods are presented in detail in the electronic appendices.

6.1 Weathering, alteration and hydration: The selection of alteration-free samples

The terms chemical weathering, alteration and hydration have been widely used in a great number of studies. In this study, we are define these terms as follows: Weathering is an at or near surface process that reflects direct interaction between the rocks and the atmosphere and/or the hydrosphere (meteoric water), at atmospheric pressure and temperature; Alteration occurs at when rocks interact with fluids at elevated temperature (> 100 °C) and exchange of elements between the fluid and the rock result in petrologically meaningful shifts in major and trace element ratios in the rock; Hydration involves the addition of water to the rock at elevated temperature by reaction to form hydrous minerals. The chemistry of the rock is not changed in a petrogenetically significant apart from the increase in LOI (loss on ignition).

By their nature, all the clasts of Moodies granite are to some degree weathered. This study has carefully selected the least weathered available material in the field. The degree of hydration observed in the rocks is highly variable. It ranged from zero hydration in medium grained micrographytic granites where

there was no replacement of feldspar minerals by mica to substantial in the most deformed volcaniclastic samples, where mica forms a significant proportion of the matrix. In most samples hydration is minor and is reflected in the sericitization of the feldspar. Thus hydration is obvious from both the petrography and LOI values of the rocks. The degree of alteration however is more difficult to asset, as no obvious chemical flux, apart for addition of water, can be established petrographically. Consequently, the degree of alteration is evaluated by considering the chemistry of the rocks, as discussed below.

We have petrologically divided the Moodies granites, into three populations according to the amount of white mica present in the alkali feldspars. The samples featured in white on figures 4a to 4b are characterised by less than 5 % of feldspar replacement (Figure 2a, 2b, 2c, 2d and 2g); the samples featured in black typically have more than 70% of feldspar replaced (Figure 2f); and the rest of the samples (in grey) are considered to contain between 5 and 70% of feldspar replaced by muscovite (Figure 2e), or remain undefined because thin sections were not produced from these samples.

Importantly, the degree of mica replacement of feldspar is uncorrelated with the K_2O content of the Moodies granites. However, as expected, the samples containing the least mica are characterised by the lowest (<55) chemical index of alteration (CIA) (Nesbitt and Young, 1982; Nesbitt and Young, 1984). This is below the value of 60 which is considered typical of average fresh granite (Fedo et al., 1995) (Figure

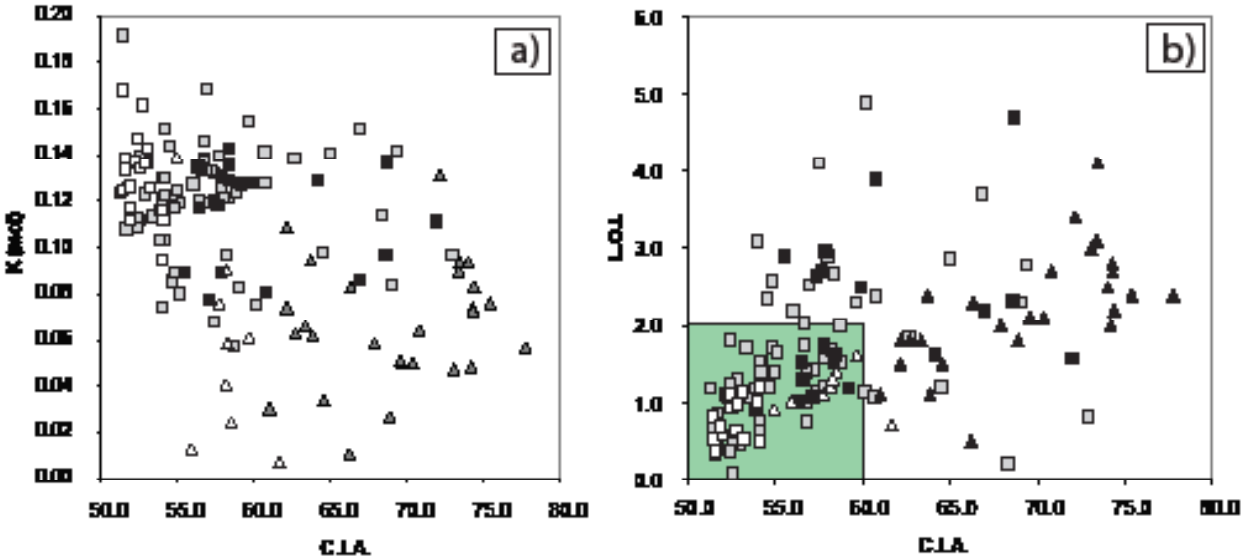

Figure 4. Binary diagram presenting the chemical index of alteration vs. the potassium and LOI content of the Moodies granites and the Theespruit felsic schists. a) Binary diagram of the Chemical Index of Alteration (CIA, Nesbit and Young, 1984), versus the molar K content of all the Moodies granites (white squares are samples that contain less than 5% of sericitic muscovite in the feldspar, black squares are samples that contain less more than 70% of sericitic muscovite in the feldspar, grey squares have medium (between 5 and 70%) amount of sericitic muscovite in the feldspar or undefined) and the Theespruit felsic schists (black triangle are the most altered samples and white triangle are the freshest samples). b) Binary diagrams comparing the Chemical Index of Alteration to the Loss On Ignitions of the Moodies granites (white squares are fresh samples, black squares are altered samples, grey squares are undefined)) and the Theespruit felsic schists (black triangle for the most altered samples and white triangles for fresh samples) (excluding one outlier included in Supplementary Table 1).

4 and 5). The Moodies granites with the most mica have CIA values over 55 (Figure 4a). The CIA values of the Theespruit schists are higher than those of the Moodies granites. The samples of the Theespruit schists with the least hydrous assemblages have CIA values ≤ 60. As for the Moodies granites, the Theespruit schists show no correlation between their hydrous mineral content and their K_2O content. The LOI value of the Moodies granites and the Theespruit schists is correlated to their CIA values, and to their sericite content (Figure 4b). As the quantity of mica increase in the rock, the LOI content of the whole rock also increases. The CIA index virtually image the breakdown of alkali feldspar in mica, so as the CIA index increases, the content of mica in the rock also increase. This explains the correlation observed between the LOI and the CIA content of the granites.

In order to use the geochemistry of the rocks to constrain their petrogenesis, it is important to the rock compositions that most faithfully reflect the original rock compositions formed on crystallization of the magmas. Consequently we restrict the following discussion to samples with the lowest LOI values < 2wt% and with C.I.A. values < 60. This selection mainly contains the samples that have the lower sericite content in the alkali feldspars. From these samples we are creating a new database, and we will restrain our work on only these samples.

The A-C*N-K (Al_2O_3-CaO*+Na_2O-K_2O) diagram (Figure 5) has been commonly used to differentiate alteration trends within collections of igneous rock compositions

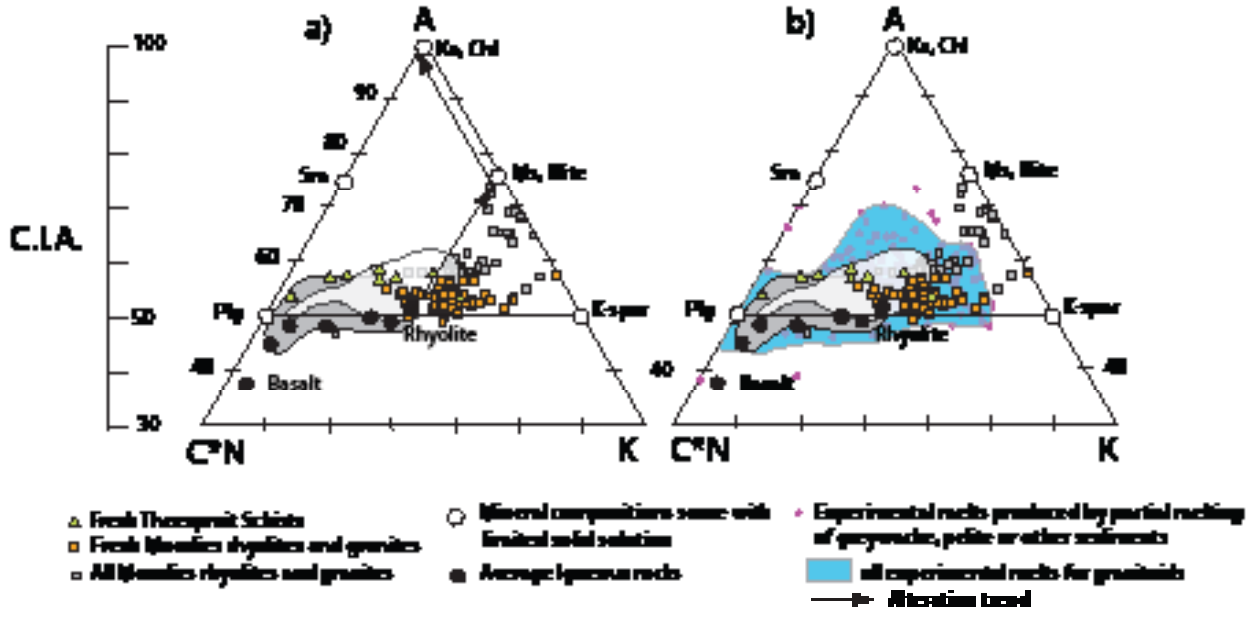

Figure 5. A-C*N-K ternary diagrams. a) The diagram displays all Moodies granites and rhyolites and the Theeespruit Formation felsic schist samples reported in this study. The dark area represents BGB TTG compositions, whilst the white field represents S-type granites worldwide. Sample hydration has no effect on the ternary plots. Arrows indicate the effect of removal of Ca or Na from pristine granites or rhyolites by weathering or hydrothermal leaching. White hexagons represent mineral compositions some with limited solid solution which is not portrayed, Chl = chlorite, plag = plagioclase, K-spar =Kfeldspar, Ms = muscovite, Ka = kaolinite, Sm = smectite, Average igneous rock compositions are from Nockolds (1954).

(Nesbitt and Young, 1984; Fedo et al., 1995). The trend towards the illite or kaolinite points is interpreted to reflect the transformation of feldspar into clay or micas (Nesbitt and Young, 1984). Thus, samples plotting on these trends are commonly seen as altered samples. There is a problem in this regard in that peraluminous granites produced from the melting of micas will have an alteration like character that reflects their source composition. This is illustrated by plotting the composition of worldwide S-type granites, as well as experimental granitoids melts on the diagram. The experimental melt and S-type granite compositions spread towards the illite and K-feldspar components and overlap substantially with the composition of the Moodies granites and the Theespruit felsic schists. In general, almost all of the rock compositions documented in this study overlap with the fields defined by S-type granite and experimental melt compositions. This suggests that our identification of the material suitable for further study has erred on the side of caution.

6.2 Mineral compositions

6.2.1. The rock forming minerals

FFeldspar compositions from the Moodies granites are dominated by K-feldspar and albite, irrespective of the rock type (Supplementary Table 2). The most Ca-rich plagioclase analysed has An12. The CaO content of some feldspars show oscillatory zoning or core/rim zoning. Plagioclase un-mixing can be observed essentially through K-feldspar exsolution in albitic plagioclase (antiphertite) and rims of perthite surrounding the antiperthite. These 2 feldspars were probably both present as ternary feldspars at high temperature during crystallisation.

Unlike the Moodies granites, no potassium feldspars have been found in the Theespruit formation schists. Plagioclases in the matrix of these rocks are bytownite (An > 75) (Supplementary Table 2). In the samples where agglomerate clasts with igneous textures are present, the feldspars analysed within the igneous textured portions are more albitic than the matrix feldspars. This indicates substantial redistribution of the K and Na within these samples. Amphibolite facies metamorphism concurrent with substantial penetrative deformation in these rocks has destroyed any K-feldspar in the protolith by reactions to produce muscovite and biotite. Plagioclase compositions in the matrix also record this metamorphic signature and the partitioning of Na between plagioclase and white mica. The only portions of the rocks that potentially record igneous mineral compositions are the igneous textures lithic clasts, where the more albitic plagioclase probably represents the composition of magmatic plagioclase. These clasts never contain K-feldspar, probably reflecting preferential preservation of K-feldspar-free domains due to the greater resistance of these domains to hydration reactions.

6.2.2. Inclusions in zircons

The zircons crystals present in the Moodies granites contain a vast range of inclusions, including apatite, monazite, quartz, biotite, muscovite, alkali feldspar, ilmenite, rutile,

plagioclase and iron-oxide (Figure 6). Poly-mineral inclusions (of quartz-feldspar-biotite) are also present in the zircons. The inclusions have azonal distribution within the host mineral. The study by Chupin et al. (1998) described melt inclusions in 3.2 Ga old Archean zircons extracted from quartzite and granitic orthogneiss in the Kaapvaal craton. These included potassic Cl-rich granitic, potassic Cl-poor granitic and tonalitic-trondhjemitic melt inclusions. Chupin et al. (1998) argued that the mineral inclusion suite found in the zircons, as well as the compositions of the melt inclusions suggests the presence of K-rich granitic magma in the Kaapvaal Craton at 3.2 Ga. Our study follows the same line of thought, and the inclusion suites observed in the zircons of the Moodies granites, their nature and localisation within the zircon grains similarly demonstrates that the zircons crystallised from K-rich granitic magmas and are not inherited from TTG-like compositions.

Scanning Electron Microscope-Energy Dispersive Spectroscopy analysis of feldspar, muscovite and biotite inclusions within zircon has identified in excess of 90 feldspar inclusions within a population of more than 600 zircons. In excess of 60 feldspars inclusions have been analysed to produce stoechiometric compositions (Sanchez-Garrido et al., 2011). Of these, only 20% are plagioclases with an anorthite component higher than 5%. Thus 80% for the analysed feldspar inclusions in zircon are alkali feldspar. Importantly, none of the plagioclase inclusions have anorthite content $\geq$ 15% (Supplementary Table 2). Most of the K-feldspar inclusions occur with Albite. In general, the anorthite component of the plagioclase inclusions is higher than the matrix plagioclase (Supplementary Table 1). This indicates that the magmatic inclusion suite preserved in the zircons was in equilibrium with the high temperature magma from which the zircons crystallised.

The biotite inclusions are often found as part of poly-mineral inclusions and have, on average, a higher Al VI and lower Al IV content than the biotite present in the thin section of the samples (Figure 7). They have Mg# ranging from 31 to 55 (not shown, Supplementary Table 2) which is lower than in the rock forming biotite. This, in the whole rock, may indicate that equilibration with a Mg-rich mineral like cordierite, which has been destroyed during metamorphism by reaction with K-feldspar and fluid to form the biotite from the matrix. The biotite inclusions have on average Ti+Al IV content higher than the rock forming biotite. Thus, the biotite inclusions in the zircons may represent primary biotite whilst the matrix biotite may be secondary. Alternatively, the both compositions may reflect igneous biotite with the differences reflecting changes in composition as crystallisation progresses. This is supported by the fact that both biotite compositions fall within the range of natural biotite and of experimental magmatic biotite present in S-type granites. Also, reactions to consume minerals such as cordierite or garnet by biotite replacement often occur in the magmatic state in granites. The nature of the mineral inclusion suite in the zircons is identical to the rock forming and accessory mineral assemblage. It is also similar to the inclusions suite in the Jack Hills zircons, which are also suggested to have crystallised from a

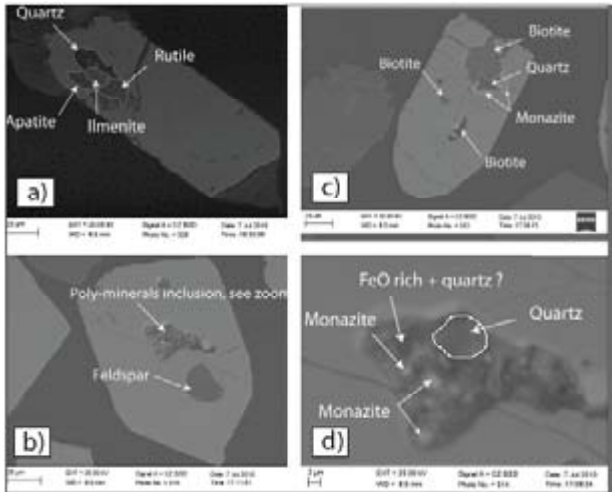

Figure 6. Representative mineral inclusion present in zircon grains of the Moodies granites.

magma derived from a sedimentary source.

6.3 Whole rock major and trace element geochemistry

It is useful to compare the composition of the Theespruit felsic schists and the Moodies granites is with a database of worldwide S-type granite compositions because of their obvious compositional similarities with these rocks and with the BGB TTG because of the overlap in and of emplacement with these plutons (Sanchez-Garrido et al., 2011).

The Moodies granites are silica (69.86 to 84.02 wt%) and potassium-rich (3.78 to 9.02 wt%) (Table 1). On the normative An-Ab-Or ternary diagram (Figure 8) all the Moodies granites fall in the granitic field and almost all on the lower (Ab-Or) part of the ternary diagram, which displays one of the characteristics of these magmas: they are K_2O-rich and CaO-poor. The same conclusion can be drawn from the Harker diagrams (Figure 9) where the majority of the Moodies granites define relatively poorly correlated inverse-correlation trends between SiO_2 and Al_2O_3, MgO, TiO_2 and FeO. Within the Moodies granites, the high levels of Na_2O and K_2O are not correlated with their SiO_2 content. The Moodies granites plot mainly in the same area as the S-type granites on most Harker diagrams and show broadly the same range of inverse-correlation between SiO_2 and Al_2O_3, MgO, TiO_2 and FeO as the S-type granites. The main differences between the Moodies granites and other types of granitoids

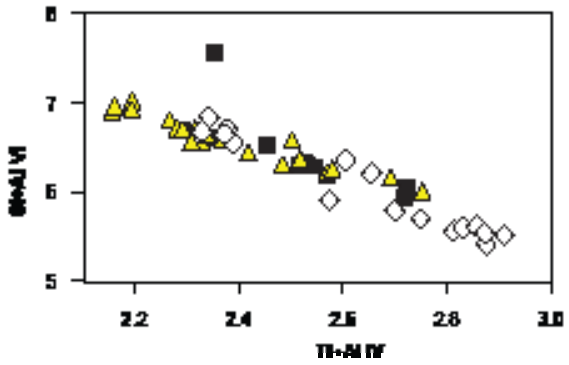

Figure 7. Binary diagrams comparing the molar composition of the biotite mineral inclusion in zircons (white diamonds) and as rock forming mineral (black squares). The yellow triangles represent biotite from the matrix of the conglomerate (Jaguin, personnal communication, Supplementary Table 1).

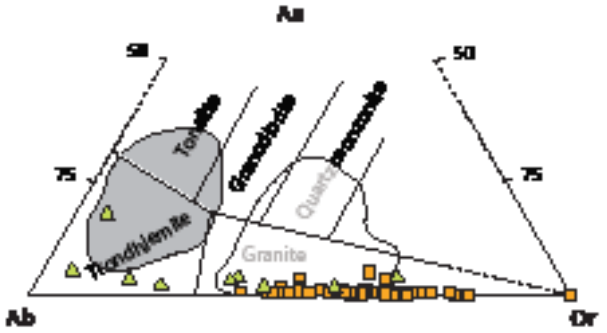

Figure 8. Ternary feldspar diagram displaying all the fresh Moodies granites (orange squares) and the fresh Theespruit felsic schists (green triangles). The field of the BGB TTG (grey field) and of S-type granites (white field) are displayed for comparison.

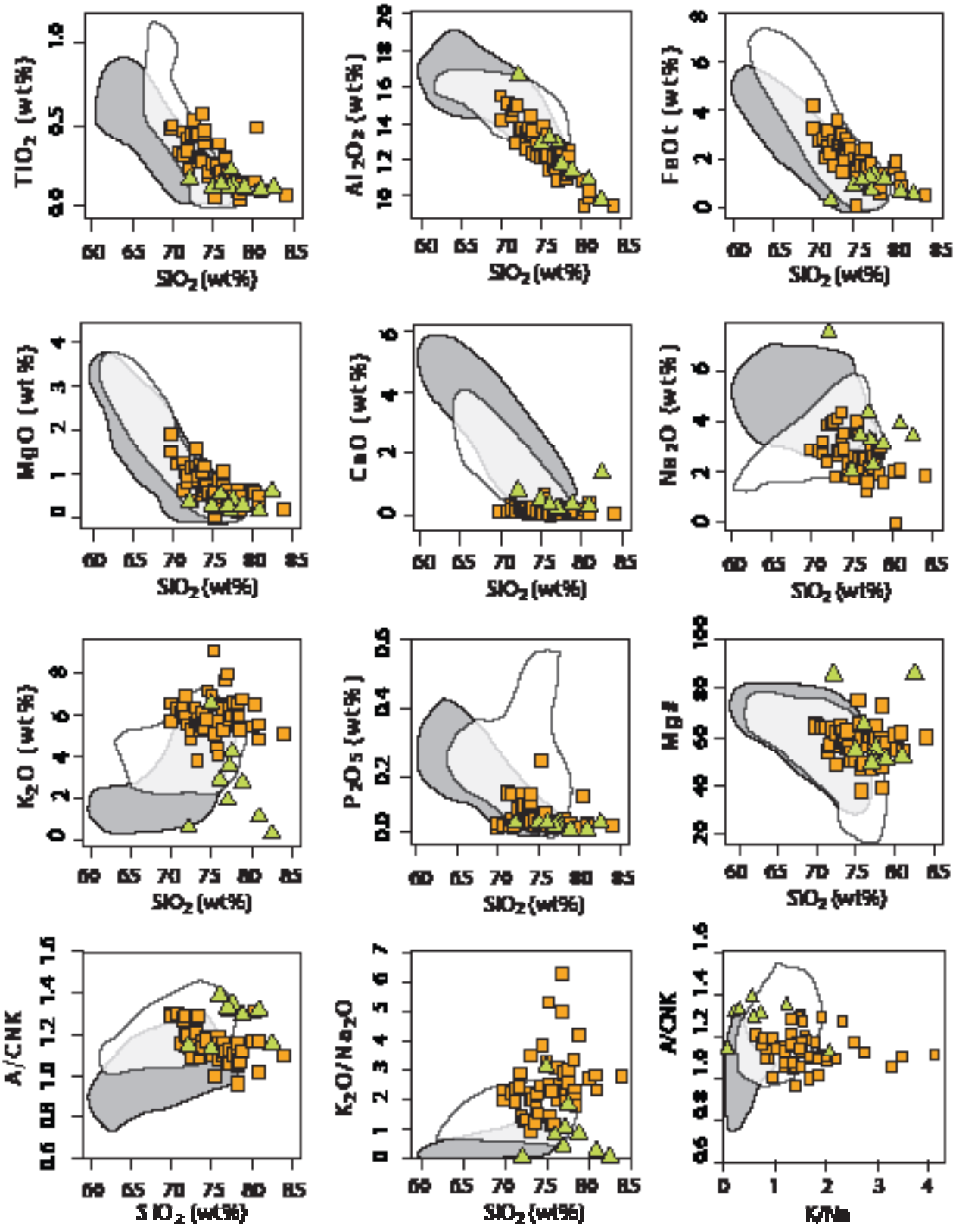

Figure 9. Harker diagrams displaying all the freshest Moodies granites (orange squares) and the Theespruit felsic schists (green triangles). The field of the BGB TTG (grey field) and of S-type granites (white field) are displayed for comparison.

(S-type and TTG) is their low CaO and P_2O_5 contents, their larger range of SiO_2 content and the behaviour of their A/CNK ratio versus SiO_2. The high SiO_2 content of both plutonic and volcanic samples indicates that this is not the result of sedimentary accumulation of quartz in the volcaniclastic rocks, but rather a consequence of magmatic quartz accumulation. This is supported by the presence of quartz phenocrysts in the whole crystallisation history of the rocks (from granites, rhyolites to volcaniclastic samples). The major population of the Moodies granites is peraluminous, and shows a negative correlation between their silica content and their A/CNK ratio.

The Theespruit felsic schists plot in the granite and trondhjemite fields of the feldspar triangle (Figure 8), and from this point of view they differ significantly from the Moodies granites. The schists are on average higher in SiO_2, MgO and lower in K_2O than the Moodies granites. The schists however share the main features of the Moodies granites chemistry i.e. they are moderately rich in Na_2O (2.03 wt% in average), have very low CaO content (0.30 wt% in average) and are potassic (3.02 wt% in average) (Figure 9, Supplementary Table 1). The Theespruit felsic schists are highly peraluminous and show no distinct correlation between the silica content and A/CNK.

The Cr content of the Moodies granites is variable and high, but is within the range of S-type granites. The Cr content of the Moodies granites ranges from 9.4 to 60.5 ppm and the Ni varies from 18.7 to 150.8 ppm (Figure 10, Supplementary Table 1). Some of the Theespruit felsic schists also display high Ni content but are in average lower in Ni than the Moodies granites. The Moodies granites and the schists have a lower Rb content than typical S-type granites, but they do plot within the lower part of the field defined by the S-type granites. Multi-element diagrams portraying the Moodies granite compositions normalized to bulk continental crust are all similar (Figure 11a) irrespective of age of sample or sampling location. The normalized element content of the Moodies granites vary in a wide range, but significantly have identical anomalies. All Moodies granites show significant negative anomalies in P, U and Sm, but variable positive to negative Sr anomaly. Compared with the granites, the BGB TTG rocks typically display the same Rb content but significantly lower K, Th and U contents, they have positive Sr anomaly and they are also on average poorer in HREE (Figure 11b). The TTG and the Moodies granites display negative Nb anomalies. The Theespruit Formation schists show a similar Ti negative anomaly to the Moodies granites, their compositions are also defined by a strong negative Sr anomaly (Figure 11b). In similarity with the Moodies granites, they display positive and variable negative K anomaly. Both Moodies granites and Theespruit schists have lower Rb and Cs content than the average S-type granites.

The chondrite normalised rare earth element (REE) patterns of all the Moodies granites are very similar, with LREE enrichment, and flat HREE content (Figure 12). Apart from 2 samples (C11X and J10), the Moodies granites do not display significant negative europium anomaly (average Eu/Eu* = 0.8) (Figure 12a).

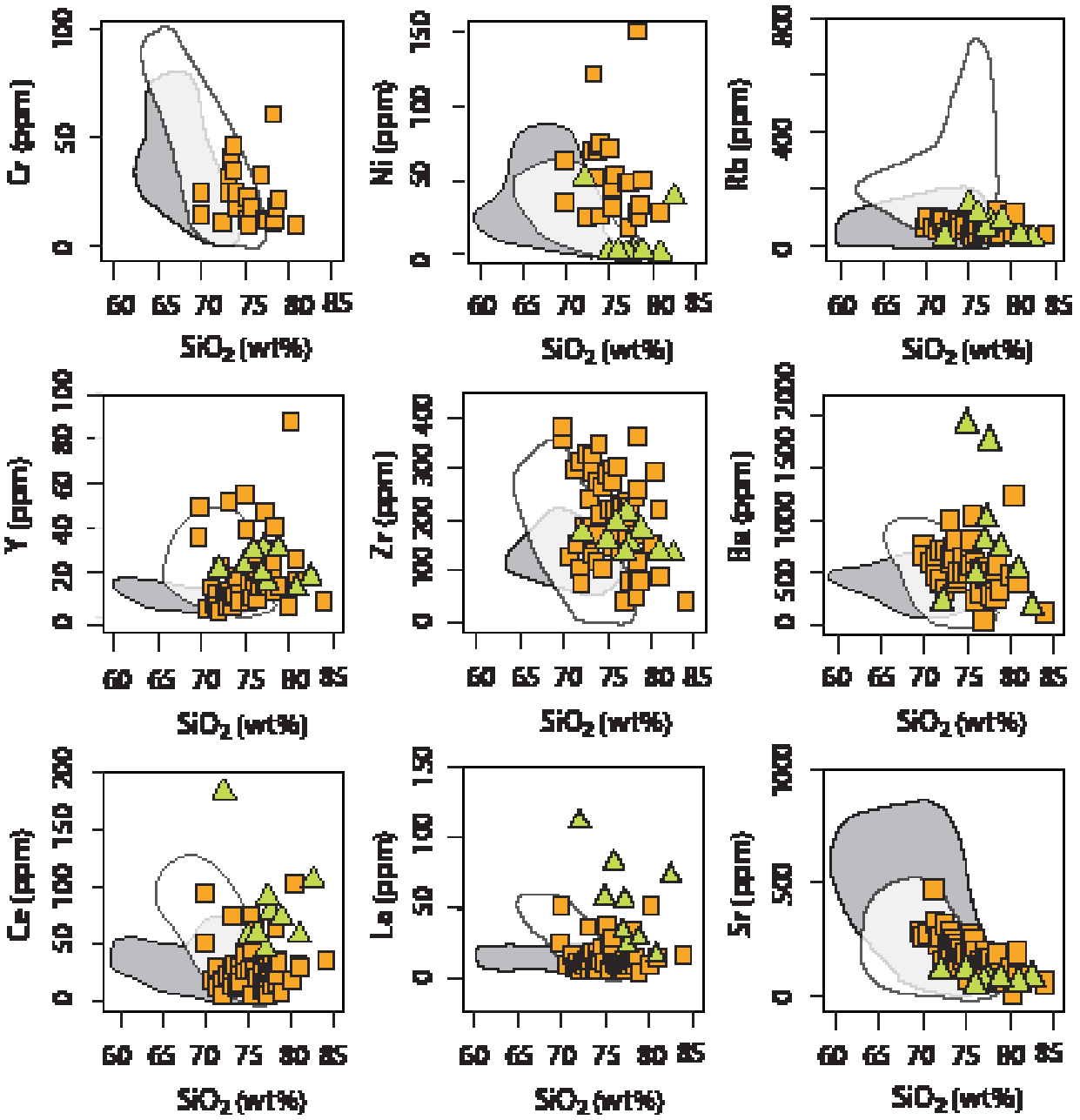

Figure 10. Harker diagram vs. trace elements displaying all the fresh Moodies granites (orange squares) and the Theespruit felsic schists (green triangles). The field of the BGB TTG (grey field) and of S-type granites (white field) are displayed for comparison.

When compared to the average of the S-type and TTG REE pattern, the Moodies granites overall have a REE normalised pattern identical to the S-type granite average. The Moodies granites differ from the TTG by their small Eu/Eu* anomaly and by their HREE pattern that is flatter than in the TTG, reflecting a higher HREE content. The Theespruit Formation felsic schists display similar REE pattern's shape i.e. depletion in LREE and flat HREE pattern but have in general higher REE content and larger Eu anomaly (average Eu/Eu* = 0.5) (Figure

12b). This is also reflected when they are compared to the S-type granites, their pattern is steeper in term of their LREE and flatter in term of their HREE content than the S-type granites. It is also clear that the schists have higher REE content than the average of the BGB TTG.

6.4 Oxygen isotope ratios in zircon and quartz

Individual zircon crystals and quartz and feldspar

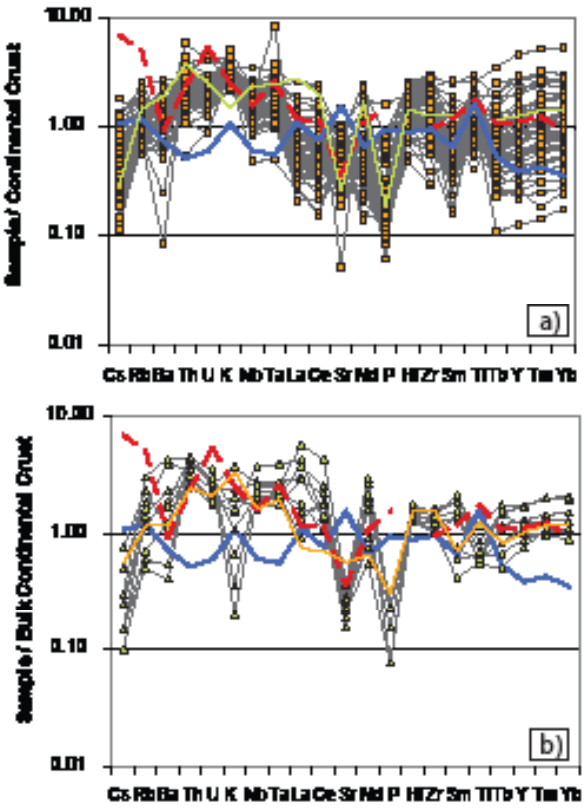

Figure 11. Trace element spider diagrams of the Moodies granites and the Theespruit felsic schists. a) trace element pattern of the fresh Moodies granites (orange squares) compared to average Barberton TTG (thick blue pattern), the average of S-type granite (red dashed thick pattern) and the average of the Theespruit schists (thin plain green pattern), b) trace element pattern of the fresh Theespruit felsic (green triangles) with the most igneous composition compared to Average Barberton TTG (thick blue pattern) the average of S-type granite (red dashed thick pattern) and the average of the Moodies granites and rhyolite (thin plain orange pattern).

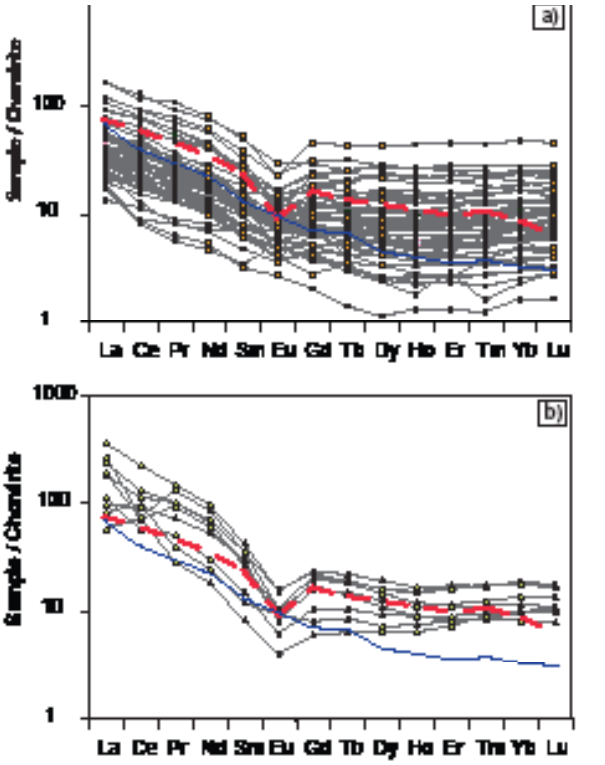

Figure 12. Rare Earth Elements diagrams of the Moodies granites and the Theespruit felsic schists. a) REE pattern of the Moodies granites. The averages of the BGB TTG (thick blue line) and of S-type granites (thick dashed red line) are displayed for comparison. b) REE pattern of the Theespruit schists. The averages of the BGB TTG (thick blue line) and of S-type granites (thick dashed red line) are displayed for comparison.

phenocrysts from the Moodies granites, as well as some whole rock powder of the same clasts were analysed for their O-isotope composition in an attempt to constrain the nature of their protholiths. Some whole rock samples of the conglomerate matrix were also analysed for whole rock $\delta^{18}O$ composition. The quartz and feldspar phenocrysts of the granites (except feldspar phenocrysts from the sampling area B) have high $\delta^{18}O$ values ranging respectively between 11.6-17 ‰ and 11.1-15.8 ‰ (Figure 13, Figure 14, Supplementary Table 4) and display a wide range of variation. In contrast, zircon crystals generally have homogeneous

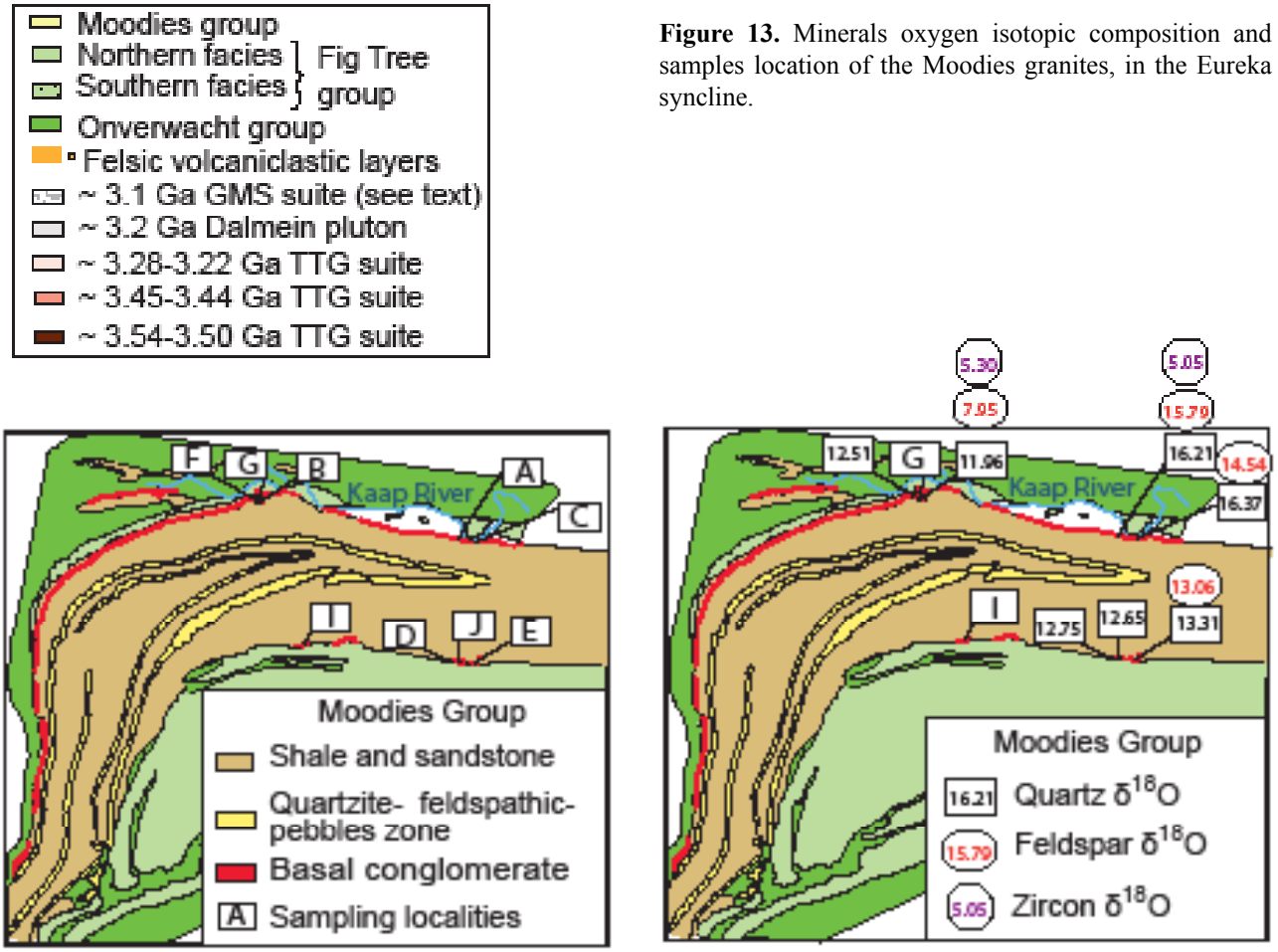

Figure 13. Minerals oxygen isotopic composition and samples location of the Moodies granites, in the Eureka syncline.

values (Figure 14, Supplementary Table 3). The $\delta^{18}O$ values of zircons are identical to mantle zircons (ca. 5.3 ‰, Valley et al., 1998) and to zircons from the TTGs of the Barberton Greenstone Belt (King, 2001). The $\delta^{18}O$ value of the two older populations of zircons analysed have similar values, in contrast, the younger population of zircon (B7 age is 3226.2 ± 8. Ma) has a $\delta^{18}O$ value of ca. 1 ‰ higher than the others.

There is a clear relationship between the sample locations and the oxygen isotopic composition of quartz and feldspar (Figure 13, Figure 14). In all localities analysed, the quartz and feldspars $\delta^{18}O$ values are not consistent with O-isotope equilibrium with zircon at magmatic temperatures. The quartz and feldspar $\delta^{18}O$ values cluster according to location and are similar for localities that are closely spatially associated (e.g. A and C, 16.2 ‰ and 16.4 ‰ respectively), but different for localities that are further away (e.g. locality B, 11.9 ‰).

The whole rock $\delta^{18}O$ values of the granite samples are in equilibrium with the $\delta^{18}O$ values of the feldspar and quartz. The whole rock $\delta^{18}O$ values of the matrix of the conglomerate hosting the granite samples are high and range between 13.4 to 16.3 ‰. There is correlation between the whole rock O-isotopic composition of the matrix and that of the granite clasts.

7. DISCUSSION

Sanchez-Garrido et al (2011) demonstrated

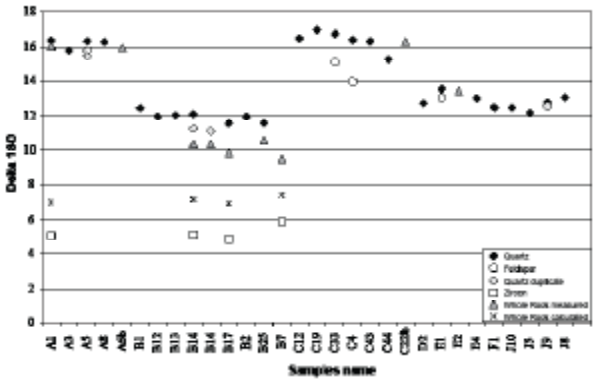

Figure 14. Oxygen isotope data in the Moodies granites and in the matrix of the Moodies conglomerate (sample A6b, C22b and E2). The differences between the measured $\delta^{18}O$ value of the whole rock and of the calculated $\delta^{18}O$ value (calculated from zircon $\delta^{18}O$ value) reflect the fact that the zircons are out of equilibrium with the rest of the main minerals (quartz and feldspars) of the rocks.

that three generations of high-K_2O, low-Ca slightly peraluminous granites were generated concurrently with TTG magmas in the Barberton greenstone belt. They concluded that the melting of a metagreywacke source at high pressure can account for the geochemical signature of these rocks. If correct, these findings imply a previously unrecognised type of granite that formed at each episode of crustal growth or recycling which constructed the proto-Kaapvaal craton. Consequently it is very important to test these hypotheses and to explore the petrogenesis of these rocks in more detail. This will be done by exploring the relationship between the assumed source compositions and the PT conditions of melting required to produce the rock compositions documented in this work. As this is best performed with knowledge of melt compositions and mineral mode of the residuum, this analysis draws on the results of relevant experimental work. Additionally, as the granites described here occur only as clasts within a conglomerate, they may represent a particular compositional predisposition to survival of weathering, erosion and transport. In this case these compositions are possibly not completely representative of the broader magmatic system. This problem is addressed by considering information from the Theespruit Formation felsic schists, which although they are less well preserved than the Moodies granites, provide information on felsic volcanic rock compositions formed at 3.55 Ga and not subsequently eroded and transported into a sedimentary deposit. Finally, what does the presence of these granitic rocks, even if they are subordinate components of the crust, tell us about the development of the early Archean continental crust? Clearly, the answer to the last question is dependent on the previous questions around their petrogenesis. Each of these topics is discussed in detail below.

7.1 The magmatic signature of the Moodies granites

In this study we have considered a subset of Moodies granites that were selected as the freshest samples available. Several primary arguments can be put forward to demonstrate that these rock compositions represent material that accurately reflects magmatic compositions: 1) The Moodies granites show typical magmatic textures defined by unaltered minerals in the freshest samples. These textures indicate rapid ascent, emplacement and crystallization, or eruption with no discernable post crystallization modification; 2) additionally, in the A-CN-K diagram the Moodies granites plot in the same field occupied by worldwide S-type granites. More importantly, their compositions also

overlap with those of experimental granitic melts from metasedimentary sources which by definition can not be altered; 3) the freshest samples lack hydrous mineral in significant amount. Chlorite is only present in very small amounts (less than 5%) in few samples; biotite and/or muscovite do not represent more than 3% of the rock.; 4). The inclusion suite present in the solely magmatic zircon crystals is identical to the major mineral and accessory mineral assemblage present in the fresh granites. The presence of monazite inclusions in magmatic zircon indicates that monazite is a magmatic minerals. This argues strongly that the peraluminosity of the samples is not due to post-crystallization leaching of Ca, Na or K, but is a primary feature of the magma; 5) Plagioclase inclusions within zircon have low An contents; An11 being the highest measured An content (Sanchez-Garrido et al.).

These five findings confirm the peraluminous, K_2O-rich, CaO-poor character of the magmas. Zircons $\delta^{18}O$ values (Sanchez-Garrido et al., 2011) of 5 to 6 ‰ suggest a magma that is mantle-like in it's oxygen isotope composition, yet quartz and feldspar have variable and high $\delta^{18}O$ values (11.1‰ to 17‰ and 13‰ to 15.8‰ respectively) that are clearly out of equilibrium with the zircons, and commonly mutually out of equilibrium at reasonable magmatic temperatures (650 to 800 °C). Thus the rocks contain textural and geochemical evidence which suggest a lack of alteration, yet quartz and feldspar have clearly reset $\delta^{18}O$ values that depend on the location of the sample. The preservation of the magmatic textures in the granites supports the idea that if rock-fluid interaction(s) occurred, it was mostly through isochemical processes. In order for the rock-fluid interaction to remain isochemical, the fluid:rock ratio needs to remain relatively low (≤1). Therefore the zircons have retained their primary oxygen isotopic composition whilst quartz and feldspar have exchanged with oxygen derived from local fluid. Thus we assume that the zircons represent the initial magmatic O-isotope composition whereas the quartz and feldspar clearly reflect the O-isotope composition of the rock after rock-fluid interaction. This disequilibrium is quite common and has already been documented in study around the world, especially in magmatic settings (King et al., 1997). To explain the disequilibrium of O-isotope between the quartz and feldspars, and the zircons we need to consider an open system where the initial $\delta^{18}O$ value of the rock would be 5 ‰ and where the final $\delta^{18}O$ value of the rock would be 16‰. Potential hypotheses include the following: 1) The rock has interacted with a meteoric fluid of low $\delta^{18}O$ value (<1 ‰), at low temperature (30°C); 2) The rock has interacted with a fluid of high $\delta^{18}O$ value (>10 ‰), at low temperature (30°C); 3) The rock has interacted with a fluid of high $\delta^{18}O$ value (>10 ‰), at medium temperature (180-220°C) or finally, 4) The rock has interacted with a fluid of high $\delta^{18}O$ value (>10 ‰), at high temperature (400°C).

Nevertheless, in order for the fluid-rock interaction to remain isochemical (as evidenced by the preservation of the magmatic textures), the fluid:rock ratio needs to be relatively low. This is best achieved via hypothesis 2 and 3. It is important at this stage to note that the rocks of the Moodies Group were affected by the

3.23 Ga metamorphic event which occurred in response to terrane accretion in the Barberton Greenstone Belt. The produced greenschist facies grades of metamorphism in the areas where the Moodies granites were sampled, as is evidenced by the relatively abundant biotite in these rocks (>> 10 %) that coexists with muscovite and chlorite. Consequently, the matrix of the conglomerate and associated clastic sediments will have produced fluid via the reactions through which the clay minerals in the rocks broke down to form micas and chlorite as well as via the simplified reaction chlorite + muscovite = biotite + H_2O. This fluid production would have occurred over a broad temperature interval, probably from 200 to > 400 °C (this rules out the hypothesis number 2 as it is ineffective that as at such low temperature (30 °C) the clays of the matrix would not have been able to loose their water and therefore to generate a fluid of high $\delta^{18}O$ value.). Such fluid will be characterised by high $\delta^{18}O$ values (> 10‰) (Criss, 2008). We consider that this event is responsible for the genesis of a fluid with high $\delta^{18}O$ value (ca. 15‰) at temperature around 200°C (sub-greenschist facies) that has inherited its O-isotope composition from the matrix of the conglomerate.

Assuming an open system, such a fluid can produce the oxygen isotopic compositions recorded in quartz and feldspar of the rocks with the highest $\delta^{18}O$ values, with fluid:rock ratios that vary between 0.86 and 1.01, at 180 and 220 °C respectively. This is the total overall fluid:granites interaction ratio, the fluid:rock ratio at any point in time was certainly much lower as this interaction had millions of years to occur. At these temperature, in a closed system, the solubility of potassium, calcium, sodium, aluminium and silica in a fluid buffered by muscovite + quartz + feldspar is low (e.g. 0.04 g of K. per kg H_2O (Azimov and Bushmin, 2007)). Importantly, the fluid compositions are buffered by the quartz + chlorite + muscovite matrix will be very similar to those in the granite clasts. Consequently, this degree of fluid:rock interaction is consistent with the low degree of alteration in the clasts. Because the Moodies granites are small clasts in a large matrix conglomerate they can probably be considered as on open system. In such a system, the potential flux of elements may well be higher and will be determined by the quantity of chloride available in the system (mostly provided by the micas), nevertheless at the fluid:rock ratios proposed, and given the fact that both mineral assemblages buffer the fluid to similar compositions, the effect on the bulk rock chemistry of the clasts is likely to be negligible.

Interestingly, there is an apparent contribution in the fact that some of the rocks with the highest $\delta^{18}O$ values in quartz contain feldspar minerals with preserved graphic textures, that are completely unaffected by hydration. This suggests that water ingress along grain boundaries may have been slow enough to not a formed a fluid saturated state, thereby avoiding the water activity values that would trigger breakdown of the K-feldspar to muscovite. Alternatively, at the low temperatures considered the breakdown of feldspar minerals to mica may be kinetically limited due to the requirement of the reaction for Al mobility. Despite the low numbers of samples analysed, the lack of oxygen isotopic variation in zircons

may be interpreted to indicate a homogeneous magma composition pre-crystallisation of the zircon. The lack of $\delta^{18}O$ diversity in zircons could reflect either the homogeneity of the oxygen isotope ratios in the source or homogenisation of the magma after its separation from the source. Consequently, we propose that the exchange of oxygen between metamorphic water in matrix and the Moodies granites does not constitute major-element alteration of the granites. The exchange of oxygen in feldspar, quartz or zircon's structure will not involve structural changes. Consequently melting of material that has $\delta^{18}O$ value close to the one found in the Moodies granites zircons will be adequate to generate the Moodies granites low $\delta^{18}O$ value. Such material is common in the BGB, as both the TTG rocks (Sanchez-Garrido et al., 2011; King, 2001) and the mafic rocks are characterised by this oxygen composition. Early erosion of these rocks to produce proximal clastic sediments with a low clay content would produce sources with appropriately low $\delta^{18}O$ values. Detrital biotite in such sediments would constitute the key chemical ingredient required to generate the major element chemistry of the Moodies granites.

7.2 Are the granites representative of the broader magmatic system?

The absence of any deep-level plutonic record for the Moodies granites, as well as the presence of volcanic rocks and graphic textures in the granites indicate that they occurred only as eruptive or high-level intrusive phenomena, thereby being predisposed to weathering and erosion. The granites found in the basal conglomerate of the Moodies group however may not represent the full range of compositions that formed part during each of the three magmatic events they record as harder material and minerals that are more resistant to weathering are naturally selected during the clastic sedimentary processes. As a result, rocks with these characteristics may contribute disproportionately to the compositions of clastic sedimentary successions. Indeed studies of the Moodies group (Hessler and Lowe, 2006, Nesbitt and Young, 1996) proposed that the Barberton Greenstone Belt was subject to an aggressive weathering environment at 3.2 Ga and onwards. The Moodies conglomeratic layers contain a low proportion of labile rock types as well as ultramafic and mafic volcanic rocks which they propose did not survive the intense weathering. Indeed the plagioclase and ferromagnesian minerals from the mafic, ultramafic or felsic volcanic rock source did not resist the extreme weathering conditions and decomposed as clays or as material in solution unlike quartz and K-feldspar which have been shown to be more resistant to weathering. The lower stability of plagioclase compared to quartz and/or K-feldspar in the weathering environment is observed in modern weathering environment and is attributed to the higher susceptibility of is calcium or sodium ion to acid hydrolysis (Nesbit and Young, 1989; Nesbitt and Markovics, 1997). These observations may be taken to argue that the Moodies granites may have only recorded a portion of the magmatic system from which they are derived, with potential concurrent more calcium-rich granites having been destroyed due to preferential weathering. In

this regard, the compositions of the Theespruit Formation felsic schists are particularly useful. These rocks correlate in age with the oldest category of Moodies granites. The Theespruit schists contain agglomeritic layers that display magmatic granitic textures. Plagioclase within the lithic clasts is more albitic that recrystallised metamorphic plagioclase within the matrix. This compositional difference, illustrates that the plagioclase in the agglomerate clasts is igneous, which is in agreement with the general magmatic texture of the agglomerate. Therefore the agglomerates represent pockets of lithic material, probably original agglomerate clasts that were preserved from alteration and metamorphism due to their higher competence and to the fact that deformation partitioned around them. As such they might provide an estimate of magma composition; however their small size (< 5 cm) and relatively coarse crystal size preclude them delivering a representative whole rock composition. The presence of recrystallised glass shards pseudomorphs and the euhedral poly-mineral quartz and feldspars assemblages in agglomerate clasts described above are evidence that the main chemical features of the Theespruit schists (SiO_2 range, relatively high-K_2O, low-CaO contents, flat HREE pattern) are representative of their magmatic composition. The fact that these chemical characteristics are very similar to the primary igneous characteristics of the Moodies granites suggests that the compositions of the compositions of the Moodies granites reflect a representative sample of ca 3.55 Ga K-rich felsic magmatic event. This conclusion is extrapolated to the ca 3.45 and 3.25 K-rich felsic magma systems. .

In contrast with the Moodies granites, potassium feldspar is absent in the Theespruit felsic metavolcanic rocks despite some of the rocks containing up to 6 wt% K_2O. In average, the K_2O content of the schists are lower than the one of the granites. Indeed, we believe that the K-feldspars have completely reacted to muscovite because of the hydration which is a consequence of the deformation and of the amphibolite facies metamorphism that the rocks undergone. In these rocks the ratio of K/Na is generally lower the Moodies granites and A/CNK values are higher. This may represent the leaching of potassium from the Theespruit metavolcanic rocks during 3.23 Ga metamorphism, or the fact that the more sodic less potassic varieties represent magma compositions that are not preserves within the Moodies clast population, perhaps because such rocks were less resistant to weathering. The fact that the more sodic components of the Theespruit formation metavolcanic rocks have A/CNK values that are similar to those of the more potassic rocks (A/CNK = 1.2 to 1.4) (Figure 8) indicates that the low K/Na ratios are likely to be primary and not solely a consequence of leaching. Additionally the Theespruit schists have a wider compositional range of some trace element compared to the Moodies granites (Ba, La, Ce…) and that they have on average lower Ni content. However the main characteristics of the Moodies granites (low-CaO, high-Na_2O, flat HREE pattern…) are faithfully replicated in the schists. Thus, consideration of the combined dataset including both the Theespruit felsic lavas and

the Moodies granites gives us a better idea of the chemical range of granite magmatism in the Barberton greenstone belt at 3.55 Ga.

7.3 S-type granites

The Moodies granites are generally peraluminous (A/CNK average >1.1) with an average normative (CIPW) corundum of 2.87 %. Following the Chappel and White classification (A/CNK>1.1; normative corundum >1%), the Moodies granites and Theespruit formation felsic schists, in term of their composition, belong to the S-type granites which are generally considered as being generated through anatexis of metasedimentary rocks. The Moodies granites are similar to S-type granites in many respects: 1) they have similar average Mg# (38 and 35. respectively, Table 1, Figure 9); 2) their maficity index (FeO_t+MgO) (s.s.) are within the same range, from 0.12 to 6.09 wt% and from 0.183 to 14.71 wt%; 3) they have similar $(La/Sm)_N$ ratio (Figure 11a); 4) neither the Moodies granites nor the S-type granites show correlation between their CaO content and their Eu/Eu*; 5) the range of Sr and Th content of both type of granite is identical (Figure 10 and Table 1) and 6) the accessory mineral suite presents in the Moodies granites and as inclusion in their magmatic zircons is typical of S-type granite. However, despite these similarities, there are also some important differences: (1) the Rb content of the Moodies granites is on average approximately a quarter lower than that of S-type granites (57 ppm and 244 ppm respectively), (2) the Eu anomaly of the Moodies granites is not significantly deep (0.51 for S-type granites against 0.76 for average Moodies granites), (3) the zircons do not have inherited cores, (4) the $\delta^{18}O$ values of the zircons are low compared to the values expected for modern S-type granites zircons ($\delta^{18}O$>8 ‰), (5) the CaO content of the Moodies clasts is very low and uncorrelated with Sr (Figure 14), (6) the Moodies granites have high Ni and Cr contents for felsic rocks (7) the U concentration in S-type granites is double (6.9 ppm) that of the Moodies granites (2.7 ppm) and the $(Gd/Yb)_N$ ratio of the Moodies granites are a bit lower than the one of the S-type granites (Figure 11a).

These differences are important as they potentially reflect systematic differences in source composition and/or the conditions of melting of the BGB S-type granites relative to their younger counterparts. On one hand the high Rb, Ni and Cr contents of the Moodies granites, as well as their oxygen isotopic composition, can be regarded as inherited from the source. The $\delta^{18}O$ values of the zircons (between 5 and 6 ‰) indicates that the source did not contain high $\delta^{18}O$-minerals (such as clays) and was not typical of post-Archean pelites. On the other hand the very low CaO content of the Moodies granites, their high Sr content and their Eu/Eu* value (close to 1) is interpreted to primarily reflect the conditions under which partial melting occurred. Indeed, in rocks with where high Sr content is correlated to high CaO content (like S-type granites, BGB TTG and Archean sedimentary rocks (Figure 15)), Ca and Sr have similar behaviour and are hosted in plagioclases. However in the Moodies granites, the high Sr content is uncorrelated with their low CaO content which we believe can be explained by the fact that Ca and Sr have

behaved differently during the melting process to produce a low-CaO and Sr-rich melt. In this hypothesis the chemistry of the Moodies granites requires melting at high pressures of a source that had the CaO derived from the substantial former plagioclase component as indicated by the significant Sr content, residing within minerals that are not reactants in the partial melting process. Similar observations than the later one on have been made on some TTG rocks due to the fact that their Sr contents are also considerably high relative to the CaO contents. In this case, it has been concluded that the high Sr and relatively low CaO content of the magmas are an indication that they formed at a pressure above that at which plagioclase is a stable phase (Moyen, 2011). In the TTGs, the high pressure of melting is corroborated by their steep REE patterns (which indicate the presence of garnet as a stable phase in the residue of melting) and by their negative Nb anomaly (which requires the presence of rutile in the residue of melting). Similar arguments to those used to argue for the TTG being produced at high pressure can be put forward to explain the low CaO content of the Moodies granites. Additional evidence also indicates that the melting reaction occurred at high pressure: indeed rutile is present as a primary and early formed magmatic accessory phase in the granites, which indicates that it was likely to have been stable phase in the residuum (as shown by the slightly negative Nb anomaly (Figure 11a) and the low Nb/Ta ratio (John et al, 2010)). This illustrates that melting occurred at high pressure as in an appropriate experimental system rutile is stable above 1.8 GPa at 850 ˚C, decreasing to 1.0 GPa at 930 ˚C (Auzanneau, 2005). Additionally, in appropriate system (quartz-feldspar-biotite greywacke), plagioclase will not be stable at high pressures.

The only other possibility that could explain why the Sr of the Moodies granites is high relative to their CaO content, to which it is uncorrelated, is the following: partial melting happened during anatexis at normal pressure conditions (at conditions where plagioclase is a stable phase, <1 GPa) (Vielzeuf and Montel, 1994; Montel and Vielzeuf, 1997), but the source of the granites was very unusual as it had a “normal” CaO content (if melting happened close to the solidus) but was extremely rich in Sr. However a sedimentary source with such characteristics does not seem to exists in the Archean as there are no sediments with these characteristics either (Figure 16). Additionally, invoking melting of a weird source as the one describe above, three times seem unrealistic, therefore we argue that melting of a “normal” source (in term of Sr and CaO contents) at high pressure is the only mechanism able to reproduce the high Sr and low CaO nature of the Moodies granites.

In order to constrain the temperature of melting, we have measured the titanium content of the zircon and applied the Ti-in-zircon thermometer. The temperatures obtained range from 675 to ca. 1008 °C (with an average of ca. 794 °C, Supplementary Table 3). As all the zircon in the rocks is magmatic, the Zr solubility thermometer (Baker et al., 2002) can provide a minimum estimate of magma temperature. This produces temperature estimates of 666 to 876 ˚C, Supplementary Table 1). In combination

these adapt are considered to give an estimate of the minimum magma temperatures between 770 and 840 °C respectively. The high level intrusive and volcanic nature of the Moodies granites indicates that the magma was strongly water-undersaturated in the source and therefore able to intrude at high levels in the crust and erupt. Moreover, the chemistry of the Moodies granites appears to require the partial melting of a source that is sufficiently rich in aluminium to produce peraluminous magma (as indicated by the presence of monazite in the granites and as inclusions in the zircons, and reflected by their A/CNK ratio), that is rich in Ni and Cr, yet with variable K_2O and Na_2O contents (as required by the variable K_2O/Na_2O ratios of the granites).

The three major rock types associated with the BGB that have the potential to generate granite with characteristics similar to the Moodies granites are the TTG, K_2O-enriched mafic rocks or sediments poor in clay minerals. As concluded by Sanchez-Garrido et al. (2011) typical TTG rocks can not be the source of the granites as such rocks have Ni and Cr contents that are similar to or lower than the granites. A recent study (Schmidt et al, 2004) shows that melting at high pressure (above plagioclase stability) of a relatively K_2O-rich mafic rocks (MORB) can generate peraluminous granite compositions similar to those documented in this study. However, such melting fails to reproduce the very low CaO content that is characteristic of the Moodies granites. Moreover, melting of such a source at high pressure seem to only produce melts at high temperature (mostly >875°C) which do not correspond to the Ti-in Zircon temperatures documented in this study. In conclusion, the most suitable source for the granite appears to be clay-poor, immature sediment, rich in quartz and plagioclase i.e. a greywacke.

To summarise, the melting conditions however seem to have happened under fluid-absent conditions and at a minimum temperature between 770 and 840 °C, at pressure above the one at which plagioclase are a stable phase. Few experiments have examined the melting process of greywacke at high pressure (Auzanneau, 2005; Schmidt et al., 2004; Auzanneau et al., 2006). The most suitable experimental work we can use to discuss the validity of this process (e.g. melting of a coarse immature quartz and plagioclase rich sedimentary source, at high pressure) are the experiments done by Schmidt et al (2004) and Auzanneau (2005 and 2006). Therefore use the results of these works as a basis for modelling the major and trace elements compositions that will be produced by such melting. The challenge is to determine which of the melting reaction can produce a granitic melt with the main characteristics of the Moodies granites, e.g., with high K_2O, low CaO, high Ni, flat HREE and no significantly deep europium anomaly.

7.4 Petrogenetic modelling

7.4.1. Major elements

As discuss above, the greywacke based experiments of Schmidt et al (2004) and Auzanneau (2005) are the only suitable experiments that exist in the literature to test high-pressure (above 10 kbars) partial melting as the process relevant to the genesis

Minerals composition	Cpx	Phengite	Rutile	Quartz	Monazite	Garnet
SiO_2	55.14	48.58		100.00		38.68
Al_2O_3	17.07	28.29				20.94
Fe_2O_3	6.86	2.78				28.58
MgO	5.37	3.88				6.58
CaO	6.34	0.22				4.78
Na_2O	8.40	0.71				0.25
K_2O	0.09	9.73				0.06
TiO_2	0.59	2.52	100.00			0.83
P_2O_5	0.00				30.00	0.00
Total	99.86	95.73	100.00	100.00	30.00	98.68
Mineral Proportion	0.22	0.17	0.00	0.43	0.00	0.18
F (Melt fraction)						0.27
Kd						
Cr	30.00		80.00	0.11		4.00
Ni				0.00		
La	0.52	0.78		0.01	3200.00	0.16
Ce	0.85	0.88	0.00	0.06	3413.00	0.35
Pr	1.50	0.07			3589.00	
Nd	1.28	0.90		0.01	3726.00	0.27
Sm	1.81	1.00	0.00	0.01	2859.00	1.04
Eu	2.50	0.58		0.03	228.00	1.50
Gd	1.41	0.60		0.01	2650.00	10.00
Tb		0.70		0.01	6600.00	18.00
Dy	1.22	0.50		0.01	1429.00	26.00
Ho	2.80				920.00	28.20
Er	1.14	0.41		0.01	585.00	38.00
Tm				0.00	385.00	45.00
Yb	1.14	0.32		0.01	273.00	38.00
Lu	1.28		0.40	0.00	174.00	35.00
Ta	0.50		113.00	0.00		
Nb	0.20		51.10	0.01		0.50
Rb	0.03			0.01		0.00
Sr	0.50		0.01	0.02		0.02
Y	2.80			0.01	1231.00	34.00
Cs	0.01			0.00		
Ba	0.10			0.00	0.00	0.00

Table 1. Major elements composition (Auzanneau, 2005; experiment PC3-2001-11) and partition coefficient (modified from Montel, 1996; Harris and Inger, 1992 and London, 1997) for the relevant mineral used in the petrogenetic modelling of the Moodies granites.

of the Moodies granites. We compare the anhydrous melts generated in the experiments of Auzanneau (2005) to the sample C44 which is the most mafic rock of the Moodies granites.

Partial melting at pressures above plagioclase stability: Here we test if melting at high pressure of a metagreywacke source could produce melts with the same characteristics than the melt from which the Moodies granites arose. We choose to compare the major elements composition of the melt produced at 2.4 GPa -870°C by Auzanneau (2005) (experimental melt PC3-2001-11). Various aspects of the chemistry of this melt match well with those of the Moodies granites: this melt is granitic,

Sample name	Moodies granite C44	Source CEPV	Garnet	Rutile	Calculated melt Composition	Magma	Melt - Granite	Magma - Granite
SiO_2	69.86	71.13	38.68		72.74	68.55	2.88	-1.31
Al_2O_3	15.53	13.17	20.94		16.01	16.57	0.48	1.04
Fe_2O_3t	3.82	5.45	29.58		0.17	3.56	-3.45	-0.08
MgO	1.50	2.40	6.58		0.68	1.36	-0.82	-0.14
CaO	0.10	1.70	4.78		0.12	0.85	0.02	0.55
Na_2O	2.87	3.00	0.25		5.63	5.01	2.76	2.14
K_2O	6.52	2.41	0.08		4.30	3.81	-2.22	-2.71
TiO_2	0.49	0.71	0.83	100.00	0.34	0.48	-0.15	-0.01
Calculated Total	100.48	99.97	99.68	100.00	100.00	100.00		
Fe+Mg (molar)	0.085	0.131	0.563		0.018	0.081		
A/CNK	1.298	1.238			1.133	1.223		
R^2							33.7	15.0

Table 2. Major element chemical modelling for partial melting of a greywacke source (Auzanneau, 2005). The melt composition and magma (Melt + Garnet + Rutile) is compared to the Moodies granites.

peraluminous (A/CNK = 1.12), relatively low in CaO (0.29 wt%), mildly rich in K_2O and Na_2O (respectively 4.61 and 5.19 wt%) and fairly rich in silica (73.20 wt%). The main difference between the experimental melt and the natural rocks is that the Moodies granites include compositions that are substantially more mafic that the experimental melt composition. Indeed, the melt only has a FeO_t+MgO value of 0.71 wt% whereas sample C44, which is one of the most mafic of the granites, has FeO_t+MgO of 4.8 wt%. As the most mafic melt produced between 800 and 900 °C in the experimental work of Auzanneau (2005) contained 2.3 wt% FeO_t+MgO (Figure 15), this may indicate that some mechanism for raising the maficity of the magma is required to explain the most mafic rocks within the Moodies granite suite that does not fall in the range of the experimental melts produced by partial melting of a metagreywacke (Auzanneau, 2005; Figure 15). The fact that the maficity and titanium content of part of the Moodies granites is higher than any of the relevant experimental melts (Figure 15) demonstrates that entrainment of peritectic garnet and rutile into the melt is needed to generate magmas with maficity values that match those of the granites (e.g. Stevens et al 2007). Consequently we have calculated the sufficient amount of peritectic garnet and rutile entrained that is needed to increase the FeO_t+MgO and TiO_2 values of the experimental melt toward value close to the one of the most mafic granites (e.g. C44). Entrainment of 12% of garnet and 0.24% of rutile to the experimental melt PC3-2001-11 is necessary to generate magma that has similar maficity and TiO_2 content than one of the most mafic Moodies granite (C44). This generates a granitic magma, peraluminous, with low CaO content (0.82 wt%), high Na_2O (4.59 wt%) and Al_2O_3 (16.34 wt%). When the resultant magma compositions are compared with the major element composition of most mafic samples of the Moodies granites (C44), the main differences reside in the slightly higher CaO content and lower K_2O/Na_2O ratio of the model magma. These differences can be explained by higher alkali content in the source of the granite. This would result in the melting reaction consuming more K_2O-rich

Sample name	Moodies granite C44	Source	Garnet	Rutile	Calculated melt	Magma	Melt - Granite	Magma - Granite
Cr	14.53	67.00	40.83	818.60	10.21	14.49	4.32	-0.04
Ni	63.75	135.00			72.00	63.48	-8.26	-0.26
La	24.52	37.00	4.18		26.13	23.53	-1.61	-0.99
Ce	52.32	103.00	20.90	0.14	59.72	55.11	-7.40	2.79
Pr	5.91	10.50			6.64	5.86	-0.74	-0.05
Nd	24.20	53.00	7.19		26.62	24.32	-2.43	0.12
Sm	5.48	11.00	6.34		6.09	6.12	-0.60	0.63
Eu	1.21	1.20	1.61		1.07	1.14	0.13	-0.07
Gd	5.77	7.50	28.44		2.84	5.85	2.83	0.08
Tb	1.17	1.50	5.64		0.30	0.92	0.87	-0.25
Dy	6.84	7.50	44.39		1.71	6.72	5.13	-0.12
Ho	1.38	1.50	8.85		0.31	1.32	1.07	-0.07
Er	4.18	4.30	28.45		0.75	4.00	3.44	-0.18
Tm	0.70	0.70	4.89		0.11	0.67	0.59	-0.02
Yb	4.93	5.20	33.18		0.87	4.67	4.05	-0.26
Lu	0.78	0.80	5.35	0.06	0.15	0.76	0.83	-0.02
Ta	1.40	0.65		158.91	1.41	1.37	-0.01	-0.02
Nb	18.18	7.80	0.24	943.95	18.47	18.17	-0.31	0.01
Rb	60.11	80.00			67.78	59.76	-7.87	-0.35
Sr	289.85	145.00	8.55	2.29	327.81	289.62	-37.78	-0.22
Y	38.43	41.50	250.84		7.38	35.97	29.05	-0.46
Cs	1.51	3.20			1.71	1.50	-0.20	-0.01
Ba	763.88	730.00			866.40	763.91	-102.52	0.03
R^2							13028.79	0.88

Table 3. Traces and rare earth element chemical modelling for partial melting of a greywacke source (of an hypothetical composition). Mineral compositions are deduced from the melt composition and their partition coefficient (Table 1). The melt composition and magma (Melt + Garnet + Rutile) is compared to the Moodies granites.

phengite relative to that which occurred in the experiments, thereby also explaining, at least in part, the CaO mismatch. Additionally, melt compositions can only typically be analysed in experiments within which significant melt volumes have been produced. Consequently, such melts will be richer in the more refractory elements than those produced closer to the solidus. In this case, the experiment in question was conducted possibly as much as 70 ºC above the solidus. If the Moodies granite magmas arose from magmas produced at temperatures closer to the solidus, this could also explain the CaO mismatch. Even though the composition of the modelled magma is not a perfect match with the granites (Figure 15), the most important features (low CaO, peraluminous, high K_2O) are well replicated. This suggests that the model has validity.

7.4.2. Trace elements

We used the mineral proportion and mineral composition, as well as the melt fraction of the experiment PC3-2001-11 produced by Auzanneau (2005) to calculate the melt trace and REE composition using an equilibrium batch melting model (equation 1) (Table 1, 2 and 3) at the same melting conditions used for the major element modelling above (2.4 GPa and 870°C). As the source trace and RE elements composition is unknown, a hypothetical source

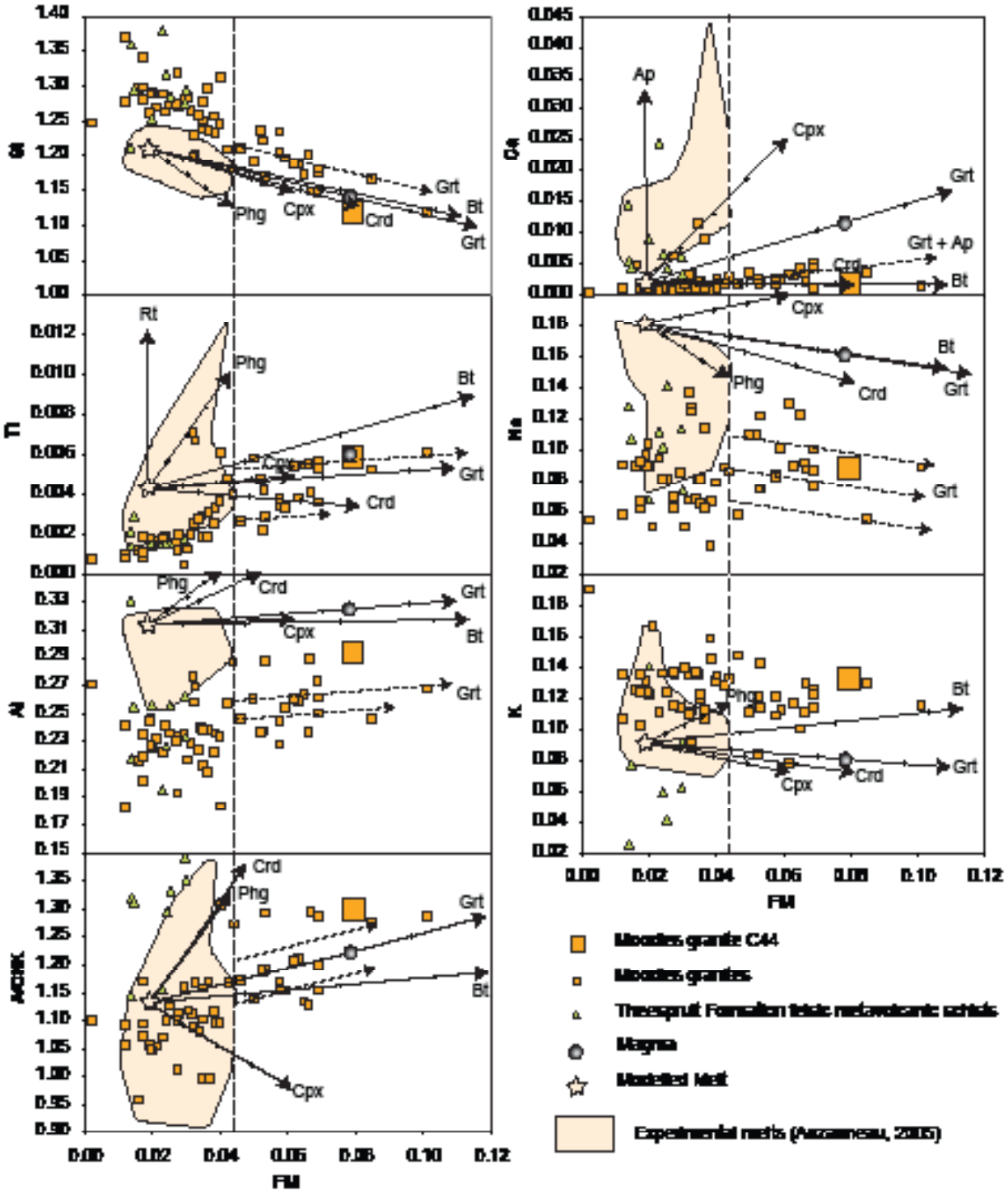

Figure 15. Anhydrous molar maficity vs. major element composition for the modelled melt and magma. The Moodies granites are figured in orange squares. The Theespruit schists are figured in green triangle. The bigger orange square represents the Moodies granitic sample that we are trying to model. The thick dashed line defines the limits of melt composition, solely based on the maficity component. Mineral entrainment to thee melt are represented as vector which are drawn with increments of 5%. Clinopyroxene, Phengite and Garnet composition are from Auzanneau 2005. The pink array represents experimental melts from melting of a greywacke source at high pressure (Auzanneau, 2005).

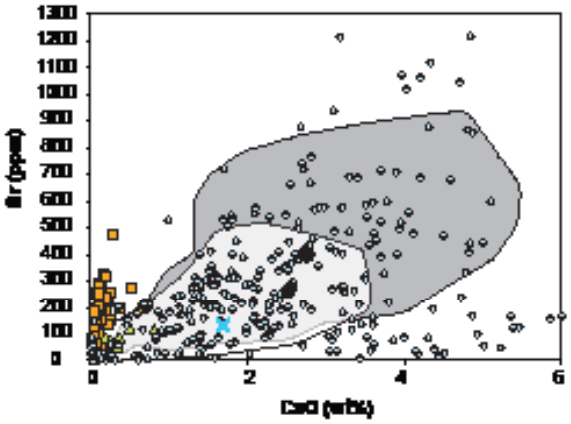

Figure 16. Binary diagrams of CaO vs. Sr content of the freshest Moodies granites (orange squares) and the Theespruit felsic schists (green triangles). The field of the BGB TTG (grey field), of S-type granites (white field) and of Archean worldwide clastic sediments (blue diamond) are displayed for comparison. Amongst the Archean sediments, the average Archean greywacke is figured as a black circle whereas the average of Archean sandstone is displayed as a black diamond. Composition of the source used for the petrogenetic modelling of the Moodies granites is displayed as a blue cross.

composition was chosen which results in a good fit between the modelled magma and the most mafic Moodies granites for all trace elements. The trace element composition of this source is then compared those of appropriate Archean clastic sediments in order to evaluate the degree to which it represents a reasonable and potentially realistic composition:

$$C^i_l = \frac{C^i_0}{D^i + F(1 - D^i)}$$

(Equation 1) and where

$$D^i = \sum_n (x_n * K^{i/l}_n)$$

In equation 1, C_{il} is the concentration of an element i in the melt, and C^i_0 the concentration of the element i in the source. F is the melt fraction, D^i is the general distribution coefficient of the element i in the solid fraction of the partial melting reaction. $Kd^{i/l}_n$ is the partition coefficient of the element i between the mineral n, and the liquid, x_n is the proportion of mineral n.

As illustrated by Figure 17 the source composition required for the modelling to match the most mafic granite compositions is in good agreement with the general characteristics of Archean clastic sediments: the slop of both LREE and HREE are not smooth but are within the range of Archean clastic sediments. The major element content (Figure 15) of the most mafic model magma has been calculated by assuming entrainment of 12 % peritectic garnet and 0.24 % of rutile entrained in the source (Table 1 and 3). Therefore we calculate the magma trace and RE element composition using the calculated melt trace and RE element, but entraining this amount of garnet and rutile. As the source composition is unknown, a hypothetical source composition was chosen which results in a good fit between the modelled magma and the most mafic Moodies granites for all trace elements. This trace element composition of this source is then compared those of appropriate Archean clastic sediments in order to evaluate the degree to which it represents a reasonable and potentially realistic composition:

As illustrated by Figure 19 the source composition required for the modelling to match the most mafic granite compositions is in good agreement with the general characteristics of Archean clastic sediments: the slope of both the HREE and LREE are within the range of Archean clastic sediments. This source is also realistic in that it has a CaO and Sr content in good agreement with Archean clastic sediments in general (Figure 16). The Ni and Cr content

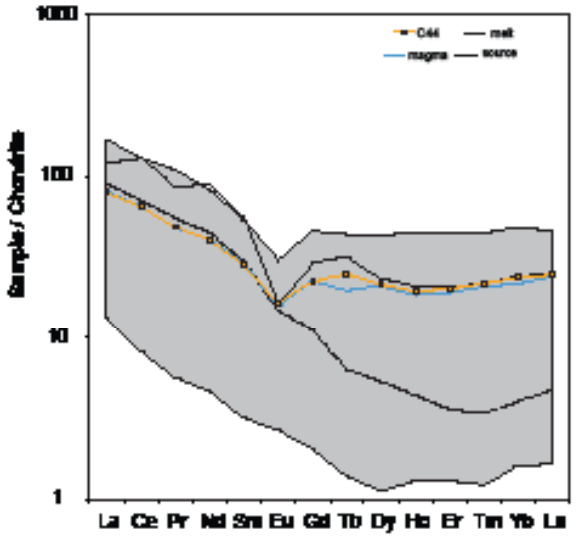

Figure 17. REE diagram (normalised to chondrite) comparing the range of the Moodies granites REE pattern (in grey array) with magma and melts pattern. The melt and magma calculated for the chemical modelling of the Moodies granites are represented, respectively in dashed line and thick blue line. The REE pattern of the source used for the chemical modelling (in case of peritectic phases entrainment) is figured as a thick black line. The sample C44 to which the melt and magma composition are compared is represented in orange.

of the source (135 and 67 ppm respectively) are also within the range shown by Archean clastic sediments (Supplementary Table 1): the Ni and Cr content of average Archean sandstones and greywackes are respectively ca. 79 and 114 ppm and ca. 83 and 194 ppm. This suggests that such HREE-rich Archean sediment used as the source for the Moodies is a viable and a plausible hypothesis.

Figure 18 compares the compositions of the Moodies granites with model granite compositions where the compositional array is expressed solely as a function of variable proportion of garnet entrainment to a single leucocratic melt composition. In terms of their maficity index, most of the Moodies granites fall within the potential compositional range of melts, as defined by the experiments of Auzanneau (2005). The granites with maficity index higher than 0.43 probably do not represent melts but can be explained by entrainment of peritectic phases (here garnet, rutile and probably apatite) to the melt. The large range of variation observed in the major and trace elements composition (Na, Si, Ca, K …) (Figure 15 and 18) can be explained by compositional variability in the source. This is particularly pertinent to these rocks which are not part of only one magmatic suite. It is likely that that source compositional variation plays an important role in shaping compositional variation within each of the three age populations, as there is no correlation between the chemistry and the age of the granites.

Genesis of peraluminous, K_2O-rich, CaO-poor magmas is a process that is not well known on the early Archean. Here we demonstrate that such magmas can be generated either through partial melting of a very unusual source, at "normal" pressure and temperature, or through partial melting of a "normal" source, at high pressure and "normal" temperature. However even if partial melting at low pressure of an unusual source manages to reproduce magma composition in good agreement with the average of the Moodies granites it fails to reproduce the composition of the granites with the highest maficity. Moreover, the partial melting of this unusual source during the three episode magma genesis from which the Moodies granites arose seems unlikely. In contrast, partial melting at unusual conditions (high pressure) manages to produce both average composition and

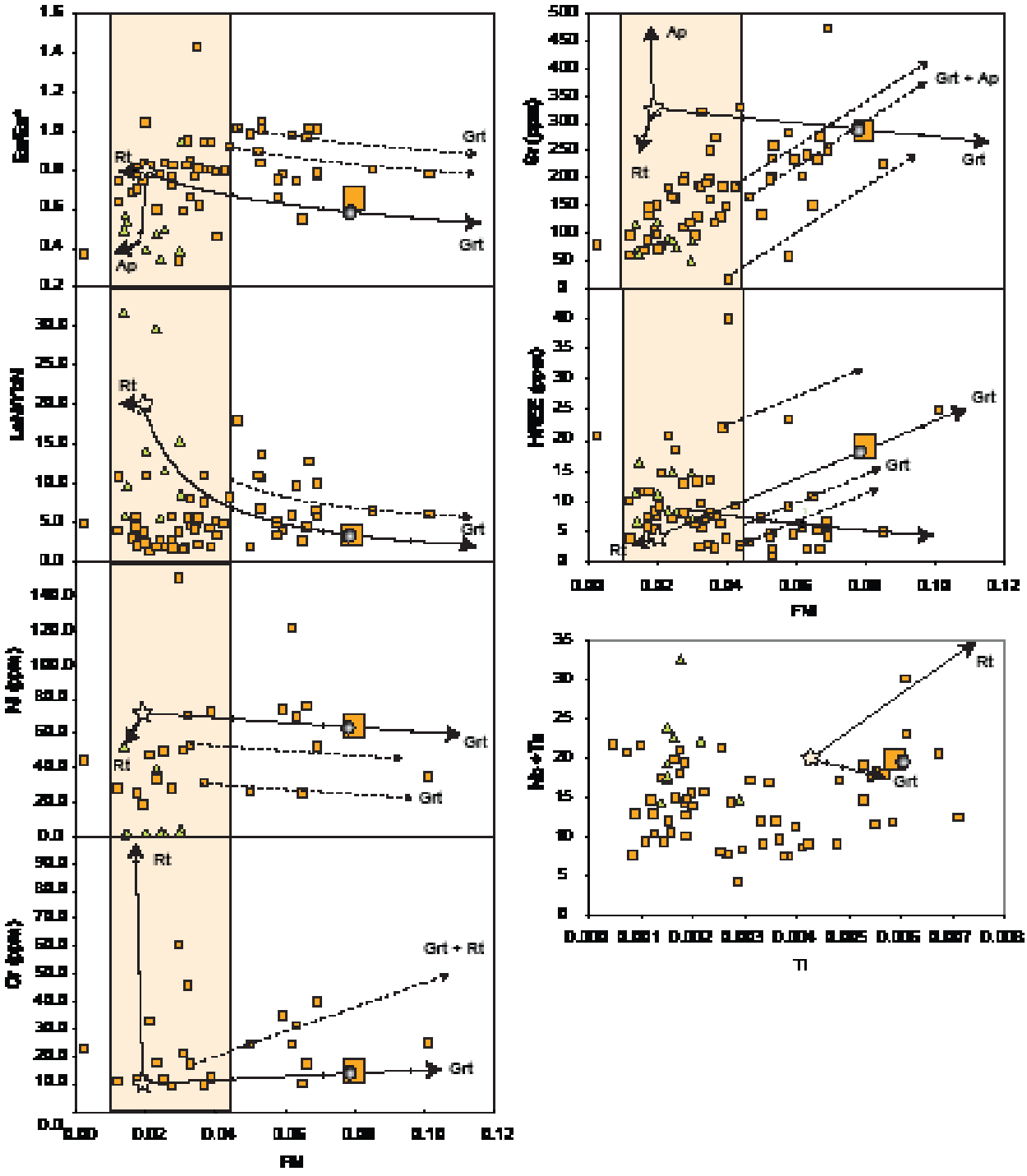

Figure 18. Anhydrous molar maficity vs. trace element composition for the modelled melt and magma. The Moodies granites are figured in orange squares. The Theespruit schists are figured in green triangle. The bigger orange square represents the Moodies granitic sample that we are trying to model. The thick dashed line defines the limits of melt composition, solely based on the maficity component. Mineral entrainment to thee melt are represented as vector which are drawn with increments of 5%. Clinopyroxene, Phengite and Garnet composition are from Auzanneau 2005. The pink array represents experimental melts from melting of a greywacke source at high pressure (Auzanneau, 2005).

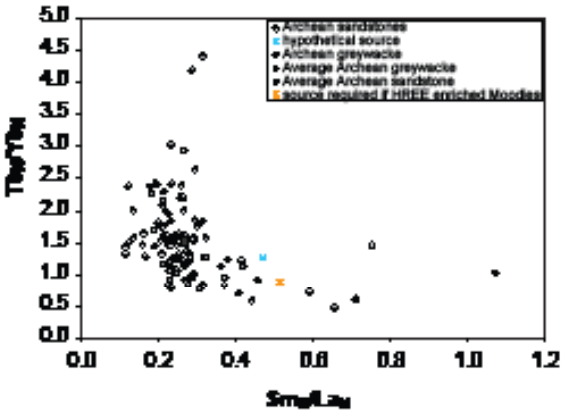

Figure 19. Diagram showing the slope of LREE and HREE (normalised to chondrite) in Archean greywacke and sandstone. The composition of the source used in the partial melting modelling is included as a blue cross (in case of garnet entrainment). The orange cross symbolise the composition of the source required for the chemical modelling if no peritectic phases entrainment is considered. Amongst the Archean sediments, the average Archean greywacke is figured as a black circle whereas the average of Archean sandstone is displayed as a black diamond.

the most mafic composition of the Moodies granites. Additionally, these conditions of pressure and temperature are not so unusual for the BGB, indeed it has been shown that the TTG of the BGB were generated through similar conditions of pressure and temperature (Moyen et al, 2007).

8. IMPLICATIONS FOR THE GENERAL HYPOTHESIS OF K_2O METASOMATISM IN THE BGB

As the chert horizons in Barberton are in general rich in potassium (Rouchon and Orberger, 2008, Hofmann and Harris, 2008), it is also often assumed that the same process (K-Si- metasomatism) was responsible for the K-rich nature of all of the felsic material in the Belt. Strangely, it does not appear to have been considered that the deposition of cherts over K_2O-rich volcanic layers could lead to K_2O increase in the cherts during later metamorphism that drives devolatilization of the K_2O-rich metavolcanic rocks. The potential effect of K_2O-rich volcanic layers can be observed in the chemistry of the Fig Tree group sediments. Indeed this group represents a sediment basin that received the bulk of the detritus from rocks like the Moodies granites. The average composition of the sediments of the northern facies of the Fig Tree group is similar in many ways to the composition of the Moodies granites: it is K_2O-rich, CaO-poor peraluminous. It is then possible that the ca. 3.2 Ga population of the Moodies granites had filled the northern Fig Tree basin. Recycling of potassium from the proto-continental crust into the sediments in the upper crust may then have been a process more efficient than the cycle of erosion/alteration/recycling of TTG to generate the sources for the late potassic batholiths that constitute the volumetrically dominant Granodiorite-Monzogranite-Syenite (GMS) suite of the BGB. This could then explain how the potassic-rich rocks of the GMS suite were generated from a TTG dominant continental crust.

9. CONCLUSIONS

In this study we showed that the composition of the granites and rhyolites from the Moodies group are magmatic. Additionally we proved that the Moodies granites and rhyolites are representative of the magmatic system they

are coming from. However they do not form one single magmatic suite: the felsic schist of the Theespruit formation could be an example of analogous material that are part of the same magmatic event and that have potentially the same source that the Moodies granites.

The Moodies granite have been shown to be analogous to modern S-type granites in many ways, however the differences between the modern S-type granites and the Moodies granites are important as they reflect the composition of the source and the conditions of melting.

We demonstrate that the Moodies granites are generate via low degree partial melting of a HREE-enriched metagreywacke source at high pressures conditions.

In conclusion we infer that the presence of the Moodies granites may result in enrichment in potassium of the proto continental crust.

ACKNOWLEDGEMENTS

Gary Stevens acknowledges the National Research Foundation (NRF, South Africa) funding through the SARChI program. Gary Stevens, Jean-François Moyen, and Hervé Martin acknowledge joint the Centre National de la Recherche Scientifique and NRF funding. We extensively thank Lauren K. Andrews for her major role in the sampling of the Theespruit felsic schists and for her dataset of these rocks. Additionally we thank Justine Jaguin for her analysis of the Moodies conglomerate biotites. We thank Chris Harris for his very helpful reviews of earlier versions of the manuscript.

REFERENCES

Anhaeusser, C.R., (1969). A comparison of pebble and fold deformation in the Nelspruit granite contact aureole, Barberton Mountain Land. Transaction of the Geological Society of South Africa 72, 49-60.

Armstrong, R.A., Compston, W., De Wit, M.J. and Williams, I.S., (1990). The stratigraphy of the 3.5-3.3 Ga Barberton greenstone belt revisited: a zircon ion microprobe study. Earth and Planetary Science Letters 101, 90-106.

Auzanneau, E., (2005). Etude expérimentale des relations de phases dans les metasediments a haute pression et haute température: Application à la croûte continentale subduite. PhD, 290 p.

Auzanneau, E., Vielzeuf, D. and Schmidt, M. W., (2006). Experimental evidence of decompression melting during exhumation of subducted continental crust, Contributions to mineralogy and petrology 152, 125-148.

Azimov, P., Ya and Buschmin, S.A., (2007). Solubility of minerals of metamorphic and metasomatic rocks in hydrothermal solutions of varying acidity: thermodynamic modelling at 400-800ºC and 1-5 kbar. Geochemistry International 45, 1210-1234.

Baker, D. R., Conte, A. M., Freda, C. and Ottolini, L., (2002). The effects of halogens on Zr diffusion and zircon dissolution in hydrous metaluminous granitic melts. Contributions to Mineralogy and Petrology 142, 666-678.

Barker, F. and Arth, J.G., (1976). Generation of trondhjemitic-tonalitic liquids and Archean bimodal trondhjemite-basalt suites. Geology 4, 596-600.

Belcher, R.W. and Kisters, A.F.M., (2006). Progressive adjustments of ascent and emplacement controls during incremental construction of the 3.1 Ga Heerenveen batholith, South Africa, Journal of Structural Geology 28, 1406-1421.

Bell, C.M., (1967). The Geology of the Farm Heemstede 33 and Portions of the Farms Schultzenhorst 31 and Mendon 32 in the Barberton Mountain Land, Ms.C. Thesis, Natal University, Durban, unpublished.

Byerly, G.R., Kröner, A., Lowe, D.R and Walsh,

M.M., (1996). Prolonged magmatism and time constraints for sediment deposition in the early Archean Barberton greenstone belt: evidence from the upper Onverwacht and Fig Tree groups, Precambrian Research 78 ,in: A. Kröner, A. Nutman, Editors , The Oldest Rocks on Earth, pp. 125–138.

Byerly, G.R., Lowe, D.R., Wooden, J.L. and Xie, X., 2002. An Archean Impact Layer from the Pilbara and Kaapvaal Cratons. Science 297, 1325-1327.

Carey, S. and Sparks, R.S.J., (1986). Quantitative models for the fall-out and dispersal of tephra from volcanic eruptions columns, Bulletin of Volcanology 48, 109-125.

Cherniak, D.J., (2010). Cation Diffusion in Feldspars. Reviews in Mineralogy & Geochemistry 72, 691-733.

Chupin, S.V, Chupin, V.P., Barton Jr., J.M, and Barton, E.S., (1998). Archean melt inclusions in zircon from quartzite and granitic orthogneiss from South Africa: Magma compositions and probable sources of protholiths. European Journal of Mineralogy 10, 1241-1251.

Cloete, M., 1991. An overview of metamorphism in the Barberton greenstone belt. In: Ashwal, L.D. (Ed.), Two Cratons and an Orogen-Excursion Guidebook and Review Articles for a Field Workshop through Selected Archaean Terranes of Swaziland, South Africa and Zimbabwe, IGCP Project 280, Dept. of Geology, Univ. Witwatersrand, Johannesburg, pp. 85–98.

Condie, K.C., (1993). Chemical composition and evolution of the upper continental crust: Contrasting results from surface samples and shales. Chemical Geology 104,, 1-37.

Condie, K.C., Archean greenstone belts, 434 pp., Elsevier, Amsterdam, 1981.

Criss, R.E., (2008), Terrestrial oxygen isotope variations and their implications for planetary lithospheres. Reviews in Mineralogy and Geochemistry 68, 511-526.

De Ronde, C.E.J and Kamo, S.L., (2000). An Archaean arc-arc collisional event: a short-lived (ca 3 Myr) episode, Weltevreden area, Barberton Greenstone Belt, South Africa. Journal of African Earth Sciences 30, 219-248.

De Ronde, C.E.J. and de Wit, M.J., 1994. Tectonic history of the Barberton greenstone belt, South Africa: 490 million years of Archean crustal evolution. Tectonics 13, 983-1005.

de Ronde, C.E.J. and Kamo, S.L., 1994. An Archaean arc-arc collisional event: a short-lived (ca. 3 Myr) episode, Weltevreden area, Barberton greenstone belt, South Africa. Journal of African Earth Sciences 30, 219-248.

de Wit, M. J., Armstrong, R., Hart, R. J. and Wilson, A. H., (1987). Felsic igneous rocks within the 3.3-to 3.5- Ga Barberton Greenstone Belt: high crustal level equivalents of the surrounding tonalite-trondhjemite terrain, emplaced during thrusting. Tectonic 6 (5), p.529-549.

de Wit, M.J., Fripp, R.E.P. and Stannistreet, I.G., (1983). Tectonic and stratigraphic implications of new field observations along the southern part of the Barberton Greenstone Belt. Special Publication of the Geological society of South Africa 9, 21-29.

de Wit, M.J., Furnes, H. and Robins, B., (2011). Geology and tectonostratigraphy of the Onverwacht Suite, Barberton Greenstone Belt, South Africa. Precambrian research, v.186, p. 1-27.

Diener, J.F.A., Stevens, G., Kisters, A.F.M, and Poujol, M., (2005). Metamorphism and exhumation of the basal parts of the Barberton greenstone belt, South Africa: Constraining the rates of Mesoarchaean tectonism. Precambrian Research 143, p.87-112.

Diergaardt, B.N., Stevens, G. and Moyen, J.-F., (2011). 3.45 Ga potassic rhyolites of the Hooggenoeg formation: Barberton Greenstone Belt, 23rd Congress of African Geology, Johannesburg, Janvier 2011.

Dziggel, A., Knipper, S. Kisters, A.F.M. and Meyer, F.M. (2006). P-T and structural evolution during exhumation of high-T, medium-P basement rocks in the Barberton Mountain Land, South Africa. Journal of Metamorphic Geology 24, 535-551.

Dziggel, A., Stevens, G., Poujol, M., Anhaeusser, C.R. and Armstrong, R.A. (2002). Metamorphism of the granite-greenstone terrane south of the Barberton greenstone belt, South Africa: an insight in the tectono-thermal evolution of the 'lower' portions of the Onverwacht Group. Precambrian Research 114, 221–247.

Farver, J.R., (2010). Oxygen and Hydrogen Diffusion in Minerals. Reviews in Mineralogy and Geochemistry 72, 447-507.

Fedo, C.M. Nesbitt, H.W. and Young, G.M., (1995) Unravelling the effects of potassium metasomatism in sedimentary rocks and paleosols, with implications for paleoweathering conditions and provenance. Geology 23 (10), 921-924.

Fenn, P.M., (1986). On the origin of graphic granite. American mineralogist 71, 325-330.

Foley, S., Tiepolo, M., and Vannucci, R., (2002). Growth of early continental crust controlled by melting of amphibolite in subduction zones. Nature 417, 837-840.

Gay, N.C., (1969). The analysis of strain in the Barberton Mountain Land, eastern Transvaal, using deformed pebbles. Journal of Geology 77, 377–396.

Harris, N.B.W. and Inger ,S., (1992). Trace element modelling of pelite-derived granites. Contributions to Mineralogy and Petrology 110, p. 46-56.

Hessler, A.M. and Lowe, D.R., (2006). Weathering and sediment generation in the Archean: An integrated study of the evolution of siliciclastic sedimentary rocks of the 3.2 Ga Moodies Group, Barberton Greenstone Belt, South Africa. Precambrian Research 151, p. 185-210.

Heubeck, C. and Lowe, D.R., (1994). Depositional and tectonic setting of the Archean Moodies Group, Barberton Greenstone Belt, South Africa, Precambrian Research 68, 257-290.

Heubeck, C.E. and Lowe, D.R., (1999). Sedimentary petrography and provenance of the Archean Moodies Group Barberton Greenstone Belt. In D. Lowe, G. Byerly, Editors , Geological Evolution of the Barberton Greenstone Belt, South Africa, Boulder, pp. 259-286 (Geological Society of America Special Paper 329).

Hofmann, A. and Harris, C., (2008). Silica alteration zones in the Barberton greenstone belt: A window into subseafloor processes 3.5–3.3 Ga ago, Chemical Geology 257, 221-239

Jahn, B.M., Glikson, A.Y., Peucat, J.J and Hickman, A.H., (1981). REE geochemistry and geochronology of Archaean silicic volcanics and granitoïds from the Pilbara block, Western Australia. Geochimica and Cosmochimica Acta 45, 1633–1652.

John, T., Klemd, R., Klemme, S., Pfänder, J. A., Hoffmann, J. E. and Gao, J., (2010). Nb–Ta fractionation by partial melting at the titanite–rutile transition: Contributions to Mineralogy and Petrology, doi: 10.1007/s00410-010-0520-4.

Kamo, S.L. and Davis, D.W., (1994). Reassessment of Archean crustal development in the Barberton Mountain Land, South Africa, based on U-Pb dating. Tectonics 13, 167–192.

King, E. M., (2001). Oxygen isotope study of magmatic source and alteration of granitic rocks in the Western United States and the Superior Province, Canada. unpublished PhD, University of Wisconsin - Madison.

King, E.M., Barrie, C.T. and Valley, J.W., (1997). Hydrothermal alteration of oxygen isotope ratios in quartz phenocrysts, Kidd Creek mine, Ontario: magmatic values are preserved in zircons. Geology 25, 1079-1082.

Kisters, A.F.M. and Anhaeusser, C.R., (1995). The structural significance of the Steynsdorp pluton and anticline within the tectono-magmatic framework of the Barberton Mountain Land. Journal of the Geological Society of South Africa 98, 43-51.

Kisters, A.F.M., Stevens, G., Dziggel, A. and Armstrong, R.A., (2003). Extensional detachment faulting and core-complex formation in the southern Barberton granite–greenstone terrain, South Africa: evidence for a 3.2 Ga orogenic collapse. Precambrian Research 127, 355-378.

Kisters, A.F.M., Stevens, G., Van Reenen, D., 2004. Excursion Field Guide: The Kaapvaal Traverse. 17–23 July 2004. Geoscience Africa, University of Witswaterrand, Johannesbourg.

Kröner, A. and Compston, W., (1988). Ion microprobe ages of zircons from Early Archean pebbles and greywacke, Barberton Greenstone Belt, southern Africa. Precambrian Research 38, 367–380.

Kröner, A., Byerly, G.R. and Lowe, D.R., (1991).

Chronology of early Archaean granite-greenstone evolution in the Barberton Mountain Land, South Africa, based on precise dating by single zircon evaporation. Earth and Planetary Science Letters 193, 41–54.

Kröner, A., Hegner, E., Wendt, J.I. and Byerly G. R., (1996). The oldest part of the Barberton granitoid-greenstone terrain, South Africa: evidence for crust formation between 3.5 and 3.7 Ga. Precambrian Research 78, 105-124.

Lackey, J. S., Valley, J. W., Chen, J. H. and Stockli, D. F., (2008). Dynamic Magma Systems, Crustal Recycling, and Alteration in the Central Sierra Nevada Batholith: the Oxygen Isotope Record. Journal of petrology 49 (7), 1397-1426.

Lackey, J.S., Valley, J.W., Chen, J.H. and Stockl, D.F., (2008). Dynamic Magma Systems, Crustal Recycling, and Alteration in the Central Sierra Nevada Batholith: the Oxygen Isotope Record. Journal of Petrology 49, 1397-1426.

Lana C., Tohver E. and Cawood, P., (2010). Quantifying rates of dome-and-keel formation in the Barberton granitoid-greenstone belt, South Africa. Precambrian Research 177, 199-211.

London, D., (1997). Estimating Abundances of Volatile and Other Mobile Components in Evolved Silicic Melts Through Mineral–Melt Equilibria. Journal of Petrology 38, 1691-1706.

London, D., (2008). Pegmatites. Canadian Mineralogist, Special Publication 10.

Lowe D.R., (1999). Geologic evolution of the Barberton Greenstone Belt and vicinity. In Lowe, D.R., Byerly, G.R., Editors , Geologic Evolution of the Barberton Greenstone Belt, Boulder, pp. 287–312 (Geological Society of America Special Paper 329).

Lowe, D.R. (1982). Comparative sedimentology of the principal volcanic sequences of Archean greenstone belts in South Africa, Western Australia, and Canada: implications for crustal evolution. Precambrian Research 17, 1–29.

Lowe, D.R. and Byerly, G.R., (2007). An Overview of the Geology of the Barberton Greenstone Belt and Vicinity: Implications for Early Crustal Development. Developments in Precambrian Geology 15, 481-528.

Lowe, D.R., 1994. Accretionary history of the Archean Barberton Greenstone Belt (3.55-3.22 Ga), southern Africa. Geology 22, 1099-1102.

Martin, H, (1986). Effect of steeper Archean geothermal gradient on geochemistry of subduction-zone magmas, Geology 14, 753-756.

Martin, H. and Moyen J.-F. (2002). Secular changes in tonalite-trondhjemite-granodiorite composition as markers of the progressive cooling of the Earth. Geology 30, 319–322.

Martin, H. and Moyen, J-F. (2005). The Archaean-Proterozoic transition: sanukitoid and Closepet type magmatism, Mineralogical Society of Poland, Special paper, 26.

Martin, H., (1987). Petrogenesis of Archaean Trondhjemites, Tonalites, and Granodiorites from Eastern Finland: Major and Trace Element Geochemistry, Journal of Petrology 28, 921-953.

Montel, J.-M. and Vielzeuf, D., 1997. Partial melting of metagreywackes, Part II. Compositions of minerals and melts. Contributions to Mineralogy and Petrology 128, 176-196.

Montel, J.M., (1996). Géochimie de la fusion de la croûte continentale. University of Blaise Pascal, Clermont-Ferrand

Moyen, J.-F. and Stevens, G., (2006). Experimental constraints on TTG petrogenesis: implications for Archean geodynamics, in: Benn, K., Mareschal, J.-C., Condie, K.C. (Eds.), Archean geodynamics and environments. AGU monograph 164, 149-178.

Moyen, J-F. (2011). The composite Archaean grey gneisses: Petrological significance, and evidence for a non-unique tectonic setting for Archaean crustal growth. Litho 123, 21-36.

Moyen, J-F., Stevens, G., Kisters, A. F.M. and Belcher, R.W., (2007). TTG Plutons of the Barberton Granitoid-Greenstone Terrain, South Africa. Developments in Precambrian Geology 15, 607-667.

Nair, R. and Chacko, T., (2008). Role of oceanic plateaus in the initiation of subduction and origin of the continental crust. Geology 36, 583-586.

Nesbitt, H.W. and Markovics, G. (1997). Weathering

of granodioritic crust, long-term storage of elements in weathering profiles, and petrogenesis of siliciclastic sediments. Geochimica and Cosmochimica. Acta 61, 1653–1670.

Nesbitt, H.W. and Young, G.M. (1982). Early Proterozoic climates and plate motions inferred from major element chemistry of lutites. Nature 299, 715–717.

Nesbitt, H.W. and Young, G.M. (1989). Formation and diagenesis of weathering profiles. Journal of Geology 97, 129–147.

Nesbitt, H.W. and Young, G.M. (1996). Petrogenesis of sediments in the absence of chemical weathering: effects of abrasion and sorting on bulk composition and mineralogy, Sedimentology 43, 341-358.

Nesbitt, H.W., Young, G.M. (1984). Prediction of some weathering trends of plutonic and volcanic rocks based on thermodynamic and kinetic considerations. Geochimica and Cosmochimica Acta 48, 1523–1534.

Nockolds, S.R., (1954). Average chemical compositions of some igneous rocks. Geological Society of America Bulletin 65, 1007–1032.

Prouteau, G., Scaillet, B., Pichavant, M. and Maury, R.C. (1999). Fluid-present melting of ocean crust in subduction zones. Geology 27, 1111-1114.

Rapp, R. P., Watson, E.B. and Miller, C.F. (1991). Partial melting of amphibolite/eclogite and the origin of Archean trondhjemites and tonalites, Precambrian Research 51, 1-25.

Rapp, R.P., Shimizu, N. and Norman, M.D. (2003). Growth of early continental crust by partial melting of eclogite. Nature 425, 605-609.

Reimer, T.O., Condie, K.C., Schneider, G. and Georgi, A. (1985). Petrography and geochemistry of granitoid and metamorphic pebbles from the early Archean Moodies Group, Barberton Mountain Land, South Africa. Precambrian Research 29, 383–404.

Rouchon V. and Orberger, B., (2008). Origin and mechanisms of K-metasomatism of ca. 3.4–3.3 Ga volcaniclastic deposits and implications for Archean seawater evolution: examples from cherts of Kittys Gap (Pilbara craton, Australia) and Msauli (Barberton Greenstone Belt, South Africa). Precambrian Research 165, 169–189.

Sanchez-Garrido, C.J.M.G, Stevens, G., Armstrong, R.A., Moyen, J-F., Martin, H. and Doucelance, R., (2011). Diversity in Earth's early felsic crust: Paleoarchean peraluminous granites of the Barberton Greenstone Belt, Geology 39, 963-966.

Schmidt, M. W., Vielzeuf, D. and Auzanneau, E. (2004). Melting and dissolution of subducted crust at high pressures: the key role of white micas. Earth and planetary science letters 228, 65-84.

Schoene, B. and Bowring, S.A., (2007). Determining accurate temperature–time paths from U–Pb thermochronology: An example from the Kaapvaal craton, southern Africa, Geochimica et Cosmochimica Acta 71, 165-185.

Singh, J. and Johannes, W., (1996) Dehydration melting of tonalites. Part II. Composition of melts and solids. Contributions to Mineralogy and Petrology 125, 26-44

Stel, H., (1992). Diagnostic microstructures for primary and deformational quartz rods in graphic granites, American Mineralogist 77, 329-335.

Stevens, G. and Moyen, J.-F., (2007). Metamorphism in the Barberton Granite Greenstone Terrain: a record of Paleoarchean accretion, Developments in Precambrian Geology 15, 669-698.

Tarney, J. Weaver, B.L. and Drury S.A., (1979). Geochemistry of Archaean trondhjemitic and tonalitic gneisses from Scotland and E. Greenland, F. Barker, Editor, in Trondhjemites, Dacites and Related Rocks, Elsevier, Amsterdam, 275–299.

Tegtmeyer, A.R. and Kröner, A., (1987). U-Pb zircon ages bearing on the nature of early Archean greenstone belt evolution, Barberton Mountain Land, southern Africa. Precambrian Research 36, 1–20.

Valley, J.W., Kinny, P.D., Schulze, D.J. and Spicuzza, M.J., (1998). Zircon Megacrysts from Kimberlite: Oxygen Isotope Variability Among Mantle Melts. Contributions to Mineralogy and Petrology 133, 1–11.

Van Kranendonk, M.J., Kröner, A., Hegner, E. and Connelly, J., (2009). Age, lithology and

structural evolution of the c. 3.53 Ga Theespruit Formation in the Tjakastad area, southwestern Barberton Greenstone Belt, South Africa, with implications for Archaean tectonics. Chemical Geology 261, 115–139.

Van Niekerk, C.B. and Burger, A.J. (1978). The age of the Moodies conglomerate boulders. Special Publication of the Geological Society of South Africa 4, 99–106.

Vielzeuf, D. and Montel, J.-M., 1994. Partial melting of metagreywackes. Part I. Fluid-absent experiments and phase relationships. Contributions to Mineralogy and Petrology 117, 375-393.

Visser, D.J.L. (1956). The geology of the Barberton area, Geological Society of South Africa Special Publication 15, p. 253 (Compiler).

Xie, X., Byerly, G.R. and Ferrell, R.E., 1997. IIb trioctahedral chlorite from the Barberton Greenstone Belt: crystal structure and rock composition constraints with implications to geothermometry. Contributions to Mineralogy and Petrology 126, 275-291.

Chapter 4: Presentation of the publication

This paper submitted to Chemical Geology, is first-authored by Miss Sanchez-Garrido Cynthia. It describes the samarium and neodymium isotopic composition of the Meso- and Paleo-Archean granites that were the object of the previous paper. This works aims to constraint in detail the isotopic radiogenic signature of the studied granites. This paper also describes the Sm-Nd signatures of the regional Tonalite-Trondhjemite-Granodiorite. This work tries to determine what the Archean mantle characteristics were and how it affected the TTG Sm-Nd characteristics and their signature. Finally, this paper discusses the consequences of the Sm-Nd signatures of the TTG on their petrogenesis model. All calculations and data acquisitions (except Lu-Hf and U-Pb (on LA-ICP MS) isotopic composition of zircons) were lead by Miss Cynthia Sanchez-Garrido under the supervision of Professor Gary Stevens, Professor Hervé Martin, Professor Jean-François Moyen and Doctor Régis Doucelance. Hafnium isotopic composition of the zircons grains were analysed by Dr. Farina. U-Pb dating of zircons by LA-ICP MS was performed by Doctor Dirk Frei. Sm-Nd samples preparation was done mostly by Miss Sanchez-Garrido, helped by Ms Chantal Bosq.

Successive taping of an old reservoir to form Paleo- and Meso-Archean felsic granitic crust: A Sm/Nd and Lu/Hf isotopic study of granitic clasts within the basal conglomerate of the Moodies group, Barberton Mountain Land, South Africa

Sanchez-Garrido, C.J.M.G[a, b, c, d], Doucelance, R.[b, c, d], Martin, H.[b, c, d], Moyen, J-F.[e, b, c], Stevens, G.[a], Farina, F.[a], Frei, D.[a], Gerdes, A.[f] and Bosq, C.[b, c, d]

[a] Center for Crustal Petrology, Department of Earth Sciences, University of Stellenbosch, South Africa Private Bag X-1, Matieland 7602, South Africa

[b] Clermont Université, Université Blaise Pascal, Laboratoire Magmas et Volcans, BP 10448, F-63000 Clermont-Ferrand, France

[c] CNRS, UMR 6524, LMV, F-63038 Clermont-Ferrand, France

[d] IRD, R 163, LMV, F-63038 Clermont-Ferrand, France

[e] Université Jean-Monnet, Laboratoire Magmas et Volcans, Département de Géologie 23 rue du Docteur Michelon, 42023 Saint Etienne, France

[f] Institut für Geowissenschaften, Goethe-Universität, Altenhöferallee 1, 60438 Frankfurt, Germany

Keywords: *Paleo-Archean granites; Kaapvaal Craton, Sm-Nd isotopes, Lu-Hf isotopes*

Abstract

Earth's oldest preserved granitoid crust dates back to the Paleo-Archean and consists predominantly of sodic Tonalite-Trondhjemite-Granodiorite (TTG) granitoids that arose through the partial melting of hydrated metabasalts. In contrast, granites (sensu-stricto), typically appear relatively late in the plutonic record of the old cratons. However, a recent study has demonstrated the presence of Paleo- and Meso Archean granitic and rhyolitic pebbles (s.s.) in the Barberton Greenstone Belt, which are coeval to regional TTG granitoids. Significantly, these pebbles are 26 Ma to 350 Ma younger than the first granitic batholiths described in the Barberton Greenstone Belt. Here we have examined the Sm-Nd and Lu-Hf isotopes of the granitic and rhyolitic pebbles in order to constrain their genesis and better understand their link with TTG granitoids. The Sm-Nd and Lu-Hf isotopic systems revealed a mildly crustal nature of the granites. The Sm-Nd system also showed that the granites were not produced by the melting of regional coeval TTG. Additionally, the depleted model ages calculated for the granitic clasts demonstrated that the protolith, of the sedimentary source of these granites, was extracted from the depleted mantle between at least 3.7 and 3.9 Ga ago. This implies that the recycling of the source of the granite could have started as earlier as 3.9 Ga, and that the Earth was already able to recycle rocks and generate continental crust at that time. This means that rocks which

were produced ca.3.7-3.9 Ga ago, must have subsequently been brought to the surface, eroded and then melted to generate granites, all within 150 Ma. Furthermore, this process happened three times and the source of the granites was similar in all three successive events, perhaps suggesting some kind of vertical dynamic system. Thus the findings of this work are of great importance for the understanding of geodynamic systems which characterised the Archean Earth.

1. INTRODUCTION

Relatively K-rich granites (senso stricto) are common components of the post-Archean upper continental crust (Taylor and McLennan, 1985; Rudnick and Gao, 2003). In contrast, during Archean times, granitoid magmatism was characterised by the more sodic Trondhjemitic, Tonalitic and Granodioritic (TTG) suite of rocks (e.g. Jahn et al. 1981; Condie, 1993; Martin, 1994). The K_2O/Na_2O is typically 0.42 in TTGs, but near unity (0.85) in the post-Archean continental crust (Rudnick and Gao, 2003). This classically reflects the importance of crustal recycling in shaping the composition of the upper continental crust, whereas TTG magmas traduce growth of the continental crust through its derivation by melting of metamafic sources (e.g. Barker and Arth, 1976; Tarney et al., 1979; Condie, 1981; Martin, 1986; Rapp et al., 1991; Nair and Chacko, 2008). Granites (senso stricto) are also present in the Archean but are mostly known in the late Archean, usually at the end of the craton stabilisation. However, until recently, it was commonly assumed that all K-rich Archean granitoids (except sanukitoids) were generated through intra-crustal anatexis of pre-existing continental crust (TTG-like material), with their different chemical varieties being related to melting conditions (depth of melting) and source composition (Sylvester, 1994; and Moyen et al., 2003, for review).

In this paper we report on an unusual variety of granite, which is preserved only as pebbles in the basal conglomerate of the Moodies group, in the Barberton Greenstone Belt (BGB) in South Africa. The pebbles consist of K-rich metaluminous to peraluminous granites and rhyolites that formed during 3 separate magmatic episodes at ca 3.55, 3.45 and 3.23 Ga (Sanchez-Garrido et al., 2011). These episodes coincide with the emplacement of the TTG plutons (Steynsdorp (3.51 Ga), Vlakplaats (3.5 Ga), Stolzburg (3.45 Ga), KaapValley (3.23 Ga) and Nelshoogte (3.21 Ga)) that formed in association with the BGB. In a recent paper, Sanchez-Garrido et al. (2011) showed that the geochemical composition of the Moodies granites and rhyolites precludes their derivation from either recycling of an older TTG-like source, or fractional crystallisation from TTG magma. In other words, the two magma types are possibly linked by geodynamic circumstance, but do not share any magmatic evolution. Consequently, the petrogenesis of theses granites, preserved in the Moodies Group as clasts, is of primary interest to

Archean continental crustal evolution as they were not generated through intra-crustal partial melting of pre-existing juvenile continental crust material but may represent new evidence of crustal components recycling by melting of sediments derived from recently formed arc rocks.

Here, we focus on the comparison between Moodies pebbles and TTGs using Sm/Nd and Lu/Hf isotopic data. For this purpose, we sampled 22 pebbles in 7 outcrops from the basal conglomerate of the Moodies group. In parallel, we studied 19 rocks amongst five different TTG plutons (Nelshoogte, KaapValley, Stolzburg, Vlakplaats and Steynsdorp plutons) in order to have a representative population of the regional TTGs. We will show that the isotopic composition of the Moodies granites and rhyolites are coherent with the petrogenetic scenario based on their geochemistry (Sanchez-Garrido et al., 2011). Moreover, we will show that they were generated by recycling of much older material, and that the TTG material may not be generated by melting of newly formed metamafic crust as suggested by earlier studies, but instead may be formed by old mafic crustal component.

2. REGIONAL SETTING AND SAMPLE DESCRIPTION

The Barberton Granite-Greenstone Terrane (Fig. 1) is a composite terrane that forms the oldest nucleus to the Kaapvaal Craton. It consists in the 3 main lithologies typical of Archean terrains: 1) a TTG gneissic basement, which includes the "Ancient Gneiss complex" (ACG) that has been dated as far as 3.644 ±0.004 Ga (Kröner, 2007). In fact, TTG emplaced during several tectono-metamorphic events, from 3.644 Ga up to 3.216 Ga (Moyen et al., 2007; Kamo and Davis, 1994); 2) The BGB, which consists of both volcanic and sedimentary rocks, emplaced between 3.55 and 3.21 Ga; 3) Late calc-alkaline mozogranitic (s.l.) plutons (Granodiorite-Monzogranite-Syenite (GMS) suite and Dalmein pluton), which intruded the greenstone belt between 3.2 and 2.6 Ga (Davies, 1971; Hawkesworth et al., 1975; Barton et al., 1983).

More recent works showed that, apart from the AGC, the TTG plutons emplaced during 3 main chronological events: 3538-3509 Ma (Vlakplaats and Steynsdorp), 3470-3443 Ma (Stolzburg) and 3227-3216 Ma (Nelshoogte, KaapValley, Badplaas) (de Ronde et al., 1994; Kamo and Davis, 1994; Kisters et al., 2010). The ca 3450 Ma plutons have been proposed to have formed syn-orogenically (de Wit et al., 1992, Schoene et al., 2008) whereas the ca 3230 Ma TTGs were associated with the amalgamation of distinct terranes along the Inyoka-Inyoni fault system (Lowe, 1994; de Ronde and Kamo, 2000; de Ronde and de Wit, 1994; de Wit et al., 1992).

The BGB itself consists of the three lithostratigraphic units of the Swaziland Supergroup that have markedly different characteristics (Viljoen and Viljoen, 1969; Anhaeusser, 1983; Lowe and Byerly, 1999).

i) The lowermost 3550–3250 Ma Onverwacht Group consists predominantly of submarine, shallow-water, ultramafic to mafic volcanic rocks with komatiitic to komatiitic basaltic compositions. These rocks have been

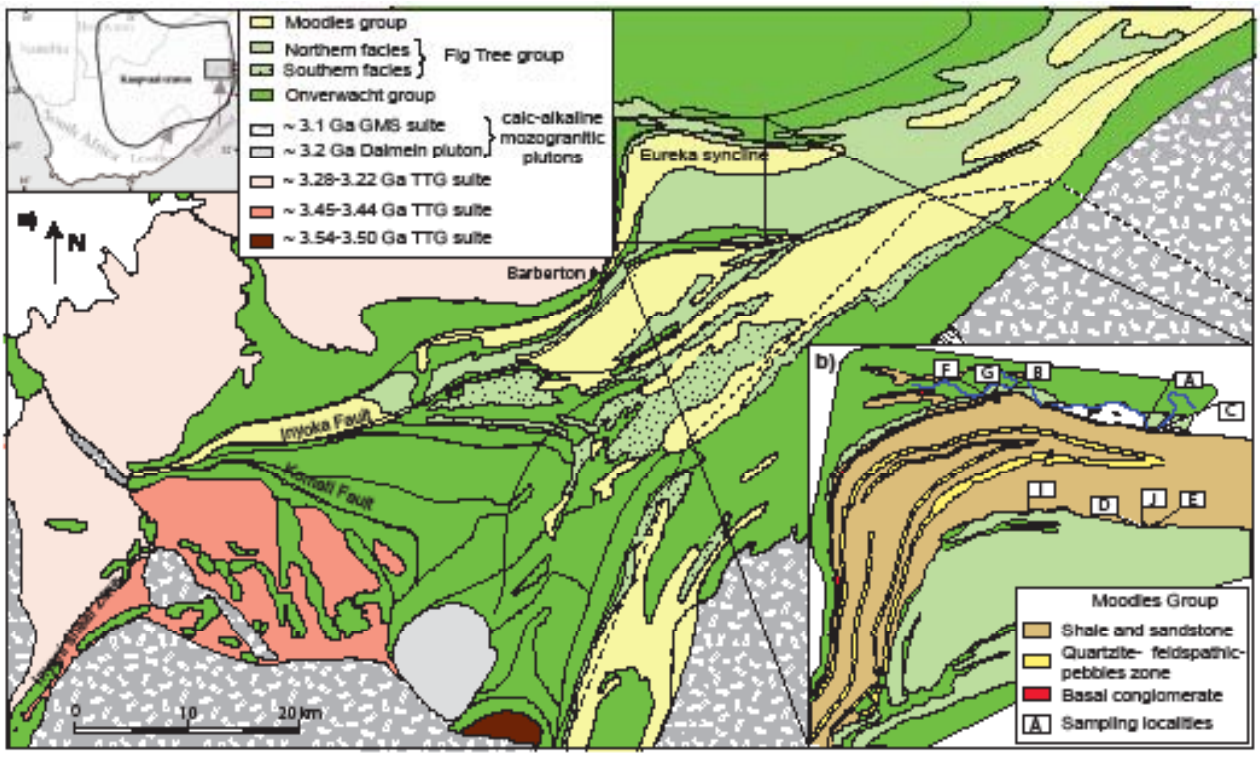

Figure 1. Simplified geological map of the Barberton Greenstone Belt (BGB), highlighting the stratigraphy of the BGB and the ages of the TTGs and younger granitic rocks. The rocks to the south of the Komati Fault have been metamorphosed to amphibolite facies grades as a result of 3230 Ma orogeny, including potassic and felsic volcaniclastic sediments of the Fig Tree Group. The inset represents a detailed geological map of the Eureka Syncline indicating the sample locations of Moodies clasts.

interpreted to represent Archean ocean floor that experienced typical seafloor metamorphism shortly after formation between 3490 and 3450 Ma (de Wit et al., 1987a; de Ronde and de Wit, 1994). The mafic-ultramafic units are interbedded with felsic volcanic rocks, thin cherts, and banded iron formations (BIF). Felsic volcaniclastic units within the lower Onverwacht Group are unique and have been proposed to represent high-level equivalents of TTG plutons of the same age as those intruding the BGB (de Wit et al., 1987b). In addition to the chemical sedimentary rocks that typify the rest of the Onverwacht Group, rare potassic clastic sedimentary layers are also developed within the Theespruit and Sandspruit Formations (Dziggel et al., 2006) that are part of the lowermost Onverwacht Group present mostly in the southern part of the BGB.

ii) The 3260–3250 Ma Fig Tree Group unconformably overlies the Onverwacht Group and it is unconformably overlain by the 3225–3215 Ma Moodies Group (e.g., Lowe, 1999). The Fig Tree Group consists in terrigenous and chemical sediments (shales, BIF, chert-clast in conglomerate, turbiditic greywackes), as well as in intermediate and felsic volcaniclastic rocks (dacitic to rhyodacitic volcaniclastic and volcanic rocks and thin bed of tuffs). These Fig Tree sediments were deposited in an alluvial to shallow-marine fan environment.

iii) The Moodies Group is the youngest group of the Swaziland Supergroup. Its minimum age of deposition has been constrained between

3224 ± 6 Ma and 3207 ± 2 Ma (Tegtmeyer and Kröner, 1987; Heubeck and Lowe, 1994, 1999) and its deposition was completed by 3109 ± 10 Ma (Kamo and Davis, 1994, Heubeck, 1993). The Moodies group is made up of coarse-grained clastic sediments and consists largely of conglomerates and quartzites, as well as shales, BIF and minor volcanics. These rocks have the general character of flysch and molasse assemblages, respectively. Rocks of both Fig Tree and Moodies groups were deposited during active deformation (e.g., Lowe, 1999). This is particularly prominent in the Moodies Group where angular unconformities between units, abundant eroded detritus from the underlying Fig Tree Group, as well as basaltic lavas and tuffs are interpreted to reflect deposition in deforming basins, such as allochthonous piggyback basins, as well as documenting a close association with an arc-terrane during the later stages of evolution (Heubeck and Lowe, 1994; de Ronde and de Wit, 1994). A recent study (Heubeck and Lowe, 1994), focusing on the basal conglomerate of the Moodies group located on the Eureka Syncline (Fig. 1), on the northern part of the belt, and based notably on the thickness variability, compositions of the clasts and paleocurrents, has proposed that most Moodies sediments were coming from the northern part of the BGB. The basal conglomerate of the Moodies group contains pebbles and cobbles of tuff, rhyolite, granite, chert, jaspilite, quartz vein, BIF, shale, silicified ultramafic rocks coming from both the Fig Tree and the Onverwacht groups, in a quartz-rich sandstone like matrix. These granitic and rhyolitic clasts are the subject of the present paper. A detailed map of the sample locations is shown in the inset of figure 1.

The clasts consist mainly in quartz and feldspar bearing tuff, microgranite, medium grained micrographytic granite, and quartz-feldspar-phyric rhyolite; their typical mineral textures are shown in figure 2. They display pristine magmatic textures ranging from microgranular (consistent with crystallisation in sub-volcanic magma chambers) to volcaniclastic textures. Thus, these rocks did not crystallised at great depth but rather formed at surface or within very shallow-level magma chambers.

3. PREVIOUS WORK

Sanchez-Garrido et al. (2011) recently performed an exhaustive SHRIMP U-Pb dating of zircon crystals extracted from the granite pebbles. Associated with 2 previous known SHRIMP analyses for these clasts (Compston and Kröner, 1988), they concluded that the ages of the pebbles cluster in 3 groups corresponding to ages of protolith emplacement at ca. 3519-3554, ca. 3438-3486 and ca. 3210-3295 Ma. In addition, the youngest age constraints the maximum age of deposition of the conglomerates at ca. 3210 Ma.

Two main hypotheses were proposed in order to account for the genesis of the granites and rhyolites, now present as boulders in the basal conglomerate of the Moodies group.

1) Based on a geochemical approach, Reimer at al. (1985) proposed that the granitic clasts were derived from granites from which much residual plagioclase was removed. Therefore the authors concluded that the granites represent evolved liquids produced by fractional crystallisation of a parental magma

generated by melting of TTG or granulite facies gneiss.

2) In contrast, the recent study by Sanchez-Garrido et al. (2011) demonstrated that the granites cannot be derived through recycling of TTG-like source neither by fractional crystallisation nor partial melting. The authors rather proposed that the source of the granitic clasts might be immature sediments deposited on the top of an oceanic lithosphere, and consumed during the destruction of the latter.

The low CaO content of the clasts (0.6 and 0.1 wt%, cf. Sanchez-Garrido et al., 2011) compared to that of TTGs (4 to 1.5 wt%), as well as the higher average Ni content of the clasts (27-96 ppm) compared to that typical of TTGs (< 50 ppm), preclude any magmatic derivation of the clast parental magmas from TTG, including by means ofpartial melting, fractional crystallisation or AFC, etc. For instance, derivation of clast parental magmas by fractional crystallisation of TTG magmas would fractionate amphibole and/or biotite, as well as opaque minerals (magnetite, ilmenite), all with $Kd_{Ni}^{min/liq} >> 1$, and then strongly impoverish the differentiated magma in Ni. This is in opposition with what is observed: the clasts are Ni-richer than their potential TTG parental magma. Similar conclusions can be made from the lack of correlation between the low CaO content of the clasts and their Eu/Eu*, as derivation of clast parental magmas by fractional crystallisation of TTG via plagioclase fractionation will generate deep Eu/Eu*, which are not observed in the clasts (Sanchez-Garrido et al. 2011). In addition, it can also be concluded that Moodies clast cannot derive of melting of the same source as TTG. Indeed such a mafic source (amphibolite) is unable to generate (even at very low degrees of melting < 20%) magmas, or close to the solidus, with both very high K_2O and Ni contents and high Mg#.

Consequently, geochemical data militate against the scenario proposed by Reimer et al. (1985). They are rather consistent with the conclusions of Sanchez-Garrido et al. (2011) who assessed that the parental magma of clasts cannot derive from TTG either through partial melting or fractional crystallisation. It must be concluded that the Moodies clasts derived from another source. As proposed by Sanchez-Garrido et al. (2011) this source may be a relatively immature sediment, rich in quartz and plagioclase, and that melted at high pressure, above the plagioclase stability field. This sediment also need to be Ni- and Cr-rich in order to reproduce the high Ni and Cr content of the clasts, which may indicate involvement of minor mafic or ultramafic component in the source of the clasts.

4. RESULTS

4.1 Analytical procedures

4.1.1. Sm-Nd procedure

Sm/Nd data of the clasts and TTG are reported in Table 1. The samples were crushed using a stainless steel jaw crusher and a representative fraction was powered in an agate ball mill at the Department of Earth Sciences of the Stellenbosch University (South Africa).

Procedures for dissolution of whole-rock powders, Sm and Nd separation, and mass

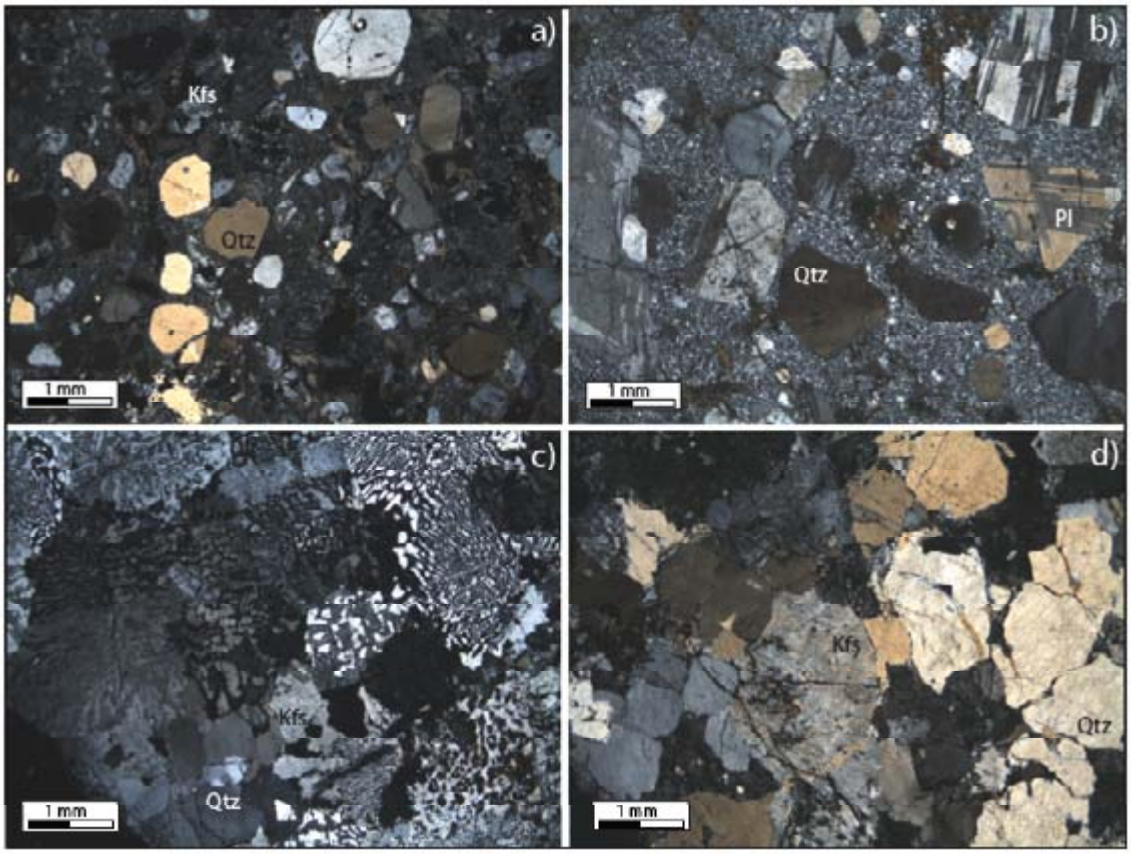

Figure 2: Representative thin section images of the different clasts population
a) Volcanoclastic sample (J5) in which quartz and alkali feldspar represent the main phenocrysts present here.
b) Typical mineral textures in crossed polarized light from a representative rhyolitic clast (B25). This rock is a quartz-K-feldspar-plagioclase-phyric rhyolite showing rounded quartz phenocrysts, an abundance of large euhedral K-feldspar phenocrysts and smaller euhedral plagioclase phenocrysts.
c) A crossed polarized light image of the typical mineral textures in a representative sample medium grained micrographic granite (C33). The texture is characterized by micrographic K-feldspar and quartz intergrowths within which K-feldspar is always present as the nucleus.
d) Fine grain granitic sample (D2). The igneous texture is preserved. Quartz and Kfs represent the main minerals of the rock, Pl (alkali fd) and biotite are present in a smaller amount.

spectrometric techniques were carried out at the Laboratory "Magmas et Volcans" of the Blaise Pascal University (Clermont-Ferrand, France). Acid-digestion of sample powders (100-200 mg) was realized using a HF-HNO_3-$HClO_4$ mixture and a high-pressure bomb (210˚C during 2 days ½). Sm-Nd purification and extraction were performed through the ''cascade'' procedure (AG50X4, TRU Spec. and Ln Spec. columns) described in Pin et al. (1994). Nd Blanks for the total procedure were < 2 ng.

Sm-Nd concentrations and the $^{147}Sm/^{144}Nd$ ratio were determined by isotope dilution, using a ^{150}Nd-^{149}Sm tracer solution. Sm isotopes were measured by thermal ionization mass spectrometry (TIMS) using a fully automated VG-54E mass spectrometer, loaded onto Ta filaments. A typical run consists in at least 5 cycle blocks of measurements with a ^{152}Sm ion beam of 0.5 V. Nd isotope ratios were measured on a TRITON Tl TIMS instrumentation, loaded onto double W filaments. A typical run consists in at least 9 10-cycle blocks of measurements with 30s baseline to allow the full rotation of

the virtual amplificatory system. Sm data were normalised to $^{152}Sm/^{147}Sm = 1.783$. $^{143}Nd/^{144}Nd$ ratios were corrected for mass-fractionation using a power-law and $^{146}Nd/^{144}Nd=0.7219$; they were also normalized to the AMES-Rennes standard using $^{143}Nd/^{144}Nd=0.51196$. Repeated analyses of the AMES-Rennes Nd standard during the period of data acquisition gave $^{143}Nd/^{144}Nd= 0.511958 \pm 0.000004$ (n=9).

4.1.2. LA-ICP MS U-Pb dating of zircons

U-Pb dating of zircons from 4 samples were done by LA-ICP MS. These samples analysed are the same than the one previously analysed for U-Pb by SHRIMP (Sanchez-Garrido et al., 2011). Dating of these grains was necessary to correct the Lu-Hf analysis from the age of the samples.

All U–Pb age data obtained at the Geological Survey of Denmark and Greenland in Copenhagen were acquired by laser ablation - single collector - magnetic sectorfield - inductively coupled plasma - mass spectrometry (LA-SF-ICP-MS) employing a Thermo Finnigan Element 2 mass spectrometer coupled to a NewWave UP213 laser ablation system. All age data presented here were obtained by single spot analyses with a spot diameter of 30 µm and a crater depth of approximately 15–20 µm. The methods employed for analysis and data processing are described in detail by Gerdes and Zeh (2006) and Frei and Gerdes (2009). For quality control, the Plešovice (Sláma et al., 2008) and M127 (Nasdala et al., 2008; Mattey, 2010) zircon reference materials were analysed, and the results were consistently in excellent agreement with the published ID-TIMS ages. Full analytical details and the results for all quality control materials analysed are reported in Table 1 in the electronic supplementary material. The calculation of concordia ages and plotting of concordia diagrams were performed using Isoplot/Ex 3.0 (Ludwig, 2003a, 2003b).

U-Pb ages for the 4 zircon crystals analysed are identical to previously reported SHRIMP ages for the same samples (Sanchez-Garrido et al., 2011).

4.1.3. LA-ICP MS Lu-Hf isotope analysis

Lutetium, hafnium and ytterbium isotopes were analysed in zircon crystals from 4 samples of the Moodies granitic clasts (Table 2) that were also analyse for Sm/Nd isotopes. They were measured at the Goethe University Frankfurt with a Thermo-Finnigan Neptune multicollector ICP-MS coupled to a New Wave Research UP-213 laser system with a teardrop shaped, low volume laser cell, following the procedure described by Gerdes and Zeh (2006, 2009). Data were collected in static mode (^{172}Yb, ^{173}Yb, ^{175}Lu, $^{176}Hf–Yb–Lu$, $1^{77}Hf$, ^{178}Hf, ^{179}Hf, ^{180}Hf) during 55 seconds of laser ablation. Where possible the “Lu–Hf–Yb laser spot” of 40 µm diameter was drilled “on top” of the 20–30 µm “U–Pb laser spot” previously analysed. Care was taken to drill exactly in the same domain (core or rim), which was previously used for U–Th–Pb isotope analyses. These domains were carefully selected on the basis of CL-images. During few ablation sessions the laser position had to be re-adjusted slightly, i.e., by manually moving the laser in x–y direction. This was necessary when the signal strength for ^{180}Hf fell below the critical intensity of 1 volt

	Ech Name	T = Age (Ga)	± 2sig	%	[Sm] Ech ppm	± 2sig	%	143Nd/144Nd Ech meas. (CI)	± 2sig	[Nd] Ech ppm	±	%
Moodies	**B7**	3.226	0.000000008	*0.0083*	3.69	0.02	0.5	0.510792	0.000005	19.64	0.10	0.5
Moodies	**C33X**	3.267	0.000000005	*0.0049*	2.77	0.01	0.5	0.510928	0.000005	13.89	0.07	0.5
Moodies	**B13**	**3.273**	0.000000100	*0.1000*	5.81	0.03	0.5	0.510941	0.000004	29.28	0.15	0.5
Moodies	**J10**	3.277	0.000000007	*0.0066*	5.82	0.03	0.5	0.510679	0.000005	32.08	0.17	0.5
Moodies	***B2***	*3.420*	*0.000000010*	*0.0100*	*1.44*	*0.01*	#	*0.510993*	*0.000005*	*7.29*	*0.04*	#
Moodies	***B14***	*3.450*	*0.000000004*	*0.0038*	*1.04*	*0.01*	#	*0.510679*	*0.000004*	*5.82*	*0.03*	#
Moodies	**J8Y**	3.452	0.000000007	*0.0069*	2.38	0.01	0.5	0.510649	0.000007	12.90	0.07	0.5
Moodies	***B1x***	*3.454*	*0.000000004*	*0.0038*	*2.22*	*0.01*	#	*0.510670*	*0.000004*	*12.46*	*0.06*	#
Moodies	**E4**	3.456	0.000000004	*0.0044*	2.66	0.01	0.5	0.510685	0.000004	14.17	0.07	0.5
Moodies	**D2**	3.463	0.000000150	*0.1500*	4.43	0.02	0.5	0.510570	0.000004	24.63	0.13	0.5
Moodies	**B12**	3.466	0.000000010	*0.0096*	1.18	0.01	0.5	0.510608	0.000007	6.49	0.04	0.5
Moodies	**C4**	3.473	0.000000002	*0.0021*	2.03	0.01	0.5	0.510527	0.000003	11.61	0.06	0.5
Moodies	**E1X**	**3.516**	0.000000073	*0.0730*	2.76	0.01	0.5	0.510206	0.000003	17.54	0.10	0.5
Moodies	***B25***	***3.524***	*0.000000150*	*0.1500*	*1.62*	*0.01*	#	*0.510998*	*0.000005*	*7.90*	*0.04*	#
Moodies	***A3***	*3.527*	*0.000000004*	*0.0038*	*0.85*	*0.00*	#	*0.511022*	*0.000005*	*3.76*	*0.02*	#
Moodies	**A5X**	3.534	0.000000005	*0.0045*	2.73	0.02	0.6	0.510444	0.000003	15.79	0.08	0.5
Moodies	***A8***	*3.534*	*0.000000005*	*0.0053*	*1.45*	*0.01*	#	*0.511056*	*0.000005*	*5.91*	*0.03*	#
Moodies	***C19***	*3.537*	*0.000000004*	*0.0035*	*8.85*	*0.05*	#	*0.510809*	*0.000005*	*48.35*	*0.25*	#
Moodies	***F1***	*3.538*	*0.000000008*	*0.0081*	*3.34*	*0.02*	#	*0.510684*	*0.000004*	*18.57*	*0.10*	#
Moodies	**A1**	3.538	0.000000004	*0.0044*	2.68	0.01	0.5	0.510898	0.000006	12.89	0.07	0.5
Moodies	**A1**	3.538	0.000000004	*0.0044*	2.70	0.01	0.5	0.510901	0.000010	12.83	0.07	0.5
Moodies	**B17**	3.542	0.000000004	*0.0038*	2.40	0.01	0.5	0.510907	0.000005	11.85	0.06	0.5
Moodies	**J9X**	3.555	0.000000010	*0.0097*	4.00	0.02	0.5	0.510513	0.000004	22.57	0.12	0.5
Moodies	**C43**				2.78	0.01	0.5	0.510801	0.000004	14.91	0.08	0.5
Moodies	**C44**				4.31	0.02	0.5	0.511086	0.000003	20.54	0.11	0.5
Moodies	**C12**				2.18	0.01	0.5	0.510584	0.000005	12.57	0.07	0.5
Moodies	**J5X**				1.84	0.01	0.5	0.510519	0.000003	10.59	0.05	0.5

Table 1a. Sm-Nd isotopic data of the Moodies granitic clasts. Data filters are represented in italic.

	Ech Name	147Sm/144Nd	± 2sig	Model Age (CHUR)[1] Ga	±	%	143Nd/144Nd Ech Initial	± 2sig	epsNd CHUR t=T	± 2sig
Moodies	**B7**	0.114	0.001	3.394	0.034	1.00	0.508371	0.000018	-1.43	0.35
Moodies	**C33X**	0.120	0.001	3.432	0.040	1.16	0.508325	0.000019	-1.27	0.37
Moodies	**B13**	0.120	0.001	3.382	0.038	1.13	0.508345	0.000019	-0.73	0.36
Moodies	**J10**	0.110	0.001	3.443	0.032	0.93	0.508303	0.000018	-1.46	0.34
Moodies	***B2***	*0.119*	*0.001*	*3.240*	*0.036*	*1.12*	*0.508300*	*0.000020*	*2.19*	*0.38*
Moodies	***B14***	*0.108*	*0.001*	*3.365*	*0.031*	*0.91*	*0.508222*	*0.000019*	*1.42*	*0.36*
Moodies	**J8Y**	0.112	0.001	3.571	0.036	1.00	0.508102	0.000019	-0.87	0.38
Moodies	***B1x***	*0.107*	*0.001*	*3.370*	*0.029*	*0.87*	*0.508216*	*0.000018*	*1.42*	*0.35*
Moodies	**E4**	0.114	0.001	3.589	0.036	0.99	0.508090	0.000019	-1.01	0.37
Moodies	**D2**	0.109	0.001	3.590	0.032	0.89	0.508082	0.000018	-0.99	0.35
Moodies	**B12**	0.110	0.001	3.573	0.035	0.97	0.508090	0.000019	-0.76	0.38
Moodies	**C4**	0.105	0.001	3.536	0.029	0.83	0.508105	0.000017	-0.27	0.34
Moodies	**E1X**	0.095	0.001	3.658	0.025	0.67	0.507995	0.000016	-1.33	0.31
Moodies	***B25***	*0.124*	*0.001*	*3.464*	*0.043*	*1.25*	*0.508100*	*0.000021*	*0.94*	*0.41*
Moodies	***A3***	*0.137*	*0.001*	*4.130*	*0.068*	*1.64*	*0.507828*	*0.000023*	*-4.33*	*0.45*
Moodies	**A5X**	0.105	0.001	3.643	0.032	0.88	0.507998	0.000019	-0.81	0.37
Moodies	***A8***	*0.148*	*0.001*	*4.956*	*0.107*	*2.17*	*0.507598*	*0.000025*	*-8.67*	*0.49*
Moodies	***C19***	*0.111*	*0.001*	*3.248*	*0.031*	*0.94*	*0.508221*	*0.000019*	*3.66*	*0.37*
Moodies	***F1***	*0.109*	*0.001*	*3.390*	*0.031*	*0.90*	*0.508143*	*0.000019*	*2.15*	*0.36*
Moodies	**A1**	0.126	0.001	3.756	0.049	1.32	0.507952	0.000022	-1.61	0.43
Moodies	**A1**	0.127	0.001	3.808	0.054	1.41	0.507929	0.000023	-2.05	0.45
Moodies	**B17**	0.122	0.001	3.561	0.043	1.20	0.508039	0.000021	0.22	0.41
Moodies	**J9X**	0.107	0.001	3.622	0.031	0.87	0.507996	0.000018	-0.29	0.36
Moodies	**C43**	0.112	0.001	3.334	0.032	0.97				
Moodies	**C44**	0.127	0.001	3.400	0.044	1.31				
Moodies	**C12**	0.105	0.001	3.413	0.029	0.85				
Moodies	**J5X**	0.105	0.001	3.538	0.029	0.83				

Table 1a (continued). Sm-Nd isotopic data of the Moodies granitic clasts. Data filters are represented in italic.

	Ech Name	T_{DM}^2 Ga One stage model	T_{DM}^3 Ga Two-stage model	T_{DM}^4 Ga Regression model	delta T^2	delta T^3	delta T^4
Moodies	**B7**	3.56	3.51	3.46	-0.33	-0.29	-0.23
Moodies	**C33X**	3.60	3.56	3.50	-0.34	-0.29	-0.23
Moodies	**B13**	3.56	3.51	3.46	-0.29	-0.24	-0.18
Moodies	**J10**	3.59	3.55	3.50	-0.31	-0.27	-0.22
Moodies	***B2***	*3.45*	*3.39*	*3.33*	*-0.03*	*0.03*	*0.09*
Moodies	***B14***	*3.52*	*3.48*	*3.43*	*-0.07*	*-0.03*	*0.02*
Moodies	**J8Y**	3.70	3.66	3.61	-0.25	-0.21	-0.16
Moodies	***B1x***	*3.53*	*3.48*	*3.43*	*-0.07*	*-0.03*	*0.02*
Moodies	**E4**	3.72	3.68	3.63	-0.26	-0.22	-0.17
Moodies	**D2**	3.71	3.67	3.63	-0.25	-0.21	-0.16
Moodies	**B12**	3.70	3.66	3.61	-0.23	-0.20	-0.15
Moodies	**C4**	3.66	3.62	3.58	-0.19	-0.15	-0.10
Moodies	**E1X**	3.75	3.72	3.68	-0.23	-0.20	-0.16
Moodies	***B25***	*3.64*	*3.59*	*3.53*	*-0.11*	*-0.07*	*-0.01*
Moodies	***A3***	*4.18*	*4.16*	*4.12*	*-0.65*	*-0.63*	*-0.60*
Moodies	**A5X**	3.75	3.71	3.67	-0.21	-0.18	-0.14
Moodies	***A8***	*4.79*	*4.82*	*4.85*	*-1.26*	*-1.28*	*-1.32*
Moodies	***C19***	*3.43*	*3.38*	*3.33*	*0.10*	*0.15*	*0.21*
Moodies	***F1***	*3.55*	*3.50*	*3.45*	*-0.01*	*0.04*	*0.09*
Moodies	**A1**	3.87	3.84	3.79	-0.33	-0.30	-0.25
Moodies	**A1**	3.91	3.88	3.83	-0.38	-0.34	-0.30
Moodies	**B17**	3.71	3.67	3.61	-0.17	-0.13	-0.07
Moodies	**J9X**	3.73	3.70	3.65	-0.18	-0.14	-0.10
Moodies	**C43**	3.51	3.46	3.41			
Moodies	**C44**	3.59	3.54	3.48			
Moodies	**C12**	3.56	3.52	3.47			
Moodies	**J5X**	3.66	3.62	3.58			

1 Jacobsen and Wasserburg (1980) and Goldstein et al. (1984) values for Chondritic Uniform Reservoir (CHUR)

2 Single, closed-system evolution since the formation of the Earth. Increase of the $^{143}Nd/^{144}Nd$ ratio of the depleted mantle from a chondritic value to 0.51315 (average MORB) in 4.55 Ga results in an actual value of 0.2137 for the $^{147}Sm/^{144}Nd$ ratio.

3 Double, closed-system evolution. From initial to 3.0 Ga, the silicate Earth evolves with a $^{147}Sm/^{144}Nd$ of 0.209; from 3.0 Ga to actual, continuous continental crust extraction until εNd_{DM}=10. This corresponds to a present day $^{147}Sm/^{144}Nd$ of 0.220 (Boyet and Carlson, 2006).

4 DM evolution - $\varepsilon Nd_{DM}(T) = 0.25T^2-3T+8.5$, as proposed by DePaolo (1981).

Table 1a (continued). Sm-Nd isotopic data of the Moodies granitic clasts. Data filters are represented in italic.

	Ech Name	T = Age (Ga)	± 2sig	%	[Sm] Ech ppm	± 2sig	%	143Nd/144Nd Ech meas. (CI)	± 2sig	[Nd] Ech ppm	±	%
NLS	**NLS 7.2/08**	3.21	0.000000010	0.0096	1.82	0.01	0.5	0.511223	0.000004	8.51	0.04	0.5
NLS	**NLS 8.1/08**	3.21	0.000000010	0.0096	2.08	0.01	0.5	0.510882	0.000004	11.03	0.06	0.5
NLS	**NLS 5.3/08**	3.21	0.000000010	0.0096	1.22	0.01	0.5	0.510407	0.000004	8.01	0.04	0.5
NLS	**NLS 5.1/08**	3.21	0.000000010	0.0096	3.31	0.02	0.5	0.511559	0.000004	13.68	0.07	0.5
NLS	**NLS 2.2/08**	3.21	0.000000010	0.0096	1.66	0.01	0.5	0.510391	0.000005	10.96	0.06	0.5
KV	**KV 3.1/08**	3.23	0.000000010	0.0096	2.92	0.02	0.5	0.510987	0.000005	14.89	0.08	0.5
KV	**KV 4.1/08**	3.23	0.000000010	0.0096	3.10	0.02	0.5	0.511138	0.000004	14.90	0.08	0.5
KV	**KV 1.1/08**	3.23	0.000000010	0.0096	2.80	0.01	0.5	0.510862	0.000004	15.00	0.08	0.5
KV	**KV 2.1/08**	3.23	0.000000010	0.0096	2.05	0.01	0.5	0.510857	0.000006	10.94	0.06	0.5
ST	**ST-J7**	3.450	0.000000010	0.0096	1.62	0.01	0.5	0.510444	0.000003	9.64	0.05	0.5
ST	**ST-J19**	3.450	0.000000010	0.0096	2.08	0.01	0.5	0.510478	0.000006	12.25	0.06	0.5
ST	**ST-J23**	3.450	0.000000010	0.0096	1.42	0.01	0.5	0.510485	0.000004	8.27	0.04	0.5
ST	**ST-J33**	3.450	0.000000010	0.0096	1.76	0.01	0.5	0.510801	0.000006	9.02	0.05	0.5
ST	**ST-J6**	3.450	0.000000010	0.0096	1.84	0.01	0.5	0.510499	0.000004	10.62	0.06	0.5
VLK	**VLK 2/08**	3.500	0.000000010	0.0096	3.31	0.02	0.5	0.510621	0.000005	18.90	0.10	0.5
STEY	**STEY 2.2/08**	3.510	0.000000010	0.0096	3.16	0.02	0.5	0.510584	0.000005	18.88	0.10	0.5
STEY	**STEY 1.4/08**	3.510	0.000000010	0.0096	2.61	0.01	0.5	0.510588	0.000004	14.23	0.07	0.5
STEY	**STEY 1.5/08**	3.510	0.000000010	0.0096	1.46	0.01	0.5	0.510387	0.000004	8.56	0.04	0.5
STEY	**STEY 1.7/08**	3.510	0.000000010	0.0096	5.20	0.03	0.5	0.510914	0.000004	25.07	0.13	0.5

Table 1b. Sm-Nd isotopic data of the Barberton Greenstone Belt TTG.

	Ech Name	147Sm/144Nd	± 2sig	Model Age (CHUR)[1] Ga	±	%	143Nd/144Nd Ech Initial	± 2sig
NLS	**NLS 7.2/08**	0.129	0.001	3.194	0.044	1.38	0.508487	0.000020
NLS	**NLS 8.1/08**	0.114	0.001	3.242	0.032	1.00	0.508466	0.000018
NLS	**NLS 5.3/08**	0.092	0.001	3.261	0.021	0.64	0.508454	0.000014
NLS	**NLS 5.1/08**	0.146	0.001	3.263	0.068	2.08	0.508458	0.000022
NLS	**NLS 2.2/08**	0.091	0.001	3.260	0.021	0.65	0.508454	0.000015
KV	**KV 3.1/08**	0.118	0.001	3.222	0.036	1.11	0.508460	0.000019
KV	**KV 4.1/08**	0.126	0.001	3.236	0.041	1.28	0.508452	0.000019
KV	**KV 1.1/08**	0.113	0.001	3.241	0.032	0.98	0.508451	0.000017
KV	**KV 2.1/08**	0.113	0.001	3.266	0.033	1.02	0.508438	0.000018
ST	**ST-J7**	0.101	0.001	3.518	0.027	0.77	0.508131	0.000017
ST	**ST-J19**	0.102	0.001	3.505	0.029	0.82	0.508140	0.000018
ST	**ST-J23**	0.104	0.001	3.541	0.029	0.81	0.508118	0.000017
ST	**ST-J33**	0.118	0.001	3.549	0.039	1.11	0.508118	0.000020
ST	**ST-J6**	0.105	0.001	3.557	0.029	0.82	0.508108	0.000017
VLK	**VLK 2/08**	0.106	0.001	3.395	0.029	0.86	0.508170	0.000018
STEY	**STEY 2.2/08**	0.101	0.001	3.291	0.026	0.79	0.508233	0.000017
STEY	**STEY 1.4/08**	0.111	0.001	3.652	0.035	0.95	0.508013	0.000019
STEY	**STEY 1.5/08**	0.103	0.001	3.667	0.029	0.80	0.507999	0.000017
STEY	**STEY 1.7/08**	0.125	0.001	3.691	0.048	1.30	0.508005	0.000022

Table 1b (continued). Sm-Nd isotopic data of the Barberton Greenstone Belt TTG.

	Ech Name	epsNd CHUR t=T	± 2sig	T_{DM}^2 Ga One stage model	T_{DM}^3 Ga Two-stage model	T_{DM}^4 Ga Regression model	delta T^2	delta T^3	delta T^4
NLS	**NLS 7.2/08**	0.43	0.39	3.44	3.38	3.31	-0.23	-0.17	-0.10
NLS	**NLS 8.1/08**	0.02	0.34	3.44	3.38	3.33	-0.23	-0.17	-0.12
NLS	**NLS 5.3/08**	-0.22	0.28	3.41	3.37	3.32	-0.20	-0.16	-0.11
NLS	**NLS 5.1/08**	-0.13	0.44	3.56	3.49	3.41	-0.35	-0.28	-0.20
NLS	**NLS 2.2/08**	-0.21	0.29	3.41	3.37	3.32	-0.20	-0.16	-0.11
KV	**KV 3.1/08**	0.42	0.36	3.43	3.38	3.32	-0.20	-0.15	-0.09
KV	**KV 4.1/08**	0.26	0.38	3.46	3.41	3.34	-0.23	-0.18	-0.11
KV	**KV 1.1/08**	0.25	0.34	3.43	3.38	3.32	-0.20	-0.15	-0.09
KV	**KV 2.1/08**	-0.01	0.35	3.45	3.40	3.35	-0.22	-0.17	-0.12
ST	**ST-J7**	-0.36	0.32	3.64	3.60	3.56	-0.19	-0.15	-0.11
ST	**ST-J19**	-0.19	0.34	3.63	3.59	3.55	-0.18	-0.14	-0.10
ST	**ST-J23**	-0.61	0.34	3.66	3.63	3.58	-0.21	-0.18	-0.13
ST	**ST-J33**	-0.61	0.39	3.69	3.65	3.60	-0.24	-0.20	-0.15
ST	**ST-J6**	-0.81	0.34	3.68	3.64	3.59	-0.23	-0.19	-0.14
VLK	**VLK 2/08**	1.69	0.35	3.54	3.50	3.45	-0.04	0.00	0.05
STEY	**STEY 2.2/08**	3.19	0.34	3.45	3.41	3.36	0.06	0.10	0.16
STEY	**STEY 1.4/08**	-1.13	0.37	3.76	3.73	3.68	-0.25	-0.22	-0.17
STEY	**STEY 1.5/08**	-1.40	0.34	3.76	3.73	3.69	-0.25	-0.22	-0.18
STEY	**STEY 1.7/08**	-1.29	0.42	3.82	3.78	3.73	-0.31	-0.27	-0.22

1 Jacobsen and Wasserburg (1980) and Goldstein et al. (1984) values for Chondritic Uniform Reservoir (CHUR)

2 Single, closed-system evolution since the formation of the Earth. Increase of the 143Nd/144Nd ratio of the depleted mantle from a chondritic value to 0.51315 (average MORB) in 4.55 Ga results in an actual value of 0.2137 for the 147Sm/144Nd ratio.

3 Double, closed-system evolution. From initial to 3.0 Ga, the silicate Earth evolves with a 147Sm/144Nd of 0.209; from 3.0 Ga to actual, continuous continental crust extraction until eNdDM=10. This corresponds to a present day 147Sm/144Nd of 0.220 (Boyet and Carlson, 2006).

Table 1b (continued). Sm-Nd isotopic data of the Barberton Greenstone Belt TTG.

(Gerdes and Zeh, 2009). Nitrogen (~0.005 l/ min) was introduced via a Cetac Aridus into the Ar sample carrier gas to enhance sensitivity (~10–20%) and to reduce oxide formation.

All analyses with ^{180}Hf signal strength <1 volt have been removed. Additional outliers were removed by using an automated outlier test that was implemented by Gerdes and Zeh. Then, all remaining ratios were used to calculate the average $^{176}Hf/^{177}Hf$ and the standard error (2 SE) for each spot analysis. All data were adjusted relative to the JMC 475 $^{176}Hf/^{177}Hf$ ratio of 0.282160. The effect of the inter-element fractionation on the Lu/Hf was estimated to be about 6 % or less based on analyses of the GJ-1 and Plesoviče zircon. Accuracy and reproducibility were checked by repeated analyses (n = 57 and 10, respectively) of reference zircon GJ-1 and Plesoviče.

For calculation of the epsilon Hf ($\varepsilon_{Hf(t)}$) value, the chondritic uniform reservoir (CHUR) was used as recommended by Bouvier et al (2008): values of $^{176}Lu/^{177}Hf$, $^{176}Hf/^{177}Hf$ and constant decay of 0.0336, 0.282785 and 1.867 x 10-11 yr-1 are used respectively. Initial $^{176}Lu/^{177}Hf_{(i)}$ and $\varepsilon_{Hf(t)}$ for all analysed zircon domains were calculated using the apparent concordant Pb-Pb ages obtained for the respective domains. When the Pb-Pb age of the domain was found discordant, concordant Pb-Pb age of the co-genetic domains was used for the calculation of $^{176}Lu/^{177}Hf_{(i)}$ and $\varepsilon_{Hf(t)}$.

4.2 Sm-Nd results

4.2.1. Moodies clasts

Contrary to major and trace element geochemistry, the radiogenic isotopic composition of rocks is time dependant, consequently, the data discussion will be organized following the crystallisation age of the clasts' parental magmas (Sanchez-Garrido et al.; 2011).

- The 3.54 Ga group

The granitic clasts display a wide range of variations of their initial $^{143}Nd/^{144}Nd$ (corrected for radioactive decay using U-Pb SHRIMP crystallisation ages) from 0.507598 to 0.508221 (ε_{Nd} values comprised between -8.7 and +3.7, see Table 2 and Fig. 4). Such a scatter; however, is mainly related to samples A3 and A8 that display very negative ε_{Nd} of -8.7 and -4.5. The $f_{Sm/Nd}$ factor ranges from -0.2481 to -0.4377 with an average of -0.3945. The Sm/Nd ratio of the clasts are variable (0.17-0.24) but average typical crustal value of 0.20 (Table 2).

- The 3.45 Ga group

The granitic clasts of this group also have an important scatter in their initial $^{143}Nd/^{144}Nd$, with values ranging from 0.508082 to 0.508300 (ε_{Nd} range between -1 and +2.2, Table 2). The $f_{Sm/Nd}$ factor, however, displays less scattered values from -0.3848 to -0.4477 (average $f_{Sm/Nd}$ = -0.4388). Compared to the older group of clasts, the range of the Sm/Nd ratio is limited between 0.17-0.20 and is lower (average 0.18).

- The 3.26 Ga group

The 3.2 Ga clasts all have negative ε_{Nd} values ranging from -0.73 to -1.5 ($^{143}Nd/^{144}Nd$ initial ratio ranging between 0.508303 and 0.508371, Table 2). The $f_{Sm/Nd}$ factor varies between -0.3874 and -0.4424. The Sm/Nd ratio of these

clasts is the less scattered and average a value of 0.19.

The scatter of ε_{Nd} values increase with crystallisation age (Fig. 4), although this observation could be biased by the possible under-sampling of the younger group of pebbles (only 4 samples compared to 9 for the older group). It also appears that initial $^{143}Nd/^{144}Nd$ ratio decrease with the increasing age of the clasts (not shown).

By considering data in groups defined by U-Pd age, the data do not allow drawing whole-rock isochrons in a $^{147}Sm/^{144}Nd$ vs. $^{143}Nd/^{144}Nd$ diagram (MSWD values >>1 traducing the low quality of alignment) except for 3.2 Ga clasts. However, the limited spread in Sm/Nd ratio for the latter samples results in a large error of 790 Ma for a calculated age of 3.603 Ga, thus statistically indistinguishable from the U-Pb crystallisation age (Fig. 5). The absence of Sm-Nd isochrons for clasts which have been shown to be of the same age asks the question of the opening of the Sm/Nd system since the crystallisation of the pebbles (via Sm/Nd fractionation post-crystallisation or Nd-isotopic disequilibrium), which is of particular importance for the interpretation of $^{143}Nd/^{144}Nd$ initial ratios in terms of sources.

4.2.2. Barberton Greentsone Belt TTGs plutons

Collectively, analysed TTGs show a large variation in their Nd initial ratios, with values ranging from 0.508006 to 0.508465 (Table 2). Plutons; however, show more coherent initial compositions, with the exception of sample

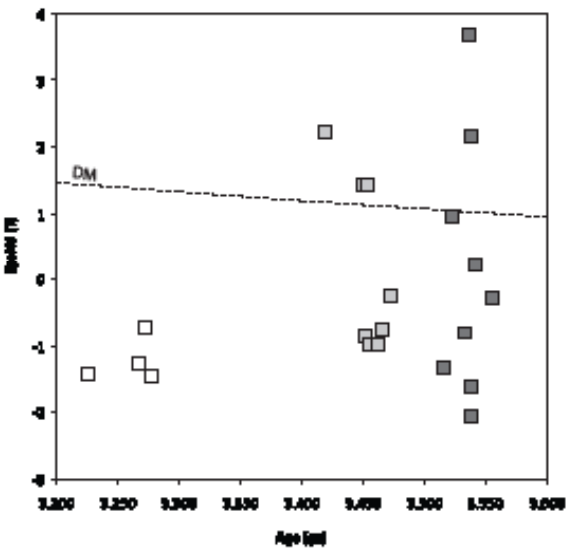

Figure 3. ε_{Nd} vs. age of crystallisation for Moodies granitic clasts (squares). The colour of the symbol is organised according to the age group of the granitic clasts. The Depleted Mantle evolution (dashed line) has been calculated assuming a simple, closed-system evolution since the formation of the Earth. Increase of the $^{143}Nd/^{144}Nd$ ratio of the depleted mantle from a chondritic value to 0.51315 (average MORB) in 4.55 Ga results in an actual value of 0.2137 for the $^{147}Sm/^{144}Nd$ ratio.

STEY 2.2/08 from Steynsdorp.

Sm/Nd data measured for Nelshoogte, KaapValley and Stolzburg define Sm-Nd whole-rock isochrons giving ages of 3253 ± 140 Ma (MSWD = 0.41), 3335 ± 640 Ma (MSWD = 0.21) and 3367 ± 510 Ma (MSWD=0.33), respectively (Fig. 6). Note that larger errors for KaapValley and Stolzburg ages compared to Nelshoogte are resulting from the small variation in the Sm/Nd data only.

Steynsdorp Sm/Nd data; however, do not allow defining an isochron in the $^{147}Sm/^{144}Nd$ vs. $^{143}Nd/^{144}Nd$ diagram. The data seem to be scattered in two groups. Three (over 4) of the analysed points fit on an isochron giving an age of 3537 Ma ± 440 Ma (MSWD = 0.16), whereas the fourth measured sample are significantly outside. When plotted in the same diagram, data by Kröner et al. (1996), together

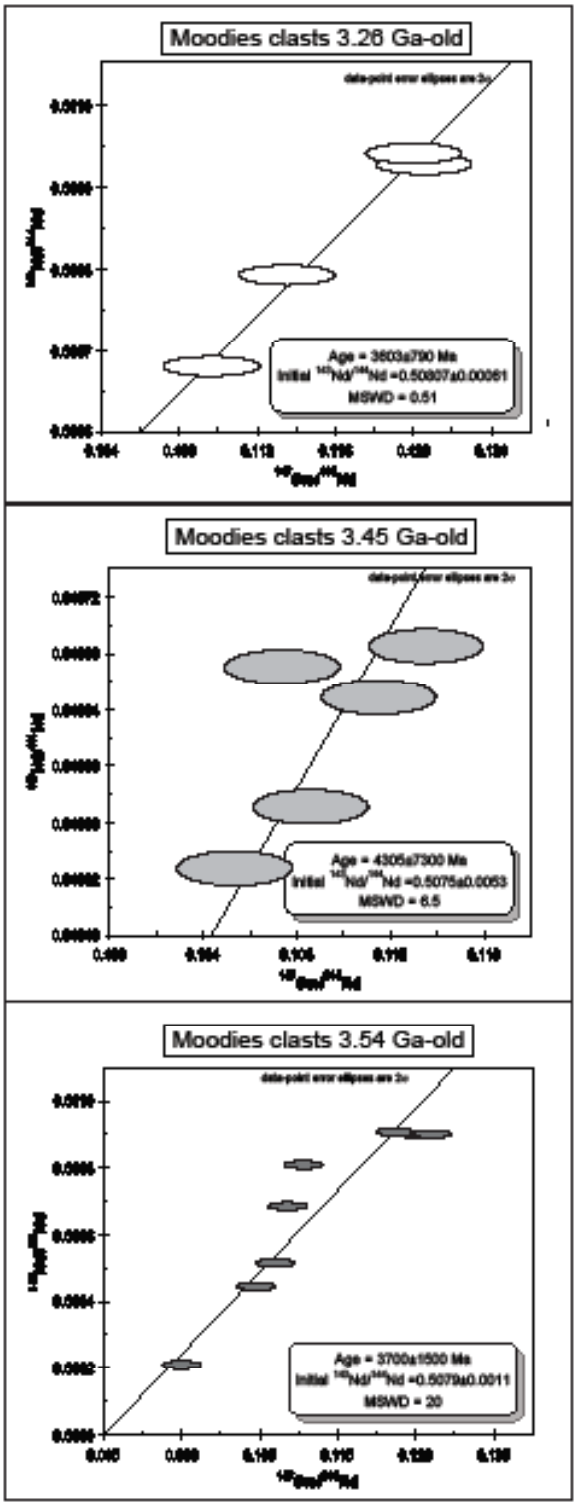

Figure 4. Sm-Nd isochron diagrams for Moodies clasts. All diagrams were built using the Isoplot v.3.41b software of Ludwig (2003a, 2003b).

with ours, define two distinct lines, suggesting that the Steynsdorp pluton (gneissic unit) is formed by composite units. This is evidenced by the difference of the geochemistry of the pluton as well as the difference in ages (Moyen et al., 2007). The regression line of 6 whole-rock Sm-Nd analyses samples (3 from Kröner et al., 1996, together with 3 of this study) of the Steynsdorp pluton gives an age of 3697 ± 120 Ma (MSWD = 0.18, see Figure 6). The data that do not fit on this 3697 Ma isochron plot on a 3509 Ma isochron.

Whatever the pluton we consider, the isochron ages are indistinguishable from the true U-Pb zircon crystallisation ages previously measured: KaapValley = 3227 Ma, Nelshoogte = 3236 Ma, Stolzburg = 3455 Ma, and Steynsdorp = 3509 Ma (Kamo and Davies, 1994). This indicates that the Sm/Nd system of those whole rocks remained closed since magma crystallisation, contrary to the Moodies clasts. Using reference-isochron diagrams (we use published U-Pb ages for plutons), we calculate initial ε_{Nd} values to be +0.5, +1.4, -1.5 and -0.9 for the Nelshoogte, KaapValley, Stolzburg and Steynsdorp (3509 Ma) plutons, respectively. The absence of positive correlation between the ε_{Nd} and the crystallisation age of the TTGs implies that they do not have a unique source.

4.3 Lu-Hf results

The result of the Lu-Hf analyses of zircon crystals are shown in the Table 2 and figure 7. We have studied 28 single magmatic zircon grains extracted from 4 samples of the Moodies granites, for Lu-Hf analyses. The Moodies granites' zircons show that they are

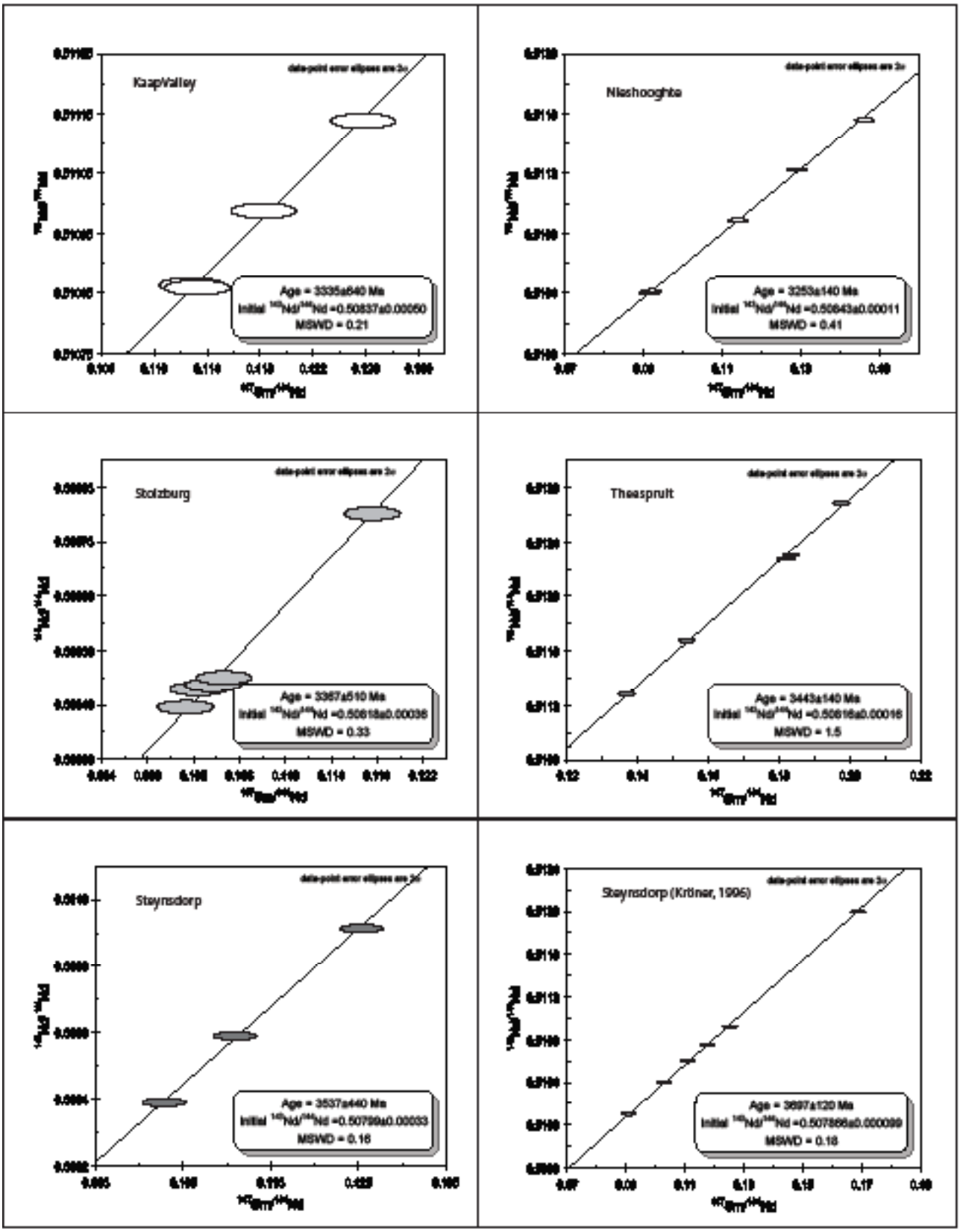

Figure 5. : Sm-Nd isochron diagrams for TTGs. All diagrams were built using the Isoplot v.3.41b software of Ludwig (2008).

all crystallised in quite evolved crustal rocks as indicated by their low $^{176}Lu/^{177}Hf$ ratios (Table 1). The granites have initial $\varepsilon_{Hf(t)}$ values that are all negative and span in a fairly wide range, from – 0.4 to -7.8. In contrast, they display a rather narrower range of model ages (calculated from Lu/Hf) from 4 Ga to 3.55 Ga. Even when taking into account that the number of sample analysed for Lu-Hf is small, the granites still display model ages difference between the younger (ca. 3.45) and older (ca. 3.55 Ga) populations. The youngest granite has Depleted Mantle (DM) ages (T_{DM}) in average ca. 3.60 Ga whereas the oldest granite has T_{DM} age ca. 3.76 Ga. In both case this indicates that the source of the zircons could have been extracted from the mantle 150 and 210 Ma before the crystallisation of the granites.

	$^{176}Yb/^{177}Hf$	±2σ	$^{176}Lu/^{177}Hf$ [a]	±2σ	$^{178}Hf/^{177}Hf$	$^{180}Hf/^{177}Hf$	Sig_{Hf} [b] (V)	$^{176}Hf/^{177}Hf$	±2σ [c]	$^{176}Hf/^{177}Hf_{(t)}$ [d]	εHf(t) [d]	±2σ [c]	T_{NC} [e] (Ga)	T_{NC} [e] (Ma)	age [f] (Ma)	±2σ
A5 46	0.1011	200	0.00317	52	1.46717	1.88647	10	0.280621	48	0.280404	-2.8	1.7	3.76	3756	3552	29
B1 004	0.0316	28	0.00116	8	1.46711	1.88649	7	0.280587	20	0.280510	-1.8	0.7	3.61	3606	3436	10
B1 010	0.0222	24	0.00083	8	1.46728	1.88656	5	0.280591	30	0.280536	-0.4	1.1	3.55	3546	3454	11
B1 012	0.0192	20	0.00070	7	1.46710	1.88650	7	0.280574	22	0.280527	-1.2	0.8	3.57	3573	3432	26
B1 013	0.0231	20	0.00080	5	1.46716	1.88649	7	0.280576	24	0.280524	-1.7	0.9	3.59	3588	3418	12
B1 014	0.0141	12	0.00058	4	1.46706	1.88645	6	0.280582	20	0.280544	-0.4	0.7	3.54	3535	3443	10
B1 015	0.0141	18	0.00055	6	1.46714	1.88653	7	0.280545	21	0.280509	-1.3	0.7	3.60	3598	3455	10
B1 020	0.0197	18	0.00078	5	1.46709	1.88655	6	0.280574	27	0.280522	-0.9	0.9	3.57	3572	3454	18
B1 022	0.0182	16	0.00074	5	1.46720	1.88674	6	0.280580	25	0.280531	-0.5	0.9	3.55	3553	3459	17
C4 078	0.1334	118	0.00403	26	1.46727	1.88633	7	0.280732	46	0.280464	-3.0	1.6	3.69	3687	3454	7
C4 080	0.0954	102	0.00266	23	1.46712	1.88654	6	0.280668	24	0.280490	-2.0	0.8	3.64	3635	3454	7
C4 081	0.0895	93	0.00279	25	1.46713	1.88647	8	0.280699	28	0.280513	-1.2	1.0	3.59	3590	3454	7
C4 085	0.0976	79	0.00280	18	1.46733	1.88657	8	0.280650	22	0.280464	-3.0	0.8	3.69	3688	3454	7
C4 088	0.2147	225	0.00631	65	1.46728	1.88656	7	0.280893	30	0.280473	-2.7	1.1	3.67	3670	3454	7
C4 088	0.1662	191	0.00437	56	1.46722	1.88646	11	0.280749	37	0.280458	-3.2	1.3	3.70	3699	3454	7
C4 090	0.1358	112	0.00414	26	1.46719	1.88658	8	0.280780	30	0.280505	-1.5	1.1	3.61	3607	3454	7
C4 091	0.0273	26	0.00097	7	1.46708	1.88648	6	0.280593	24	0.280529	-0.6	0.9	3.56	3559	3454	7
C4 094	0.0410	43	0.00142	12	1.46718	1.88653	6	0.280619	28	0.280525	-0.8	1.0	3.57	3568	3454	7
C4 099	0.0178	15	0.00071	5	1.46710	1.88639	6	0.280576	21	0.280529	-0.6	0.7	3.56	3559	3454	11
C4 100	0.1269	113	0.00368	26	1.46704	1.88637	9	0.280731	25	0.280486	-2.2	0.9	3.64	3645	3454	7
C4 103	0.0879	104	0.00258	25	1.46715	1.88643	8	0.280690	32	0.280519	-1.0	1.2	3.58	3580	3454	7
C4 104	0.1068	96	0.00296	21	1.46717	1.88628	7	0.280700	32	0.280503	-1.6	1.1	3.61	3610	3454	7
C19 27	0.0564	81	0.00194	25	1.46731	1.88652	10	0.280425	48	0.280294	-7.8	1.7	4.00	3996	3503	18
C19 28	0.0522	58	0.00194	20	1.46714	1.88639	6	0.280611	49	0.280478	-0.5	1.7	3.62	3617	3536	10
C19 29	0.0419	39	0.00145	11	1.46734	1.88648	8	0.280514	37	0.280415	-2.9	1.3	3.74	3745	3531	10
C19 34	0.0667	89	0.00223	25	1.46725	1.88637	6	0.280587	46	0.280435	-2.2	1.6	3.71	3706	3531	10
C19 38	0.0324	31	0.00117	8	1.46711	1.88655	7	0.280494	69	0.280414	-3.1	2.5	3.75	3750	3523	10
C19 39	0.0640	66	0.00216	19	1.46724	1.88640	6	0.280566	28	0.280419	-2.7	1.0	3.74	3736	3531	10
Temora (n=6)	0.0303	148	0.00115	49	1.46716	1.88641	10	0.282685	25	0.282676	5.4	0.8	0.74		417	3
GJ-1, n=30	0.0069	8	0.00026	2	1.46717	1.88647	10	0.282002	26	0.281999	-14.3	0.9	1.98		606	6
JMC 475 (n=8)					1.46716	1.88665	15	0.282147	8							

Quoted uncertainties (absolute) relate to the last quoted figure. The effect of the inter-element fractionation on the Lu/Hf was estimated to be about 6 % or less based on analyses of the GJ-1 and Plesoviče zircon. Accuracy and reproducibilty was checked by repeated analyses (n = 30 and 6, respectively) of reference zircon GJ-1 and Temora (data given as mean with 2 standard deviation uncertainties)

(a) $^{176}Yb/^{177}Hf = (^{176}Yb/^{173}Yb)_{true} \times (^{173}Yb/^{177}Hf)_{meas} \times (M_{173(Yb)}/M_{177(Hf)})^{\beta(Hf)}$, $\beta(Hf) = \ln(^{179}Hf/^{177}Hf_{true} / {}^{179}Hf/^{177}Hf_{measured}) / \ln (M_{179(Hf)}/M_{177(Hf)})$, M=mass of respective isotope. The 176Lu/177Hf were calculated in a similar way by using the 175Lu/177Hf and b(Yb).

(b) Mean Hf signal in volt.

(c) Uncertainties are quadratic additions of the within-run precision and the daily reproducibility of the 40ppb-JMC475 solution. Uncertainties for the JMC475 quoted at 2SD (2 standard deviation).

(d) Initial $^{176}Hf/^{177}Hf$ and εHf calculated using the apparent Pb-Pb age determined by LA-ICP-MS dating (see column f), and the CHUR parameters: $^{176}Lu/^{177}Hf = 0.0336$, and $^{176}Hf/^{177}Hf = 0.282785$ (Bouvier *et al*., 2008).

(e) two stage model age in billion years using the measured $^{176}Lu/^{177}Lu$ of each spot (first stage = age of zircon), a value of 0.0113 for the average continental crust (second stage), and a juvenile crust (NC) $^{176}Lu/^{177}Lu$ and $^{176}Hf/^{177}Hf$ of 0.0384 and 0.28314, respectively.

(f) Concordant 207Pn/206Pb apparent age of the spot determined by LA-ICP-MS. Otherwise, if the age of the spot is discordant, the age represented is the apparent age for the sample (207Pb/206Pb age for <1000 and 90% concordant).

Table 2. Lu-Hf isotope data for the zircons of the Moodies granitic pebbles.

5. DISCUSSION

5.1 Alteration and the role of accessory minerals on the Sm-Nd couple (Sm/Nd fractionation)

It has been demonstrated, in many Archean terranes (Wilson and Carlson 1989; Grau et al., 1990, 1992; Rosing, 1990; Lahaye et al., 1995; Frei et al., 1999; Moorbath et al., 1997 and references therein), as in the BGB, that the Sm-Nd system was sensitive to fluid/rock interaction and metamorphism (Rosing, 1990; Gruau et al., 1990). Evidences of silicification, sericitisation (Toulkeridis et al., 1998; Hoffman and Harris ,2008) and/or hydrothermalism events have been documented in the BGB and some authors have studied the influence of these processes on the Sm/Nd system on regional rocks (komatiites, BIF and carbonates). Thus for example in the Fig Tree Group, non-clay silicic carbonates and phosphates (of secondary origin) have recrystallised due to

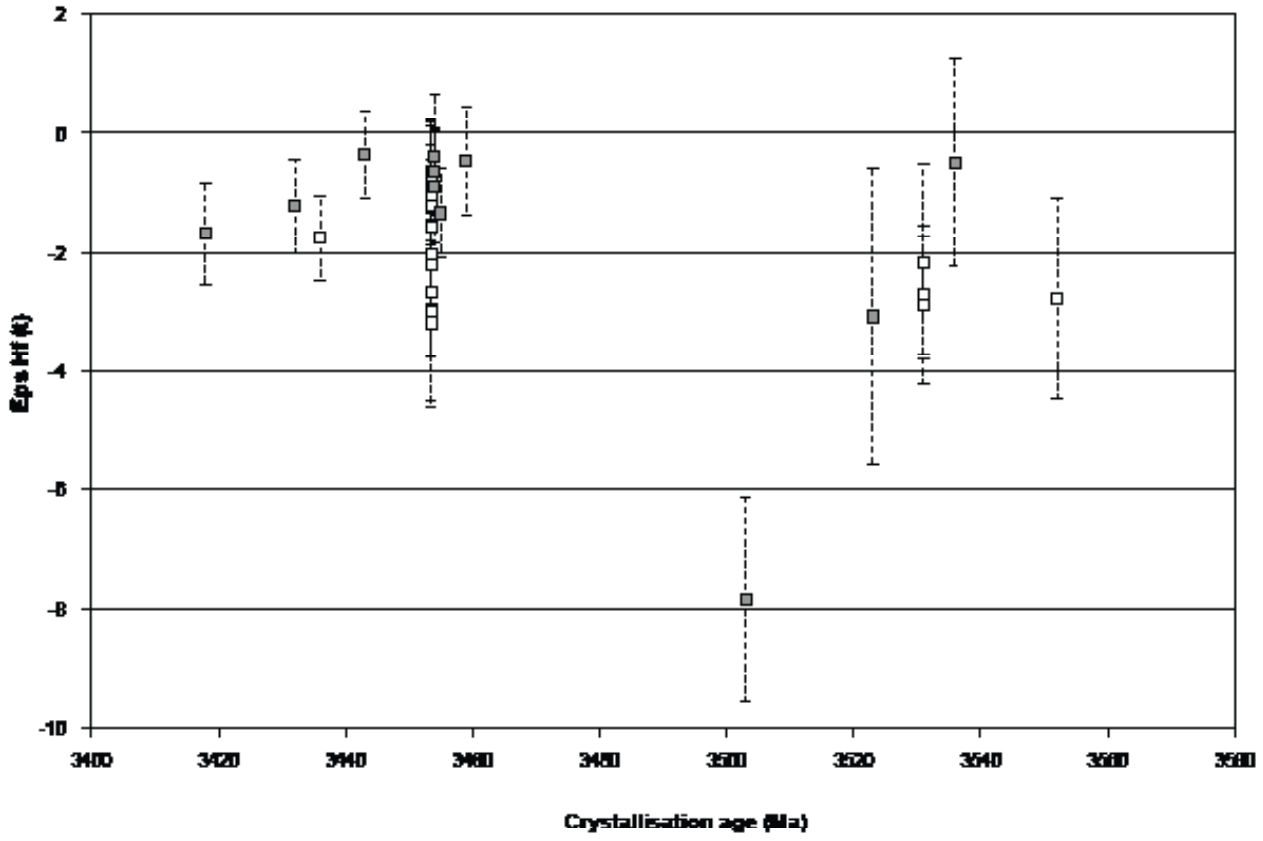

Figure 6. ε_{Hf} vs. age of crystallisation for selected Moodies clasts. The $\varepsilon_{Hf(t)}$ value of each spot (where t is the weighted mean $^{207}Pb/^{206}Pb$ age of the domain) of the granites' zircons was calculated using the U-Pb concordant age of the same analysed spot within the same zircon (Table 3). When the analysis of U-Pb in the zircon did not led to a concordant age, the concordant age of the sample, previously defined by LA-ICPMS, was used to calculate the $\varepsilon_{Hf(t)}$ of the spot (Table 3). The two different categorie of spot are plotted as white diamon when the U-Pb age concordant age of the sample was used and as grey diamond when the U-Pb concordant age of the analysed spot was used.

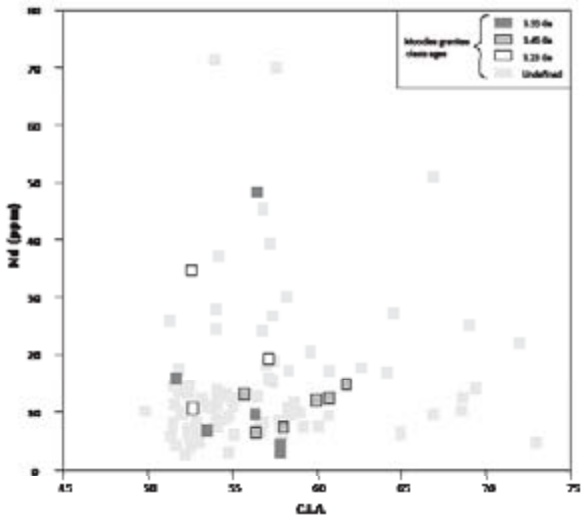

Figure 7. Chemical index of alteration (CIA, cf. Nesbitt and Young, 1982) vs. Nd content (ppm) for Moodies clasts. CIA values are from Sanchez-Garrido et al. (2011).

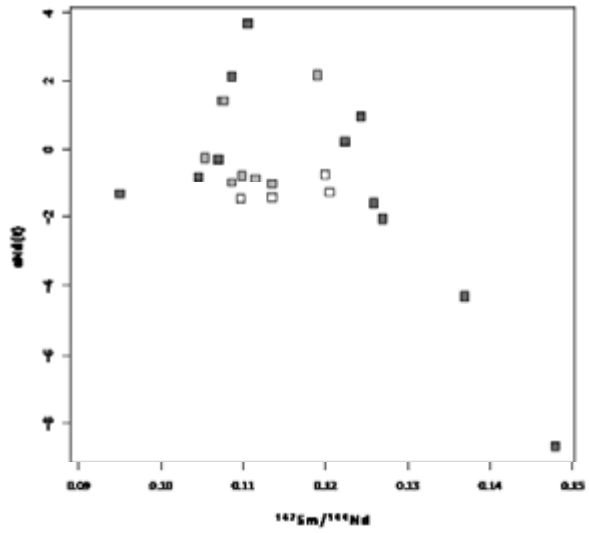

Figure 8. $^{147}Sm/^{144}Nd$ ratio vs. ε_{Nd} for Moodies clasts.

fluid-rock interaction. Toulkeridis et al. (1998) have demonstrated that in both rock types, the Sm/Nd data from had been disturbed and had recorded the respective age of recrystallisation, which corresponds to the age of the fluid/rock interaction event undergone by the carbonates. In a more general way, Rosing (1990) explained how the variation of Sm-Nd during alteration (or fluid/rock interaction or metamorphism) could induce a scatter of the initial epsilon Nd, proportional to the lapse of time between the emplacement and the secondary disturbance. The removal of Sm from a rock after its emplacement will induce a change in the Sm/Nd ratio and therefore a change of its $^{143}Nd/^{144}Nd$ isotopic ratio, consequently influencing its model age. Furthermore, the nature of the alteration and its influence on the Sm-Nd system depends on the nature of the fluid, on the primary and secondary mineral assemblage, as well as the trace element concentration of the studied rocks/minerals (Lahaye et al., 1995). As REE are mostly hosted within accessory minerals (monazite, apatite, zircon, allanite, xenotime), these minerals largely buffer/control the Sm-Nd content of rock, and alteration of these accessory minerals will affect the Sm/Nd ratio. Opening of the monazite or apatite mineral system (because of closure temperature) followed by inter-granular fluids can favour the transport of Sm or Nd out of the system and once again change the Sm/Nd ratio of the rock. Lahaye et al. (1995) argue that a large scatter in the $^{143}Nd/^{144}Nd$ initial ratio of a same co-genetic suite of rocks, as well as an isochron age different from the crystallisation age of a rock, are potential indicators of a perturbation of the Sm-Nd system.

Turning back to our samples, we have calculated their T_{CHUR} and T_{DM} model ages. The latter are dependant on the model of evolution used for DM that includes one-stage (see Fig. 4) or two-stage (Workman and Hart, 2005; Boyet and Carlson, 2006) models, as well as regression

curves between dated samples representative of the depleted mantle (DePaolo, 1981, Blichert-Toft et al.,1999; and Vervoort and Blichert-Toft, 1999). Error related to the choice of a given evolution has been evaluated by calculating three model ages corresponding to three contrasted models: 1) the single, closed-system evolution described in legend of figure 4; 2) the two-stage model proposed by Boyet and Carlson (2006); and 3) the DM evolution from DePaolo (1981). Results are reported in Table 1. They show consistent values at the level of 10-100 Ma. Such differences, however, are mainly related to the use of the ε_{Nd} time-depending evolution of DePaolo (1981) that gives an actual value of 8.5, in disagreement with measured values in MORB (around 10). When considering the single- and double-stage models only, differences range from 20 to 50 Ma. As a consequence, the choice of a given DM evolution leads to uncertainties that are lower than age differences between the three Moodies groups of clasts.

Whatever the DM evolution, a few clasts have T_{CHUR} and T_DM ages either too young compared to their crystallisation age (TC) (e.g. sample C19) or too old for the Earth history (samples A3 and A8, Table 1). Together with the lack of isochron ages, this indicates that at least some pebbles or even the entire set of pebbles underwent changes in their Sm/Nd isotopic system, which had been (at least partially) reset. According to Gruau et al. (1996) the low-Nd samples are the easiest to be reset and/or affected by the interaction with a Nd-richer fluid or magma. There is however no clear relationship between the chemical index of alteration (CIA; Nesbitt and Young, 1982) and the neodymium concentration ([Nd]) of pebbles: they are not correlated (Fig. 8). Such a feature could also result from the contamination of the magma by ancient crustal rocks. If contamination had happened, a positive correlation between the $^{147}Sm/^{144}Nd$ initial ratios and the ε_{Nd} values should be excepted because the more ancient crust would have a more negative ε_{Nd} and a lower Sm/Nd ratio (Vervoort and Blichert-Toft, 1999; Blichert-Toft et al., 1999). The absence of correlation between these two parameters (Fig. 9) argues against crustal contamination.

All the above observations suggest that in at least some of the clasts, the Sm-Nd system was reset post-crystallisation. We then can conclude that the Nd isotopic data of the clasts do not always record the initial value of the parental magma. As a direct consequence, we filtered our dataset from the most perturbed values. For this purpose, we considered as criteria the alteration level express in the petrography of the clasts (the preservation of igneous textures and unmodified feldspars, as well as the content of sericite), the incoherence of model and crystallisation ages combined with the [Nd] contents. Finally we used the chemical index of alteration (CIA) as a parameter to verify our selection of the least altered samples. This resulted in the removing of 8 samples over 22 (see italic data in Table 1).

5.2 Interpretation of the isotopic data

Moodies granite/rhyolite filtered points do not plot on a single evolution line in the $\varepsilon_{Nd(t)}$ vs. crystallisation age diagram (Fig. 10). On the contrary, clasts are scattering. This is particularly important for the 3.45 and 3.54

Ga groups with ε_{Nd} values ranging from -0.27 to -1.01 and from +0.22 to -2.05, respectively. This scattering indicates that the 3 chronologic populations of clasts have not been derived from a single source. Furthermore, ε_{Nd} are mostly negative, precluding any exclusive contribution of juvenile mantle material in their source, but rather pointing towards a contribution from a crustal component, which is in agreement with previous conclusions drawn with both major and trace element data, arguing that the clasts parental magmas might have a sedimentary origin (Sanchez-Garrido, et al., 2011).

T_{DM} model ages, that represent the time of extraction of the protolith from a Depleted Mantle, are not very helpful because the source of Moodies clasts is sediments (which might result of mixing of different sources). So, instead of T_{DM} ages, we rather consider crustal residence age (CR_{Nd}), which gives a minimum estimate of the protolith age. CR_{Nd} are calculated as T_{DM}, these age represent the age for which $\varepsilon_{Nd(t)}$ of the granite is equal to the $\varepsilon_{Nd(t)}$ of the DM. The CR_{Nd} age does not give the age at which the source of the granite was extracted from the DM but rather is an estimate of the minimum age of the protolith of the source of the granite. It illustrates the age of the protolith of the sediments that melted to generate the granites. As there are different models for the evolution of the $\varepsilon_{Nd(t)}$ of the DM through time (DePaolo, 1981; Boyet and Carlson, 2006), it is possible to calculate T_{DM} model ages or CR_{Nd} model age for two models. Whatever the DM evolution, scattering of CR_{Nd} values increases with age of crystallisation. This could be related to some evolution in the source of the clasts. Such a feature could also result either from a

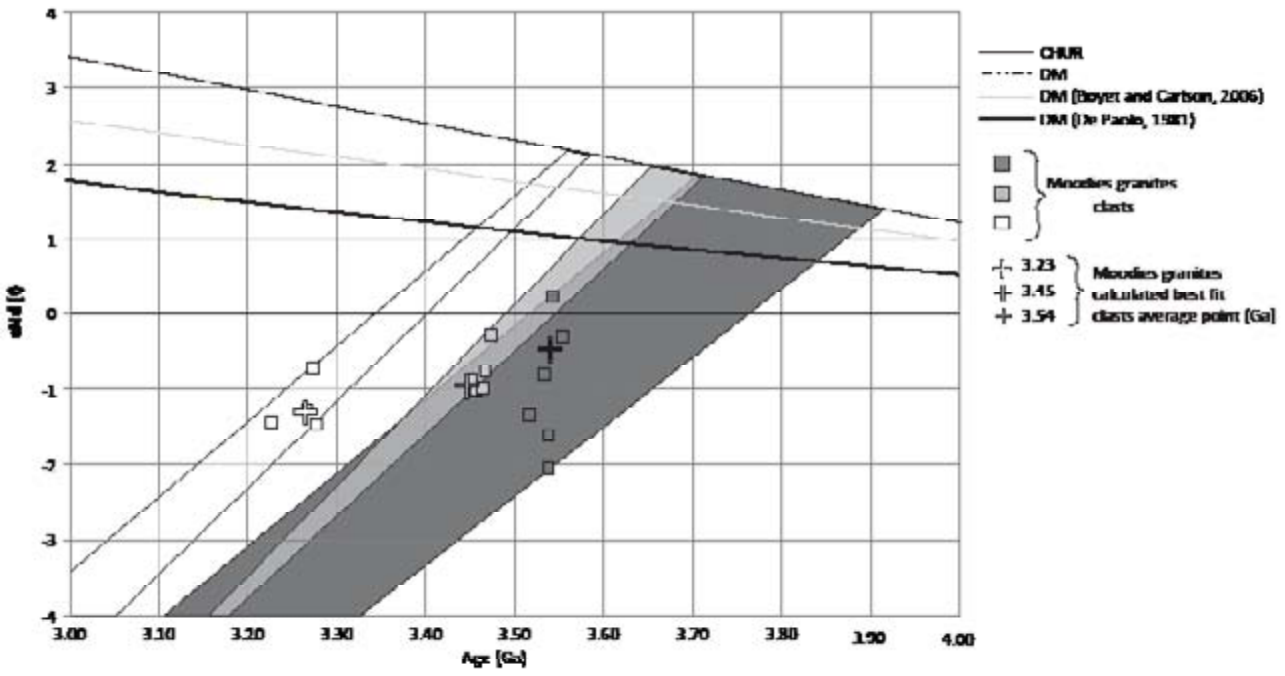

Figure 9. ε_{Nd} vs. age of crystallisation for Moodies Sm/Nd disturbance-filtered clasts. The depleted mantle evolution has been calculated assuming a simple, closed-system evolution since the formation of the Earth ($^{143}Nd/^{144}Nd = 0.51315$ and $^{147}Sm/^{144}Nd = 0.2137$).

sampling bias (small number of analysed clasts for the 3.23 Ga group) or from a difference in the genetic process that formed the 3 groups of clasts. For instance, the difference (Δt) between CR_{Nd} and crystallisation ages of granites is ca. –380 to 170 Ma for the 3.54 and between 260 to 190 Ma for the 3.45 Ga groups, whereas the 3.26 Ga clasts have a Δt of that varies between ca. 340 to 290 Ma (Fig. 11). This may suggest a longer process of formation for the youngest granites, leading to a more homogenised source of the granites, and thus in a smaller ε_{Nd} scatter.

5.2.1. Heterogeneous source

Depending on the DM model chosen, there is a large difference between the CR_{Nd} and the crystallisation age (Δt) of the granite. With the DM model of one stage, the Δt varies between ca. 380 to 170 Ma for the 3.54 Ga group of clasts, whereas the 3.26 Ga-old population of clasts have a Δt that ranges between ca. 340 to 290 Ma. With the model of evolution in two stages of Boyet and Carlson (2006) the Δt for the oldest population of clasts becomes 340-130 Ma and the Δt of the youngest group becomes 290-240 Ma. The observed variations between the Δt of the two models reflect in fact the variation of the Sm:Nd ratio between the two models. It is difficult to state what is the exact Δt is for each group. However, no matter what DM model is chosen, the Δt of the granite of each group is significant. It can not be denied that the CR_{Nd} ages of the granite are older than their crystallisation age. The Δt observed for each granite is almost constant. However the fact that the youngest population of granite has an average Δt greater than the 2 other groups of clasts may suggest a longer process of formation.

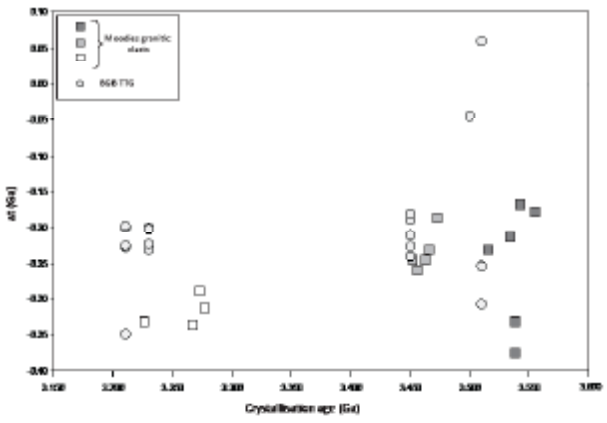

Figure 10. Δt differences between crustal residence (CR_{Nd}) and crystallisation ages vs age of crystallisation for the Moodies granitic clasts.

In a general way, we observe that according to the one stage evolution DM model, the crustal residency of the protolith of the granites started between 3.71 to 3.91 Ga years ago for the oldest population of clasts, 3.66 to 3.72 Ga years ago for the intermediate population of clasts and between 3.56 to 3.60 Ga years ago for the youngest group of granite. If however if we consider the DM evolution of DePaolo (1981), the crustal residency age of the source of the oldest population of granitic clasts starts at ca. 3.83 Ma whereas the one of the youngest population starts at ca. 3.50 Ma ago. If the scatter of the $\varepsilon_{Nd(t)}$ is considered as representative of the source, it must be concluded that the source of the Moodies was heterogeneous which leads to 2 distinct models:

1) The source of the clasts is isotopically

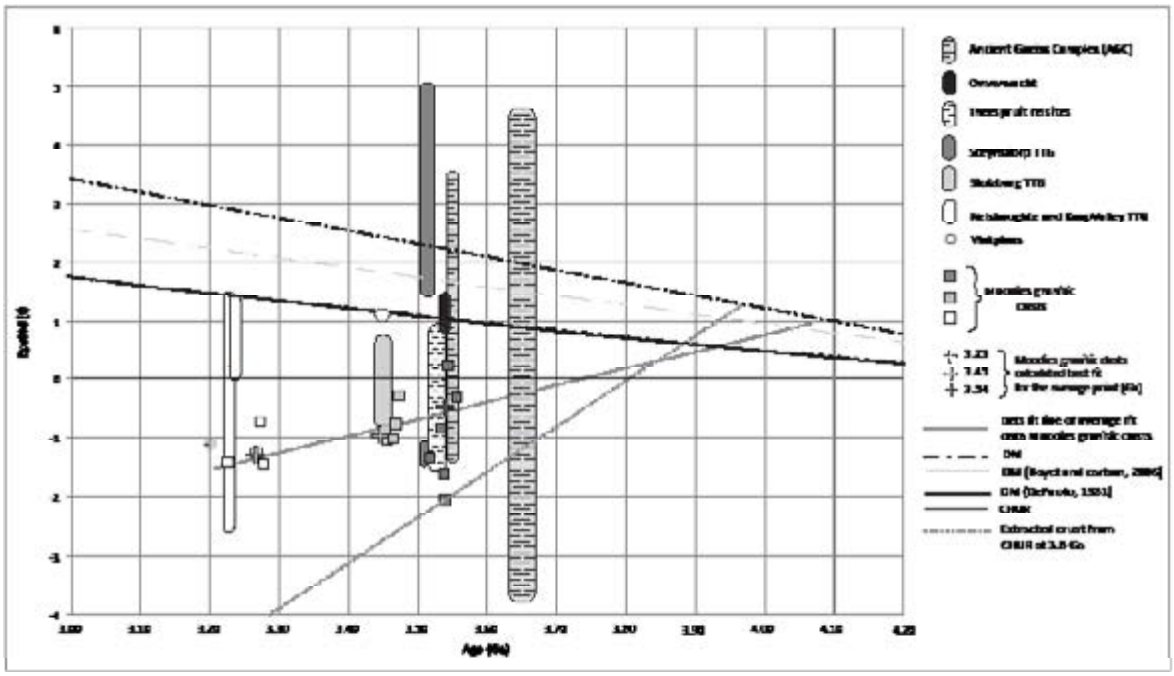

Figure 11. ε_{Nd} vs. crystallisation age for Moodies clasts, regional BGB TTGs and older formations (komatiites and komatiitic basalts from the Onverwacht group; mafic, ultramafic rocks from the Komatii formation; felsic schists from the Theespruit formation; Ancient Gneiss Complex (AGC) from the Swaziland). Data references are: Schoene et al. (2009); Carlson et al. (1983); Chavagnac (2004); Van Kranendonk et al. (2009) and Kröner et al. (1996). Crosses correspond to average initial Nd values determined for each age-group of clasts (see section 5.2.2 for details).

heterogeneous but corresponds to a unique component. Melting of immature clay-poor metasediments was proposed by Sanchez-Garrido et al. (2011) to account for the chemical characteristics of Moodies clasts. The sediments should have (if their protolith is identical in term of nature) a similar Sm/Nd signature with similar evolution (=same $f_{Sm/Nd}$) through time. Moreover, Knesel and Davidson (2002) and Patino-Douce and Harris (1998) have demonstrated that the melting of a mica-rich metasedimentary source can generate a wide spectrum of melts with wide range of trace element and isotopic signature. This could explain the scatter observed in the Moodies data: the clasts being generated through melting of metasediments identical in origin (formed by the weathering of the greenstone belt material) but with heterogeneous chemistry (e.g. due to layering of pelite/greywacke material in the source).

2) As an alternative, the scatter of the ε_{Nd} might be the result of a mixing between juvenile material extracted from a depleted mantle source at the same age that the oldest population of clasts (3.54 Ga) and an older recycled crustal component (extracted at ca. 3.9 Ga). However, there is no correlation between initial $^{147}Sm/^{144}Nd$ and ε_{Nd} for the 3 age-groups (Fig. 9) but a hazy, no significant co-variation for the youngest group to support this hypothesis. As said in section 5.2, positive correlations

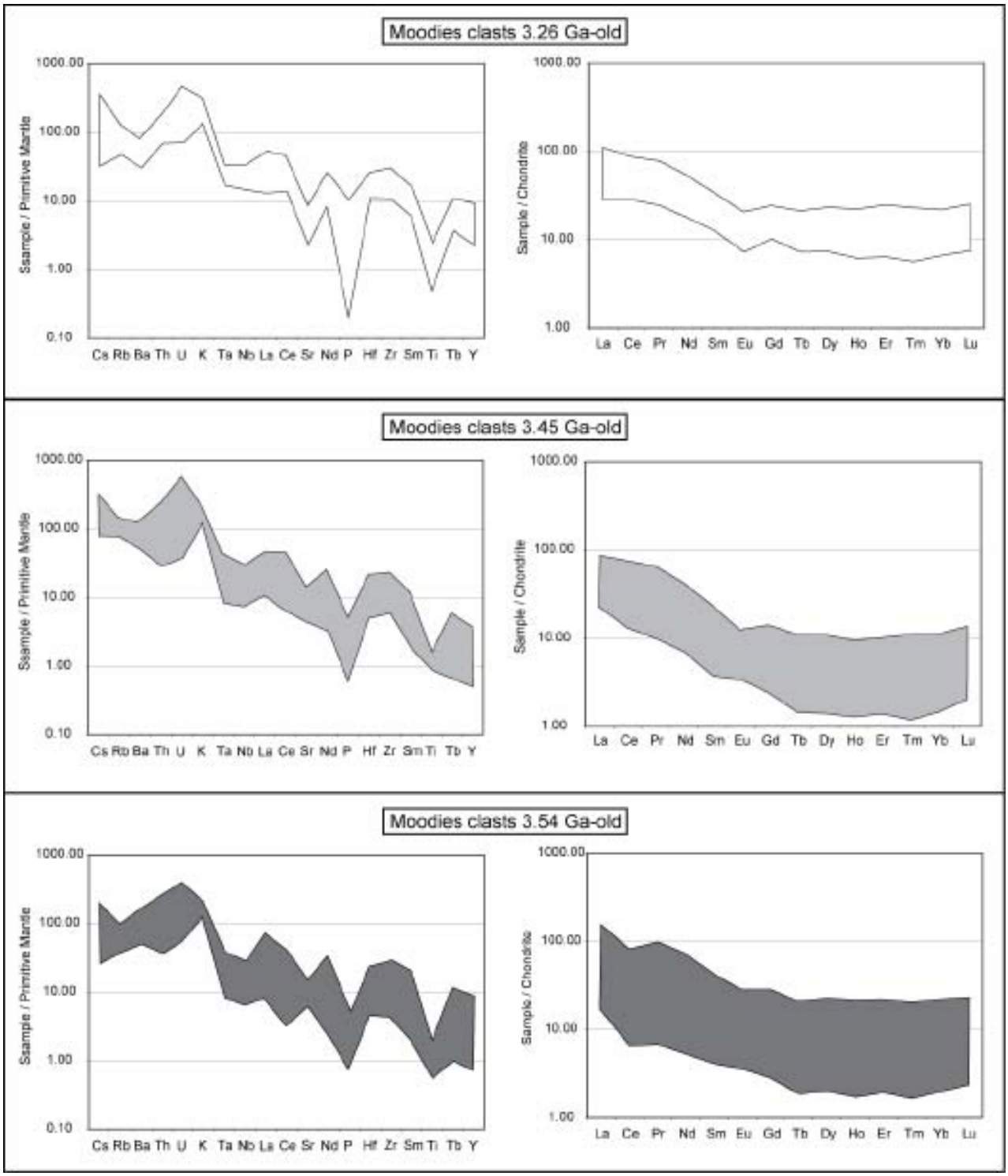

Figure 12. Primitive mantle-normalized spidergrams of Moodies clasts together with chondrite-normalized REE.

should be expected in case of contamination by older crustal rocks. Furthermore the chemistry of the clasts does not support the hypothesis of mixing for the formation of the granites: firstly, the clast chemistry is not age dependant, secondly the lack of correlation between some major elements (e.g. Na_2O or K_2O vs. SiO_2) and between most of the trace elements and SiO_2 (not shown, Sanchez-Garrido et al., in preparation) argue against such mixing. Moreover, the REE patterns (Fig. 13) of clast with extreme ε_{Nd} are similar (for instance, samples A1 and B17), which points towards similar source for those clasts rather than increasing crustal contamination. Besides, such old crustal materiel (3.9 Ga) was never sampled in the BGB (the oldest rocks of the Kaapvaal Craton are part of the AGC and have been dated up to 3.644 ± 0.004 Ga , cf. Kröner, 2007), which, albeit it does not exclude it never existed (never at the surface or not anymore), argues against the mixing model.

The possibility of assimilation-fractional crystallisation (AFC) can also be ruled out as there is no direct evidence for such process. In fact the clasts do not contain micro-xenolithic material, neither inherited zircons cores (Sanchez-Garrido et al., 2011). Moreover, as plutonic equivalent of the granite remained unknown until today, it is very difficult to infer the nature of the assimilated component (wall rock).

5.2.2. Limitation of the filtering of the data

On the other hand, the scattering of Moodies Sm/Nd data can also traduce the limitations of the filtering experiment. A few clasts could indeed present modified Sm/Nd characteristics but still display reasonable CR_{Nd} model ages compared to their crystallisation age.

In this case, we use reference-isochron diagrams (we calculate the best line fitting our measurements with a slope given by the U-Pb age) rather than ‘‘classical’’ ones to determine the Nd initial composition of each population of clasts (Fig. 14). That way we obtain the following ε_{Nd} values, -1.23, -0.91 and -0.41 for the 3.26, 3.45 and 3.54 Ga groups, respectively. Plotted in the ε_{Nd} vs. age diagram with data from the literature (Fig. 12), the 3 points fit on a single evolution line that cross-cut the CHUR at ca. 3.7 Ga, the DM (one stage evolution curve) at ca. 4.05 Ga, the DM of DePaolo (1981) at ca. 3.95 Ma and the DM (two stage evolution curve) at ca. 4 Ga. This implies that the protolith, of the source of the granites’ clasts, was identical for the 3 groups, being extracted from either a depleted mantle source ca 4.05 Ga (if the one stage evolution of the DM is considered) or a CHUR source at about 3.75 Ga, and then activated during each of the three TTG emplacement events. However, we need to stress that the CR_{Nd} age is dependant of the DM model considered and that therefore the youngest extraction age calculated corresponds to the minimum extraction age of the protolith, from the DM, which also is the minimum age of the source of the granitic pebbles.

T_{DM} ages calculated from the Sm-Nd considering the one-stage DM evolution and Lu-Hf isotopic systems are identical for 3 samples over 4 analysed (Table 4). More precisely, average T_{DM} ages calculated for each sample from Lu-Hf data analysed in zircons give identical values than whole-rock T_{DM} ages determined with the

	U-Pb age	T_{DM} Lu-Hf	T^1_{DM} Sm-Nd	T^2_{DM} Sm-Nd	T^3_{DM} Sm-Nd
Material	Zircons	Zircons	Whole rock	Whole rock	Whole rock
B1x	3.454	3.571	3.527	3.48	3.43
C4	3.473	3.623	3.660	3.62	3.58
A5X	3.534	3.756	3.747	3.71	3.67
C19	3.537	3.763	3.433	3.38	3.33

Table 3. Comparison of T_{DM} ages calculated from the whole rock Sm-Nd and from the zircon Lu-Hf system, for the granites pebbles of the Moodies group. 1) Single, closed-system evolution since the formation of the Earth. Increase of the $^{143}Nd/^{144}Nd$ ratio of the depleted mantle from a chondritic value to 0.51315 (average MORB) in 4.55 Ga results in an actual value of 0.2137 for the $^{147}Sm/^{144}Nd$ ratio. 2) Double, closed-system evolution. From initial to 3.0 Ga, the silicate Earth evolves with a $^{147}Sm/^{144}Nd$ of 0.209; from 3.0 Ga to actual, continuous continental crust extraction until $\varepsilon_{Nd(DM)} = 10$. This corresponds to a present day $^{147}Sm/^{144}Nd$ of 0.220 (Boyet and Carlson, 2006). 3) DM evolution - $\varepsilon_{Nd\ DM(t)}) = 0.25T^2$-3T+8.5, as proposed by DePaolo (1981).

Sm-Nd system. As the zircons are considered to be more resistant than other accessory mineral (apatite, for example), we are confident than the T_{DM} ages (or CR_{Nd} ages) obtained are representative of the source of the granites. Thus the latter was extracted from the depleted mantle very early in the Archean and in the history of the BGB. We can conclude from the above comparison that the filtering of the data is efficient and consider that our Sm-Nd data are representative of the source of the granitic pebbles. Moreover, we notice that the T_{DM} ages calculated using the DM evolution curve of DePaolo (1981) or Boyet and Carlson (2006) are different than the T_{DM} ages calculated using the Lu-Hf data. We therefore conclude that the one-stage evolution of the DM, for the period of time considered, match our data the best.

5.3 Regional implication and interpretations

The chemistry of the clasts precludes the regional TTGs as a reliable source, therefore, we have compared the clasts to other regional rocks that may be compatible as a source. The figure 12 displays ε_{Nd} values as a function of crystallisation age for filtered clasts, TTGs as well as some additional BGB data from the literature. The TTG data from the literature show a larger scatter than Moodies clasts, which suggests that both materials do not share a common source. If that was the case, a greater range of variations should be expected in Moodies clasts, especially for the 3.2 Ga group, when compared to Kaap Valley samples. This provides an additional argument, and it is consistent with TTGs and Moodies clasts originating from a different source, which can be clearly deduced from major and trace element data.

The T_{DM} ages of the TTGs though time correspond well to the CR_{Nd} age of the source of the clasts' protolith. It is now admitted that TTG originated by high pressure melting of an hydrous metabasalt, even if the geodynamic environment where melting took place is still a subject of controversy: overthickened mafic lower crust (Smithies, 2000) versus subducted oceanic crust (Martin, 1986). In the Kaapvaal Craton the later hypothesis is most consistent

with the geological and geodynamic history of the BGB (Moyen et al., 2006). Assuming a subducted hydrated oceanic crust as source of TTGs, the Nd isotopic signature of the later will be representative of the evolution of the subducted oceanic crust. Consequently the TDM ages of the TTGs would represent the time of extraction of the oceanic lithosphere from the depleted mantle. The average difference between the TTG T_{DM} age and their crystallisation age varies from 0.24 to 0.3 Ga. The fact that the 2 older groups of granites have the same average CR_{Nd} ages than the TTG T_{DM} ages indicates that the source of the clasts's protolith was extracted from the depleted mantle at the same time as the TTG source, and in the case of the Kaapvaal Craton, at the same time as the oceanic crust. This could indicate that the source of the clasts be related to the oceanic crust.

The Ancient Gneiss Complex (AGC) of Swaziland consists mainly in TTG but it also contains more potassic felsic rocks (e.g. Nhlangano gneiss) known to be older than the bulk of the Moodies clasts (ca.3.6 to 3.7 Ga; cf. Schoene et al, 2009). Therefore previous studies (Reimer et al., 1985; Tegtmeyer and Kroner, 1987) have considered the AGC as a suitable source for the granitic clasts of the Moodies group. The Nd isotopic data of the ACG show an important scatter, the ε_{Nd} ranging from +6.29 to -4.09, and the two old groups of clasts fit on the evolution line of the AGC trough time. This result suggests that either the clasts formed by recycling of ACG rocks or that they formed via mixing of old ACG component and juvenile material. From an isotopic point of view only, the ACG cannot be rejected as the source of

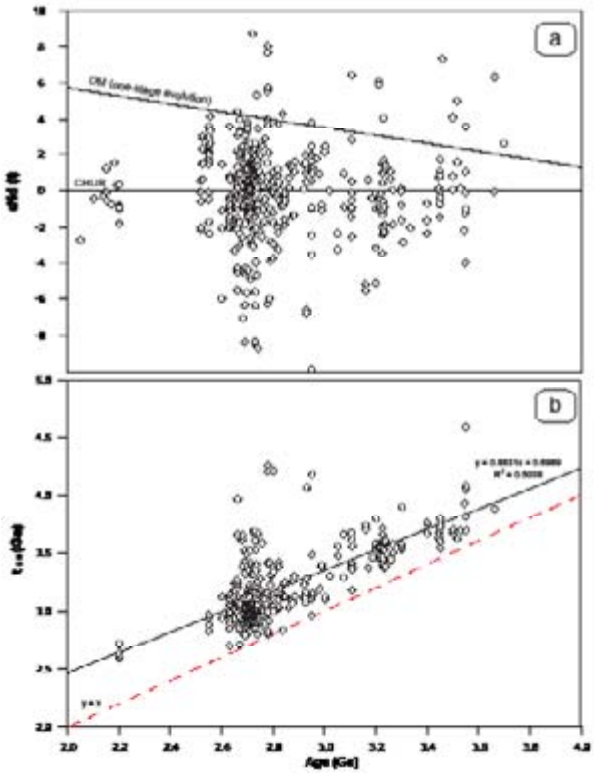

Figure 13. ε_{Nd} vs. ages of the worldwide TTG. b) Sm-Nd model ages of worlwide TTG vs age of crystallisation (single-stage evolution of DM, see figure 4) for the TTG. Data from Georoc database.

the clasts. Nevertheless the chemistry of the clasts discards their formation trough a mixing process between juvenile depleted material and crustal material. On the other hand, recent work (Sanchez-Garrido et al., 2011) has demonstrated that the clasts cannot represent upper crustal equivalents of the relatively K_2O-rich portions of the AGC, as these rocks have substantially higher CaO contents.

6. GEODYNAMICAL IMPLICATIONS

Two distinct sources can be proposed for the origin of Moodies clasts when considering

that the scatter of the Sm/Nd data is relative to post-crystallisation events or not: either altered, isotopically heterogeneous sediments or a depleted (or CHUR like), isotopically homogeneous component. Both induce drastic differences in term of geodynamics.

The coeval emplacement of TTG and the clasts magma and the absence of a genetical link between the two type of magma strongly suggest that the clasts magmas and the TTG were generated during the same geodynamic event. Assuming that TTG are generated in subduction environment (Condie, 1980; Martin, 1986; Condie, 1989; Rollinson, 1997; Barth et al., 2002; Foley et al., 2002; Kamber et al., 2002; Moyen et al., 2006; Nair et Chacko, 2008) altered sediments located on the top of the oceanic crust will consequently be able to melt contemporaneously with subducted meta-basalts (amphibolite) (Moyen et al., 2006). In other words, they can melt throughout subduction events, during which the TTG are also generated, through basalt melting. In this case, the similar geochemical characteristics of the clasts imply that their sedimentary source had originated from the same protolith(s), albeit they were deposited in different time. Such a protolith could be the weathered oceanic crust itself or material coming from the craton (crustal material and/or supracrustal greenstone material). The scattering of our data would result, in this model, from variable alteration of crustal material (like the BGB itself or TTG) at the origin of sediments, but would not fit with sediments originated from the weathering of the oceanic crust as this would product homogeneous Nd signature, and short CR age. The gap observed between the TDM and the crystallisation age of the TTG in the BGB (ca. 210 Ma in average) is surprisingly high for the Archean as high Al- Sr and HREE depleted TTG are viewed as melting product of juvenile material assuming that Archean oceanic lithosphere was probably consumed within 50 Ma (Shirley et al, 2008) but not longer than 150 Ma. The gap observed between the T_{DM} and the crystallisation age of the TTG is >200 Ma and is found in most Archean high Al, Sr and HREE depleted TTG worldwide (Figure 15). If we assume that TTG are produced by the melting of Archean oceanic lithosphere, in one melting episode and that this one was consumed within less than 50 Ma, then the T_{DM} expected should not be more than 50 Ma. But this does not seem to be the case as the average of Archean TTG T_{DM} ages worldwide is ca. 380 Ma. Knowing that the present day oceanic crust is not older than 180 Ma (Cogne et al, 2004), the residence time of the Archean lithosphere of nearly 380 Ma is unrealistic as Archean subduction is believed to be faster than present-day subduction. This challenges the hypothesis of formation of the TTG in subduction zone from depleted meta-mafic material. Another main model for the formation of Archean TTG (high Al- Sr and HREE depleted) has been proposed besides the subduction one (Foley et al, 2002; Drummond and Defant, 1990; Martin, 1987): lithospheric delamination of thickened and dense, unstable subcrustal lithosphere leads which led to upwelling and decompression melting of the asthenosphere (Bedard, 2006) or delamination and sinking leading to subduction of differentiated oceanic plateaus.

The isotopic Sm-Nd data seem to argue either against subduction of juvenile material or

against fast subduction rate (Van Hunen et al., 2008). Indeed the crustal residency time of the source of the TTG is very long. One way of producing long crustal residency time is to accumulate material without recycling, in other words, to generate an oceanic plateau. With time, the accumulated mafic material would have been layered and the high density layers (like serpentinite layers) would have sunk into the depleted mantle and melted, to form TTG magmas. Therefore, we infer that the nearly 300 Ma gap between the extraction of the TTG source from the depleted mantle and the crystallisation of the TTG magmas, correspond to multiple episodes of mantle melting leading to the formation of TTG source rocks. Additionally, this indicates that TTG genesis is not governed by a unique process which is in agreement with previously suggested ideas (Moyen et al., 2007; Moyen, 2011).

7. CONCLUSION

Previous work has evidenced the presence of a markedly low-CaO, K_2O-rich variety of calc-alkaline granite that formed concurrently with the TTGs of the BGB, during each of three documented cycles of TTG magmatism (Sanchez-Garrido et al., 2011). These granites are preserved as clasts in the basal conglomerate of one of the lithostratigraphic group of the BGB, and represent principally high level intrusions and eruptive material. The neodymium and hafnium isotopic signatures of these rocks provide information on their nature and improve our understanding of the nature of their source. Despite the high quality of the analyses, the Sm-Nd isotopic data of the clasts are challenging, such as data from other Archean terranes, they show fractionation of the Sm/Nd ratio post-crystallisation. Once the database was filtered it became clear that the source of the clasts was not a juvenile magma, and that they did not formed from one unique source that evolved through time. In contrast, the scatter of their ε_{Nd} is representative of the heterogeneity of the source of the clasts' parental magma. The clasts' parental magma formed via partial melting of sediments that had a crustal protholith of the same origin, but showing internal heterogeneity. The Sm/Nd and Lu/Hf data are in favour of the proposed immature metasedimentary source for the clasts. The TTGs and the clasts both seem to have formed from material that was extracted from the depleted mantle at the same time. The Ni and Cr content of the clasts seem to indicate the presence of a mafic component in the source of the sediments. However, despite the possible heterogeneity of the source, the source of the clasts remained the same through time, which implies the presence of a steady craton at ca. 3.9 Ga, and the activation of crustal recycling processes way before 3.1 Ga.

ACKNOWLEDGEMENTS

This research was supported by South African National Research Foundation (NRF) grant funding to Gary Stevens via the SARChI programme, as well as a PhD bursary to Cynthia Sanchez-Garrido. Gary Stevens, Jean-François Moyen, and Hervé Martin acknowledge joint the Centre National de la Recherche Scientifique and NRF funding.

REFERENCES

Anhaeusser, C. R., 1983. Contributions to the Geology of the Barberton Mountain Land, Spec. Publ. Geol. Soc. S. Afr. 9, pp. 223.

Barker, F. and Arth, J.G., 1976. Generation of trondhjemitic-tonalitic liquids and Archean bimodal trondhjemite-basalt suites. Geology 4, 596-600.

Barth, M.G., Foley, S.F. and Horn, I., 2002. Partial melting in Archean subduction zones: constraints from experimentally determined trace element partition coefficients between eclogitic minerals and tonalitic melts under upper mantle conditions. Precam. Res. 113, 323–340.

Barton, M., et al., 1983. Geochronological and Sr-isotopic studies of certain units in the Barberton granite-greenstone terrane, South Africa. Spec. Publ. Geol. Soc. S. Afr. 9, 63–72.

Bédard, J., 2006. A catalytic delaminationdriven model for coupled genesis of Archaean crust and subcontinental lithospheric mantle. Geochim. Cosmochim. Acta, 70, 747–771.

Blichert-Toft, J., Albarède, F., Rosing, M., Frei, R. and Bridgwater, D., 1999. The Nd and Hf isotopic evolution of the mantle through the Archean. Results from the Isua supracrustals, West Greenland, and from the Birimian terranes of West Africa. Geochim. Cosmochim. Acta, 63, 3901–3914.

Bouvier, A., Jeffrey D. Vervoort, J.D., Patchett, P.J., 2008. The Lu–Hf and Sm–Nd isotopic composition of CHUR: Constraints from unequilibrated chondrites and implications for the bulk composition of terrestrial planets. Earth Planet. Sci. Let. 273, 48-57.

Boyet, M. and Carlson, R.W., 2006. A new geochemical model for the Earth's mantle inferred from 146Sm–142Nd systematics. Earth Planet. Sci. Let. 250, 254-268.

Carlson, R.W., Hunter, D.R. and Baker, F., 1983. Sm–Nd age and isotopic systematics of the bimodal suite, ancient gneiss complex, Swaziland. Nature 305, 701–704.

Chavagnac, V., 2004. A geochemical and Nd isotopic study of Barberton komatiites (South Africa): implication for the Archean mantle. Lithos 75, 253–281.

Condie, K.C., 1980. Origin and early development of the Earth's crust. Precam. Res. 11, 183–197.

Condie, K.C., 1981. Archean greenstone belts, 434 pp., Elsevier, Amsterdam.

Condie, K.C., 1989, Plate tectonics and crustal evolution: Oxford, Pergamon, 476 p.

Condie, K.C., 1993. Chemical composition and evolution of the upper continental crust: Contrasting results from surface samples and shales. Chem. Geol. 104, 1-37.

Cogné, J.-P. and Humler, E., 2004. Temporal variation of oceanic spreading and crustal production rates during the last 180 My. Earth Planet. Sci. Let. 227, 427-439.

Davies, R.D., 1971. Geochronology and isotope evolution of the early Precambrian crustal rocks in Swaziland, Ph.D. Thesis, Univ. Witwatersrand, Johannesburg, p. 135

de Ronde C.E.J. and de Wit, M.J., 1994. Tectonic history of the Barberton Greenstone belt, South Africa:490 millions years of Archean crustal evolution, Tectonics 13, 983-1005.

de Ronde, C. E. J., de Wit, M. J., and Spooner, E. T. C., 1994. Early Archean (>3.2 Ga) Fe-oxide-rich, hydrothermal discharge veins in the Barberton greenstone belt, South Africa, Geol. Soc. Am. Bull. 106, 86– 104.

De Ronde, C.E.J. and Kamo, S.L., 2000. An Archaean arc-arc collisional event: a short-lived (ca 3 Myr) episode, Weltevreden area, Barberton greenstone belt, South Africa. J. Afr. Earth Sci. 30, 219-248.

de Wit, M. J. et al., 1987. Felsic igneous rocks within the 3.3 – 3.5 Ga Barberton greenstone belt: High crustal level equivalents of the surrounding tonalite trondhjemite terrain, emplaced during thrusting, Tectonics 6, 529-549.

de Wit, M. J. et al., 1992. Formation of an Archaean continent. Nature 357, 553–562.

de Wit, M. J., Hart, R. A, and Hart, R. J. ,1987. The Jamestown ophiolite complex, Barberton mountain belt; a section through 3.5 Ga oceanic crust, J. Afr. Earth Sci. 6, 681-730.

DePaolo, D., 1981. Neodymium isotopes in the Colorado

Front Range and crust–mantle evolution in the Proterozoic. Nature, 291, 193-196.

Drummond M.S. and Defant, M.J. 1990. A model for trondhjemite-tonalite-dacite genesis and crustal growth via slab melting: Archean to modern comparisons, J. Geophy. Res.. 95, 21503–21521.

Dziggel, A. et al. 2006. P-T and structural evolution during exhumation of high-T, medium-P basement rocks in the Barberton Mountain Land, South Africa, J. Metamorph. Geol. 24, 535-551.

Foley, S., Tiepolo, M., and Vannucci, R., 2002.. Growth of early continental crust controlled by melting of amphibolite in subduction zones. Nature 417, 837-840.

Frei, D. and Gerdes, A., 2009. Precise and accurate in situ U–Pb dating of zircon with high sample throughput by automated LA-SF-ICPMS. Chem. Geol. 261, 261–270.

Frei, R., Bridgwater, D., Rosing, M. and Stecher, O. 1999. Controversial Pb-Pb and Sm-Nd isotope results in the early Archean Isua (West Greenland) oxide iron formation: preservation of primary signatures versus secondary disturbances. Geochim. Cosmochim. Acta 63, 473-488.
.

Gerdes, A. and Zeh, A., 2006. Combined U–Pb and Hf isotope LA-(MC)-ICP-MS analyses of detrital zircons: comparison with SHRIMP and new constraints for the provenance and age of an Armorican metasediment in Central Germany. Earth Planet. Sci. Lett. 249, 47–61.

Gerdes, A. and Zeh, A., 2009. Zircon formation versus zircon alteration — New insights from combined U–Pb and Lu–Hf in-situ LA-ICP-MS analyses, and consequences for the interpretation of Archean zircon from the Central Zone of the Limpopo Belt. Chem. Geol. 261, 230-243.

Goldstein, S.L., O'Nions, R.K. and Hamilton, P.J., 1984. A Sm-Nd study of atmospheric dusts and particulates from major river systems. Earth Planet. Sci. Let. 70, 221-236.

Gruau, G., Chauvel, C. and Jahn, B.M., 1990. Anomalous Sm-Nd ages for the early Archean Onverwacht Group volcanics: Significance and petrogenetic implications. Contrib. Mineral. Petrol. 104, 27–34.

Gruau, G., Rosing, M., Bridgewater, D. and Gill, R.C.O., 1996. Resetting of Sm-Nd systematics during metamorphism of > 3.7 Ga rocks: implication for isotopic models of early Earth differentiation, Chem. Geol. 133, 225-240.

Gruau, G., Tourpin, S., Fourcade, S. and Blais, S., 1992. Loss of isotopic (Nd, O) and chemical (REE) memory during metamorphism of komatiites: new evidence from eastern Finland, Contrib. to Min. and Pet. 112, 66-82.

Hawkesworth, C.J., Moorbath, S., O'Nions, R.K., Wilson J.F.,1975. Age relationships between greenstone belts and "granites" in the Rhodesian Archaean craton. Earth Planet. Sci. Let. 25, 251-262.

Heubeck, C. and Lowe, D.R, 1994. Depositional and tectonic setting of the Archean Moodies Group, Barberton Greenstone Belt, South Africa, Precamb. Res. 68, 257-290.

Heubeck, C. and Lowe, D.R, 1999. Sedimentary petrography and provenance of the Archean Moodies Group, Barberton Greenstone Belt, in Lowe, D.R. and Byerly, G.R., eds, Geological evolution of the Barberton Greenstone Belt, South Africa: Boulder, Colorado, Geol. Soc. Am., Spec. paper 329, 259-286.

Heubeck, C.E., 1993. Geology of the Archean Moodies Group, central Barberton Greenstone Belt, South Africa. Ph.D. Thesis.

Hofmann, A. and Harris, C., 2008. Silica alteration zones in the Barberton greenstone belt: A window into subseafloor processes 3.5-3.3 Ga ago, Chem. Geol. 257, 221-239.

Jacobsen, S.B. and Wasserburg, G.J., 1980. Sm-Nd isotopic evolution of chondrites. Earth Planet. Sci. Let. 50, 139-155.

Jahn, B.M. et al., 1981. REE geochemistry and isotopic data of Archean silicic volcanics and granitoids from the Pilbara Block, western Australia: Implications for the early crustal evolution. Geochim. Cosmochim. Acta 45, 1633–1652.

Kamber, B.S. et al., 2002. Fluid-mobile trace element constraints on the role of slab melting and implications for Archean crustal growth models. Contrib. Min. Pet. 144, 38–56.

Kamo, S.L. and Davis, D.W., 1994. Reassessment of Archean crustal development in the Barberton Mountain Land, South Africa,

based on U-Pb dating. Tectonics 13, 167–192.

Kisters, A. F.M. Et al., 2010. Continental growth and convergence-related arc plutonism in the Mesoarchaean: Evidence from the Barberton granitoid-greenstone terrain, South Africa. Precam. Res. 178, 15-26.

Knesel, K.M. and Davidson, J.P., 2002. Insights into Collisional Magmatism from Isotopic Fingerprints of Melting Reactions. Science, 296, 2206-2208.

Kröner, A. 2007, The Ancient Gneiss Complex of Swaziland and Environs: Record of Early Archean Crustal Evolution in Southern Africa. Developments Precam. Geol. 15, 465-480.

Kröner, A. and Compston, W., 1988. Ion microprobe ages of zircons from early Archaean granites pebbles and greywacke, Barberton Greenstone Belt, southern Africa, Precamb. Res. 38, 367-380.

Kröner, A. et al. 1996. Terrane accretion in the oldest part of the Barberton granitoid-greenstone terrain, South Africa: evidence for crust formation between 3.5 and 3.7 Ga. Precamb. Res. 78, 105-124.

Lahaye, Y. et al., 1995. The influence of alteration on the trace-element and Nd isotopic compositions of komatiites. Chem. Geol. 126, 43-64.

Lowe, D. R., and Byerly, G. R. (Eds.), 1999. Geologic Evolution of the Barberton Greenstone Belt, South Africa, Spec. Pap. Geol. Soc. Am., 329.

Lowe, D.R., 1994. Accretionary history of the Archean Barberton Greenstone Belt (3.55-3.22 Ga), southern Africa. Geology 22, 1099-1102.

Lowe, D.R., 1999. Geologic evolution of the Barberton Greenstone Belt and vicinity. In Lowe, D.R., Byerly, G.R., Editors , Geologic Evolution of the Barberton Greenstone Belt, Boulder, pp. 287–312 (Geol. Soc. .Am. Spec. Paper 329).

Ludwig, K., 2003a. Isoplot/Ex version 3: a Geochronological toolkit for Microsoft Excel. Geochronology Center, Berkeley.

Ludwig, K.R., 2003b. User's Manual for Isoplot 3.00. Berkeley Geochronological Center, Special Publication No. 4, Berkeley, 71 pp.

Martin, H, 1986. Effect of steeper Archean geothermal gradient on geochemistry of subduction-zone magmas. Geology 14, 753-756.

Martin, H., 1987. Petrogenesis of Archaean Trondhjemites, Tonalites and Granodiorites from Eastern Finland: Major and trace element geochemistry, J. Petrol. 28, 921-953.

Martin, H., 1994,. The Archean grey gneisses and the genesis of the continental crust, in: Condie, K.C. (Ed.), The Archean Crustal Evolution, Developments in Precambrian Geology. Elsevier, Amsterdam, pp. 205– 259.

Mattey, J.M., 2010. Analysis of the relative decay constants of 235U and 238U by multi-step CA-TIMS measurements of closed-system natural zircon samples. Chem. Geol. 275, 186–198.

Moorbath, M., Whitehouse, M.J. and Kamber, B.S.,1997. Extreme Nd-isotope heterogeneity in the early Archaean – fact or fiction? Case histories from northern Canada and West Greenland, Chem. Geol. 135, 213-231
.

Moyen, J.-F. et al., 2003. Late Archaean granites: a typology based on the Dharwar Craton (India). Precam. Res. 127, 103-123
.

Moyen, J.-F. et al., 2007. TTG plutons of the Barberton Granitoid-Greenstone Terrain, South Africa, in: van Kranendonk, M., Smithies, R. H. and Bennett, V.B. (Eds), Earth's Oldest Rocks. Developments in Precambrian Geology 15, pp. 607-667.

Moyen, J.-F., Stevens, G. and Kisters, A.F.M., 2006. Record of mid-Archaean subduction from metamorphism in the Barberton terrain, South Africa. Nature 443, 559-562.

Moyen, J-F., 2011. The composite Archaean grey gneisses: Petrological significance, and evidence for a non-unique tectonic setting for Archaean crustal growth. Lithos 123, 21-36.

Nair, R. and Chacko, T., 2008. Role of oceanic plateaus in the initiation of subduction and origin of the continental crust. Geology 36, 583-586.

Nasdala L., et al., 2008. Zircon M257–a homogeneous natural reference material for the ion microprobe U-Pb analysis of zircon. Geostand. Geoanal Res. 32, 247–265.

Nesbitt, H.W. and Young, G.M., 1982. Early Proterozoic climates and plate motions inferred from major

element chemistry of lutites. Nature 299, 715–717.

Patiño Douce, A.E. and Harris, 1998. N. Experimental Constraints on Himalayan Anatexis. J. Petrol. 39. 689-710.

Pin, C., Briot, D., Bassin, C. and Poitrasson, F., 1994. Concomitant separation of strontium and samarium-neodymium for isotopic analysis in silicate samples, based on specific extraction chromatography. Analytica Chimica Acta 298, 209-217.

Rapp, R. P., Watson, E.B. and Miller, C.F., 1991. Partial melting of amphibolite/eclogite and the origin of Archean trondhjemites and tonalites. Precamb. Res. 51, 1-25.

Reimer, T.O, et al., 1985. Petrography and geochemistry of granitoid metamorphites pebbles from the early Archaean Moodies group, Barberton Mountainland/South Africa, Precamb. Res. 29, 383-404.

Rollinson, H., 1997, Eclogite xenoliths in west African kimberlites as residues from Archaean granitoid crust formation: Nature 389, 173–176.

Rosing, M.T., 1990. The theoretical effect of metasomatism on Sm-Nd isotopic systems. Geochim. Cosmochim. Acta 54. 1337–1341.

Rudnick, R.L. and Gao, S., 2003. Composition of the continental crust, The Crust, Vol. 3 ,in: Rudnick, R.L., Editor, (2003) Holland, H.D., Turekian, K.K., Editors , Treatise on Geochemistry, Elsevier, Oxford (2003), pp. 1–64.

Sanchez-Garrido, C.J.M.G, et al., 2011. Diversity in Earth's early felsic crust: Paleoarchean peraluminous granites of the Barberton Greenstone Belt, Geology 39, 963-966.

Sanchez-Garrido, C.J.M.G., Stevens, G., Harris, C., Moyen, J.-F., Martin, H., and Doucelance, R., in preparation. Granitic contributions to the construction of the Paleo-Archean continental crust: Insights from three generations (3.55, 3.45 and 3.23 Ga) of low-Ca rhyolites/granites in the Barberton Granite Greenstone Terrane

Schoene, B., et al., 2009. Sm–Nd isotopic mapping of lithospheric growth and stabilization in the eastern Kaapvaal craton. Terra Nova 21, 219-228.

Schoene, B., De Wit, M. J. and Bowring, S. A., 2008. Mesoarchean assembly and stabilization of the eastern Kaapvaal craton: A structural-thermochronological perspective. Tectonics 27, TC5010; doi:10.1029/2008TC002267.

Sláma J., et al., 2008. Plešovice zircon—a new natural reference material for U–Pb and Hf isotopic microanalysis. Chem. Geol. 249,1–35.

Smithies, R.H., 2000. The Archaean tonalite-trondhjemite- granodiorite (TTG) series is not an analogue of Cenozoic adakite. Earth Planet. Sci. Let. 182, 115–125.

Sylvester, P.J., 1994. Archaean granite plutons. In: Condie, K.C. (Ed.), Archaean Crustal Evolution. Developments in Precambrian Geology, vol. 11. Elsevier, Amsterdam, pp. 261–314.

Tarney, J., Weaver, B.L. and Drury, S.A., 1979. Geochemistry of Archaean trondhjemitic and tonalitic gneisses from Scotland and E. Greenland, F. Barker, Editor, Trondhjemites, Dacites and Related Rocks, Elsevier, Amsterdam, pp. 275–299.

Taylor, S.R. and. McLennan, S.M, 1985. The Continental Crust: Its Composition and Evolution Blackwell, Oxford, p. 312.

Tegtmeyer, A. R. and Kröner, A., 1987. U-Pb zircon ages bearing on the nature of early Archaean greenstone belt evolution, Barberton Mountainland, Southern Africa. Precamb. Res. 36, 1-20 .

Toulkeridis, T., et al., 1998. Sm-Nd, Rb-Sr and Pb-Pb dating of silicic carbonates from the early Archaean Barberton Greenstone Belt, South Africa evidence for post-depositional isotopic resetting at low temperature, Precamb. Res.. 92, 129-144.

Van Hunen, J. et al., 2008. tectonics of early Earth: Some geodynamic considerations.. In: Condie, K.C. and Pease, V. (Eds.), When did plate tectonics begin on planet Earth. Geological society of America Special paper 440, pp. 261–314.

Van Kranendonk, M.J., et al., 2009. Age, lithology and structural evolution of the c. 3.53 Ga Theespruit Formation in the Tjakastad area, southwestern Barberton Greenstone Belt, South Africa, with implications for Archaean tectonics, Chem. Geol. 261, 115-139.

Vervoort, J.F. and Blichert-Toft, J., 1999. Evolution of the depleted mantle: Hf isotope

evidence from juvenile rocks through time. Geochim. Cosmochim. Acta 63, 533-556.

Viljoen, M. J., and Viljoen, R. P., 1969. An introduction to the geology of the Barberton, granite greenstone terrain, Spec. Publ. Geol. Soc. S. Afr. 9, 1-20.

Wilson, A. H., and Carlson, R. W., 1989. A Sm-Nd and Pb isotope study of Archaean greenstone belts in the southern Kaapvaal Craton, South Africa: Earth Planet. Sci. Let. 96, 89–105.

Workman, R. and Hart, S.R. 2005. Major and trace element composition of the depleted MORB mantle (DMM). Earth Planet. Sci. Let. 231, 53-72.

CONCLUSION

In this thesis I have documented the petrogenesis of rare granites and rhyolites, present only as clasts in the Basal conglomerate of the Moodies Group, in the Barberton Greenstone Belt (BGB) in South Africa. These granites and rhyolites record the presence of true granites in the Paleo- and Meso-Archean. They provide clues of great importance for our understanding of the development of the earliest continental crust. The results and conclusions drawn from my work, presented in chapters 2, 3 and 4 can be summarized as follows:

1) Sensitive high resolution ion microprobe (SHRIMP) analysis of zircon grains from 22 clasts allowed me to date the age of crystallization of the granites and rhyolites. I showed that the granites and rhyolites crystallized during three episodes of magmatism, which coincided with episodes of TTG genesis and three main deformation events in the BGB.

2) The presence of Albite, Orthoclase, as well as rare plagioclase inclusions with low Anorthitic content in the zircons serves as evidence that the zircons crystallized in a K-Na-rich magma, therefore ruling out the possibility of them having been inherited from TTG magmas. Additionally I demonstrated that the mineral inclusion suites present in the zircons, e.g. monazite, apatite, alkali feldspar, biotite, rutile, ilmenite and quartz, is identical to the rock forming minerals and accessory minerals present in the clasts. This shows that the zircons crystallized from a magma very close in composition to the granites and rhyolites, and that the main chemical characteristics of the clasts (i.e. Ca-poor and K-Na-rich) are primary magmatic features. This is of great importance, as it shows that the clasts are generally little- to non-altered and that their chemistry can therefore be used to understand their petrogenesis.

3) I observed that the samples preserve magmatic and volcanic textures evidenced by delicate quartz-feldspar intergrowths. This indicates that the granites formed at surface or in shallow-level magma chambers.

4) Careful investigation of the chemistry of the granites and rhyolites allowed me to establish that they were not low level crustal equivalents of the regional TTG's, but rather share characteristics of S-type granites. The peraluminous nature of our samples, as well as their flat HREE patterns and their Sr contents similar to S-type granites, represents some of the evidence that the source of

the granites was probably meta-sediments. However, fundamental differences exist between these granites and modern S-type granites (e.g. they have a very low CaO content uncorrelated with their high Sr content, and the Rb content of the samples are lower than what is expected for S-type granites), which I attribute to their source composition or to the process and conditions of their formation. Based on the chemistry and the petrography of the granites, I conclude that they formed via partial melting of immature, quartz + biotite-bearing clastic sediments (i.e. immature greywackes). More importantly, melting took place at high pressure, above the pressure at which plagioclase is a stable phase in greywacke, at ca. 750-850 °C. These conditions of melting were tested via geochemical modeling, where I confirm that the granites could be formed through the partial melting of an immature greywacke at high pressure and medium temperature. These conditions of melting are very similar to the conditions at which TTG magmas are generated (partial melting of amphibolite at ca. 18-24 kbars). I propose that the granites present in the Moodies group were generated under the same conditions as the TTGs, during the same geodynamic event. Given that in the BGB, at least one group of the TTG plutons was formed in a subduction zone, I deduced that the granites were formed in the same setting where their source, the sediments, were most likely situated on top of the subducted oceanic crust.

5) Whole-rock oxygen isotopes, and the oxygen isotopes of individual minerals in the clasts and in the matrix of the conglomerate, show very interesting results. The $\delta^{18}O$ value of the feldspar and quartz grains of some clasts, as well as the $\delta^{18}O$ value of the whole-rock are high (ca.16 ‰), yet the $\delta^{18}O$ value of single zircon grains from the same samples are very low (ca.6 ‰). This indicates that a portion of the quartz and feldspars were altered, but that the zircons have preserved the magmatic $\delta^{18}O$ value of the source of the granite. I interpreted these differences as reflecting the interaction of the granitic pebbles with a low temperature (ca. 200 °C), high $\delta^{18}O$ fluid (ca. 16 ‰). This interaction happened at an extremely slow rate, thus preserving the magmatic textures of the feldspar grains. I infer that this fluid was induced during the 3.23 Ga greenschist-facies metamorphism which affected the BGB, including the Moodies Group. The metamorphic fluid percolated through the matrix of the conglomerate, thus recording the high $\delta^{18}O$ value of this one and cooling down by ca. 50-100 °C. The high $\delta^{18}O$ fluid was then available to react with the granitic pebbles. However, even though oxygen

isotope exchanged took place between feldspar and quartz, the low solubility of certain elements in such a low temperature fluid (like potassium, calcium and sodium) could explain how the bulk-rock composition of the granite remained unchanged relative to its magmatic composition. Despite the fact that oxygen isotope exchange happened, the lack of alteration of the feldspar and quartz, and the preservation of delicate magmatic textures, could either be explained by the kinetics of the reaction between the fluid and the grains, or by the low activity of water in the fluid (<1).

6) The $\delta^{18}O$ values of the zircons have preserved the $\delta^{18}O$ value of the magma from which the granites originated. This $\delta^{18}O$ value is similar to the $\delta^{18}O$ value of the regional TTG. This could imply that material from the TTG, such as their high-Al biotites, was involved in the sedimentary source of the granites.

7) A comparison of volcaniclastic rocks from the oldest lithological unit in the BGB and the oldest, coeval population of granite, allowed me to identify similarities between the two rock types. In fact the in-situ volcaniclastic rocks share many characteristics with the granites: they are relatively rich in K_2O, poor in CaO, peraluminous and have flat HREE patterns. I have established that these rocks are not volcanic equivalents of the TTGs, as described in previous studies, but rather the volcanic equivalents of the granites of the Moodies group. I conclude that the granitic clasts, which are a unique feature for the Paleo- to Meso-Archean, may in fact represent only a fraction of the preserved granitic material, and that volcanic material such as that from the Theespruit formation, for instance, may help us to establish the compositional range of the granitic suite.

8) Whole-rock Sm-Nd analysis of granitic and volcanic clasts allowed the determination of the minimum age of the source of the granite at ca. 3.9 Ga. Using these radiogenic isotopes, I can conclude that the source of the granites was isotopically heterogeneous but identical for the whole generation of granite. In other words, the sedimentary source of the granite was derived from the same type of protolith, but was isotopically heterogeneous. This is not an uncommon feature of sediments, which are often heterogeneous in nature, but eroded from the same general relief.

9) The Sm-Nd isotopic characteristics of the granites indicate that, 3.9 to 3.7 Ga ago, the Earth was already very effective at recycling pre-existing crustal material. More specifically, the source of the granite was presumably generated 3.7 to 3.9 Ga ago, brought to surface, weathered to become

sediment, and then taken to depth to generate the granites and rhyolites which are now present in the Moodies Group. This suggests a tectonic environment and Paleo- to Meso-Archean geodynamic processes similar to that which operates on Earth today.

10) Additionally, the study of Lu-Hf isotopes of the zircons from the clasts helps to confirm their crustal nature, as well as the minimum age of the source's protolith of the granites and rhyolites.

11) Interestingly, the Sm-Nd isotopic composition of the BGB TTGs implies that the source of the TTGs was always ca. 300 Ma older than the TTG themselves. This indicates that the TTG may not be primitive rocks but they are rather produced by melting of a source that was extracted from the Depleted Mantle at least 300 Ma before their formation. This can not correspond directly to the oceanic crust as this one was recycled within a maximum of 180 Ma after its extraction from the Depleted Mantle. We assume that the 300 Ma gap correspond to multiple episode of mantle recycling leading to the TTG source.

In conclusion, the results of my PhD shows that crustal recycling, evidenced by the partial melting of sediments, was effective on the Kaapvaal Craton long before ca. 3.2 Ga, which is the earliest known age for the appearance of widespread potassic-rich granitic magmatism on the Craton. I have demonstrated that in the BGB, true granites (senso stricto) were generated from at least 3.55 Ga onwards. These granites probably formed in a subduction zone setting, coeval with the TTG magmatism. Additionally, weathering of these low-level, shallow crustal granites represents the perfect mechanism by which to enrich the upper crust in potassium. Previous studies have argued that the late cratonization, potassic-rich granites (like the Granodiorite-Monzogranite-Syenite suite of the BGB) were generated through low degrees of partial melting of TTGs. I, in contrary, argue that these late Archean granites were formed from the recycling of previously K-rich material, located in the upper-crust, which in turn originated from the erosion of shallow-level granites and rhyolites present in the crust since 3.55 Ga. I believe that the absence of an obvious plutonic record of these shallow-level granites and rhyolites does not automatically imply a low abundance in the crust. In contrary I think that the K-rich sediments of the BGB have recorded the widespread presence of such granites. For instance, the Fig Tree Group sediments are unusually rich in potassium at a time where

mostly TTGs and komatiites are supposed to have dominated the crust. I believe that the granites were present in greater proportion than presently preserved. Preferential weathering of the granites with smaller Na:Ca ratios could explain the illusion of absence of these granites in great proportion. For instance, rocks such as the Theespruit felsic schists may represent the Na:Ca-richer equivalent of the granites.

In conclusion, the work presented in this thesis demonstrates that the early Earth was operating, in many respects, as it is today and that subduction zone processes were probably effective since the Paleo-Archean. The absence of widespread Andesitic material from the Archean rock record, and the presence of highly potassic granites, could reflect the difference between early Earth and modern Earth processes. In the modern Earth, sediments are melted at medium depth and melting of the mantle wedge is responsible for the genesis of Andesitic magmas. In the Archean, the pressure gradient was different and the proportion of clays in sediments (and therefore water content) was lower. This induced low fertility at lower pressure. High pressure partial melting seems to be one of the only viable mechanisms to explain the presence of both TTG and the Moodies granites. The low water content of these rocks precludes the melting of the mantle wedge, and explained the absence of Andesite.

Appendices

Chapter 2: Appendices

2. Data Repository description guide of Chapter 2

Table DR1: Geochemical data for the Moodies granitic clasts and TTGs associated with the Barberton Greenstone Belt

This table contains the chemical compositions of the Moodies granitic clasts, the Tonalite-Trondhjemite-Granodiorite (TTG) of the Barberton Greenstone Belt, discussed in the paper. The chemistry of the relatively potassic portion of the Ancient Gneiss Complex (AGC) figured in the table. Experimental data (Schmidt et al 2004) discussed in the paper are also part of this table. In addition this table contains information regarding the petrography and the Zr solubility temperature of the granitic clasts.

Table DR2: Stable isotope data

This table contains a summary of the data produced during SHRIMP oxygen analysis for the Moodies Group granitic and rhyolitic clasts.

Table DR3: S.E.M mineral inclusions analysis

This table contains a summary of representative data produced during SEM analysis for the Moodies Group granitic and rhyolitic clasts. A very subordinate fraction of feldspar and plagioclase inclusion within the zircon has been analysed, but only few data are presented in order give an idea of the mineral composition of the inclusion to the reader.

Table DR4: U-Pb radiogenic isotope data

This table contains a summary of the data and ages produced during SHRIMP U-Pb analysis for the Moodies Group granitic and rhyolitic clasts. A very subordinate fraction of zircon from samples A3, B25 and B14 produced younger concordant ages relative to the bulk of the grains. As these younger

zircons have Th/U < 0.4 and never occur as rims on the older population, they are interpreted to be detrital zircons of magmatic origin that have been introduced via very small amounts of matrix possibly adhering to the clasts, despite substantial efforts to clean the clasts of any matrix.

Figure DR5: Catholuminescence images of the analysed zircons

This figure documents the CL images of the clasts' zircons that were analysed via SHRIMP. The black or white ellipse indicates the place of the SRHIMP analysis. The 207Pb/206Pb age is indicated next to the analysed spot. The CL imaging did not reveal the presence of inherited cores. For some grains, both magmatic rims and core of the grain where analyzed to confirm the absence of inherited core.

Figure DR6: Concordia diagram of analysed U-Pb zircons

This figure documents the concordia diagrams drawn using the program ISOPLOT, for each samples from which zircons have been analysed by SHRIMP.

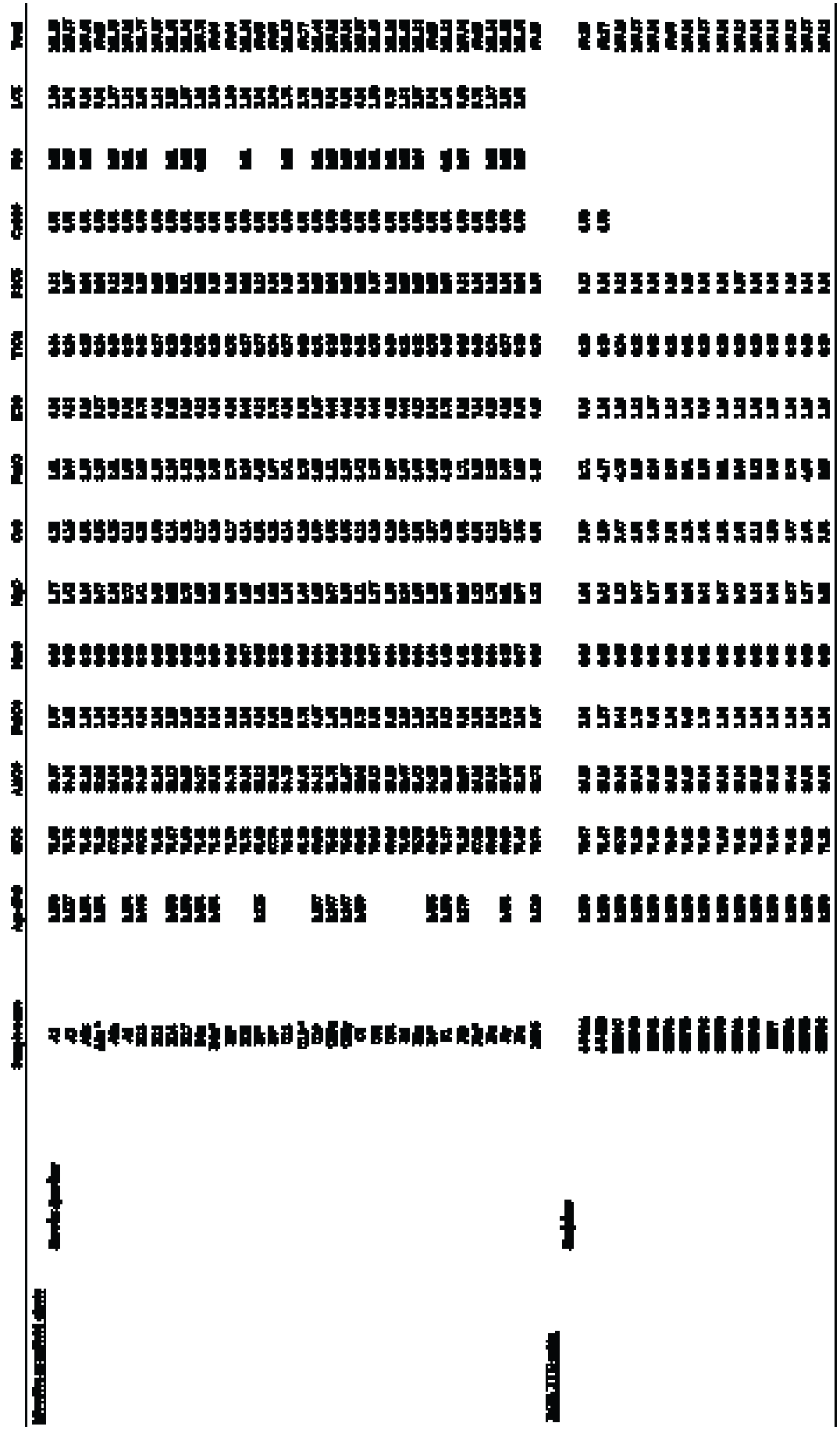

Supplementary Table DR1: Geochemical data for the Moodies granitic clasts and TTGs associated with the Barberton Greenstone Belt

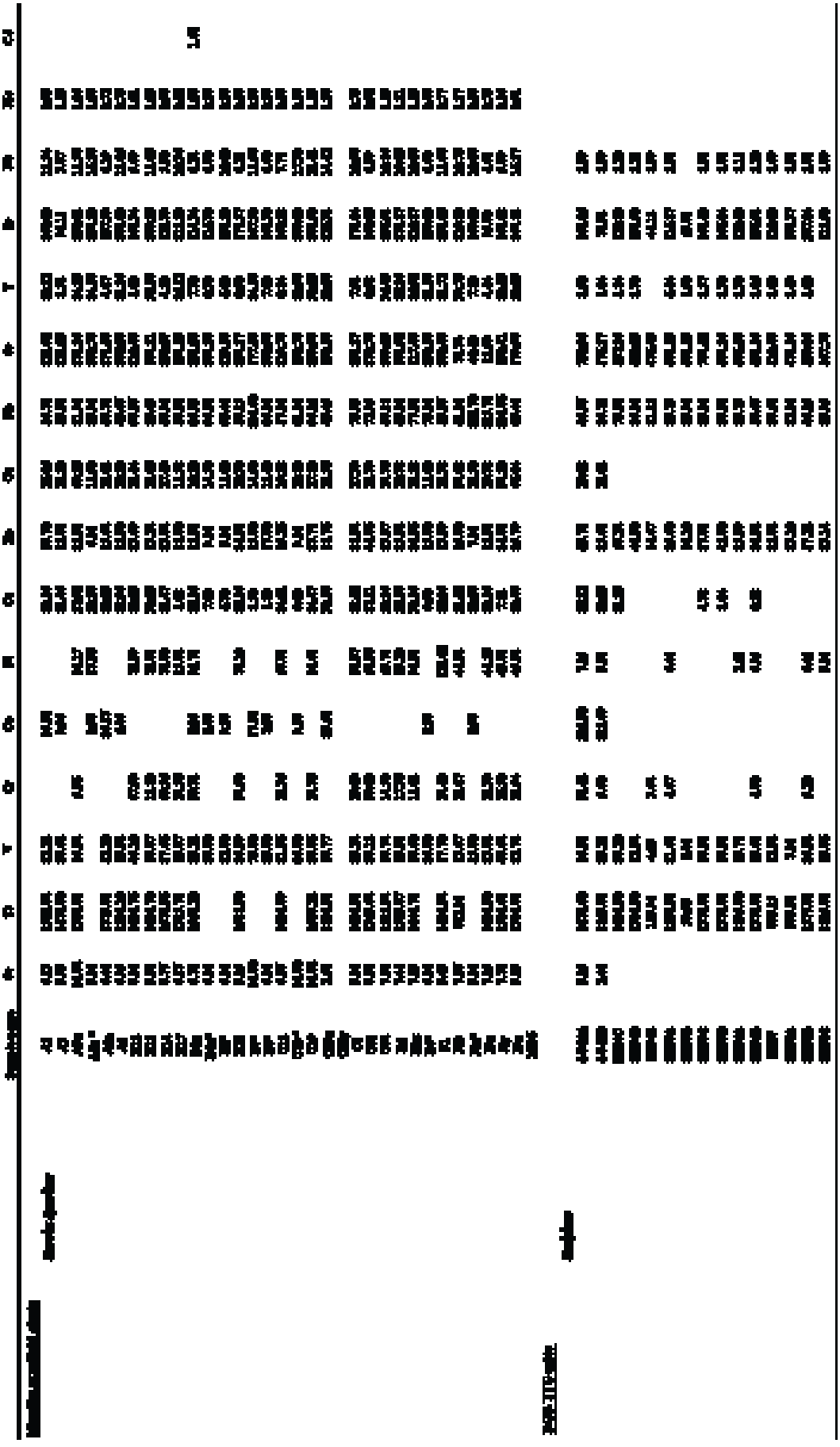

Supplementary Table DR1 (continued): Geochemical data for the Moodies granitic clasts and TTGs associated with the Barberton Greenstone Belt

Supplementary Table DR1 (continued): Geochemical data for the Moodies granitic clasts and TTGs associated with the Barberton Greenstone Belt

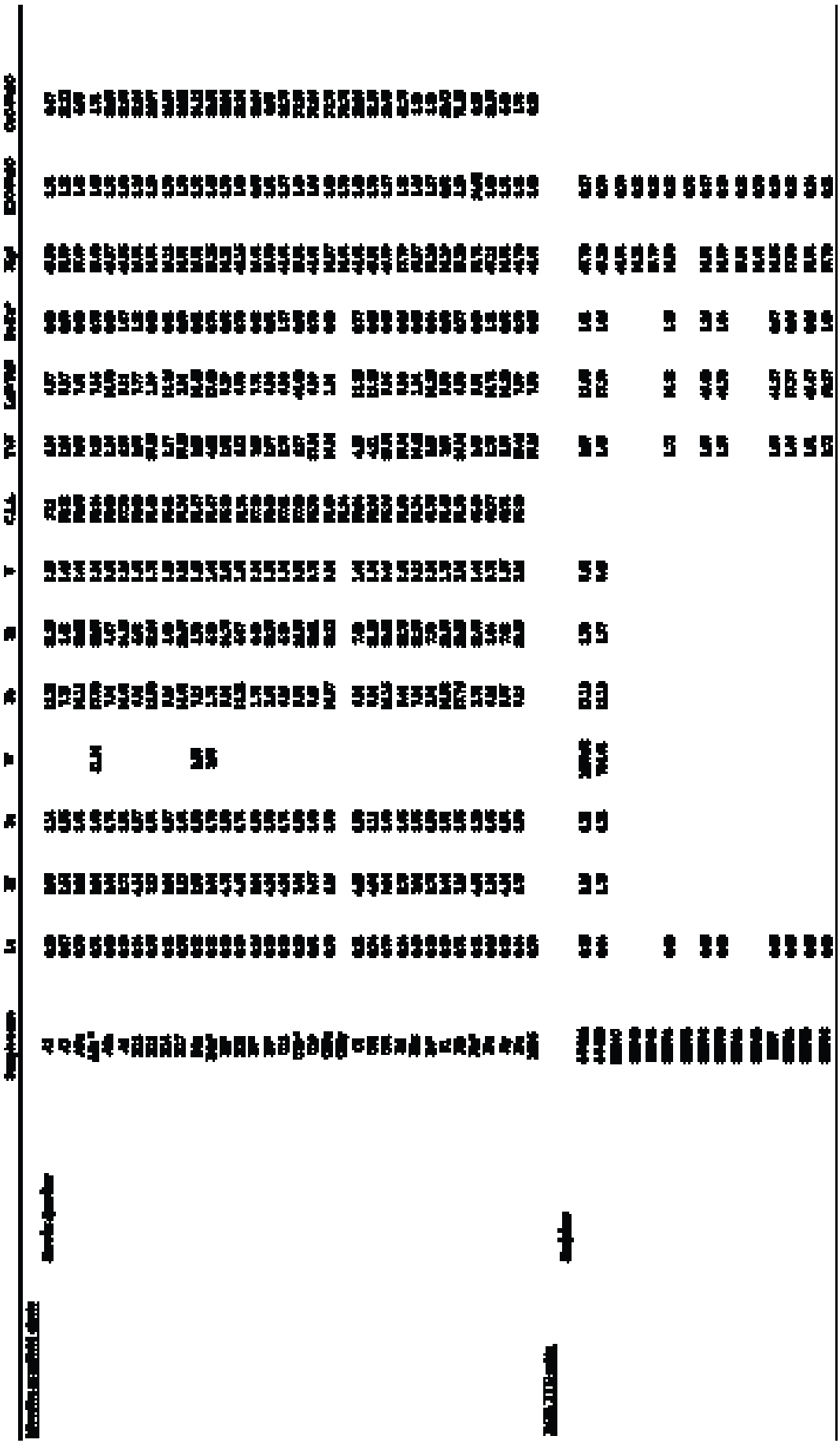

Supplementary Table DR1 (continued): Geochemical data for the Moodies granitic clasts and TTGs associated with the Barberton Greenstone Belt

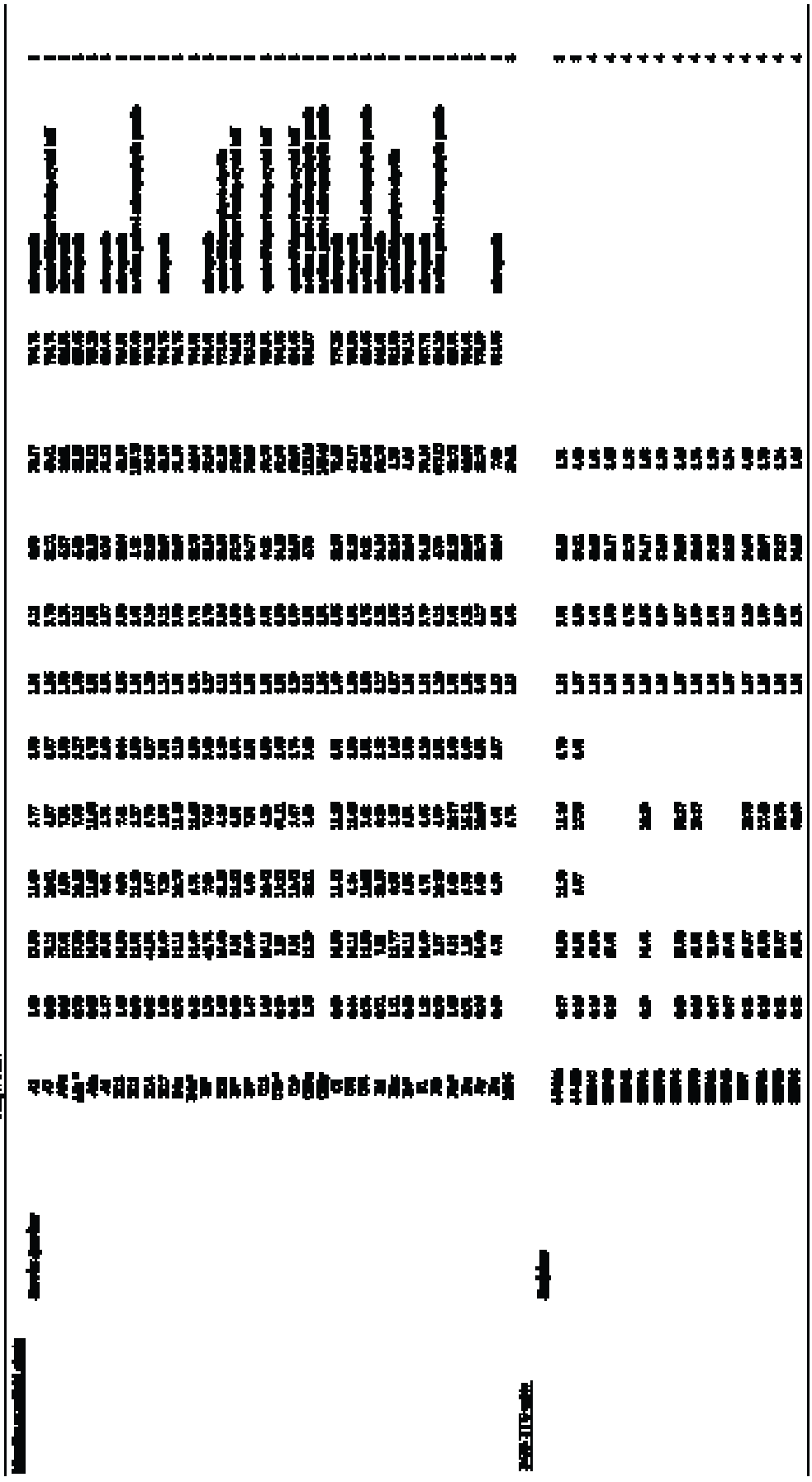

Supplementary Table DR1 (continued): Geochemical data for the Moodies granitic clasts and TTGs associated with the Barberton Greenstone Belt

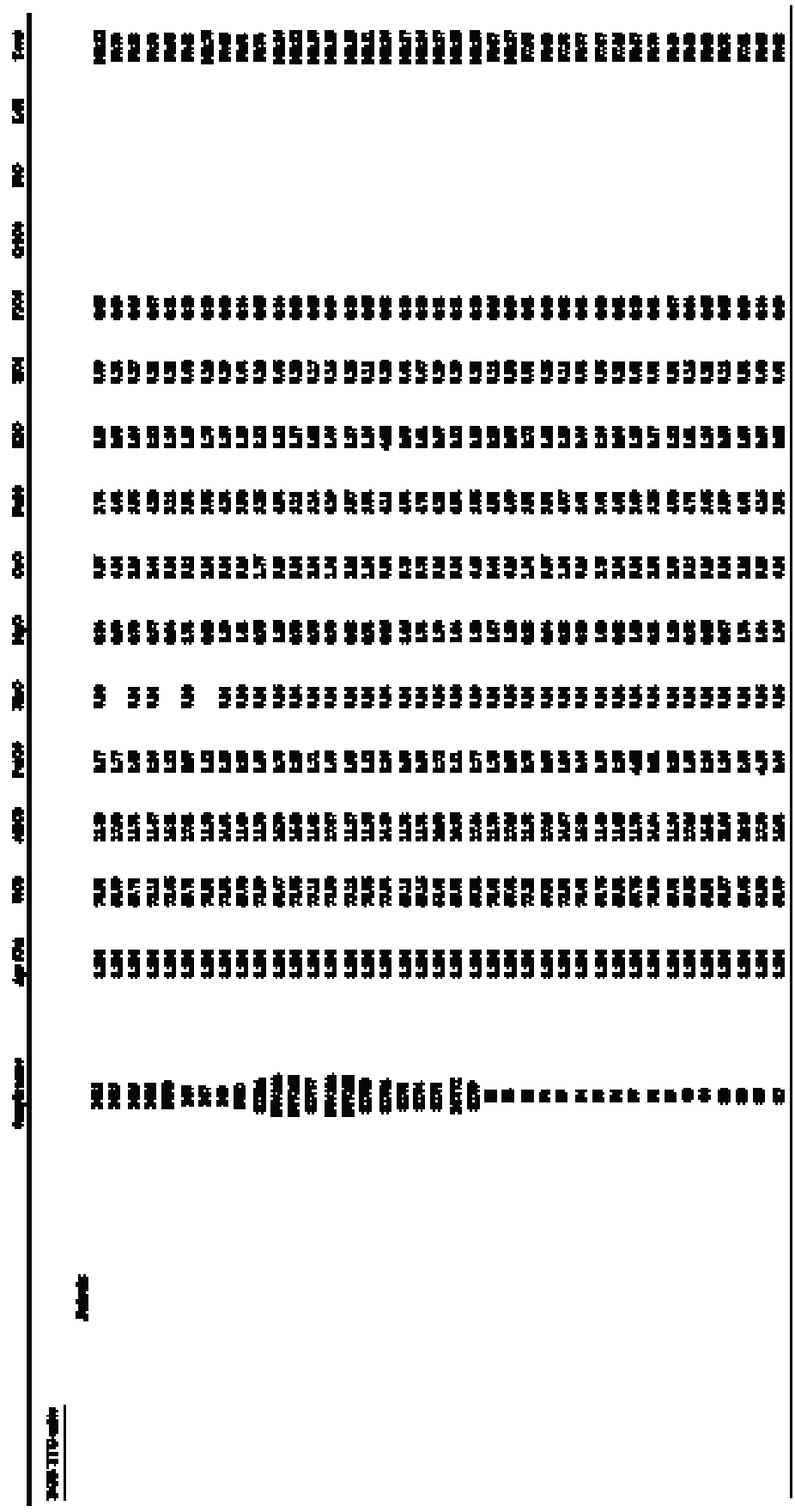

Supplementary Table DR1 (continued): Geochemical data for the Moodies granitic clasts and TTGs associated with the Barberton Greenstone Belt

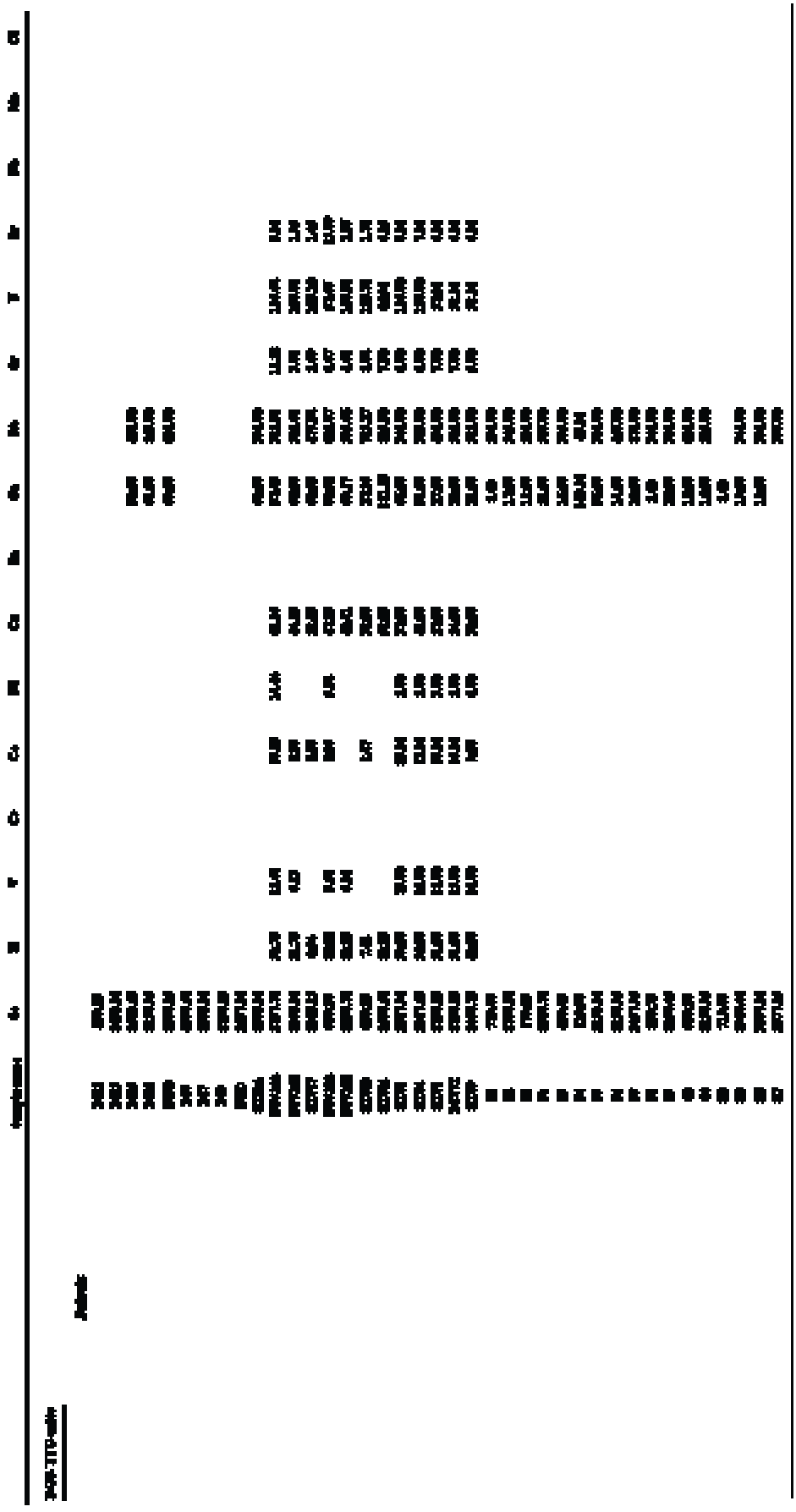

Supplementary Table DR1 (continued): Geochemical data for the Moodies granitic clasts and TTGs associated with the Barberton Greenstone Belt

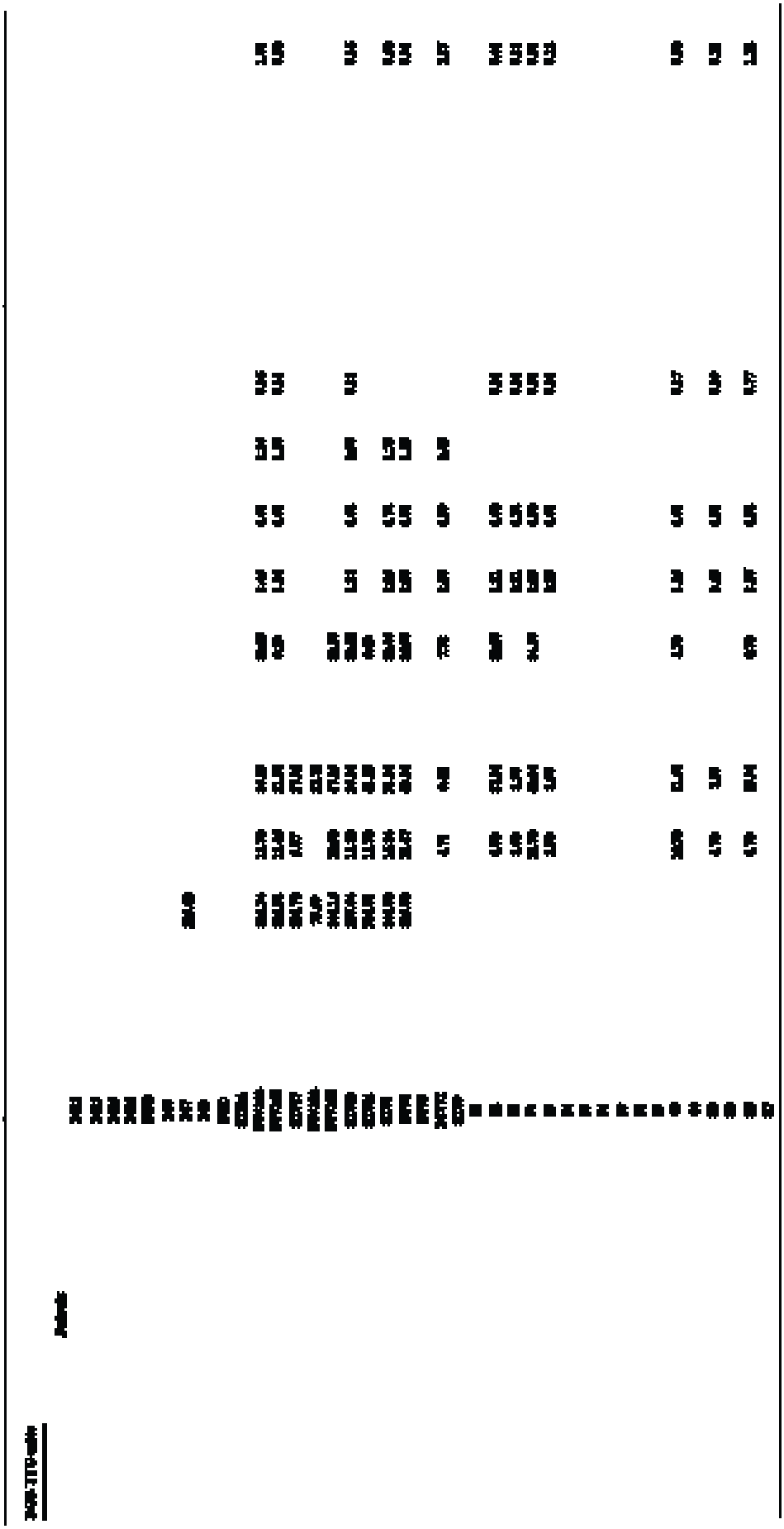

Supplementary Table DR1 (continued): Geochemical data for the Moodies granitic clasts and TTGs associated with the Barberton Greenstone Belt

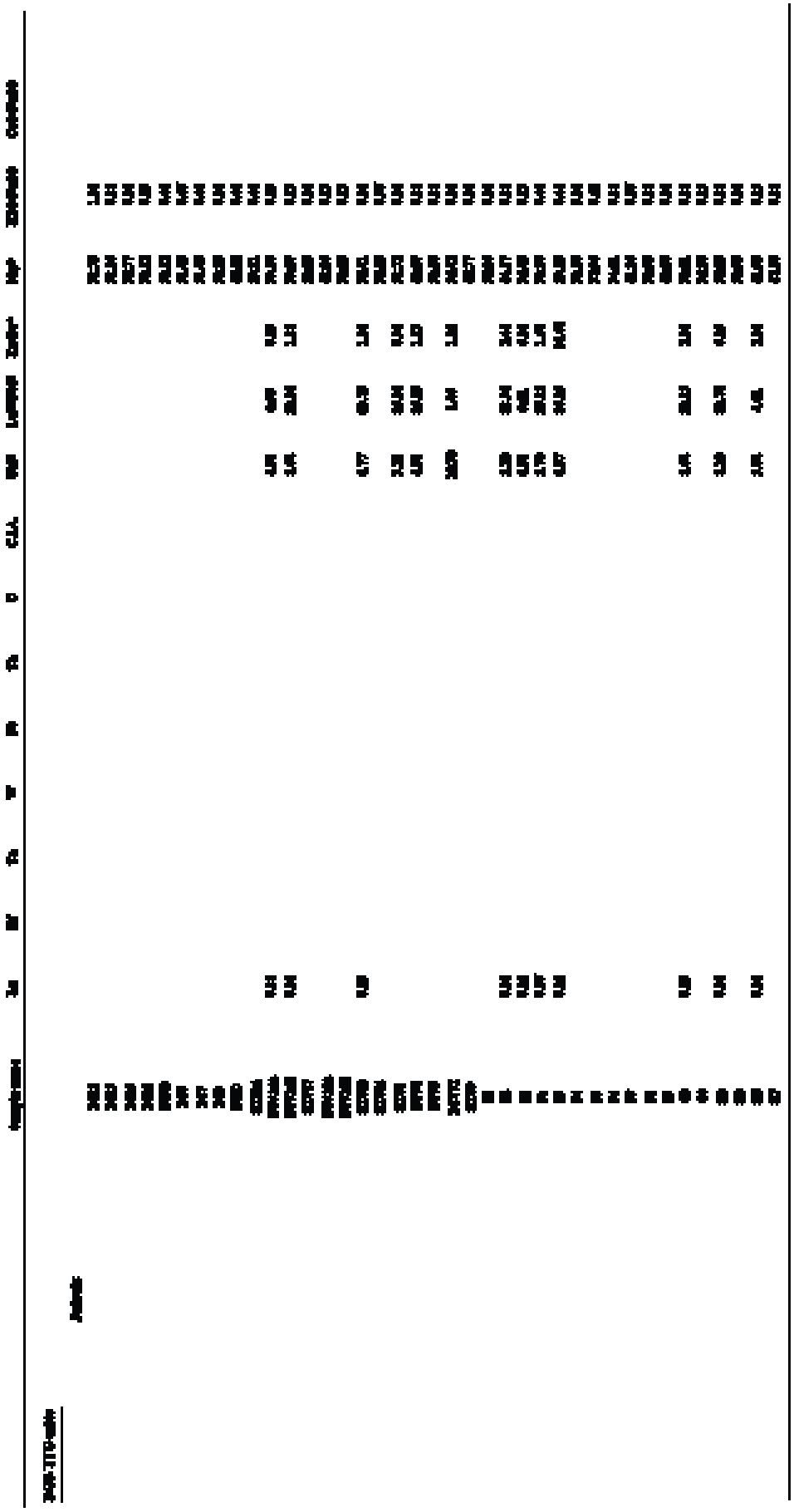

Supplementary Table DR1 (continued): Geochemical data for the Moodies granitic clasts and TTGs associated with the Barberton Greenstone Belt

Supplementary Table DR1 (continued): Geochemical data for the Moodies granitic clasts and TTGs associated with the Barberton Greenstone Belt

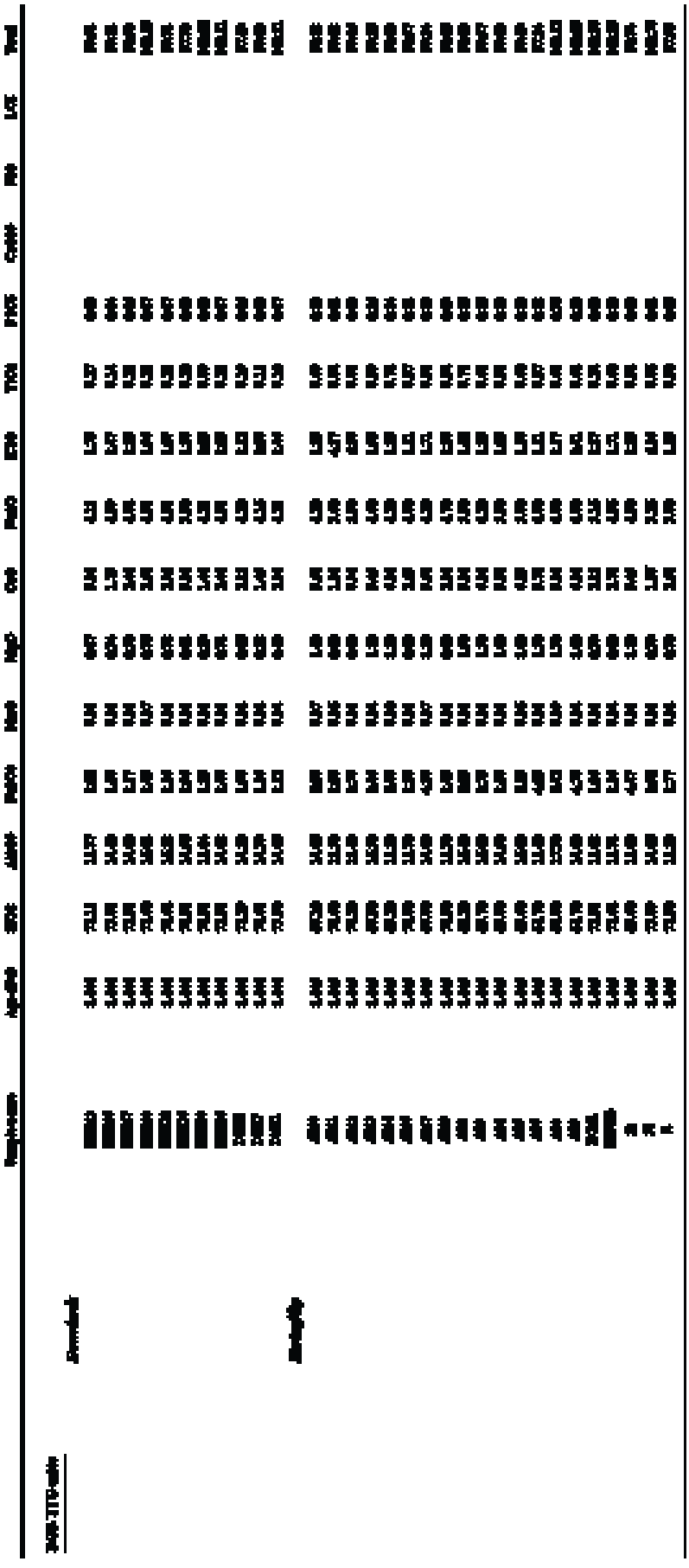

Supplementary Table DR1 (continued): Geochemical data for the Moodies granitic clasts and TTGs associated with the Barberton Greenstone Belt

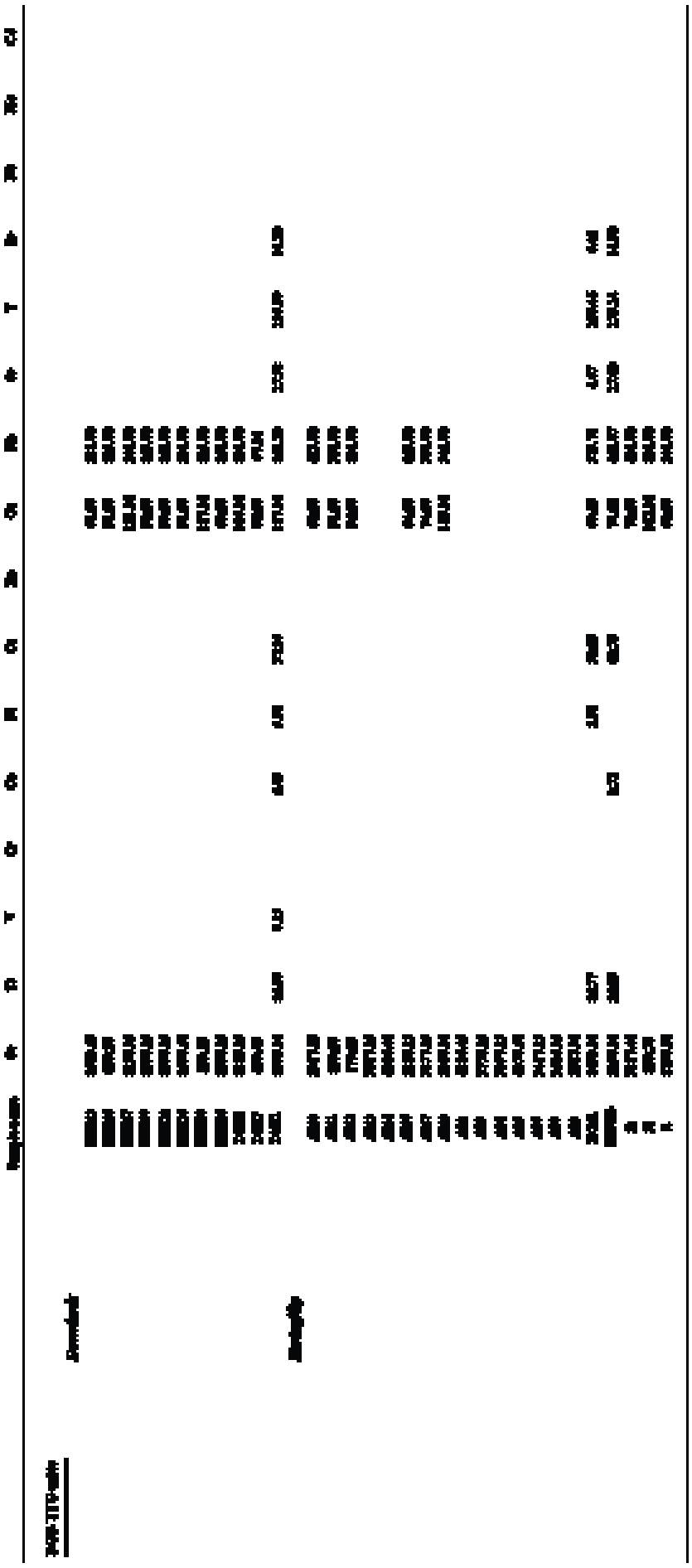

Supplementary Table DR1 (continued): Geochemical data for the Moodies granitic clasts and TTGs associated with the Barberton Greenstone Belt

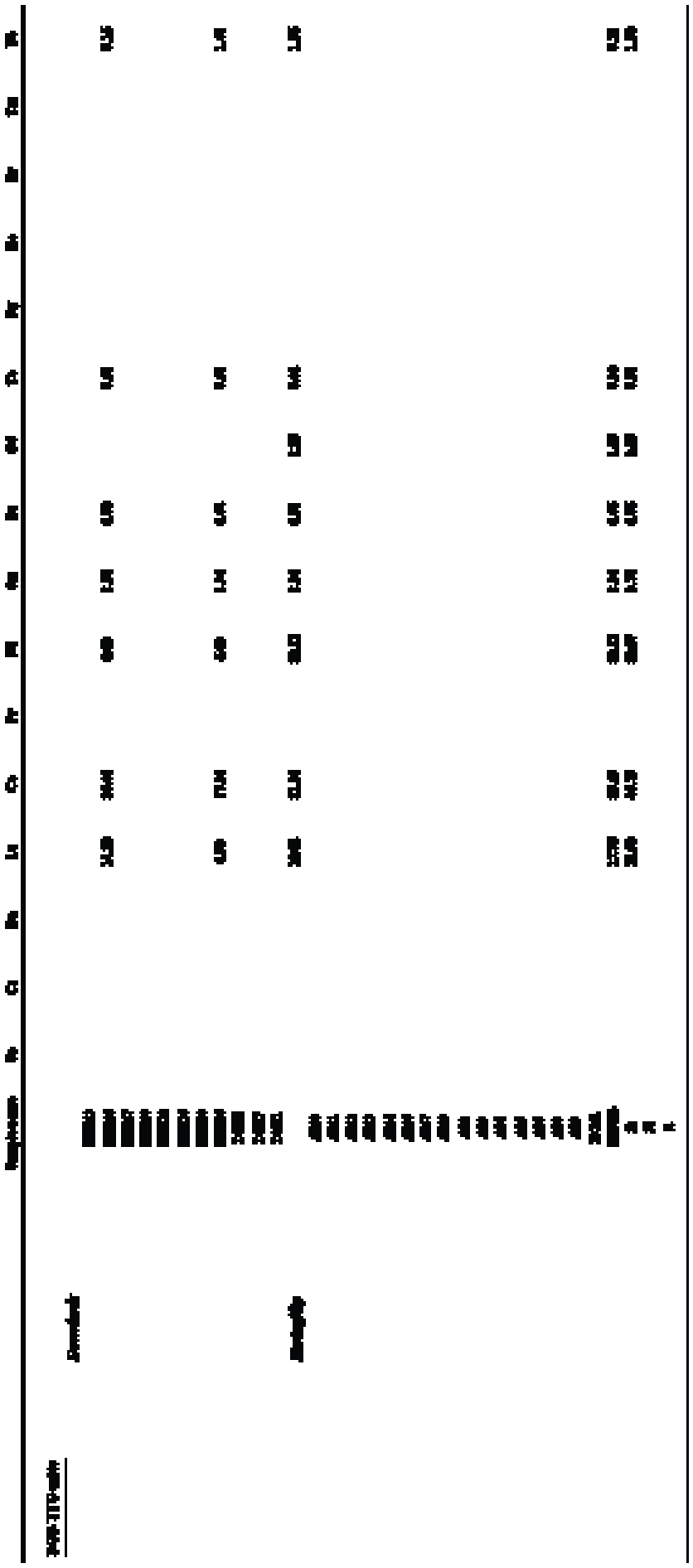

Supplementary Table DR1 (continued): Geochemical data for the Moodies granitic clasts and TTGs associated with the Barberton Greenstone Belt

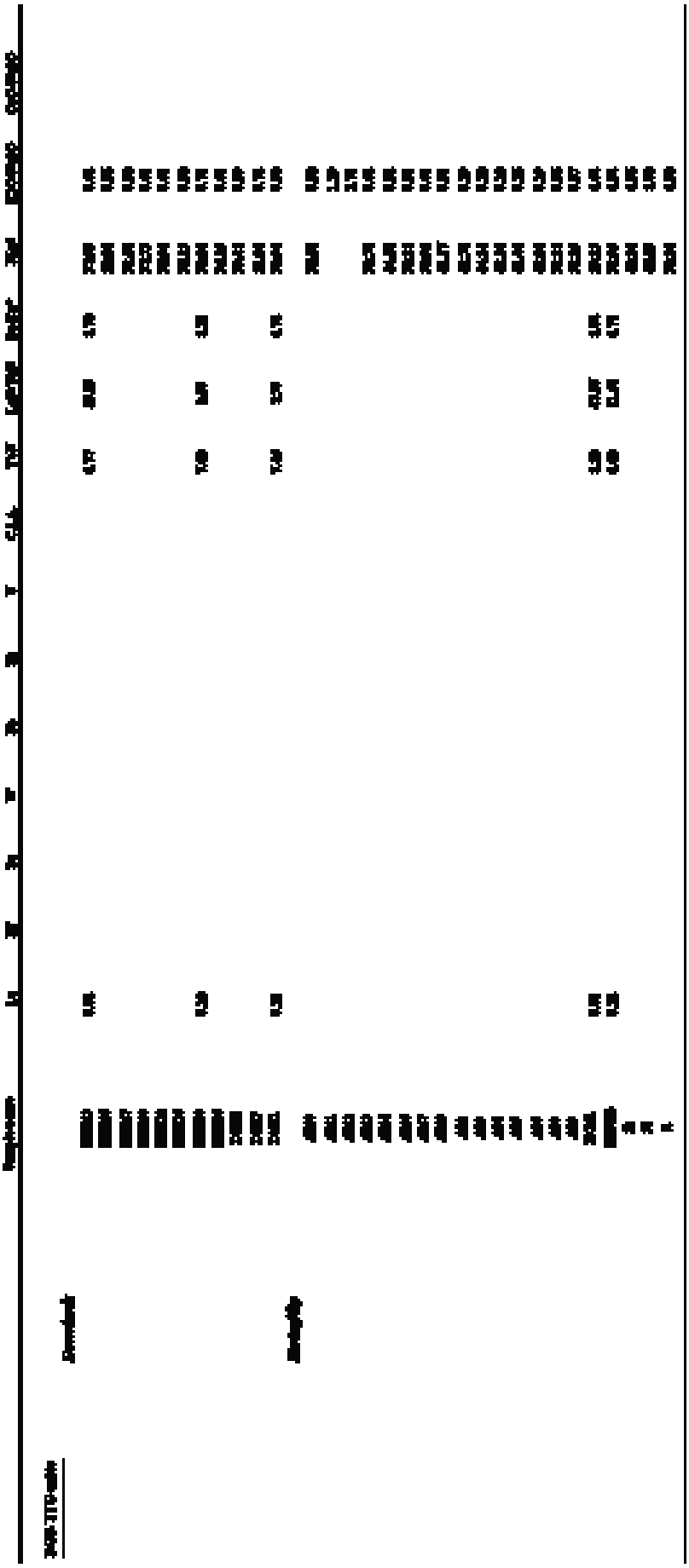

Supplementary Table DR1 (continued): Geochemical data for the Moodies granitic clasts and TTGs associated with the Barberton Greenstone Belt

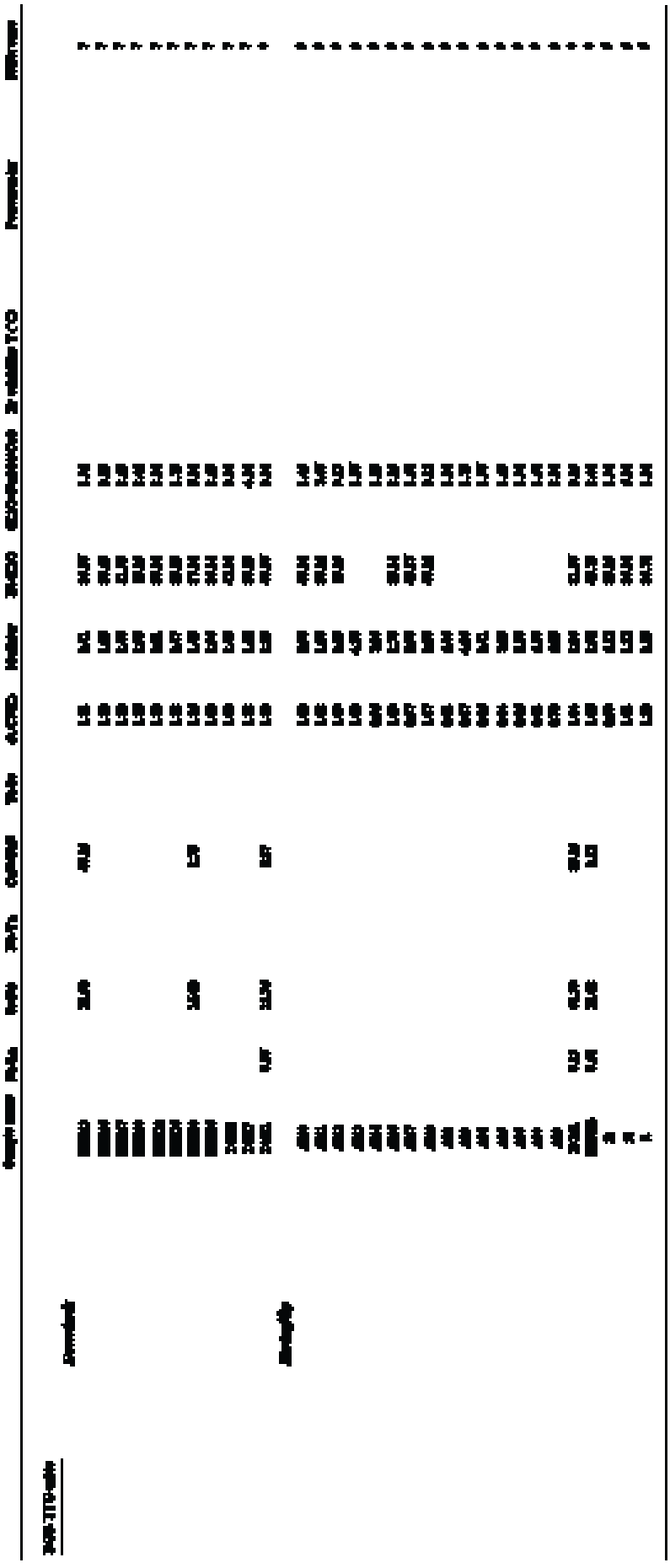

Supplementary Table DR1 (continued): Geochemical data for the Moodies granitic clasts and TTGs associated with the Barberton Greenstone Belt

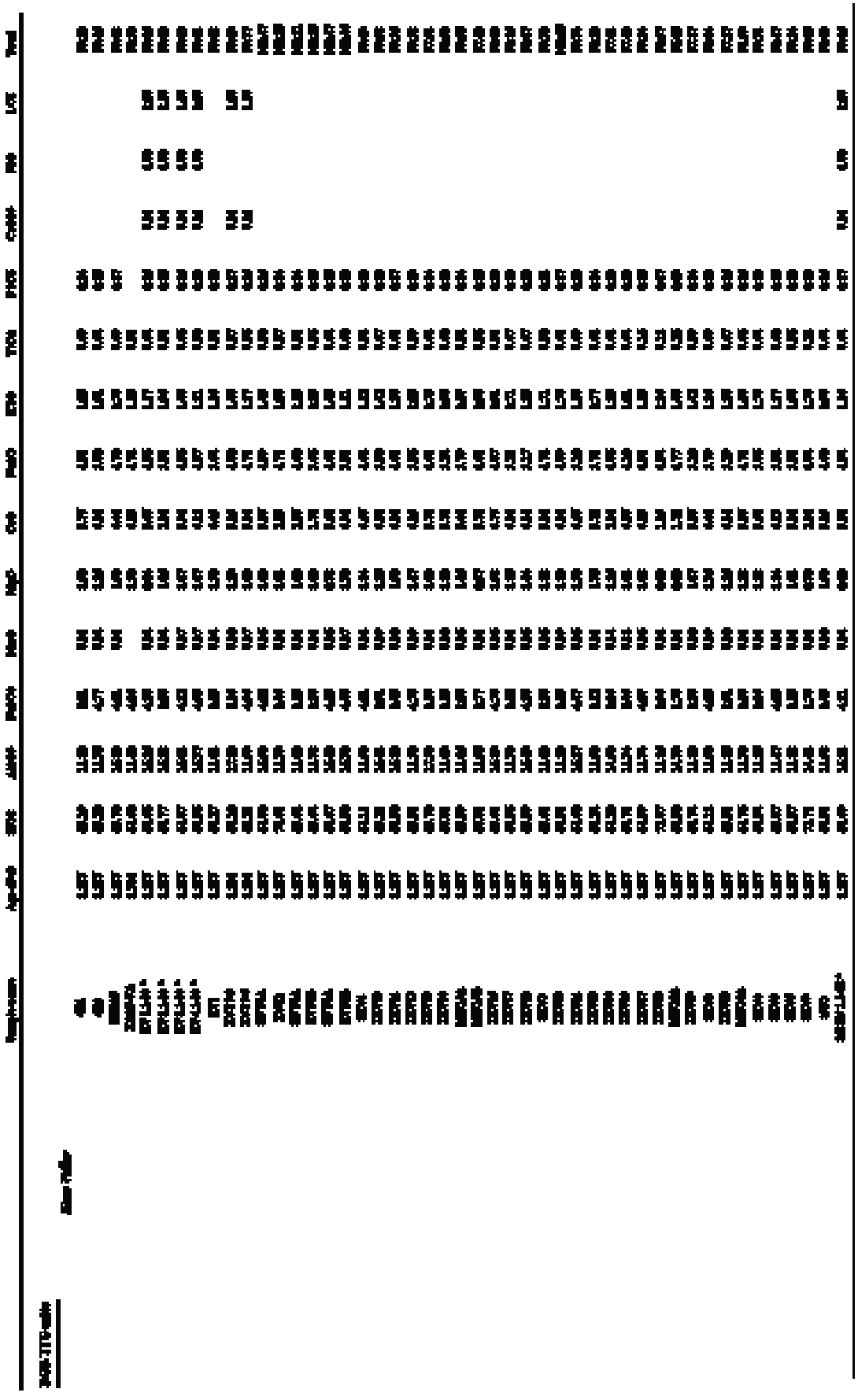

Supplementary Table DR1 (continued): Geochemical data for the Moodies granitic clasts and TTGs associated with the Barberton Greenstone Belt

Supplementary Table DR1 (continued): Geochemical data for the Moodies granitic clasts and TTGs associated with the Barberton Greenstone Belt

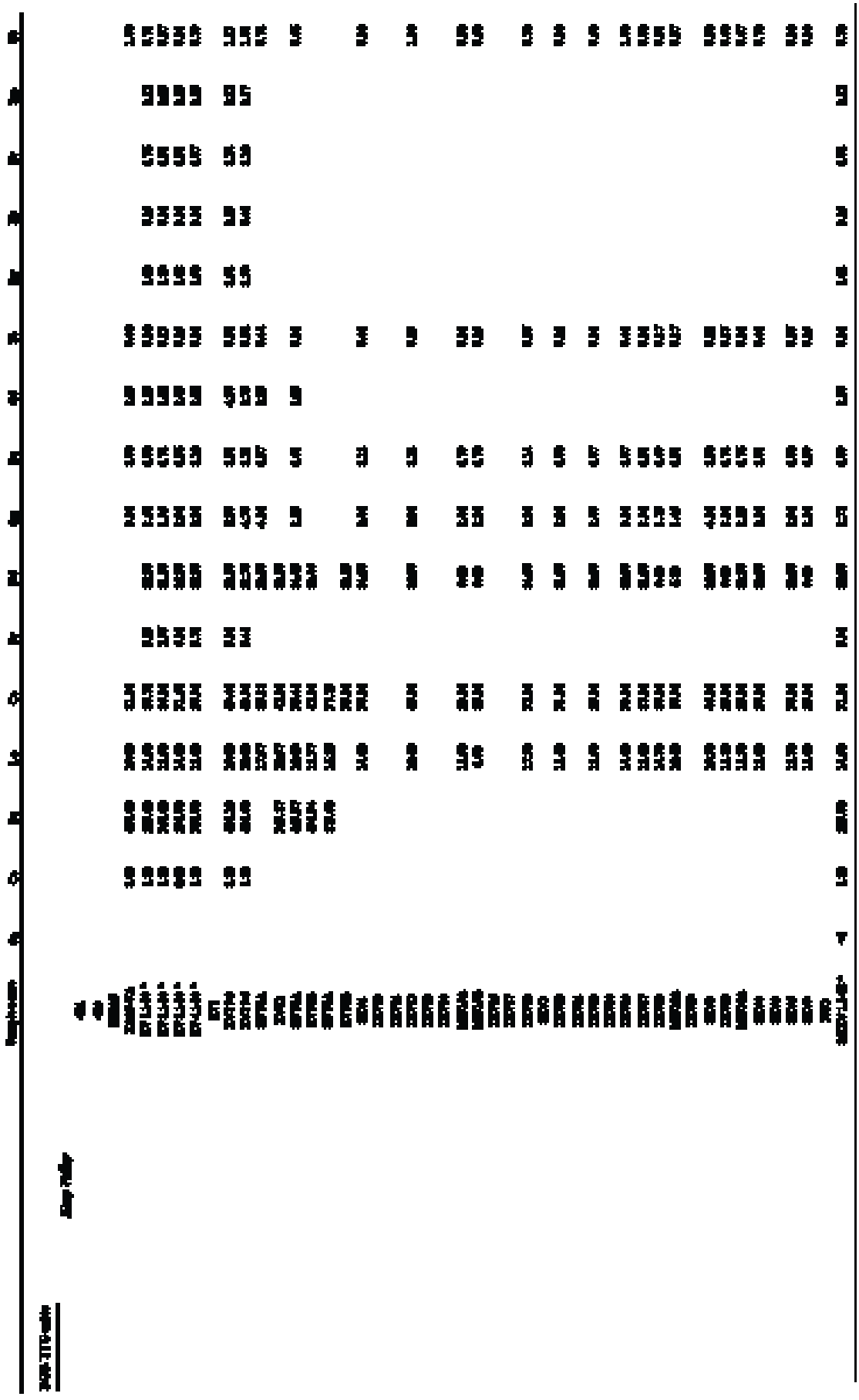

Supplementary Table DR1 (continued): Geochemical data for the Moodies granitic clasts and TTGs associated with the Barberton Greenstone Belt

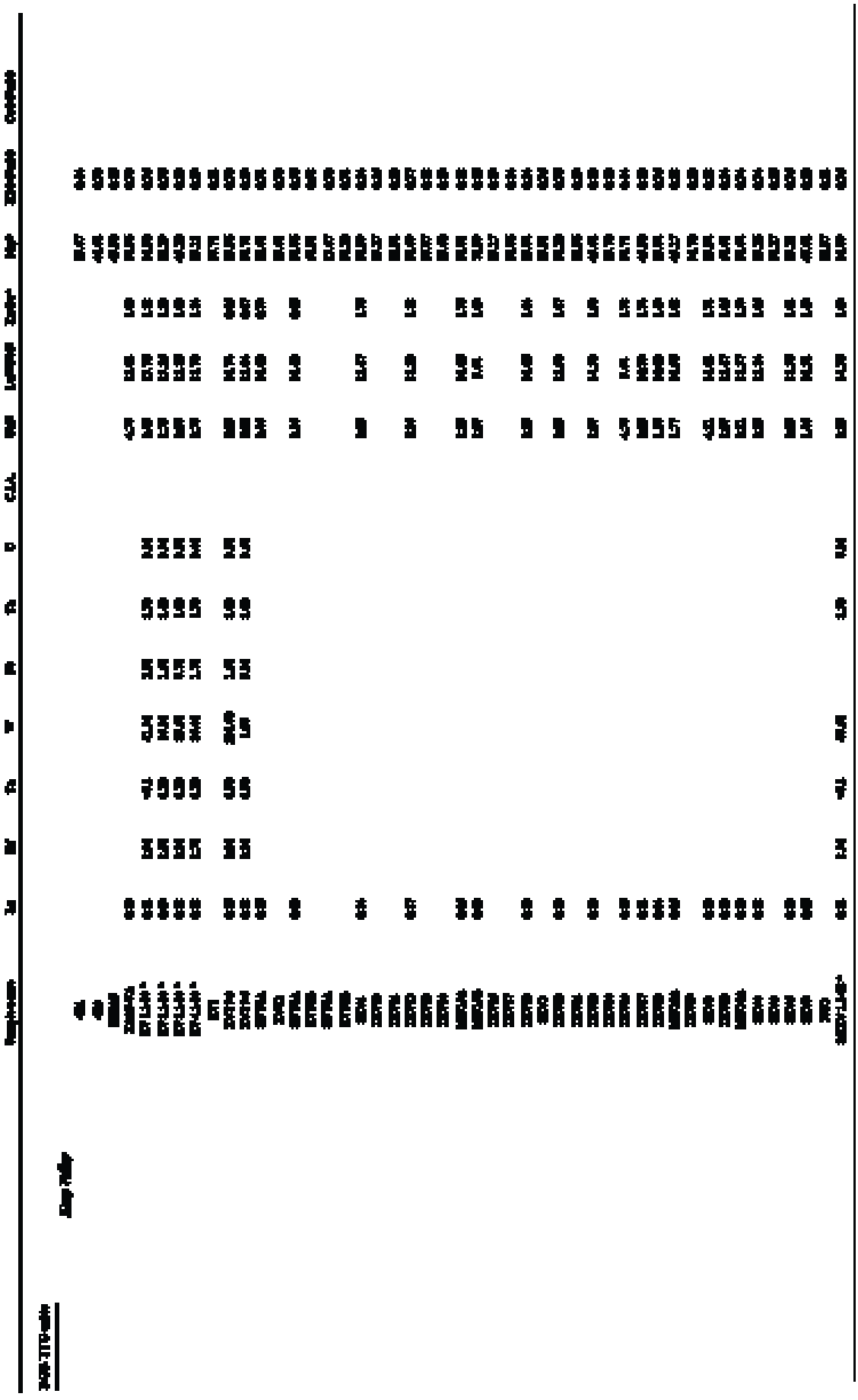

Supplementary Table DR1 (continued): Geochemical data for the Moodies granitic clasts and TTGs associated with the Barberton Greenstone Belt

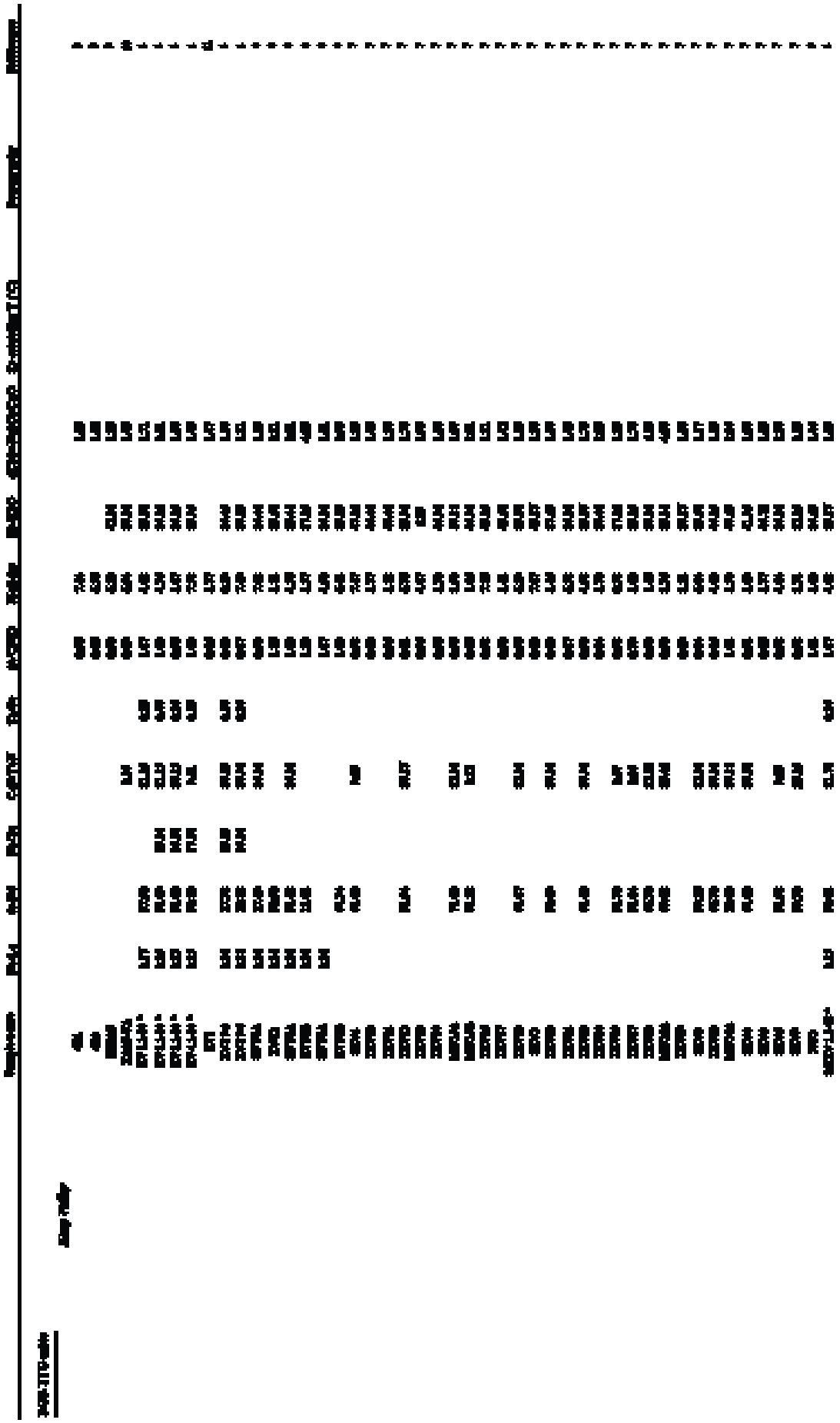

Supplementary Table DR1 (continued): Geochemical data for the Moodies granitic clasts and TTGs associated with the Barberton Greenstone Belt

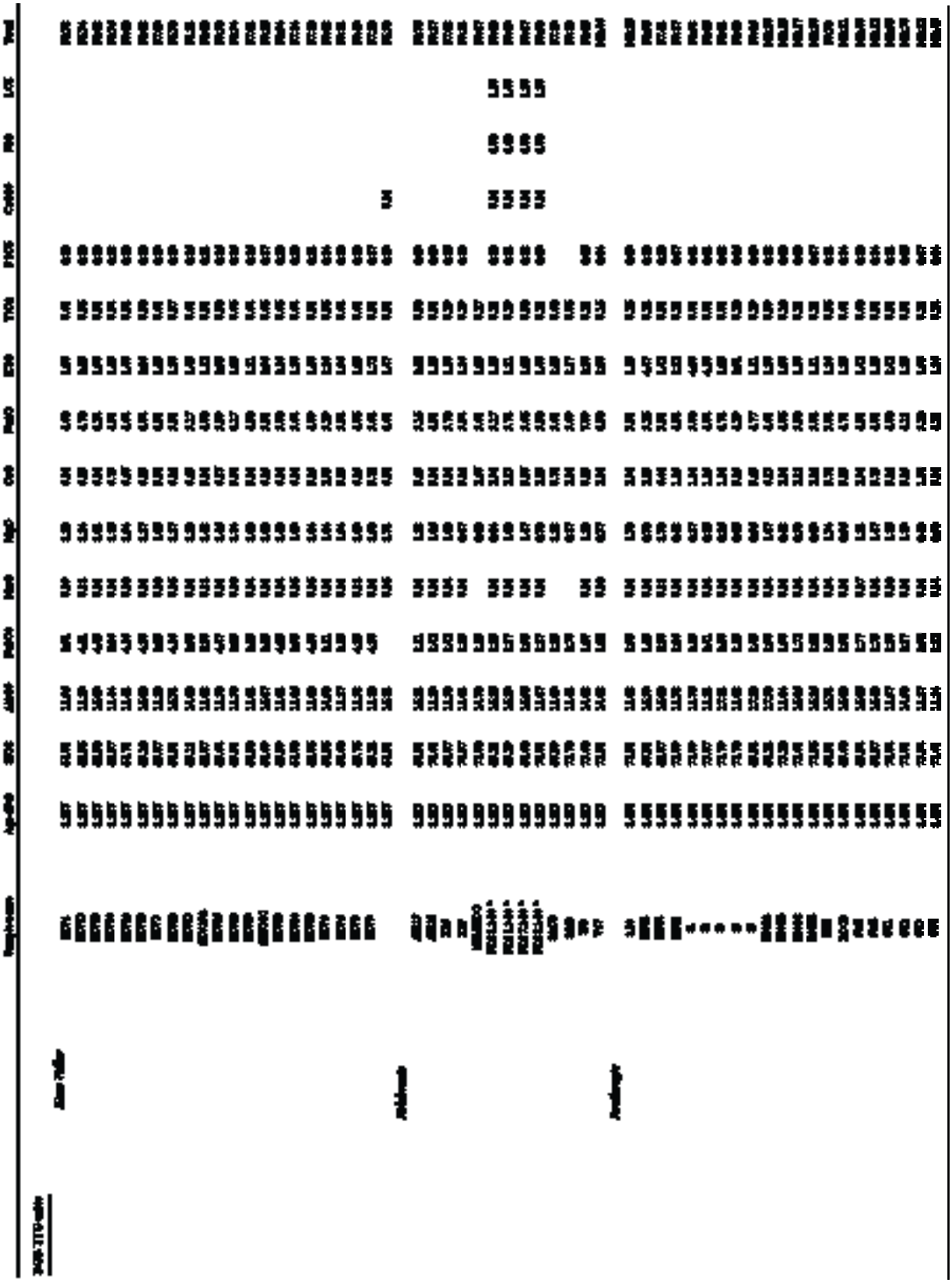

Supplementary Table DR1 (continued): Geochemical data for the Moodies granitic clasts and TTGs associated with the Barberton Greenstone Belt

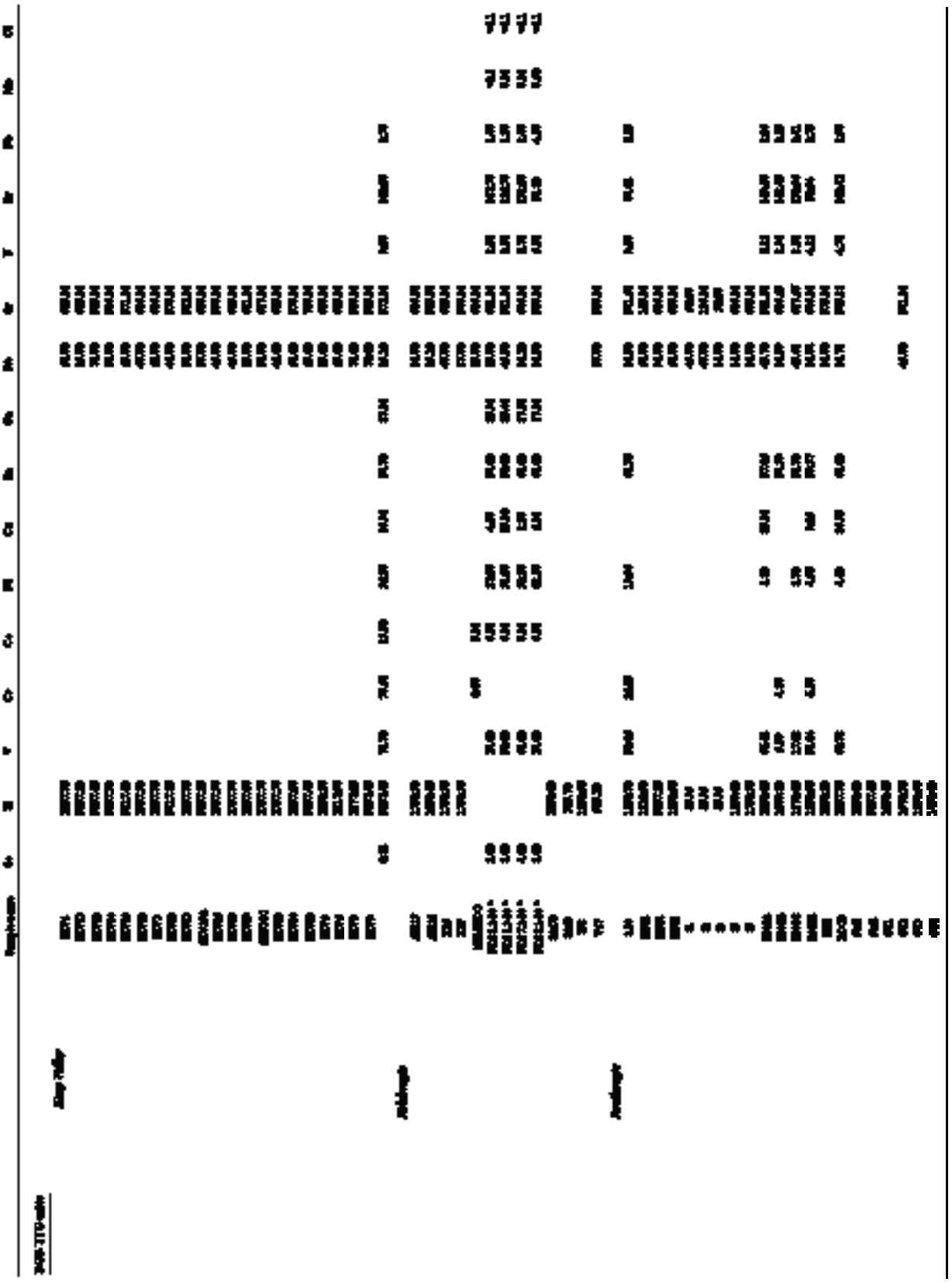

Supplementary Table DR1 (continued): Geochemical data for the Moodies granitic clasts and TTGs associated with the Barberton Greenstone Belt

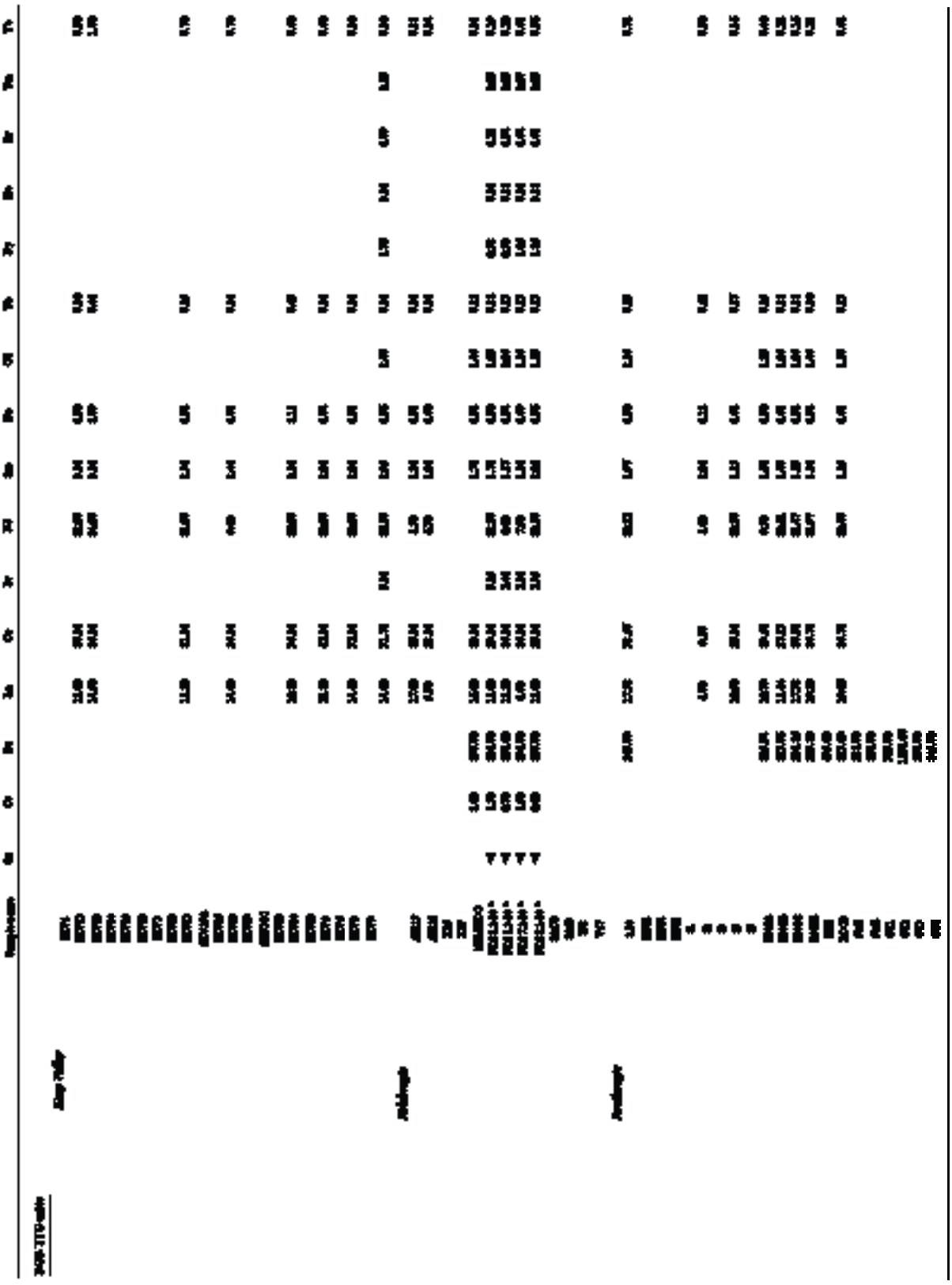

Supplementary Table DR1 (continued): Geochemical data for the Moodies granitic clasts and TTGs associated with the Barberton Greenstone Belt

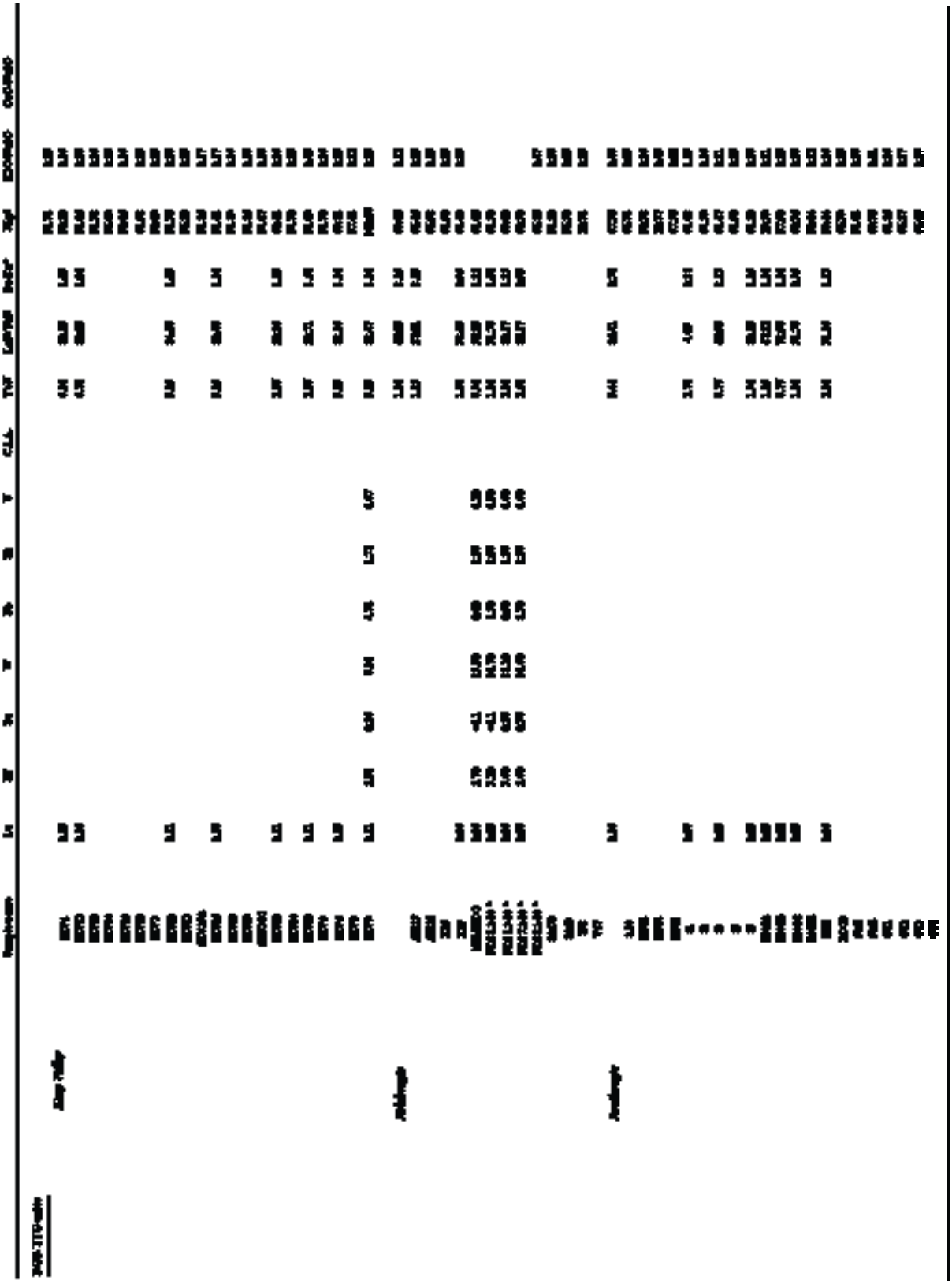

Supplementary Table DR1 (continued): Geochemical data for the Moodies granitic clasts and TTGs associated with the Barberton Greenstone Belt

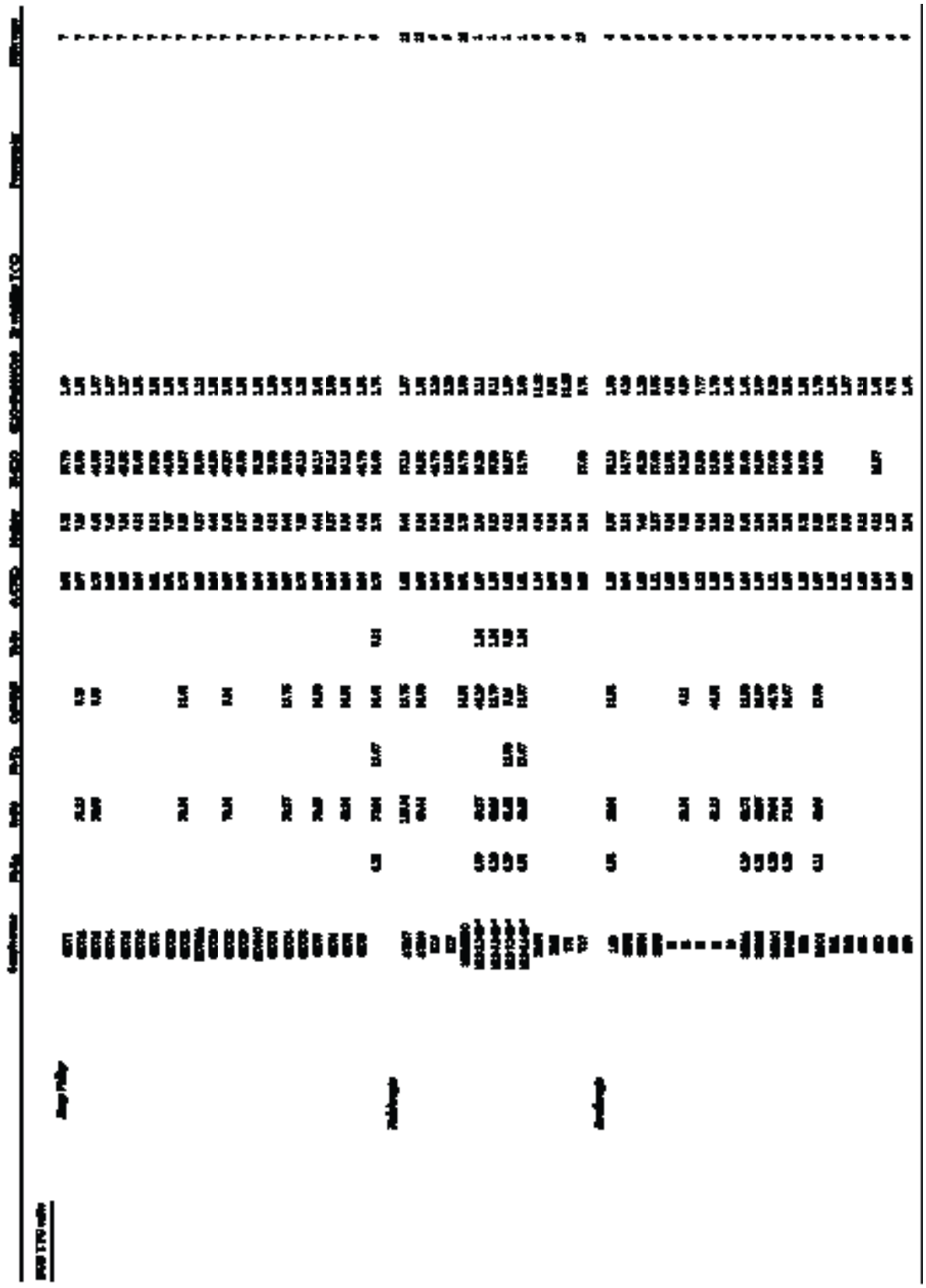

Supplementary Table DR1 (continued): Geochemical data for the Moodies granitic clasts and TTGs associated with the Barberton Greenstone Belt

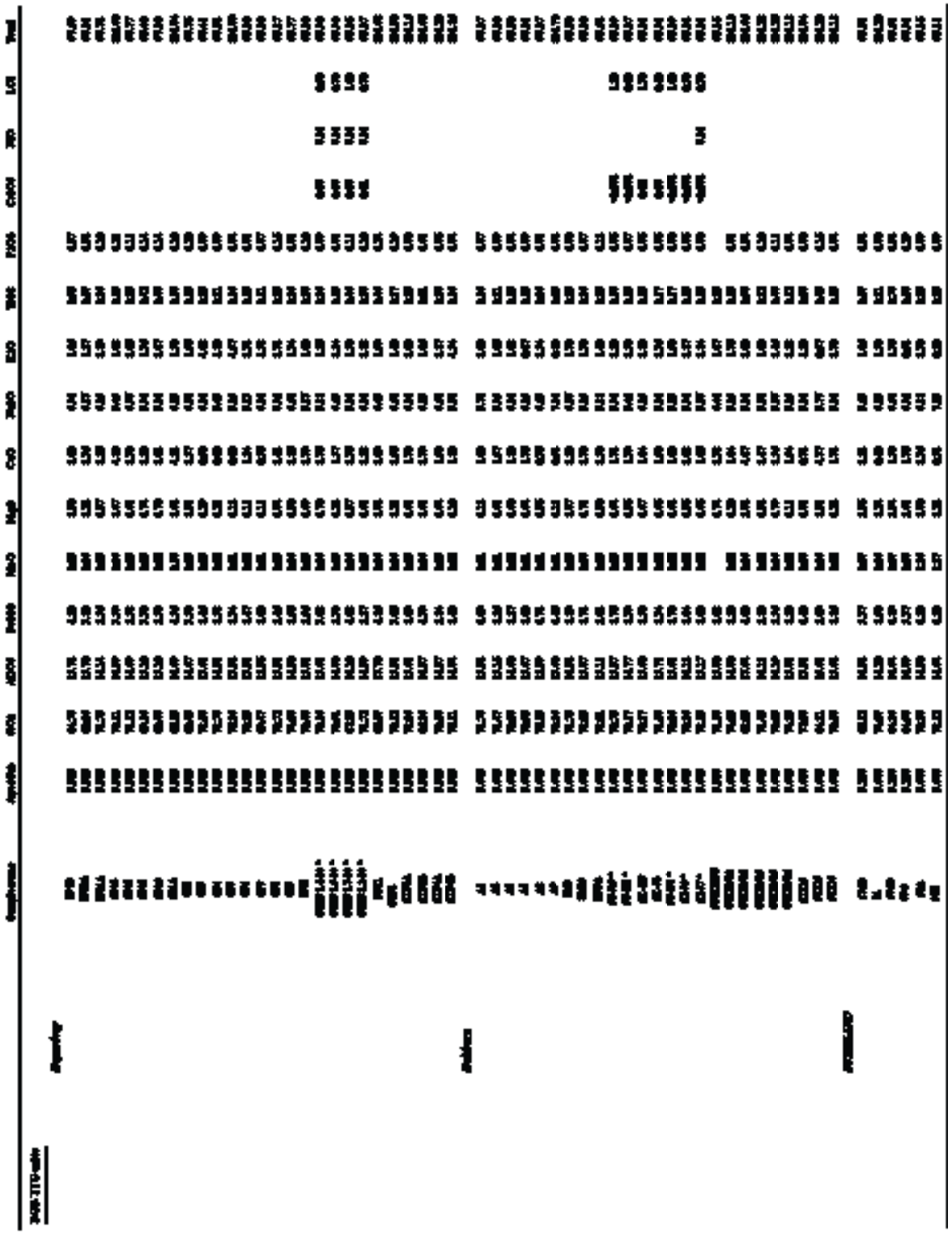

Supplementary Table DR1 (continued): Geochemical data for the Moodies granitic clasts and TTGs associated with the Barberton Greenstone Belt

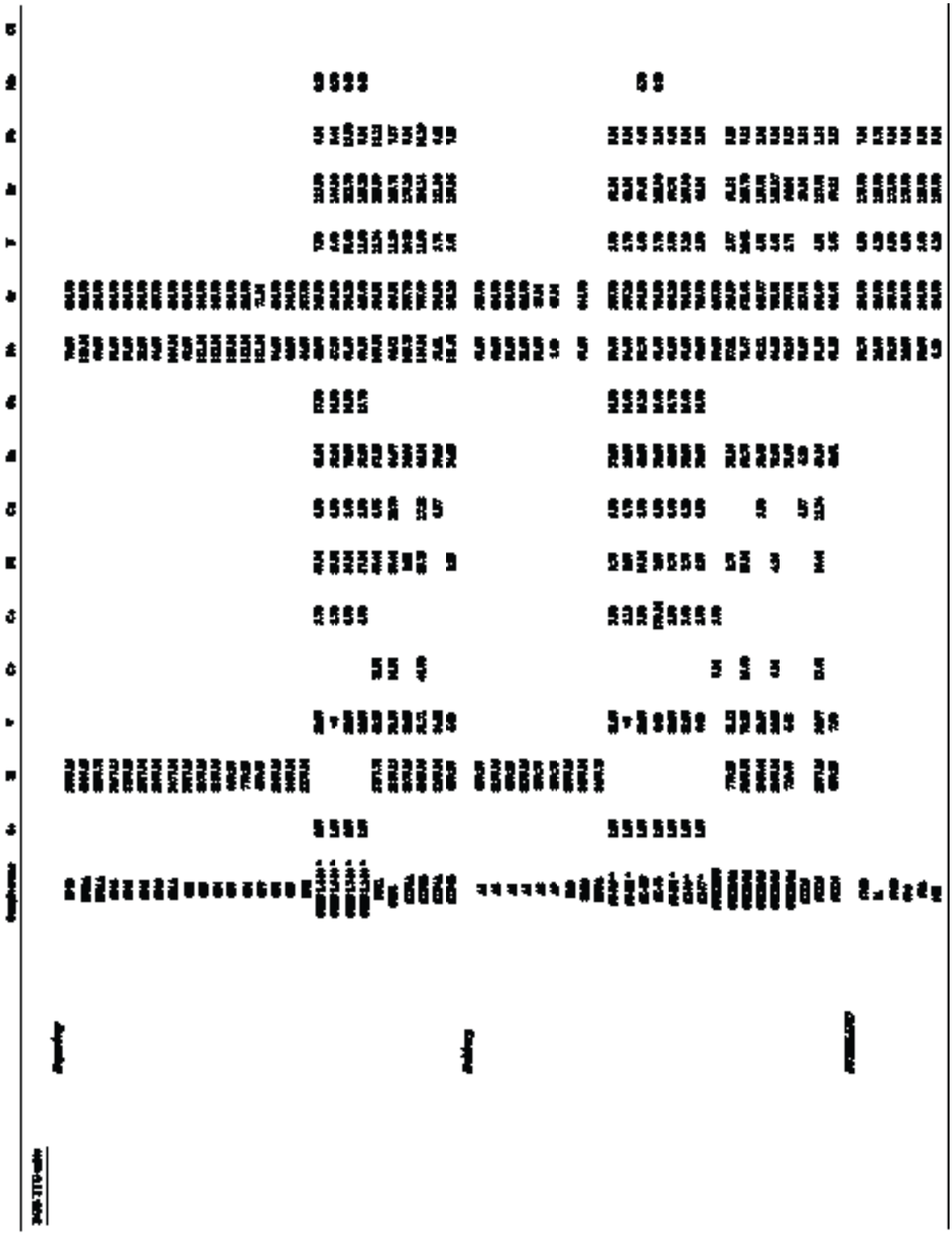

Supplementary Table DR1 (continued): Geochemical data for the Moodies granitic clasts and TTGs associated with the Barberton Greenstone Belt

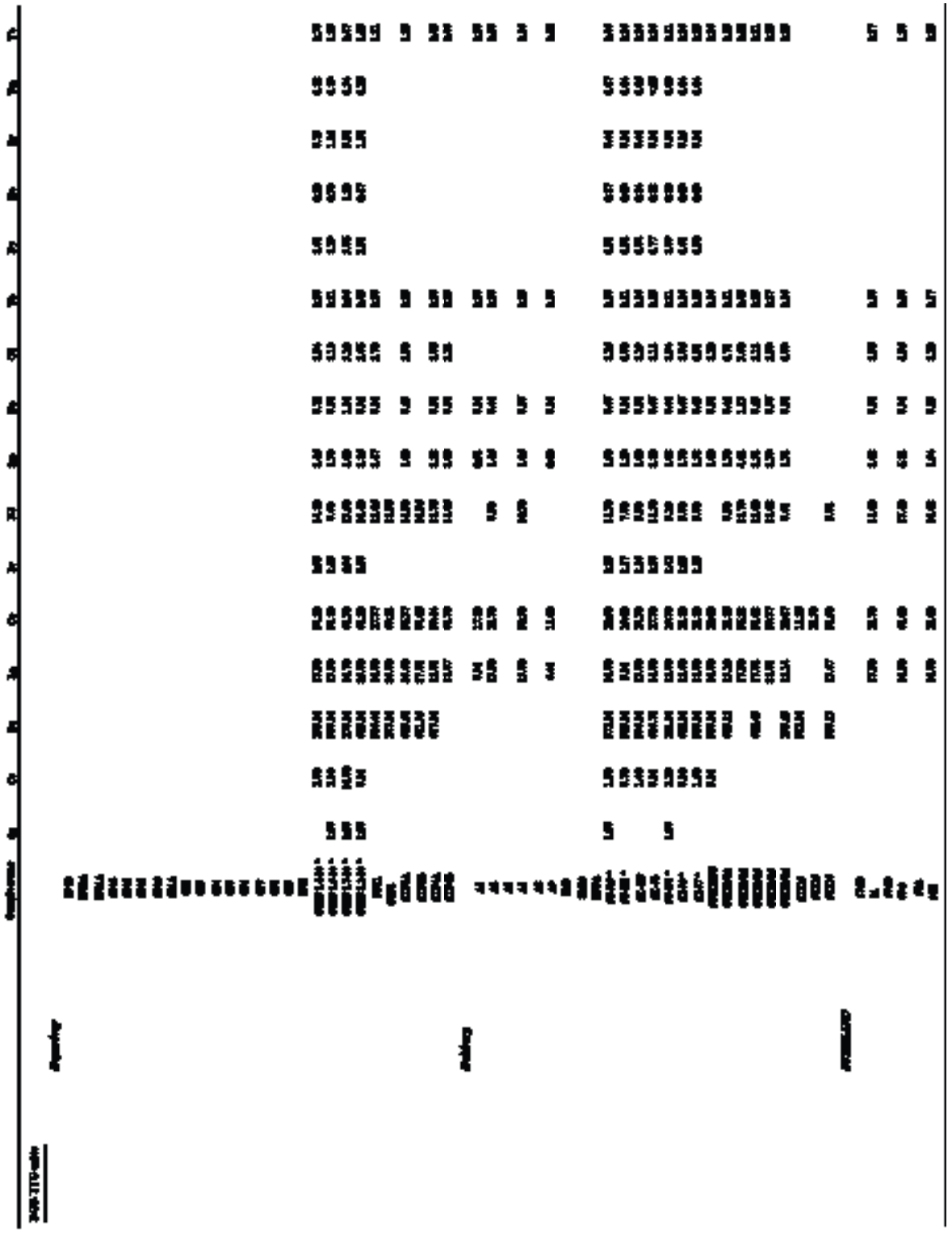

Supplementary Table DR1 (continued): Geochemical data for the Moodies granitic clasts and TTGs associated with the Barberton Greenstone Belt

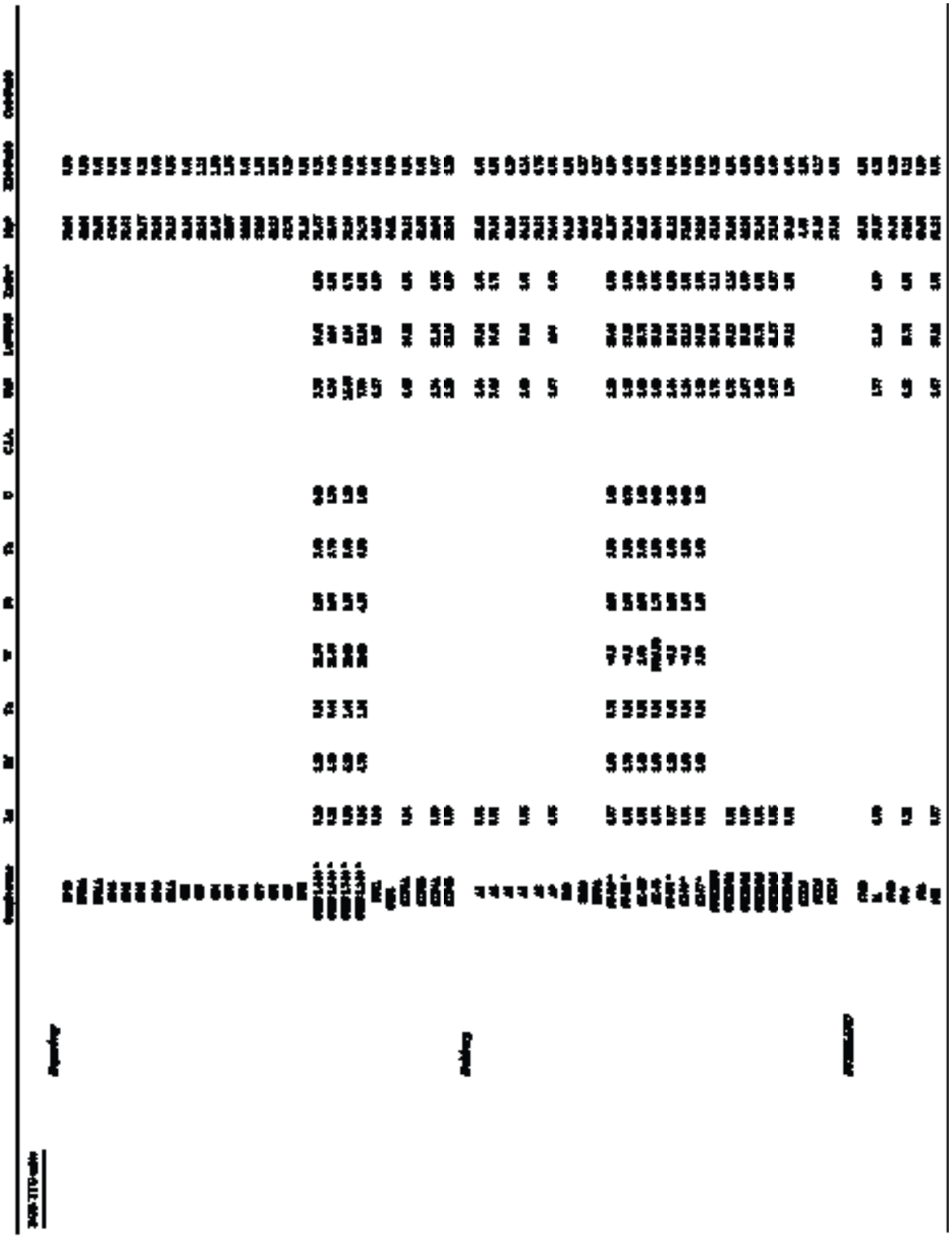

Supplementary Table DR1 (continued): Geochemical data for the Moodies granitic clasts and TTGs associated with the Barberton Greenstone Belt

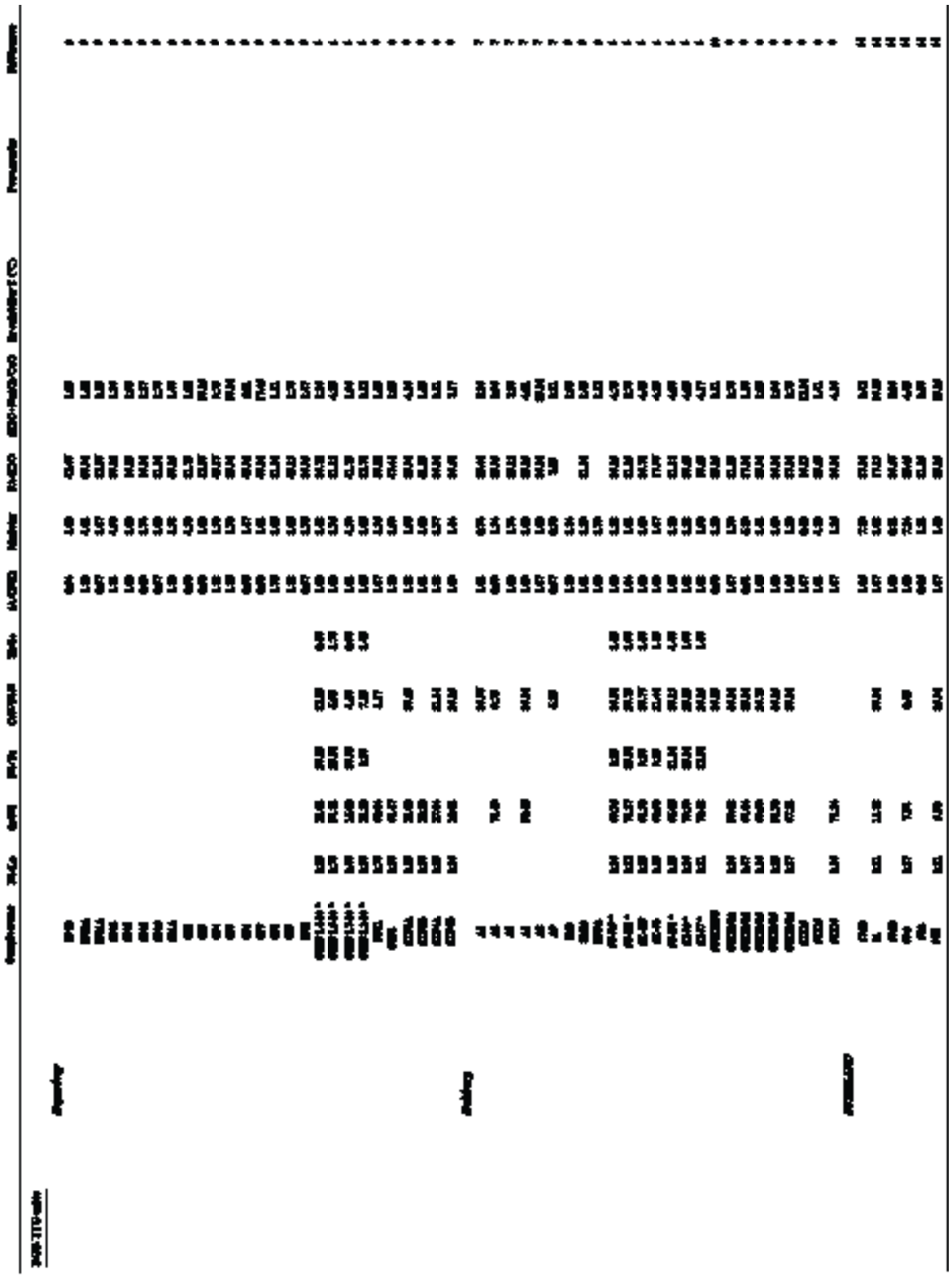

Supplementary Table DR1 (continued): Geochemical data for the Moodies granitic clasts and TTGs associated with the Barberton Greenstone Belt

Supplementary Table DR1 (continued): Geochemical data for the Moodies granitic clasts and TTGs associated with the Barberton Greenstone Belt

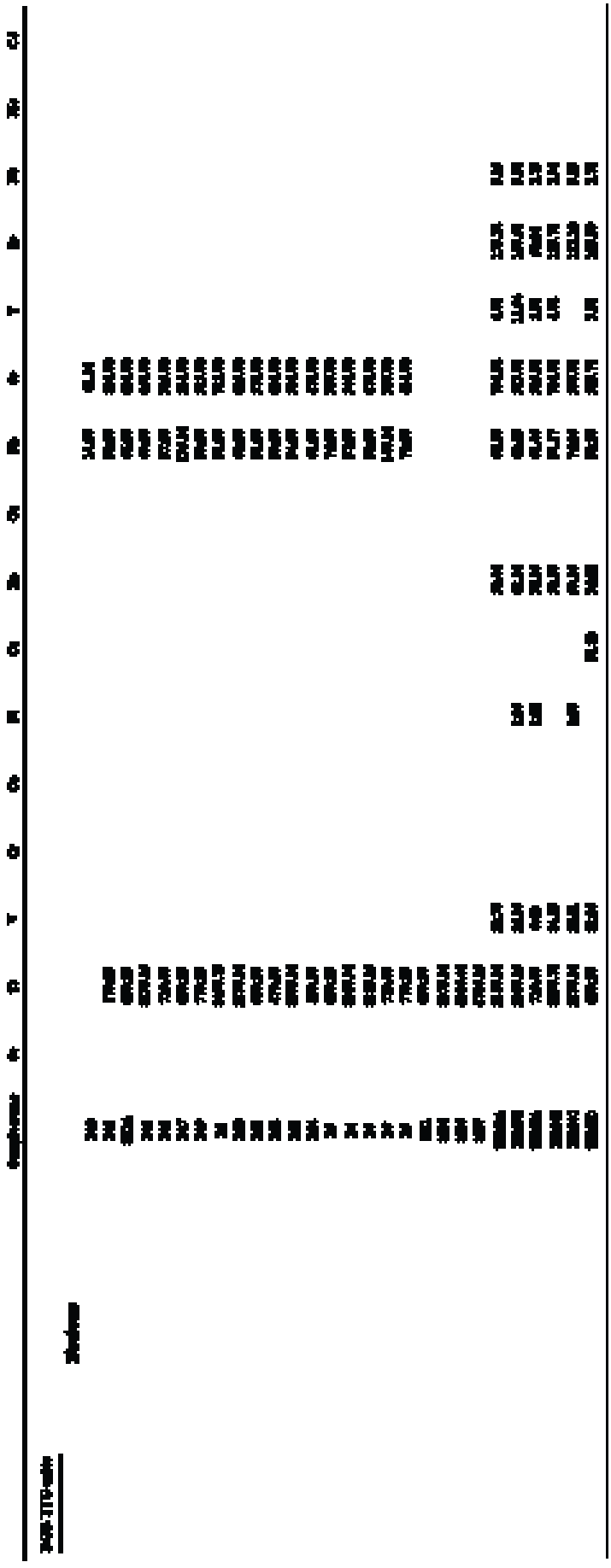

Supplementary Table DR1 (continued): Geochemical data for the Moodies granitic clasts and TTGs associated with the Barberton Greenstone Belt

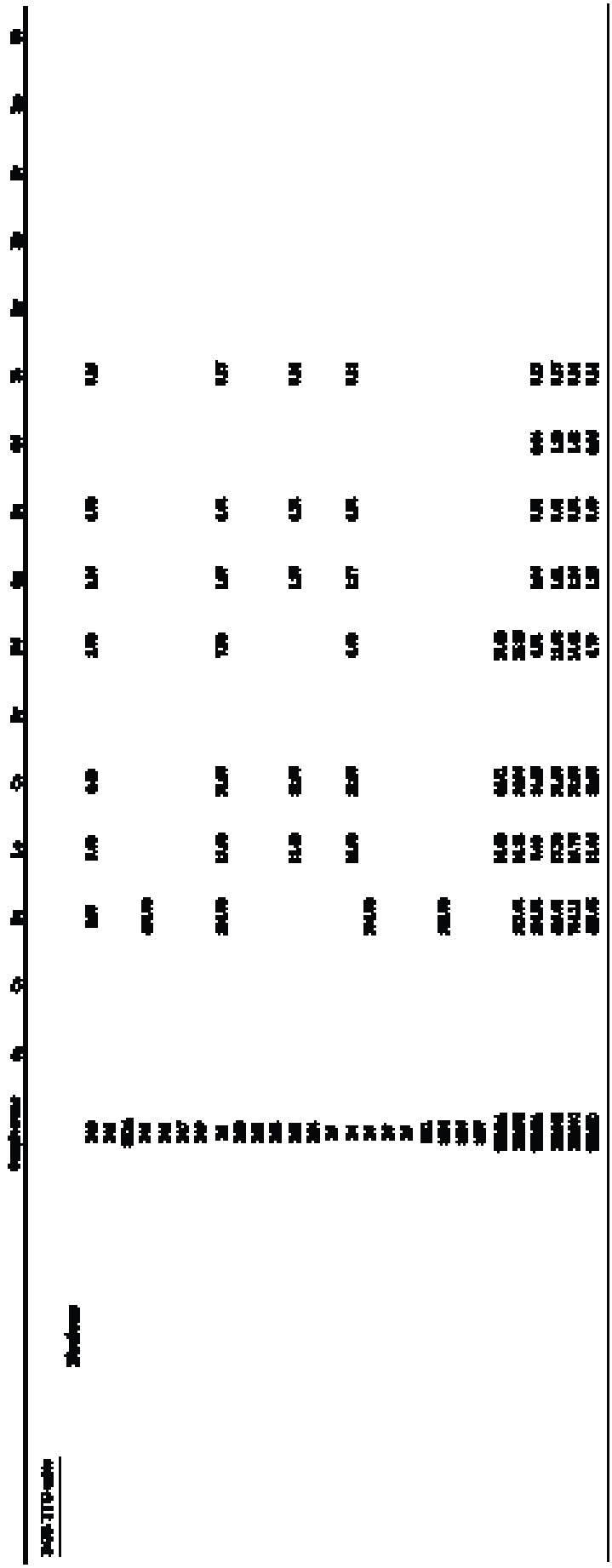

Supplementary Table DR1 (continued): Geochemical data for the Moodies granitic clasts and TTGs associated with the Barberton Greenstone Belt

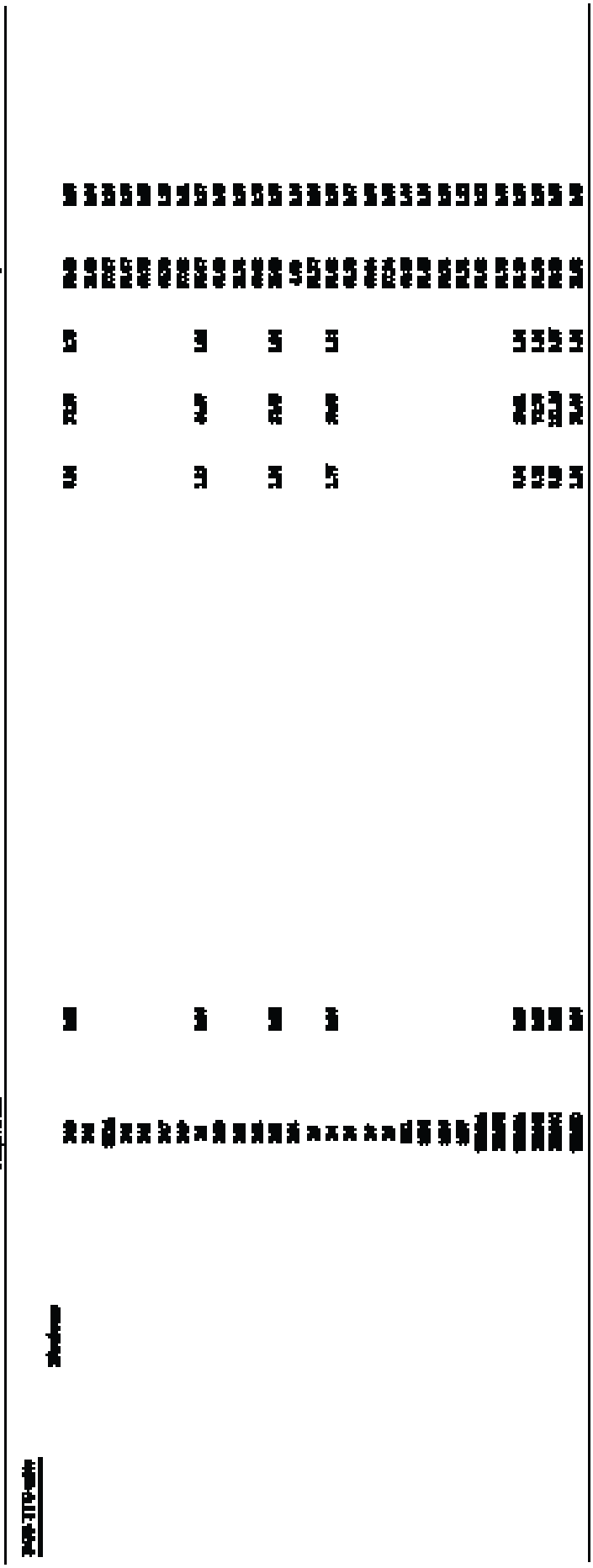

Supplementary Table DR1 (continued): Geochemical data for the Moodies granitic clasts and TTGs associated with the Barberton Greenstone Belt

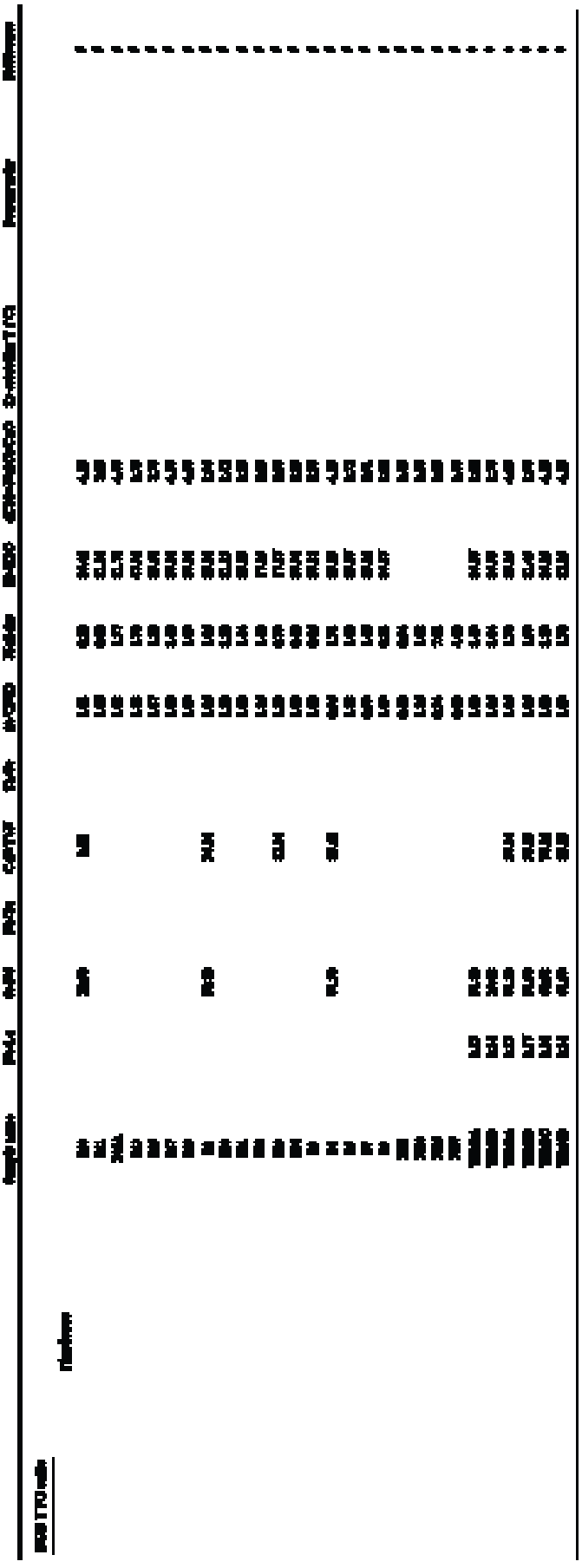

Supplementary Table DR1 (continued): Geochemical data for the Moodies granitic clasts and TTGs associated with the Barberton Greenstone Belt

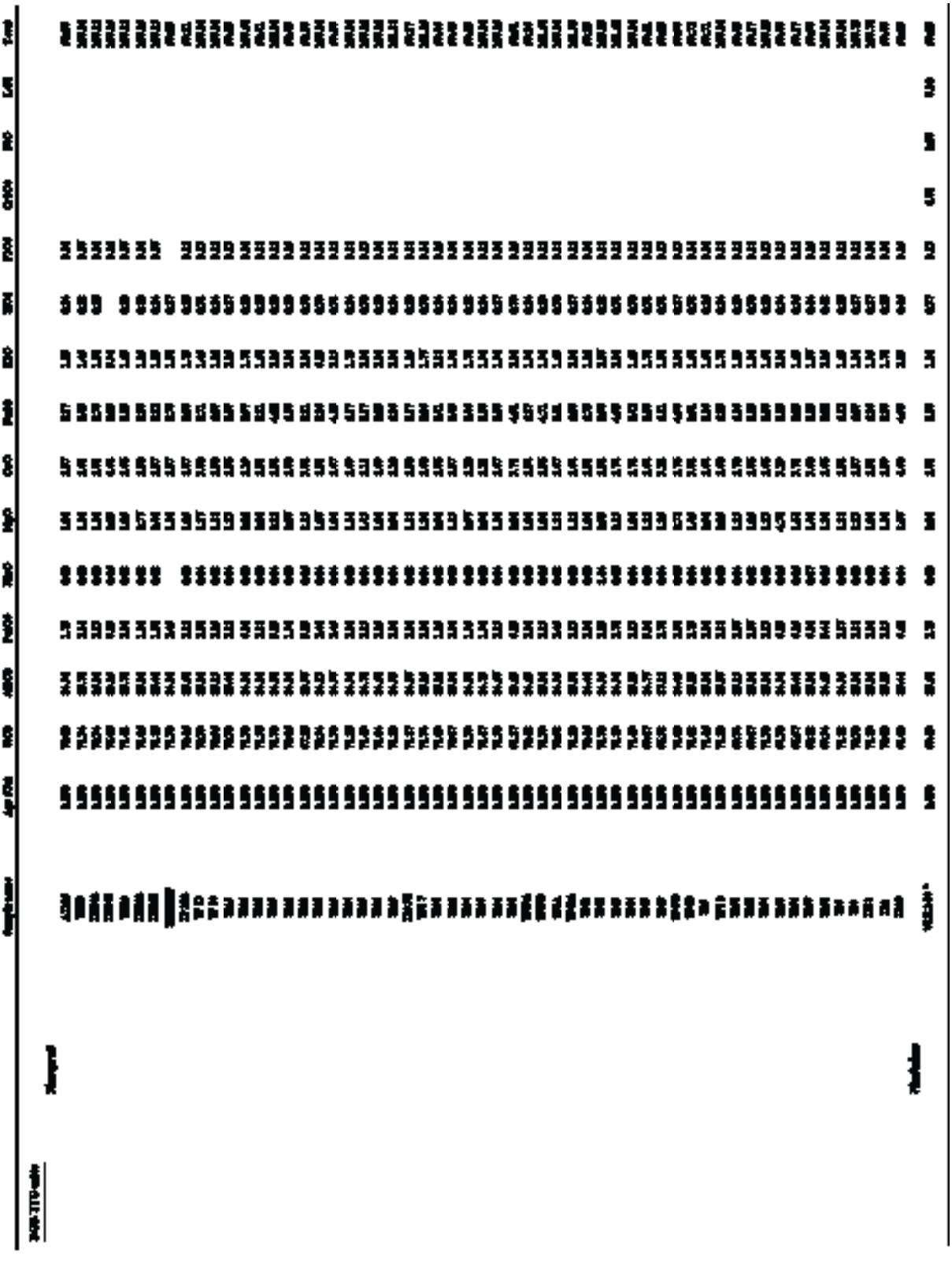

Supplementary Table DR1 (continued): Geochemical data for the Moodies granitic clasts and TTGs associated with the Barberton Greenstone Belt

Supplementary Table DR1 (continued): Geochemical data for the Moodies granitic clasts and TTGs associated with the Barberton Greenstone Belt

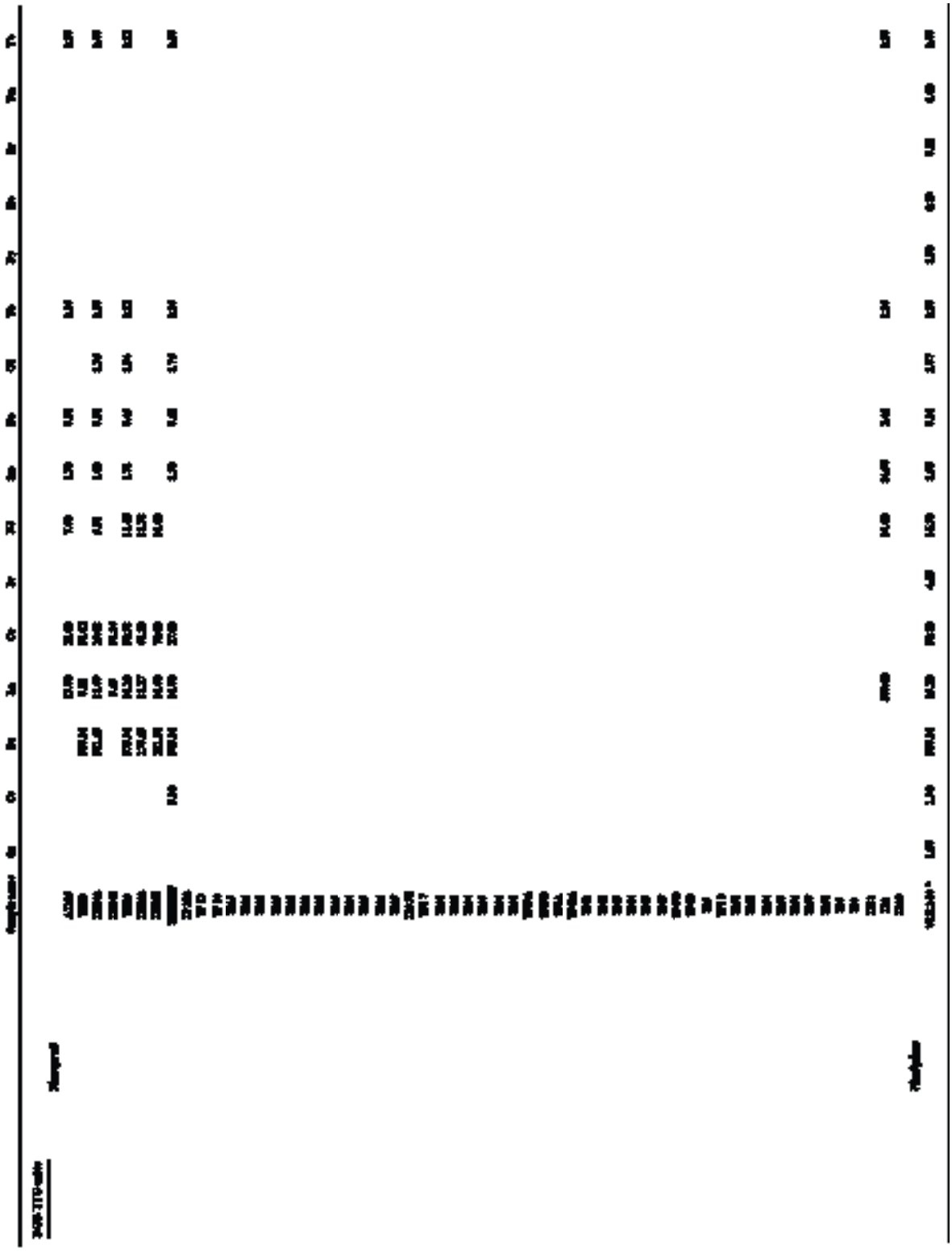

Supplementary Table DR1 (continued): Geochemical data for the Moodies granitic clasts and TTGs associated with the Barberton Greenstone Belt

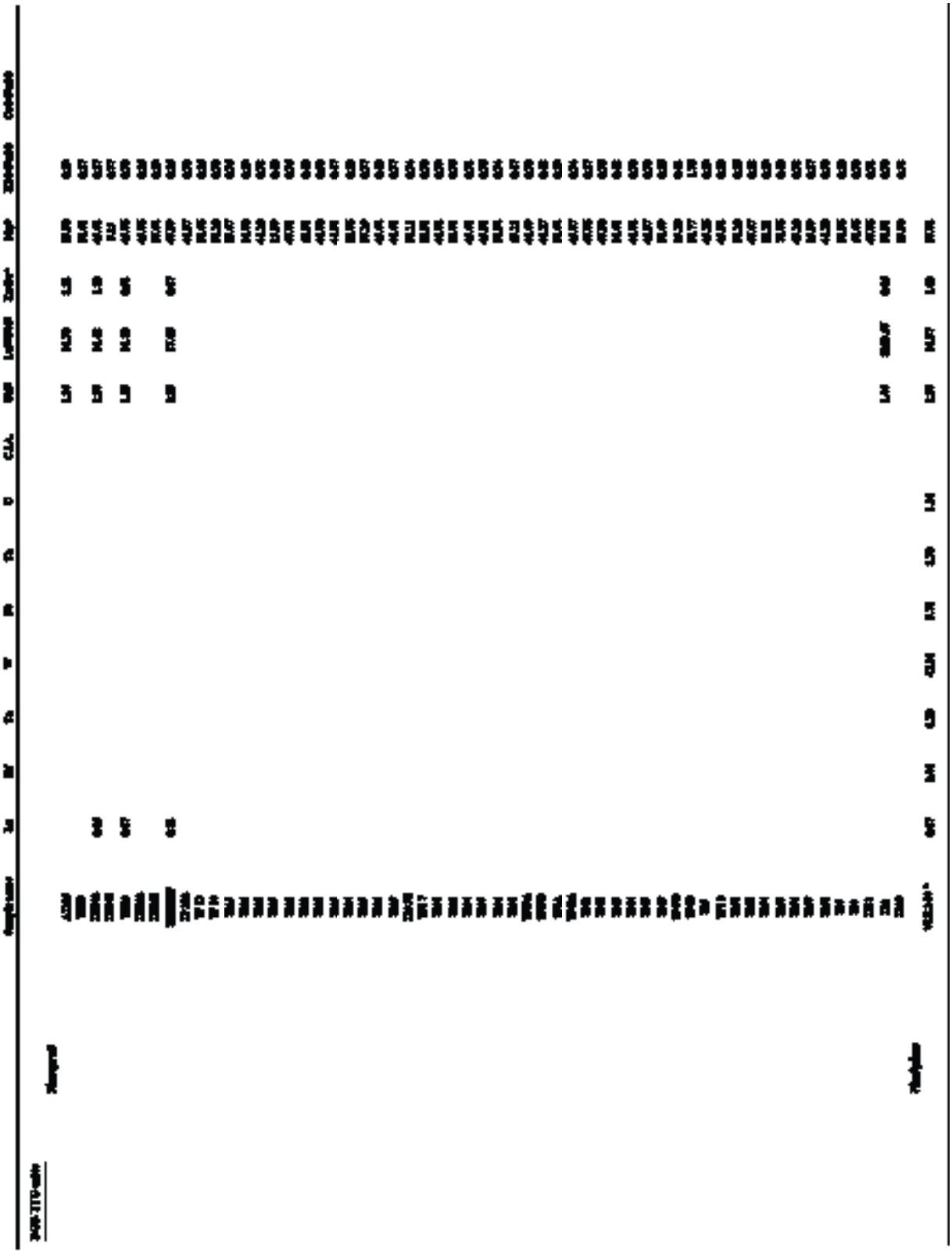

Supplementary Table DR1 (continued): Geochemical data for the Moodies granitic clasts and TTGs associated with the Barberton Greenstone Belt

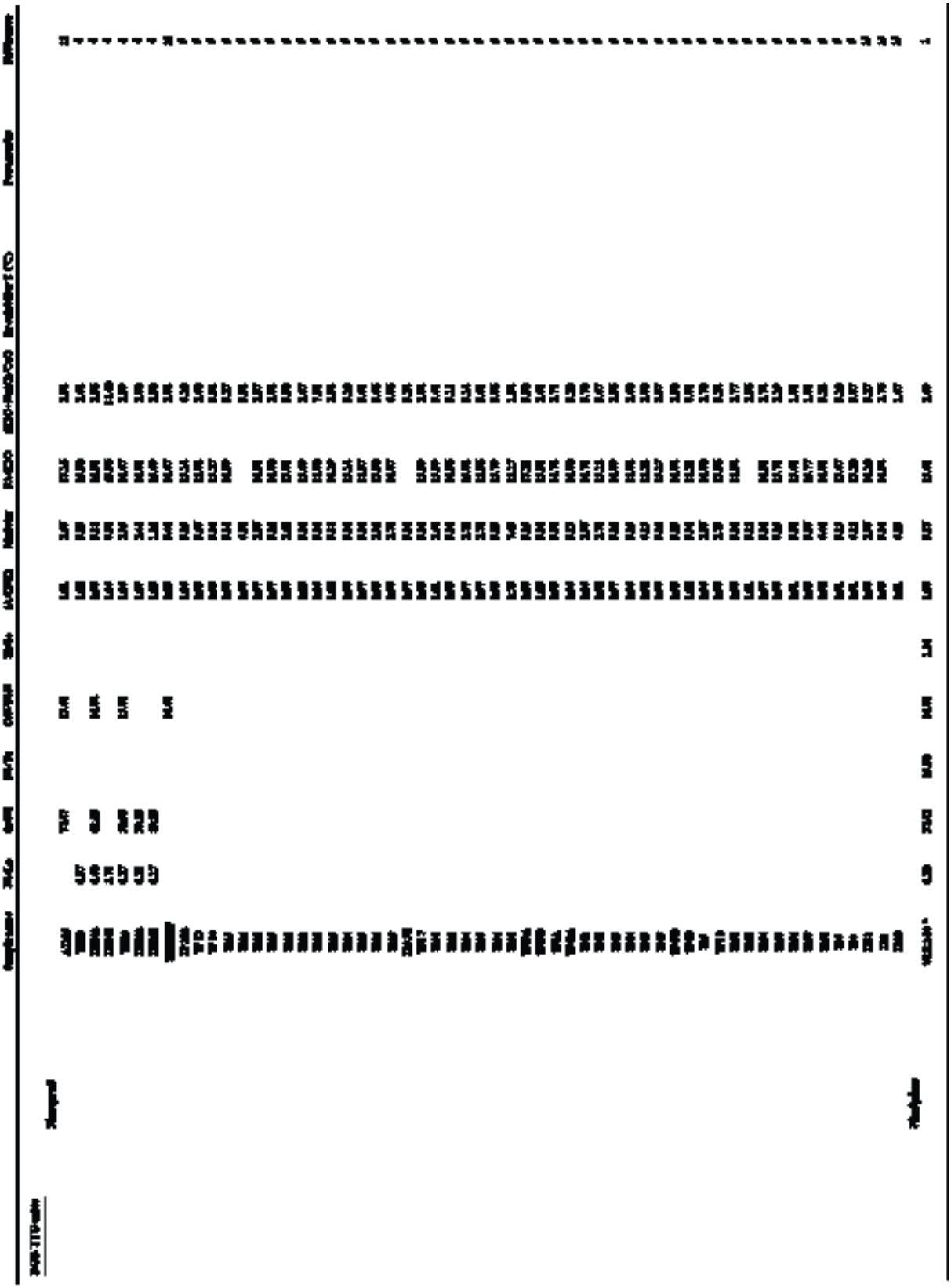

Supplementary Table DR1 (continued): Geochemical data for the Moodies granitic clasts and TTGs associated with the Barberton Greenstone Belt

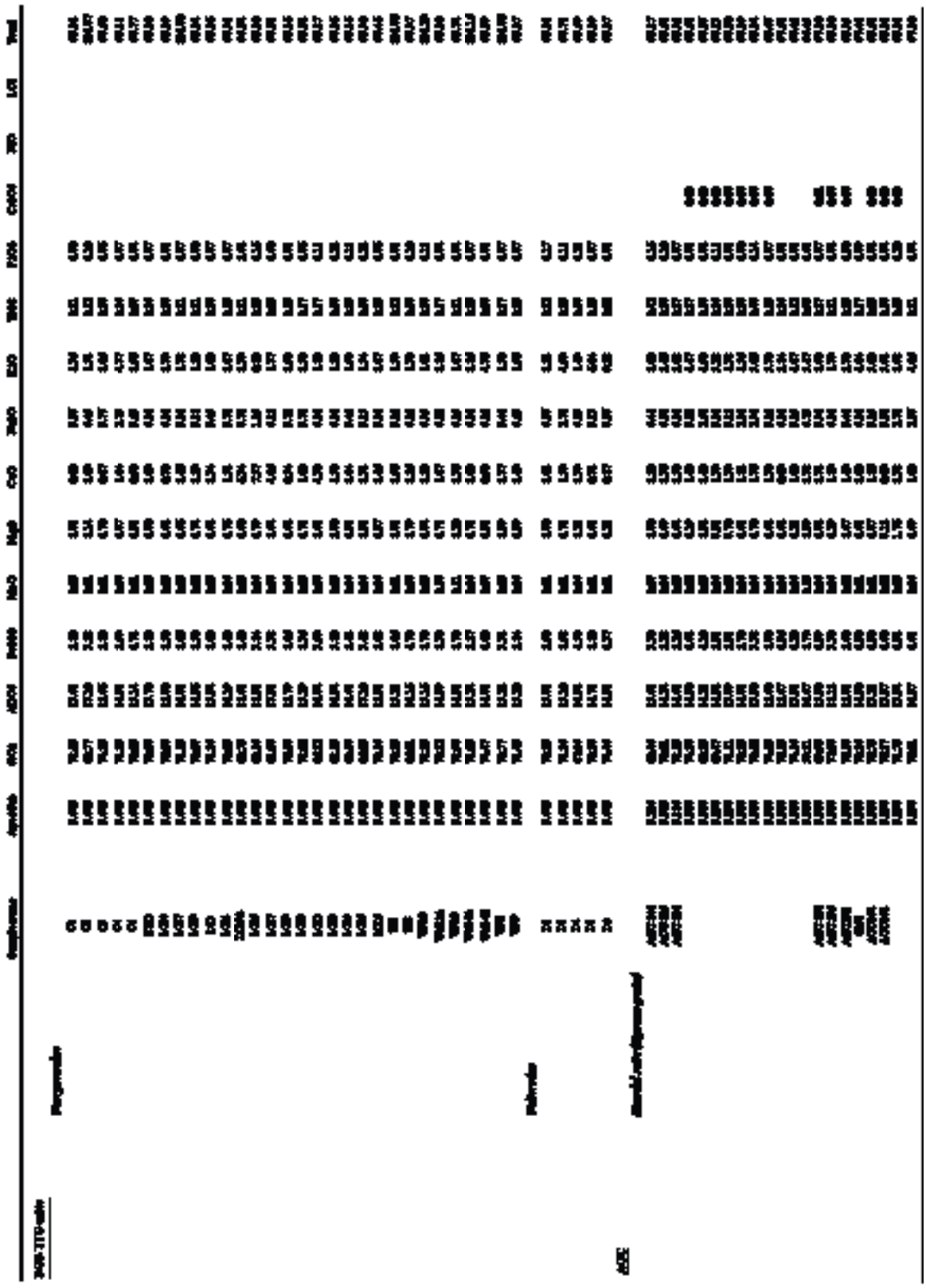

Supplementary Table DR1 (continued): Geochemical data for the Moodies granitic clasts and TTGs associated with the Barberton Greenstone Belt

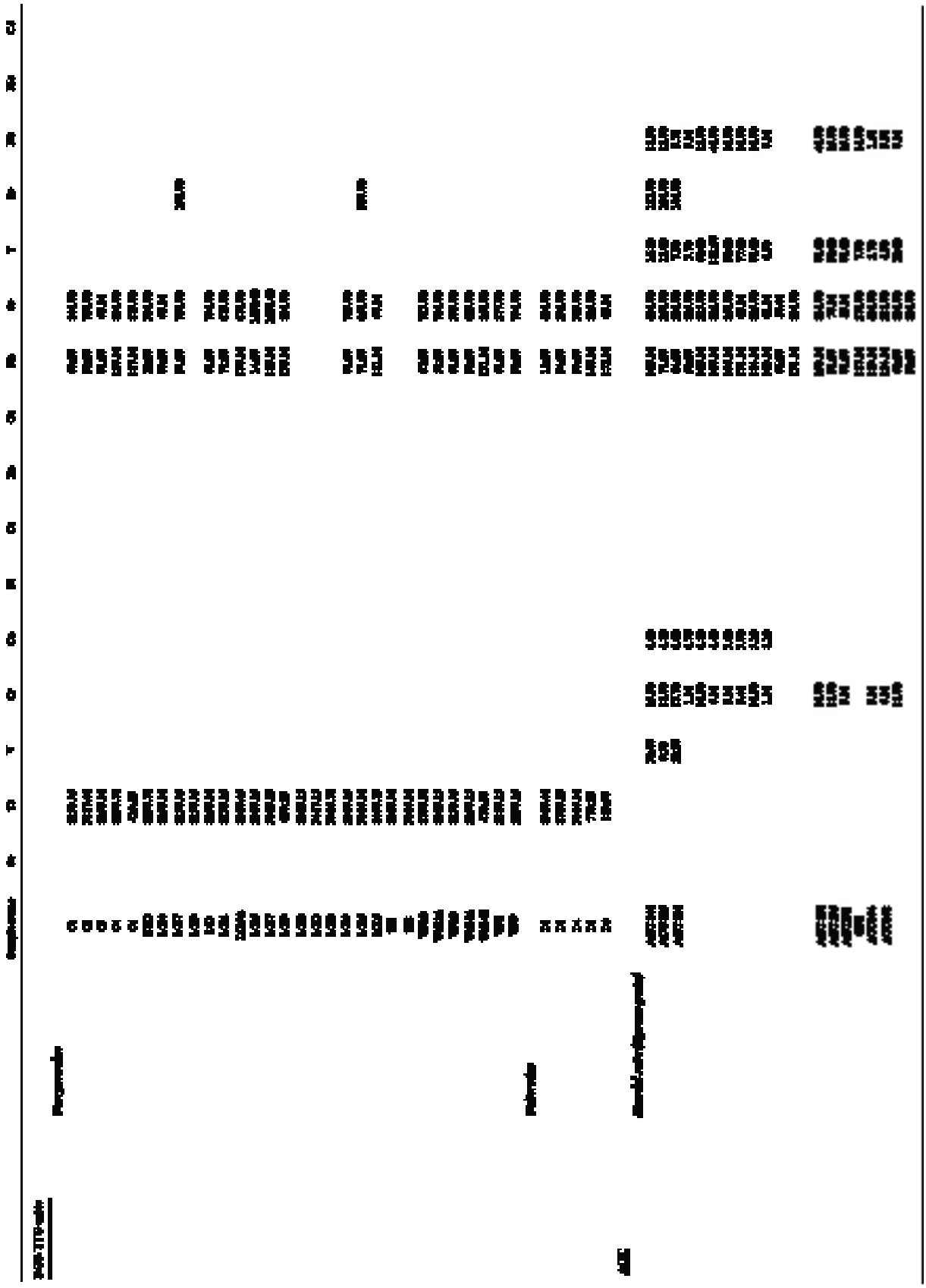

Supplementary Table DR1 (continued): Geochemical data for the Moodies granitic clasts and TTGs associated with the Barberton Greenstone Belt

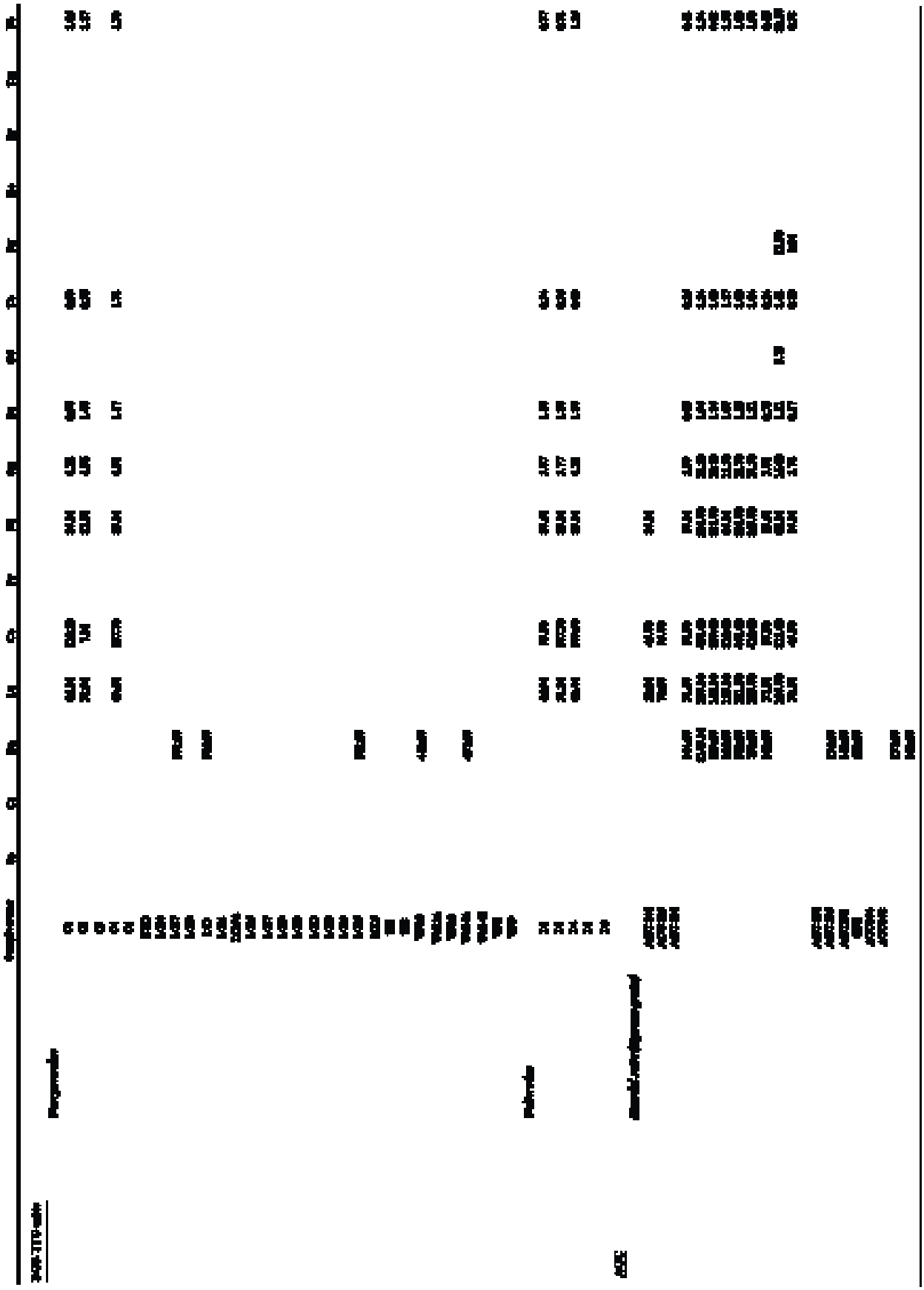

Supplementary Table DR1 (continued): Geochemical data for the Moodies granitic clasts and TTGs associated with the Barberton Greenstone Belt

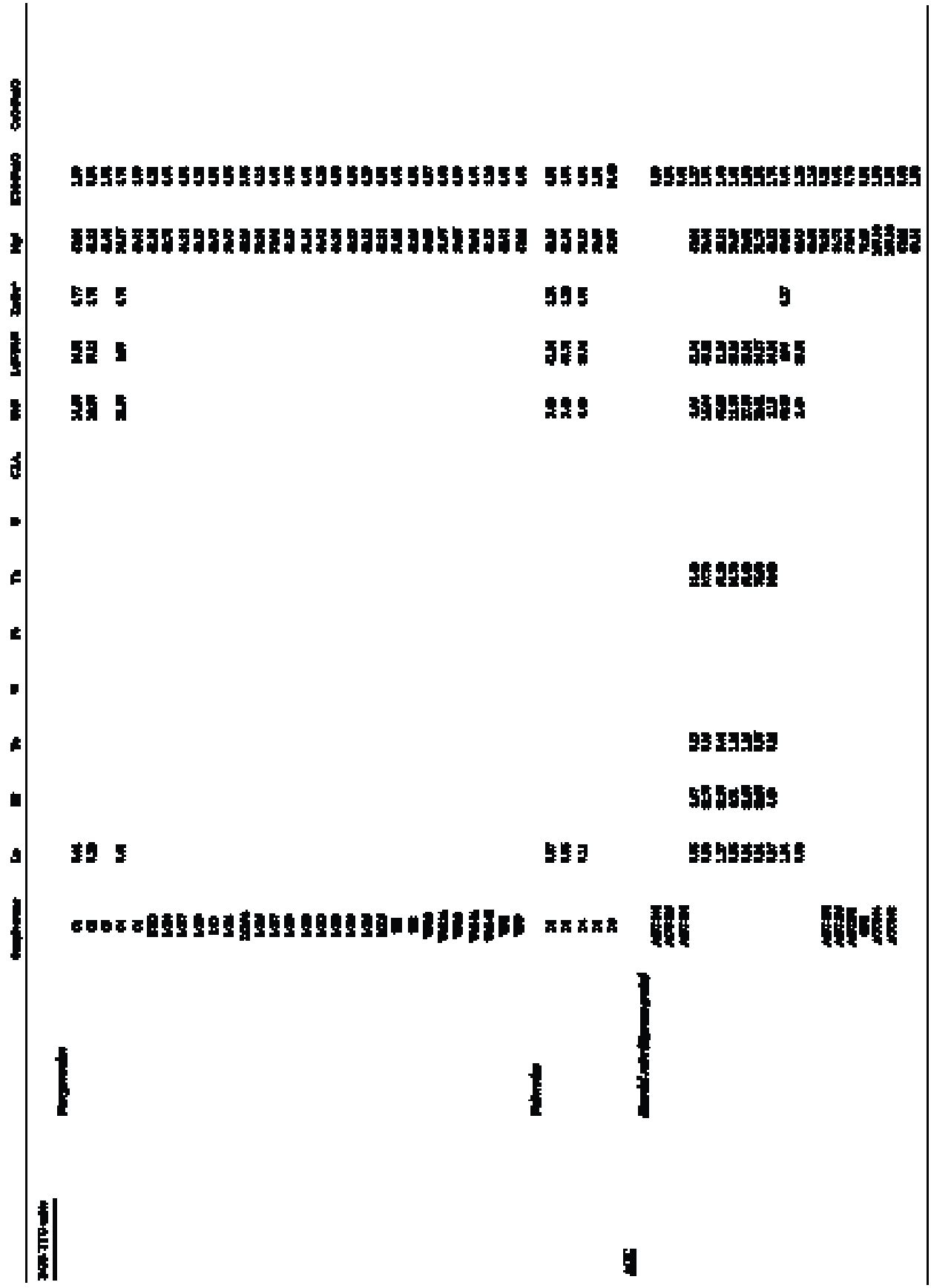

Supplementary Table DR1 (continued): Geochemical data for the Moodies granitic clasts and TTGs associated with the Barberton Greenstone Belt

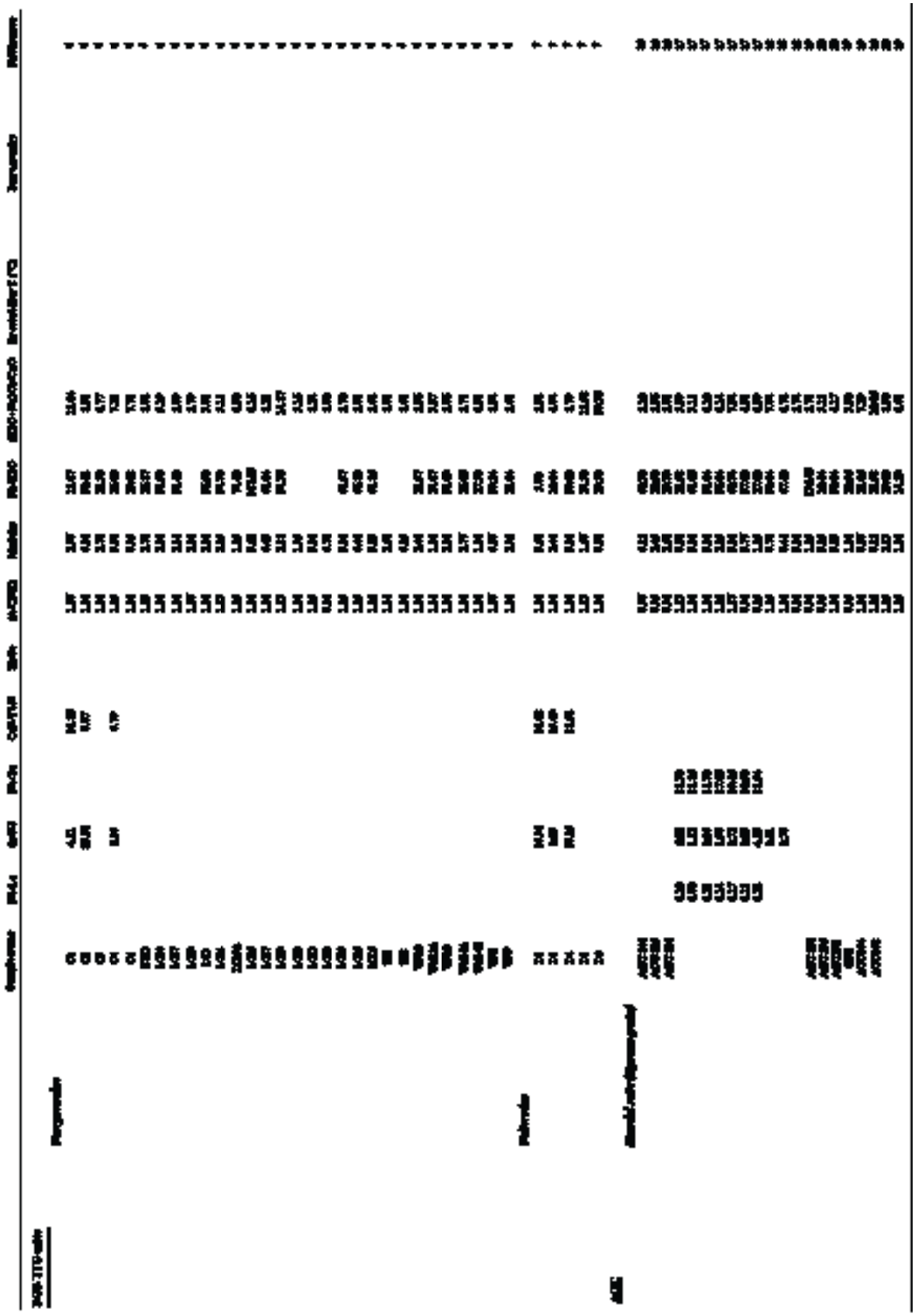

Supplementary Table DR1 (continued): Geochemical data for the Moodies granitic clasts and TTGs associated with the Barberton Greenstone Belt

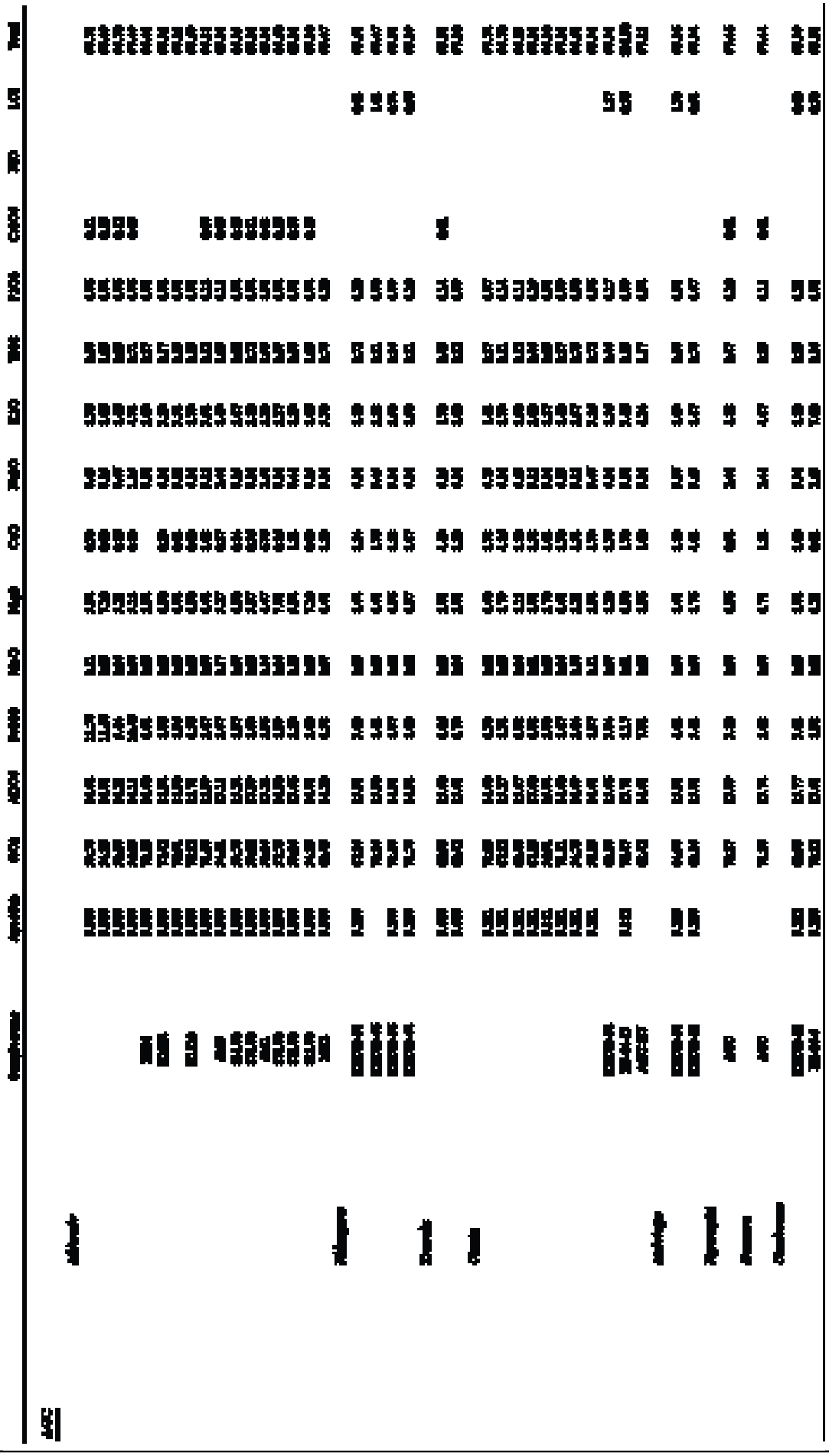

Supplementary Table DR1 (continued): Geochemical data for the Moodies granitic clasts and TTGs associated with the Barberton Greenstone Belt

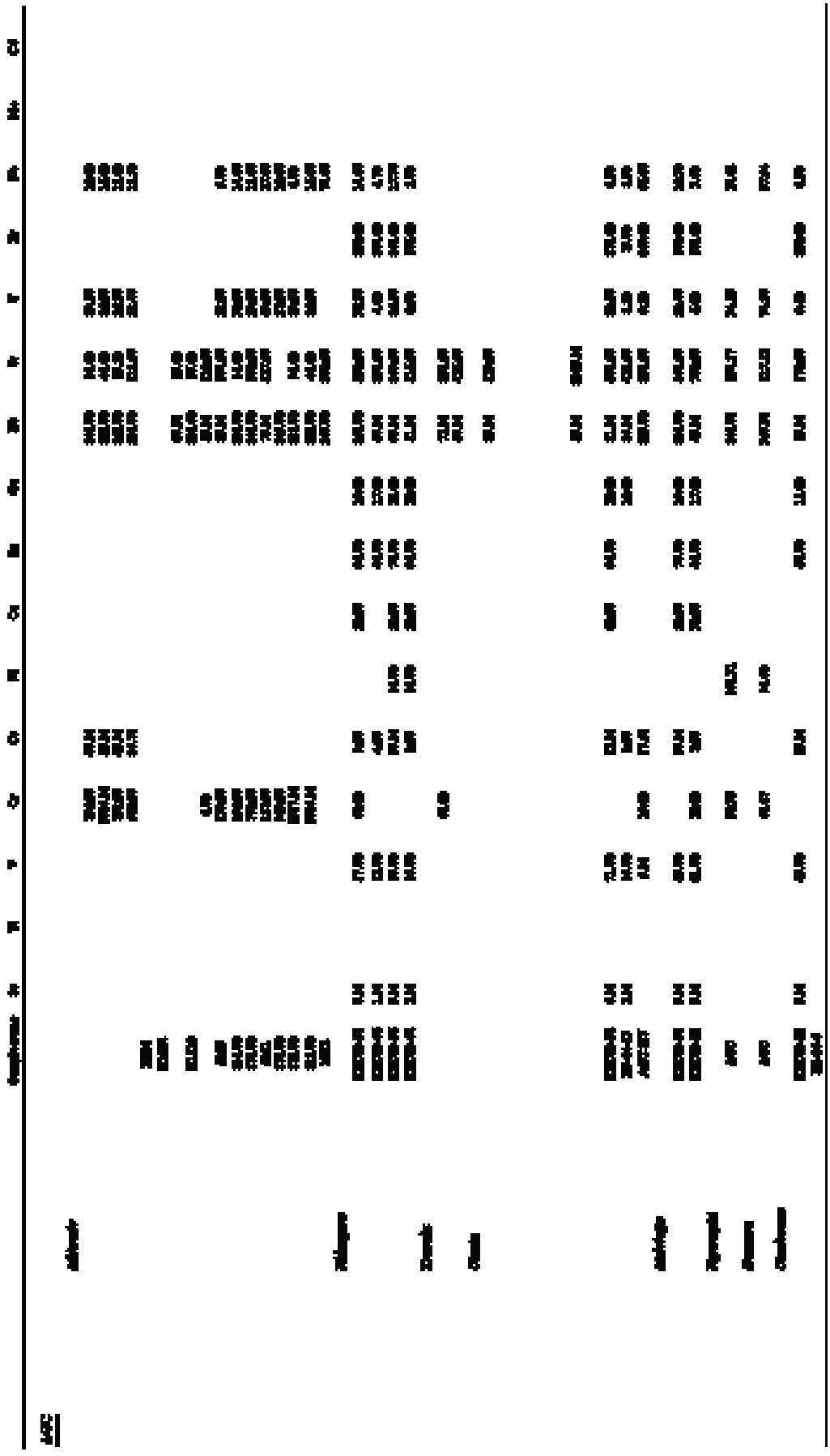

Supplementary Table DR1 (continued): Geochemical data for the Moodies granitic clasts and TTGs associated with the Barberton Greenstone Belt

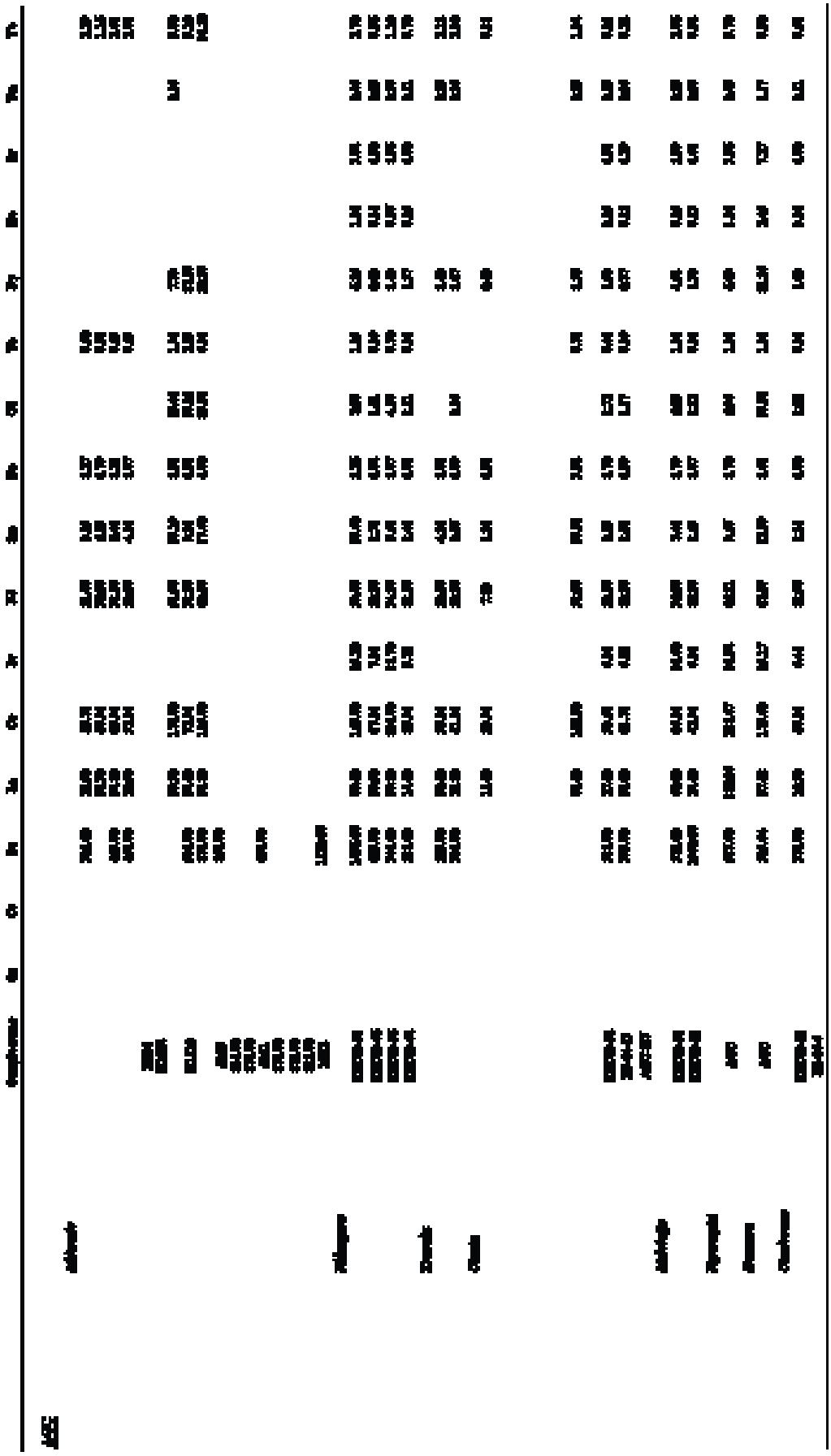

Supplementary Table DR1 (continued): Geochemical data for the Moodies granitic clasts and TTGs associated with the Barberton Greenstone Belt

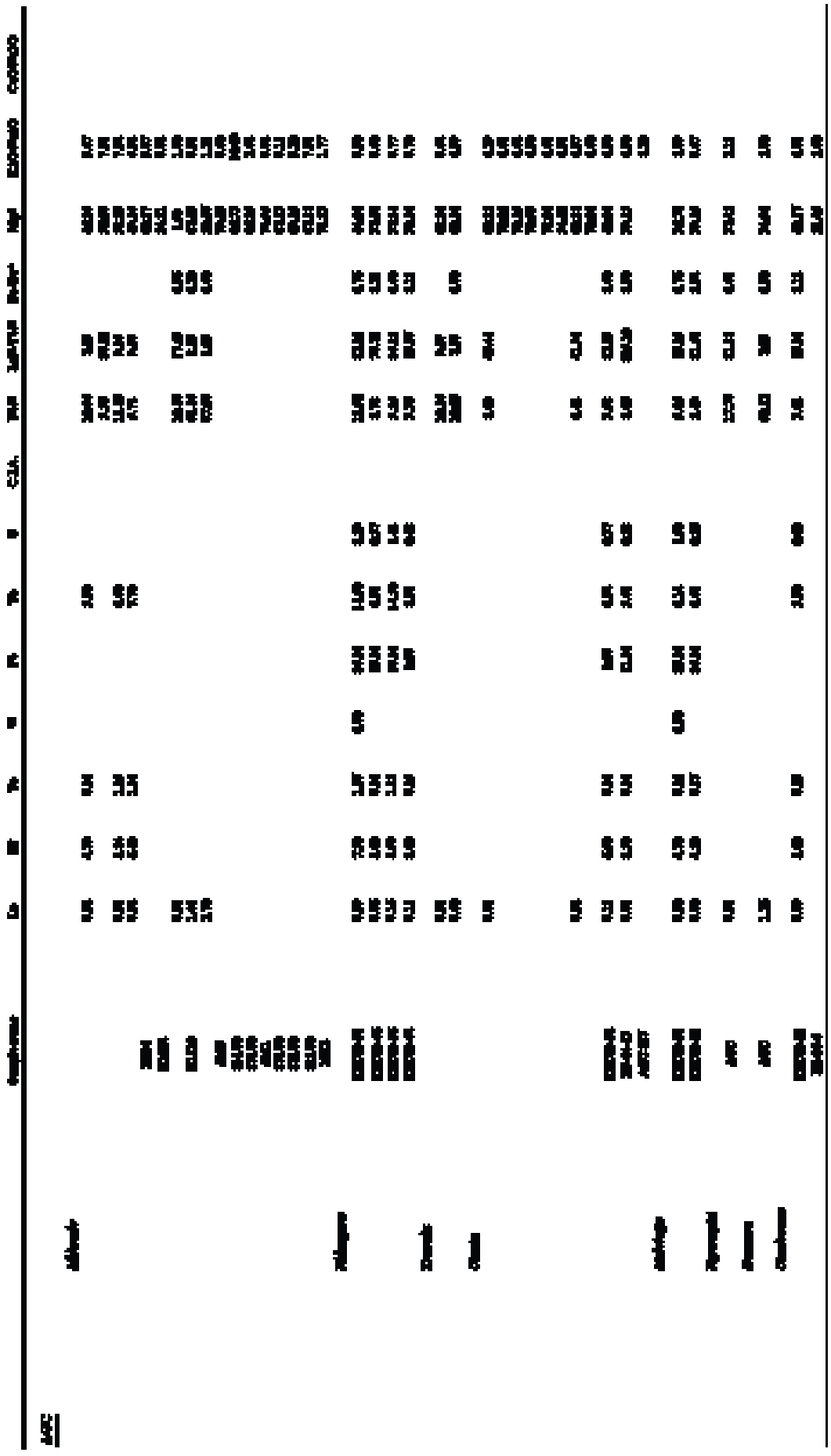

Supplementary Table DR1 (continued): Geochemical data for the Moodies granitic clasts and TTGs associated with the Barberton Greenstone Belt

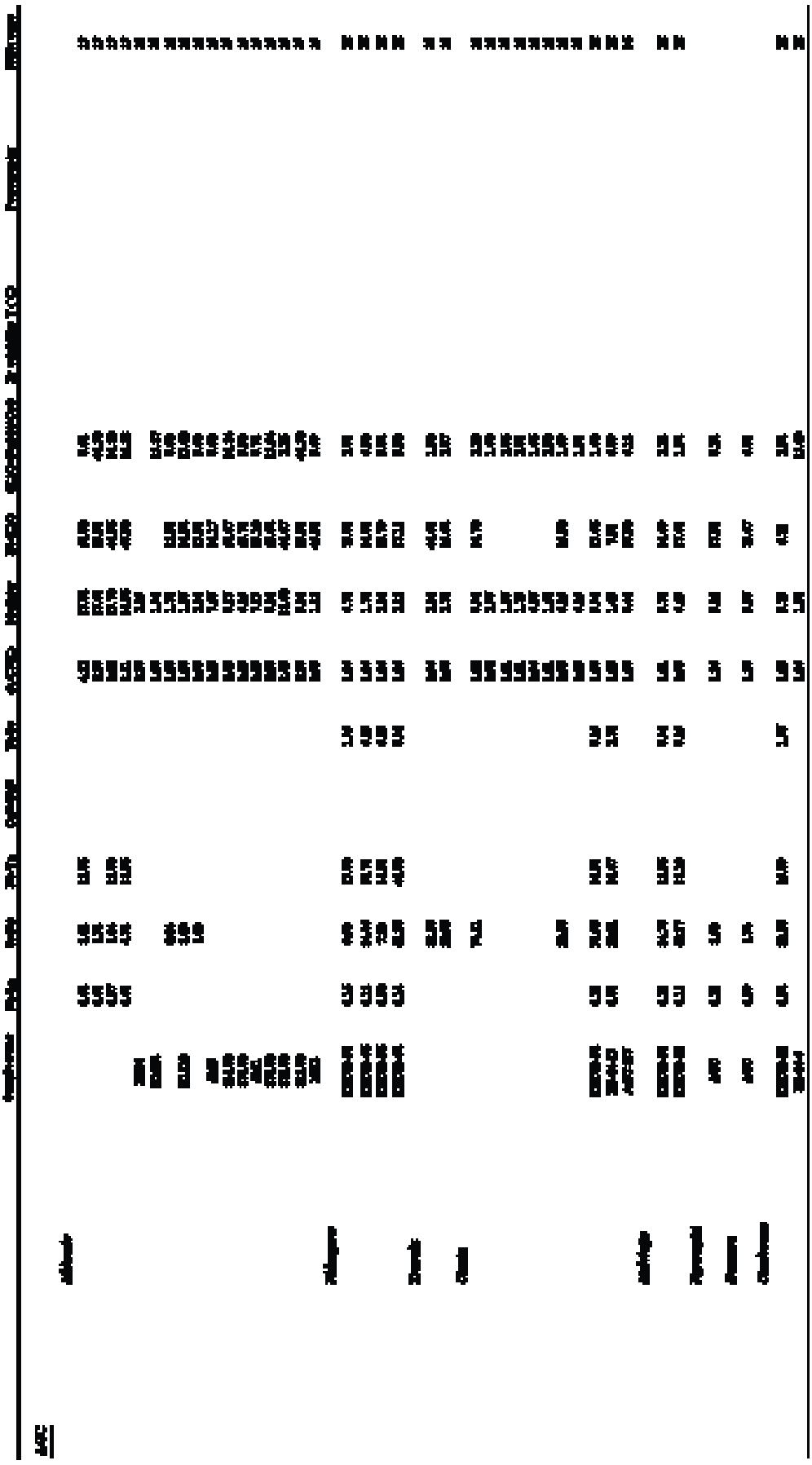

Supplementary Table DR1 (continued): Geochemical data for the Moodies granitic clasts and TTGs associated with the Barberton Greenstone Belt

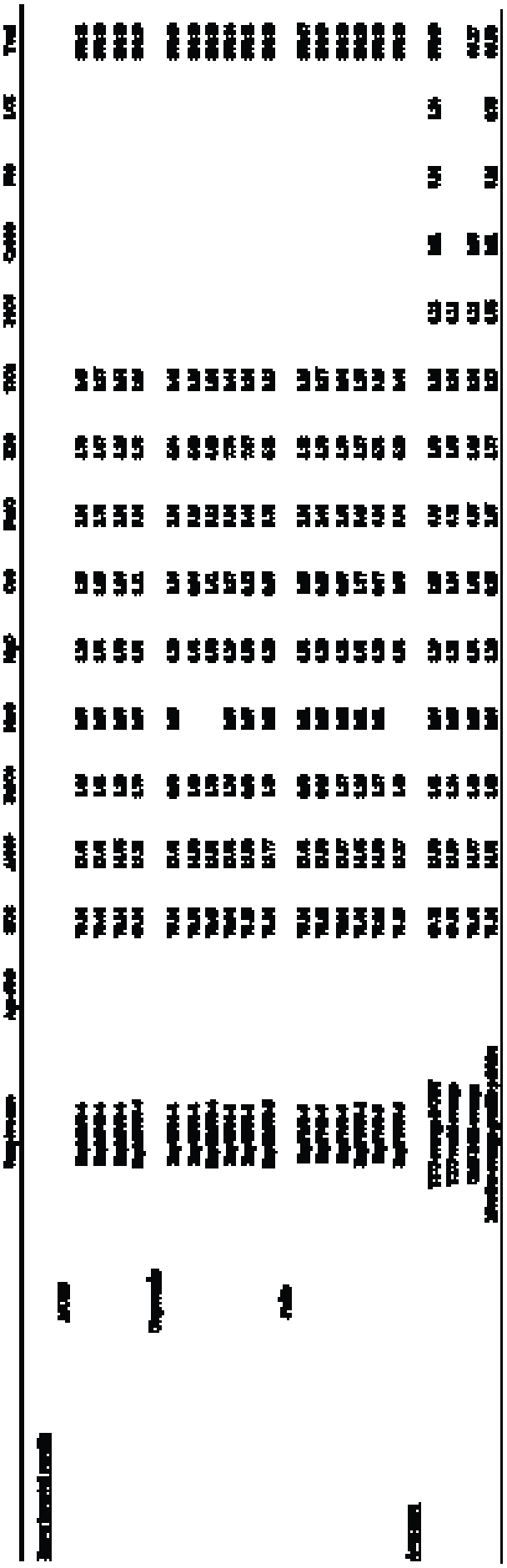

Supplementary Table DR1 (continued): Geochemical data for the Moodies granitic clasts and TTGs associated with the Barberton Greenstone Belt

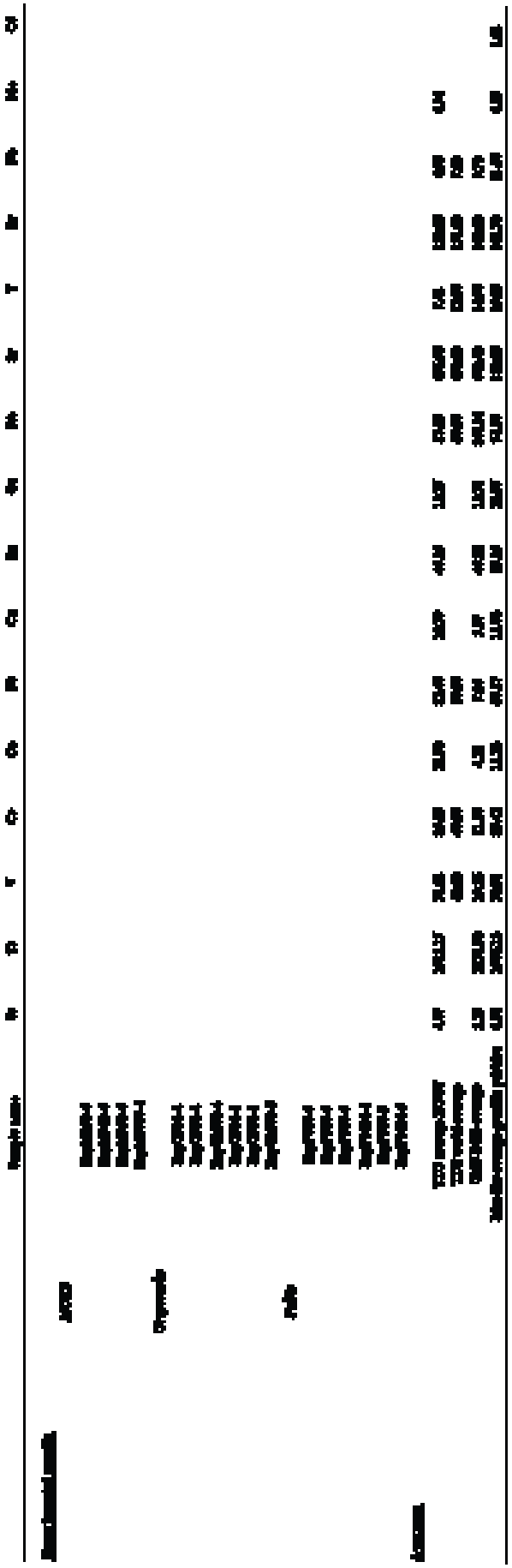

Supplementary Table DR1 (continued): Geochemical data for the Moodies granitic clasts and TTGs associated with the Barberton Greenstone Belt

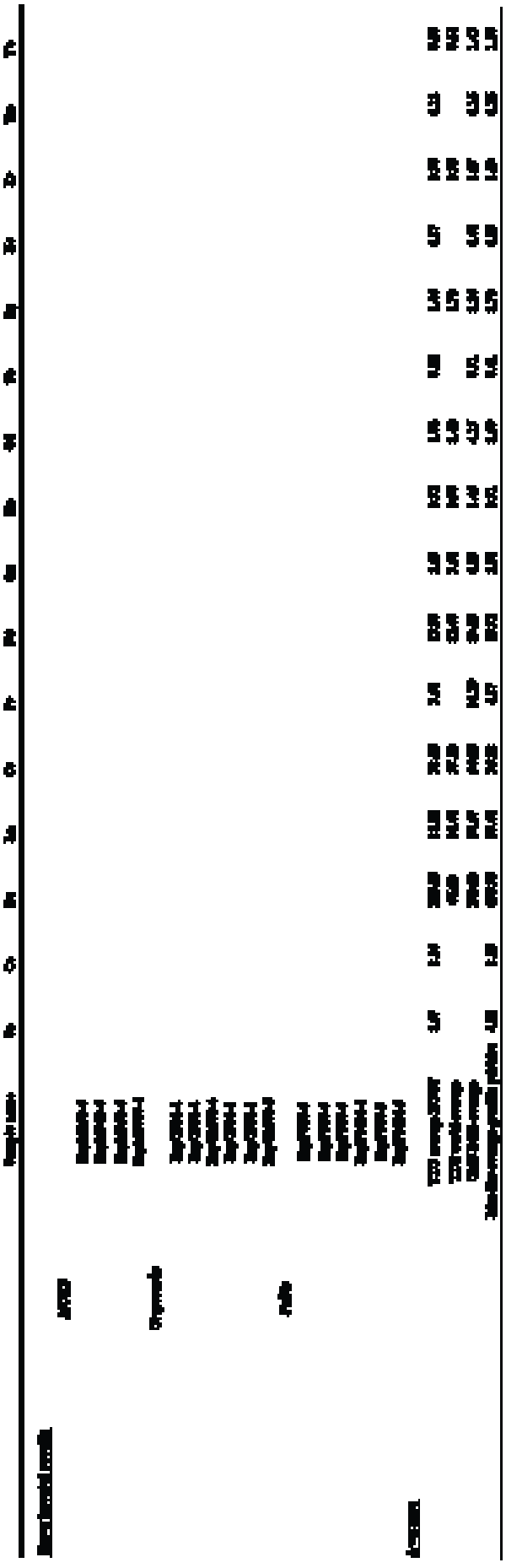

Supplementary Table DR1 (continued): Geochemical data for the Moodies granitic clasts and TTGs associated with the Barberton Greenstone Belt

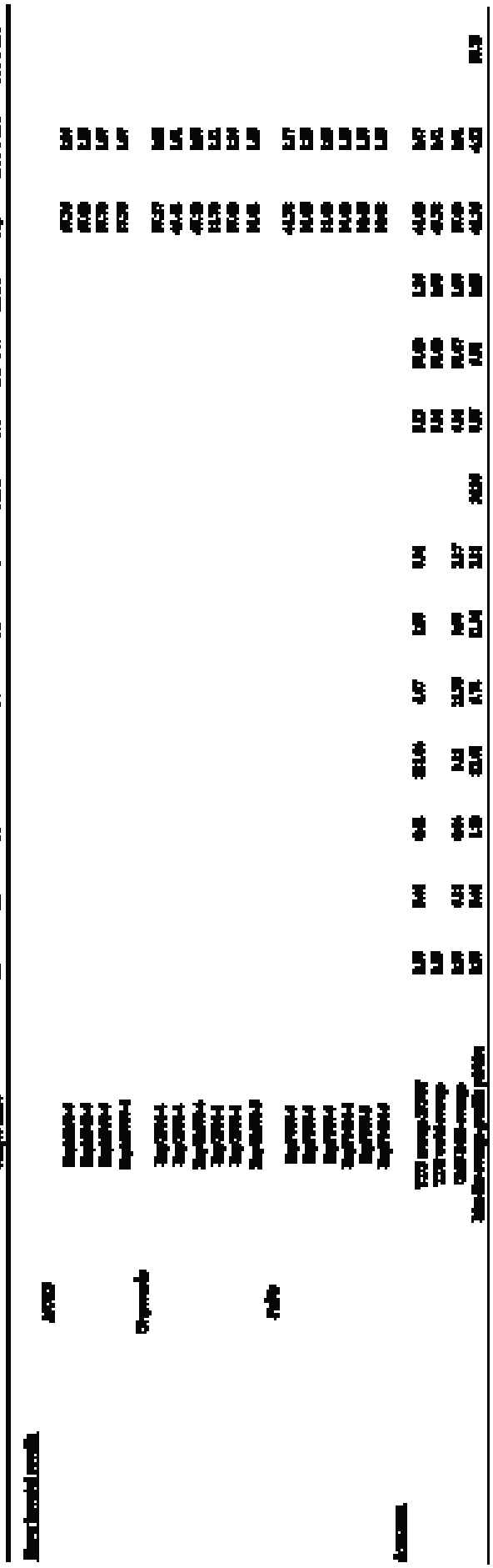

Supplementary Table DR1 (continued): Geochemical data for the Moodies granitic clasts and TTGs associated with the Barberton Greenstone Belt

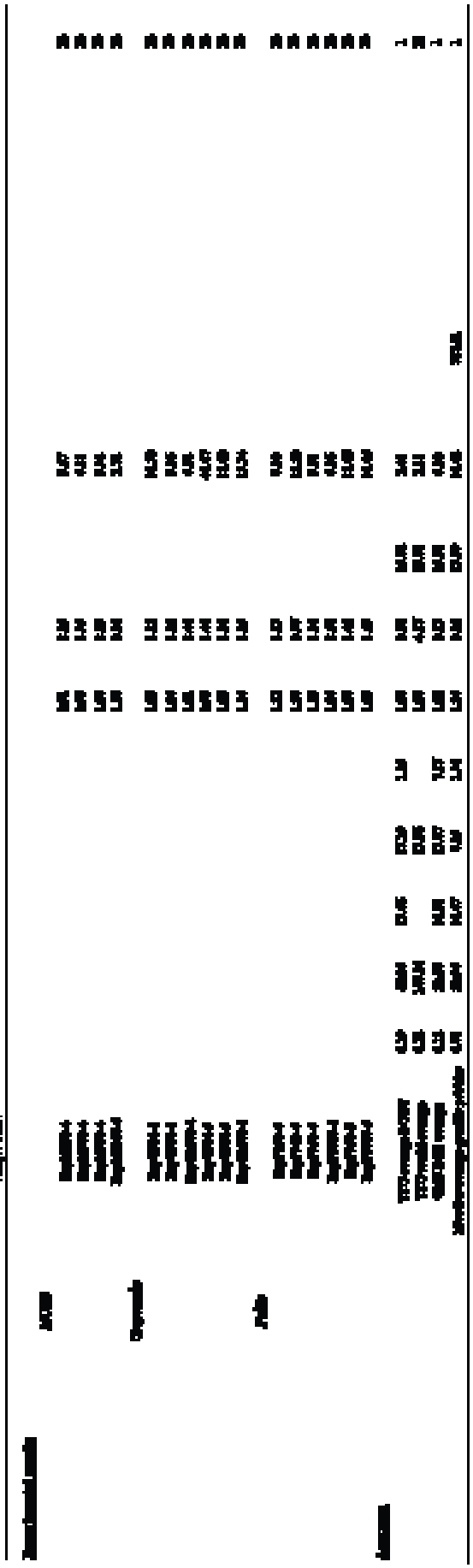

Supplementary Table DR1 (continued): Geochemical data for the Moodies granitic clasts and TTGs associated with the Barberton Greenstone Belt

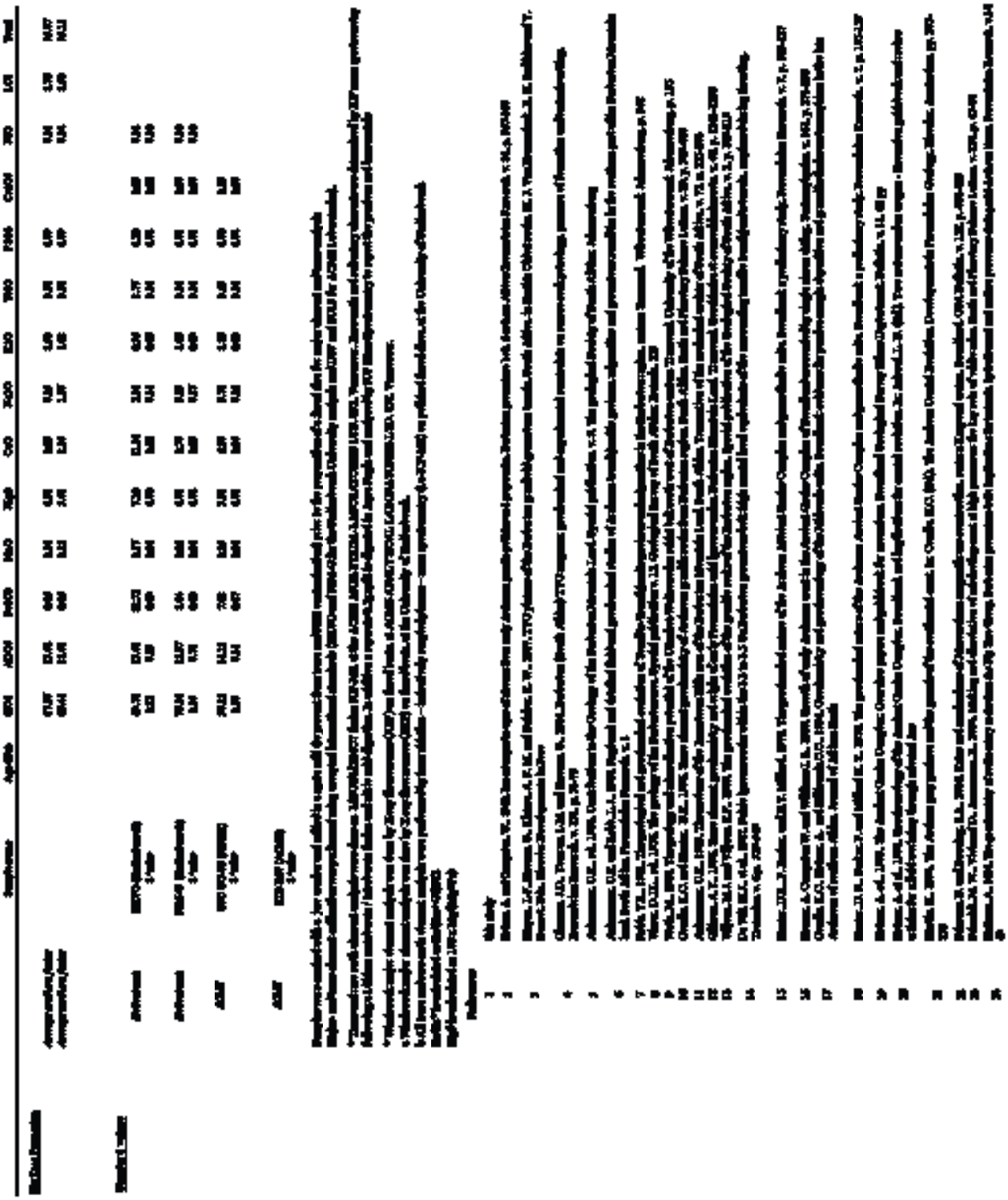

Supplementary Table DR1 (continued): Geochemical data for the Moodies granitic clasts and TTGs associated with the Barberton Greenstone Belt

Supplementary Table DR1 (continued): Geochemical data for the Moodies granitic clasts and TTGs associated with the Barberton Greenstone Belt

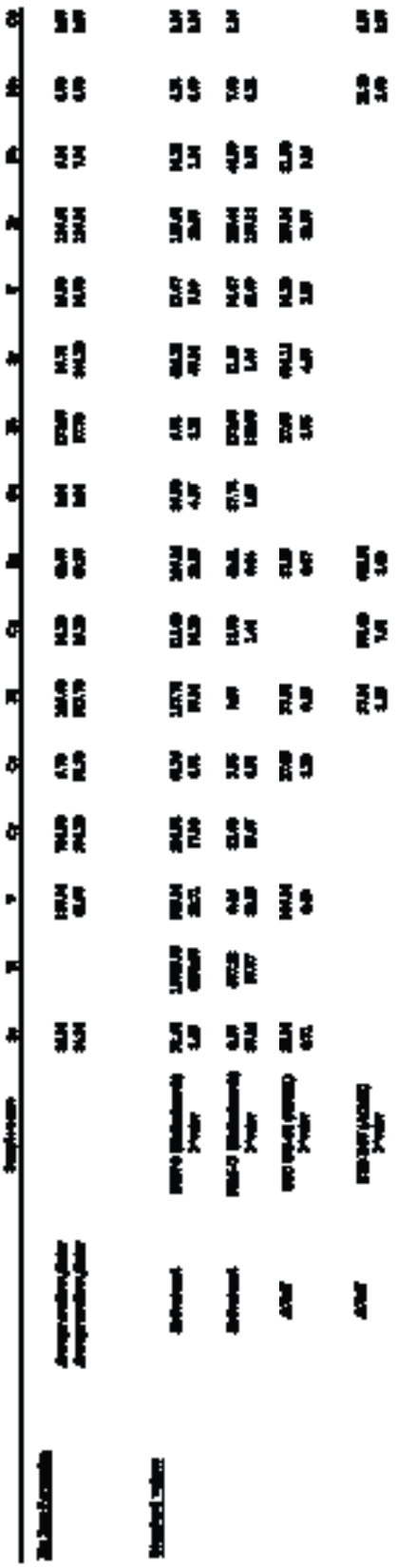

Supplementary Table DR1 (continued): Geochemical data for the Moodies granitic clasts and TTGs associated with the Barberton Greenstone Belt

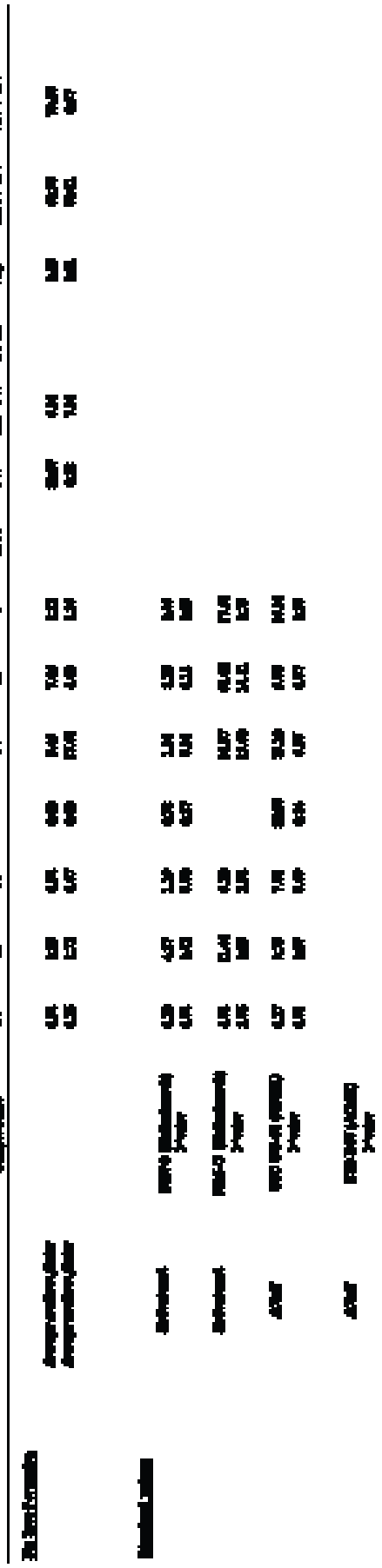

Supplementary Table DR1 (continued): Geochemical data for the Moodies granitic clasts and TTGs associated with the Barberton Greenstone Belt

Supplementary Table DR1 (continued): Geochemical data for the Moodies granitic clasts and TTGs associated with the Barberton Greenstone Belt

Sample number	Grain.spot	$^{18}O/^{16}O$	± 1σ	
A1	A1-1.1	5.28	0.17	
	A1-2.1	4.88	0.22	Mean = 5.05±0.15 [3.0%] 95% conf.
	A1-4.1	4.98	0.16	Wtd by data-pt errs only, 0 of 5 rej.
	A1-5.1	5.06	0.13	MSWD = 0.74, probability = 0.56
	A1-6.1	4.92	0.23	
B7	B7-11.1	6.27	0.26	
	B7-14.1	5.64	0.22	Mean = 5.91±0.32 [5.4%] 95% conf.
	B7-4.1	6.31	0.24	Wtd by data-pt errs only, 0 of 5 rej.
	B7-5.1	5.91	0.14	MSWD = 1.9, probability = 0.11
	B7-5.2	5.72	0.17	
B14	B14-1.1	5.14	0.21	
	B14-10.1	4.94	0.12	
	B14-3.1	5.28	0.13	
	B14-3.2	5.08	0.20	
	B14-4.1	5.31	0.19	
	B14-7.2	4.79	0.16	Mean = 5.03±0.16 [3.3%] 95% conf.
	B14-8.2	4.72	0.20	Wtd by data-pt errs only, 1 of 9 rej.
	B14-8.3	5.33	0.12	MSWD = 1.6, probability = 0.13
	B14-9.1	4.96	0.12	
B17	B17-1.1	4.70	0.15	
	B17-10.1	4.88	0.17	
	B17-11.1	5.03	0.21	
	B17-2.1	4.94	0.22	Mean = 4.90±0.15 [3.0%] 95% conf.
	B17-4.1	4.76	0.19	Wtd by data-pt errs only, 0 of 6 rej.
	B17-9.1	5.18	0.16	MSWD = 1.02, probability = 0.40

SHRIMP II oxygen isotope analysis followed the methods described by Ickert et al. (2008)[1]. The internal standard used was the Temora II zircon with a $\delta^{18}O$ value of 8.2‰ (Black et al., 2004)[2]. Oxygen isotope compositions were recalculated relative to Vienna Standard Mean Ocean Water and reported as $\delta^{18}O$ (Craig, 1961)[3].

(1) Ickert, R.B., Hiess, J., Williams, I.S., Holden, P., Ireland, T.R., Lanc, P., Schram, N., Foster, J.J., Clement, S.W., 2008, Determining high precision, in situ, oxygen isotope ratios with a SHRIMP II: Analyses of MPI-DING silicate-glass reference materials and zircon from contrasting granites. Chemical Geology, v.257, p.114–128.

(2) Black, L.P., Kamo, S.L., Allen, C.M., Davis, D.W., Aleinikoff, J.N., Valley, J.W., Mundil, R., Campbell, I.H., Korsch, R.J., Williams, I.S., Foudoulis, C., 2004, Improved Pb-206/U-238 microprobe geochronology by the monitoring of a trace-element-related matrix effect; SHRIMP, ID-TIMS, ELA-ICP-MS and oxygen isotope documentation for a series of zircon standards. Chemical Geology, v. 205, p.115–140.

(3) Craig, H., 1961, Isotopic variations in meteoric waters. Science, v.133, p.1833–1834.

Supplementary Table DR2: Stable isotope data

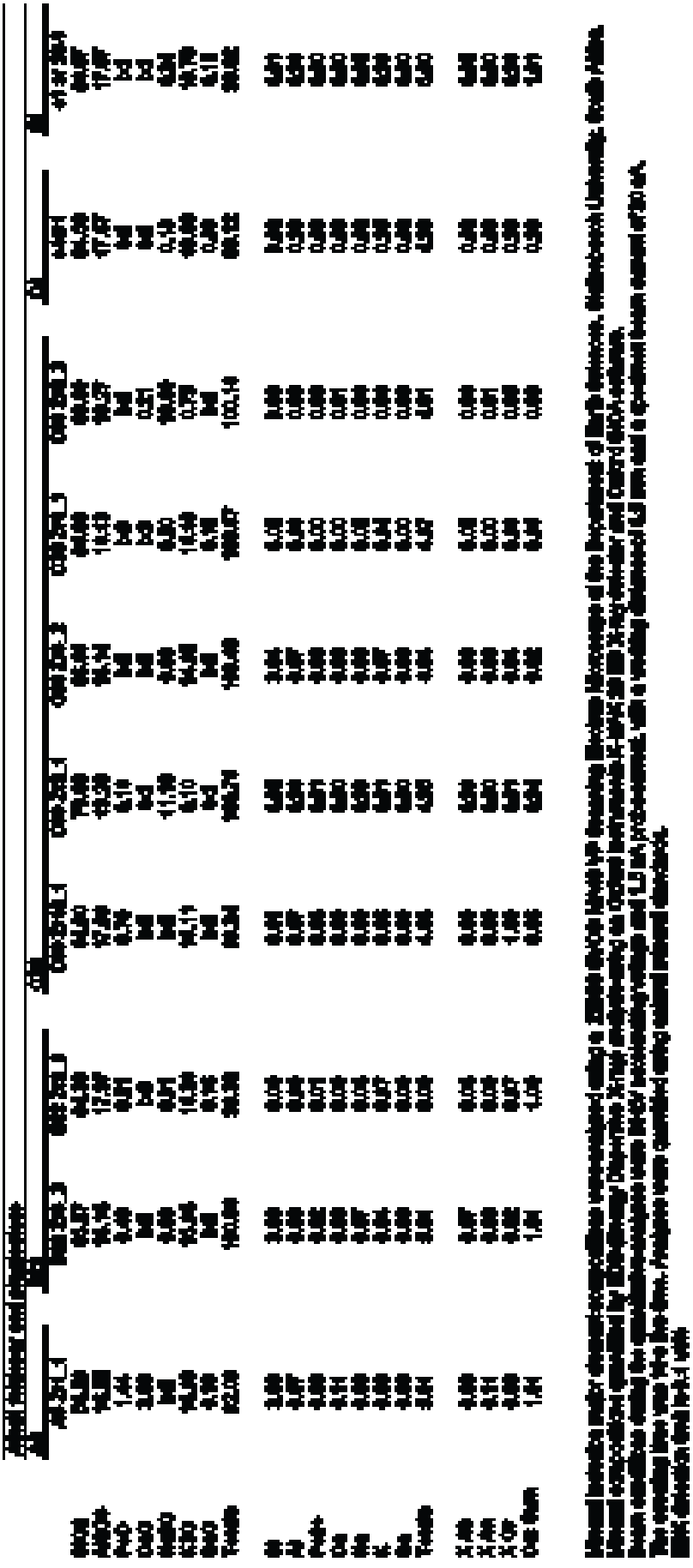

Supplementary Table DR3: SS.E.M mineral inclusions analysis

Supplementary Table DR4: U-Pb radiogenic isotope data

Supplementary Table DR4 (continued): U-Pb radiogenic isotope data

Supplementary Table DR4 (continued): U-Pb radiogenic isotope data

Supplementary Table DR4 (continued): U-Pb radiogenic isotope data

Supplementary Table DR4 (continued): U-Pb radiogenic isotope data

Supplementary Table DR4 (continued): U-Pb radiogenic isotope data

Sample name	Grain Spot	% $^{206}Pb_c$	U (ppm)	Th (ppm)	$^{232}Th/^{238}U$	$^{206}Pb^*$ (ppm)	(1) $^{206}Pb/^{238}U$ Age (Ma)	± 1σ	(1) $^{207}Pb/^{206}Pb$ Age (Ma)	± 1σ	% Discordant	(1) $^{207}Pb^*/^{206}Pb^*$	err %	(1) $^{207}Pb^*/^{235}U$	err %	(1) $^{206}Pb^*/^{238}U$	err %	err corr
JTB																		
	2.1	0.18	229	108	0.49	127.0	3214	± 28	3279	± 4	2	0.2654	0.28	23.65	1.20	0.6465	1.10	0.970
	3.1	9.37	300	351	0.95	177.0	2575	± 29	3250	± 20	20	0.2575	1.30	17.42	1.50	0.4910	1.40	0.730
	4.1	21.60	344	1064	3.20	174.0	2356	± 60	3423	± 88	31	0.2910	5.70	17.50	6.30	0.4370	3.20	0.495
	5.1	3.59	470	2652	5.67	183.0	2172	± 25	3294	±15	34	0.2679	0.93	14.80	1.60	0.4005	1.40	0.823
	6.1	10.56	240	303	1.30	156.0	2797	± 30	3315	± 12	16	0.2715	0.79	20.35	1.70	0.5432	1.50	0.879
	6.2	26.97	574	2944	5.13	180.0	1525	± 42	3156	± 55	51	0.2425	2.20	8.91	3.30	0.2665	3.10	0.832
	7.1	4.27	546	2362	4.05	144.0	1665	± 16	3229	± 13	49	0.2600	0.82	10.65	1.40	0.2940	1.10	0.805
	8.1	5.01	288	518	1.65	159.0	2614	± 25	3280	± 9	20	0.2656	0.55	18.37	1.30	0.5001	1.20	0.903
	8.2	6.48	291	253	0.90	158.0	2656	± 35	3250	± 80	19	0.2620	5.10	17.34	4.50	0.4862	1.60	0.305
	9.1	7.96	561	369	0.68	180.0	1900	± 21	3218	± 19	41	0.2555	0.83	12.07	1.50	0.3426	1.30	0.856
	10.1	23.40	290	688	2.55	128.0	2158	± 50	3042	± 62	36	0.2765	2.70	14.50	3.30	0.3950	2.80	0.720
	11.1	34.46	364	534	1.53	255.0	2765	± 100	3434	± 52	19	0.2951	2.10	21.70	5.00	0.5340	4.50	0.909
	12.1	0.11	108	58	0.57	61.6	3280	± 30	3273	± 85	0	0.2644	0.33	24.33	1.20	0.6654	1.20	0.962
	13.1	3.80	575	1151	3.18	145.0	2581	± 22	3277	± 14	30	0.2651	0.46	15.87	1.30	0.4289	1.20	0.870

The SHRIMP analytical procedures followed the methods described in Compston et al (1984) [1] and Williams (1998) [2].
The standard zircon [illegible] [3] was used to [illegible] U concentration whereas the U-Pb ratios were referenced to the zircon standard [illegible] [4].
Errors are 1-sigma; Pb_c and Pb^* indicate the common and radiogenic portions, respectively.
[illegible]
(1) Common Pb corrected using measured ^{204}Pb.
The age calculations and the concordia plots were done using Isoplot/Ex software (Ludwig, 2003) [5]

Reference

1. Compston, W., Williams, I.S. and Meyer,C., 1984, U-Pb geochronology of zircons from lunar breccia 73217 using a sensitive high-resolution ion-microprobe. Journal of Geophysic Research, B 98, p. 525-534
2. Williams, I.S., 1998, U-Th-Pb geochronology by ion microprobe, In Applications of Microanalytical Techniques to Understanding Mineralizing Processes, M.A. McKibben, W.C. Shanks III, and W.I. Ridley, Eds p. 1-35
3. Claoue-Long, J.C., et al., 1995, Two Carboniferous ages: a comparison of SHRIMP zircon dating with conventional zircon ages and 40Ar/39Ar analysis, In Geochronology, Time Scale and Global Stratigraphic Correlation, W.A. Berggren, et al., Eds p. 3-21
4. Paces, J.B. and J.D. Miller, 1993, Precise U-Pb ages of Duluth Complex and related mafic intrusions, northeastern Minnesota: geochronological insights into physical, petrogenetic, paleomagnetic and tectonomagmatic process associated with the 1.1 Ga midcontinental rift system. Journal of Geophysics research, v. 98, p. 13997-14013
5. Ludwig, K.R., 2004, User's Manual for Isoplot/Ex version 3.00-A Geochronology Toolkit for Microsoft Excel. Berkeley Geochronological Center Special publication of the Geological Society of South Africa,v. 4, p 70

Supplementary Table DR4 (continued): U-Pb radiogenic isotope data

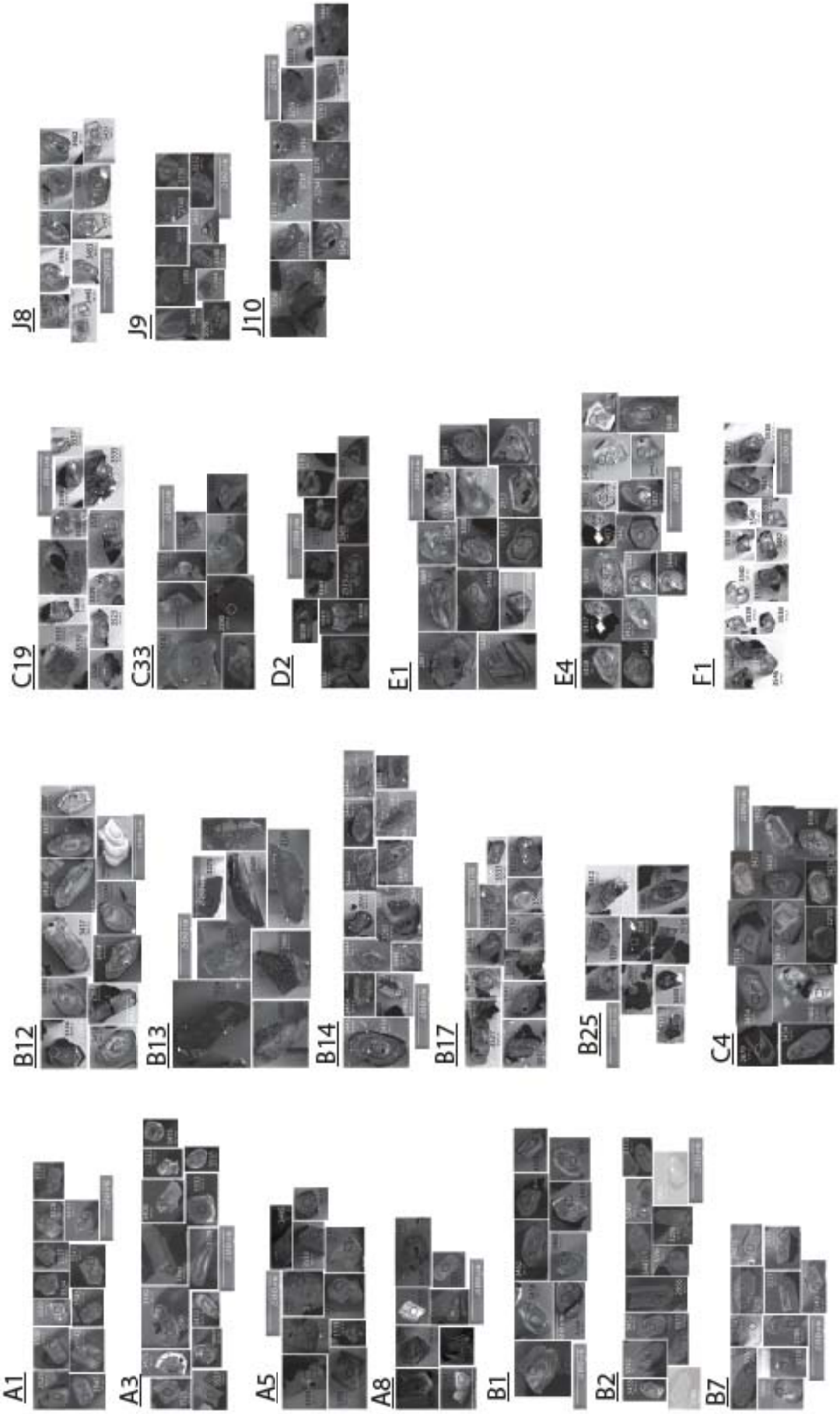

Supplementary Table DR5: Catholuminescence images of the analysed zircons

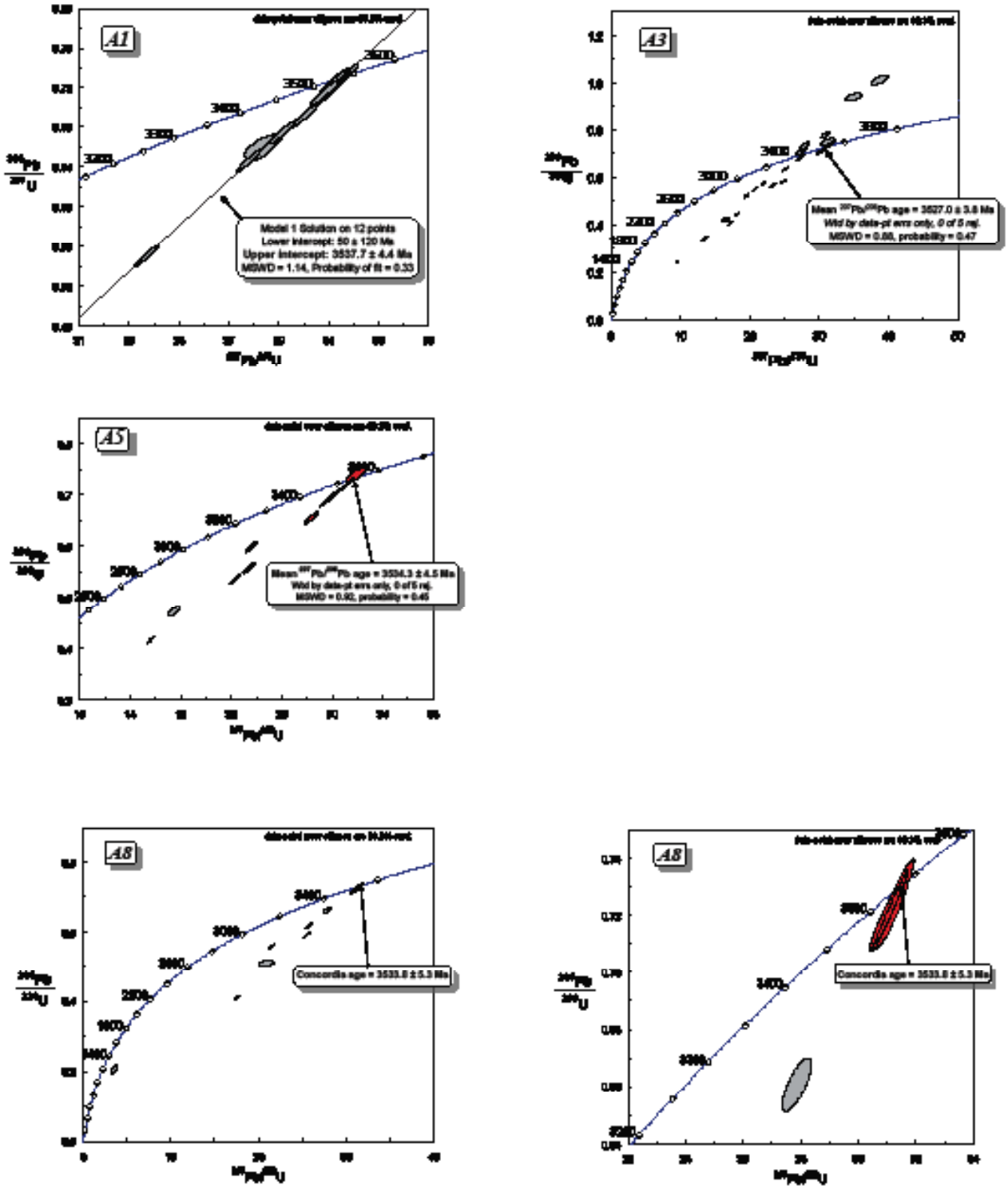

SHRIMP zircon U-Pb concordia diagram for the samples A1, A3, A5 and A8.

Supplementary Table DR6: Concordia diagram of analysed U-Pb zircons

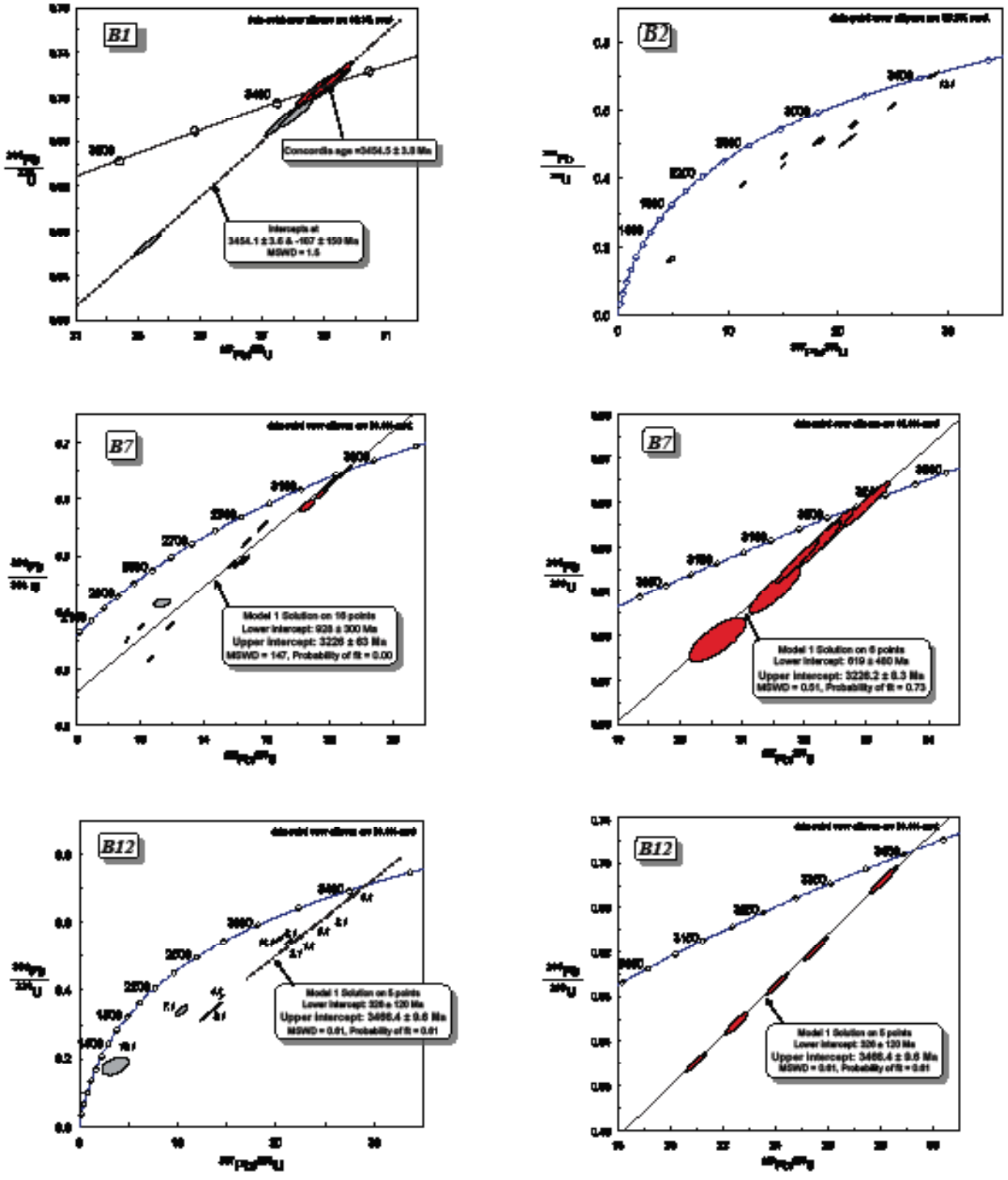

SHRIMP zircon U-Pb concordia diagram for the samples B1, B2, B7 and B12.

Supplementary Table DR6 (continued): Concordia diagram of analysed U-Pb zircons

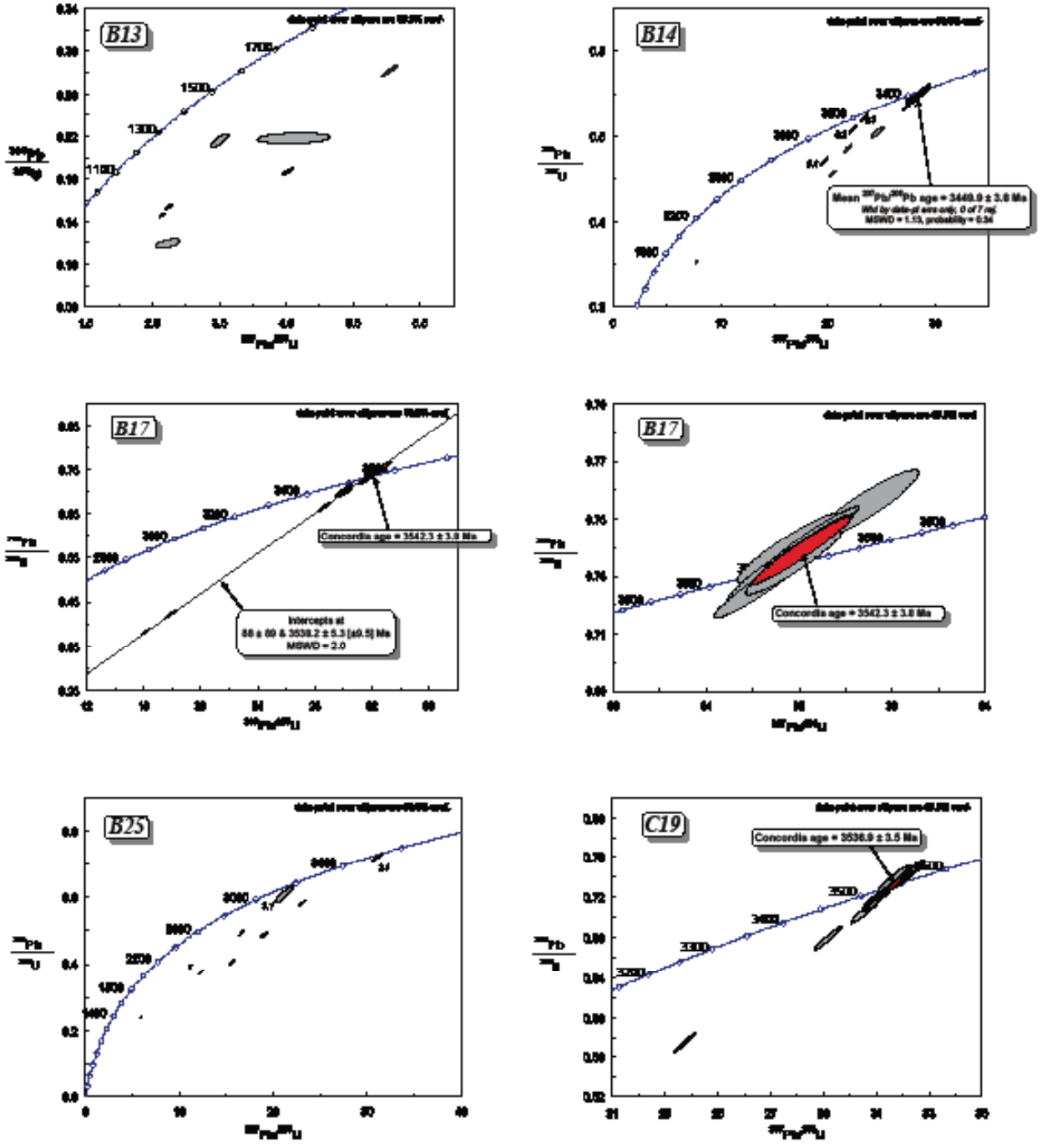

SHRIMP zircon U-Pb concordia diagram for the samples B13, B14, B17, B25 and C19.

Supplementary Table DR6 (continued): Concordia diagram of analysed U-Pb zircons

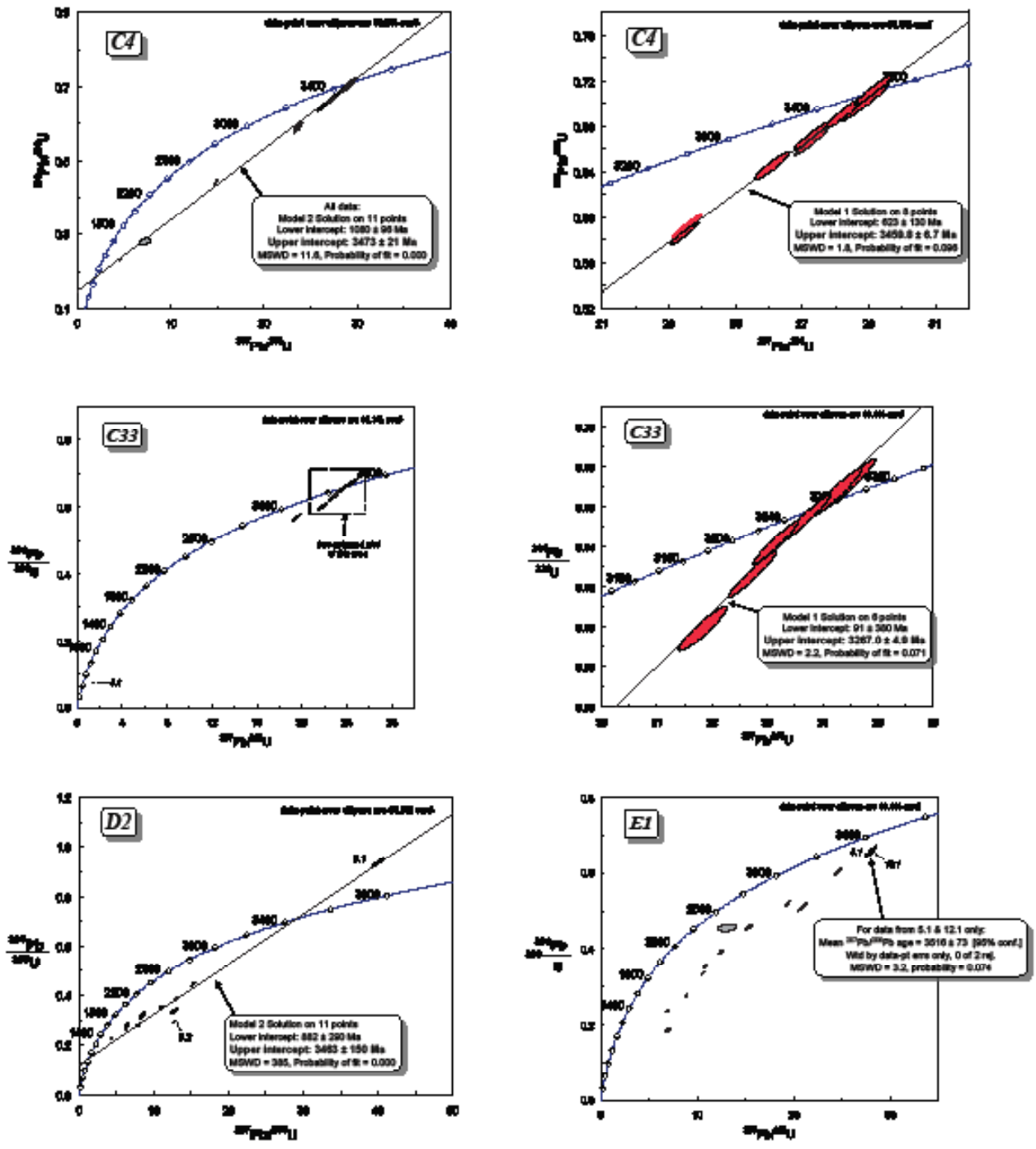

SHRIMP zircon U-Pb concordia diagram for the samples C4, C33, D2 and E1.

Supplementary Table DR6 (continued): Concordia diagram of analysed U-Pb zircons

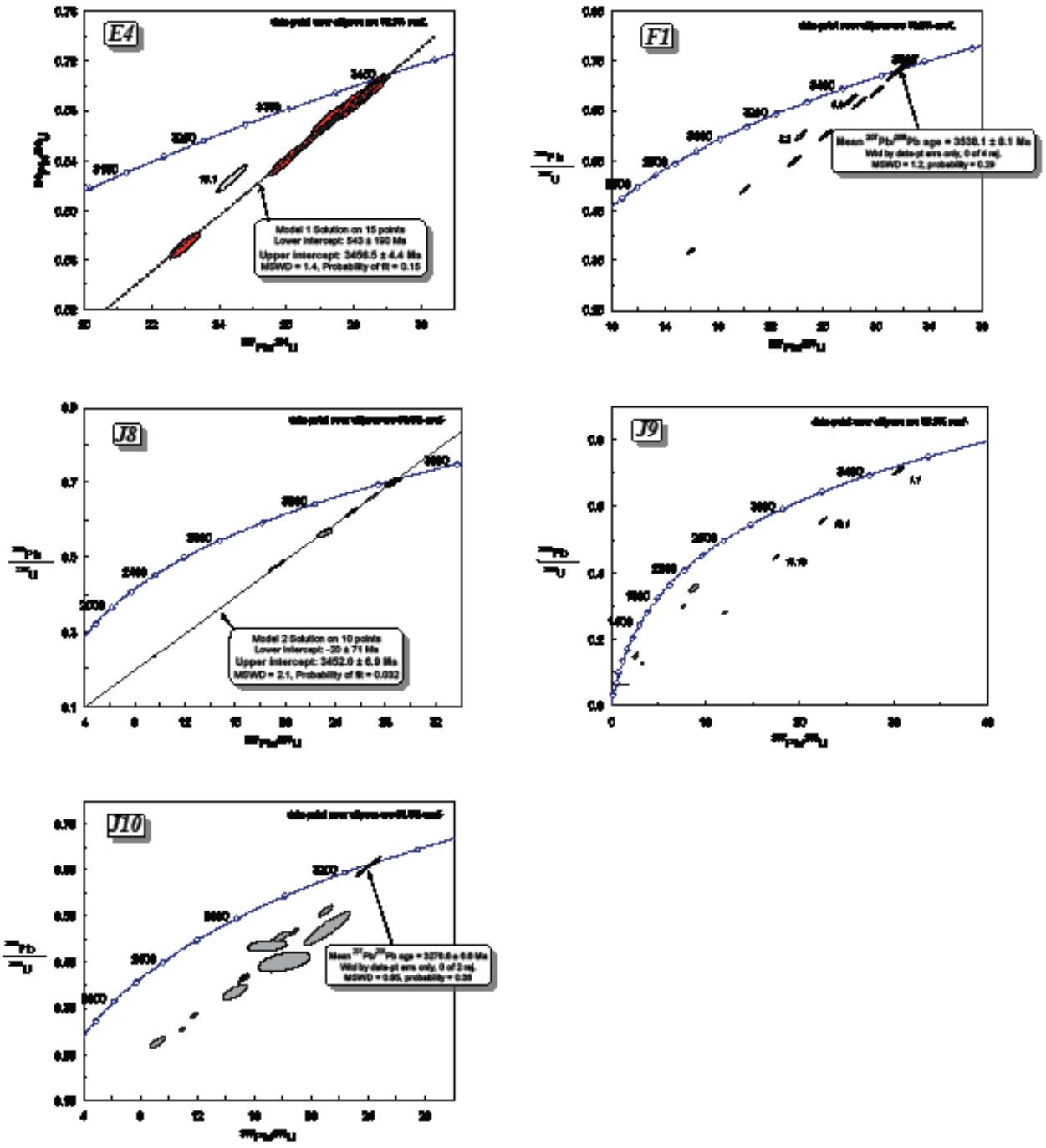

SHRIMP zircon U-Pb concordia diagram for the samples E4, F1, J8, J9 and J10.

Supplementary Table DR6 (continued): Concordia diagram of analysed U-Pb zircons

Chapter 3: Appendices

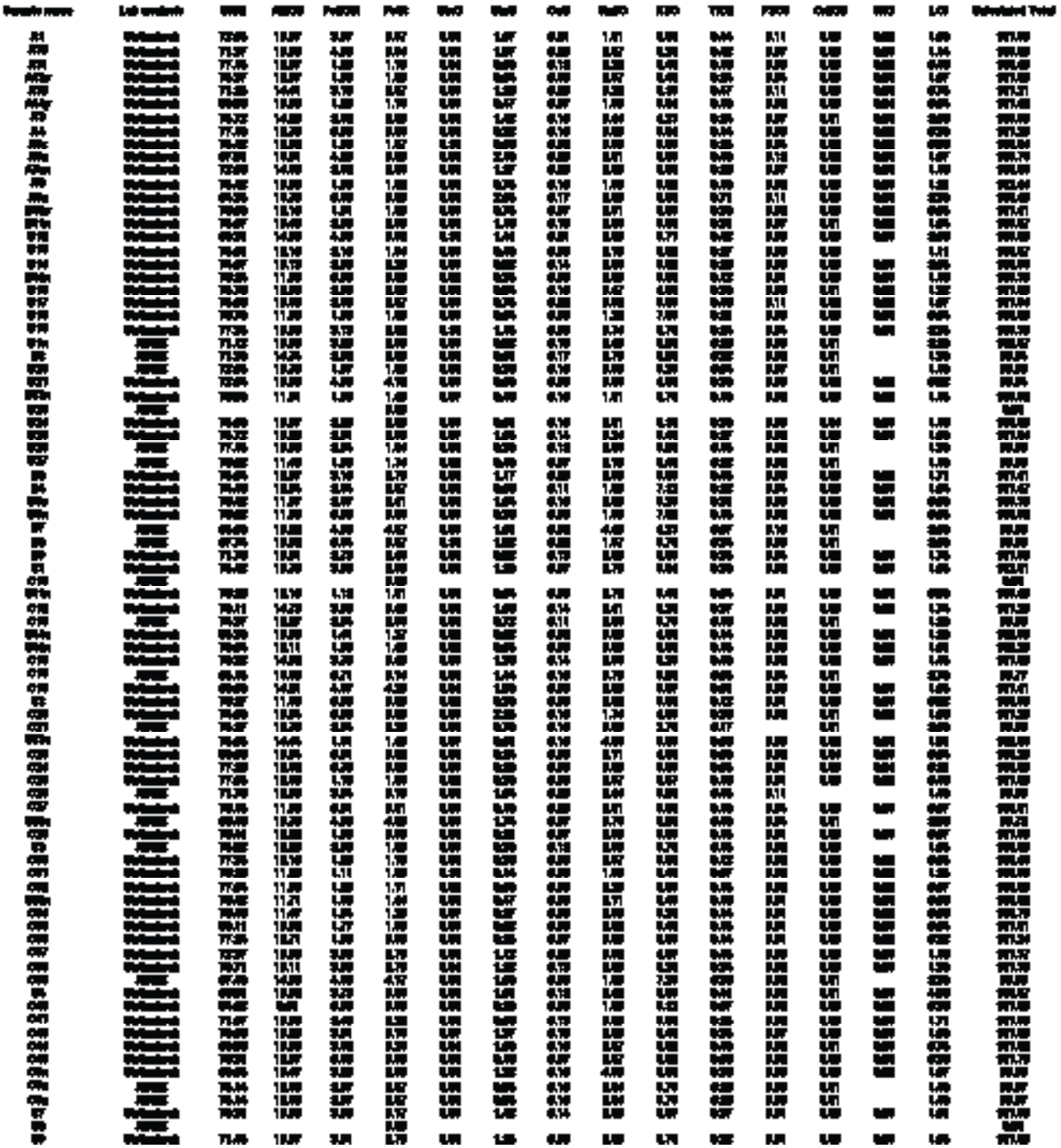

Supplementary Table 1: Geochemical data for the Moodies granitic clasts and Theespruit felsic schists associated with the Barberton Greenstone Belt

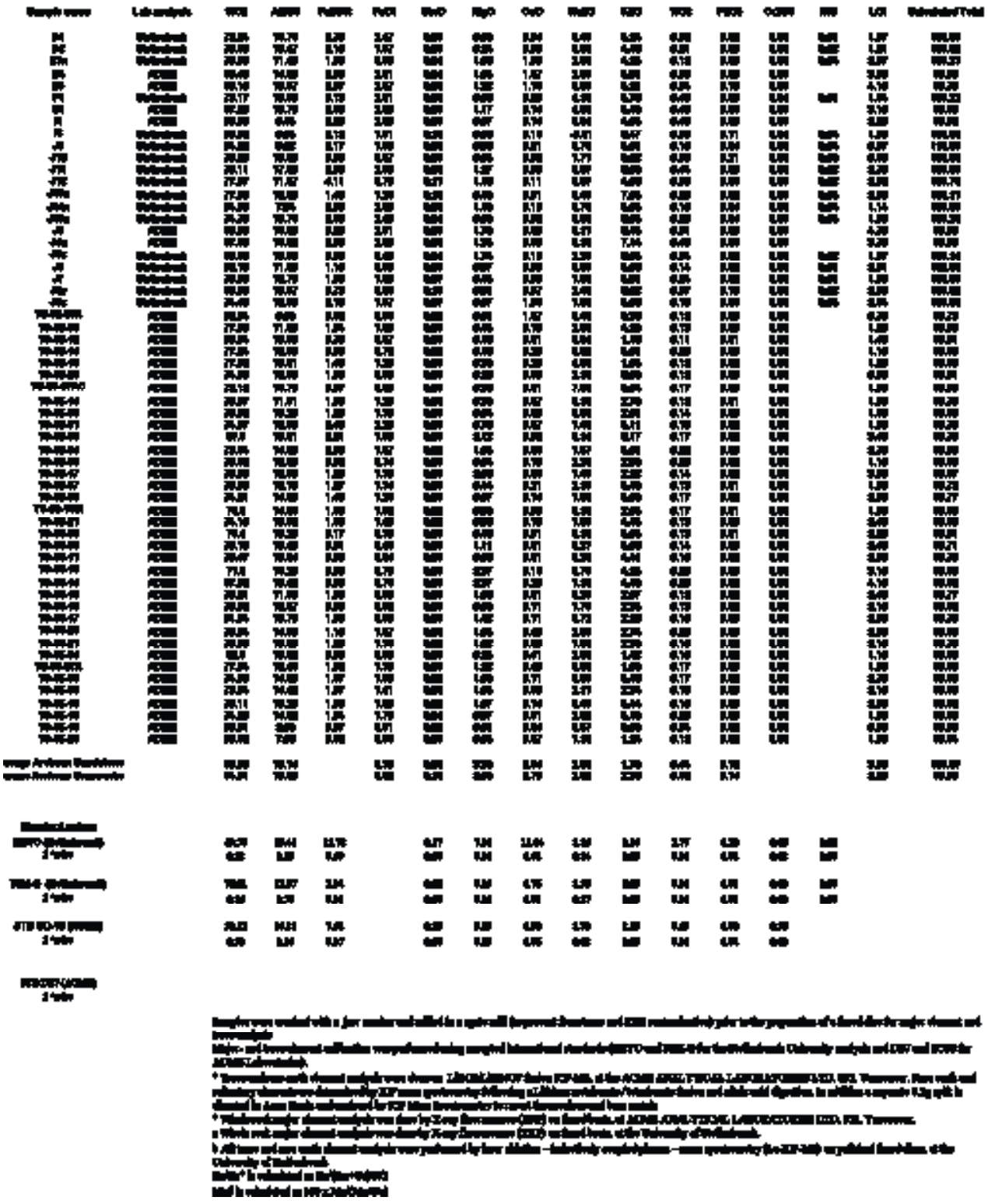

Supplementary Table 1 (continued): Geochemical data for the Moodies granitic clasts and Theespruit felsic schists associated with the Barberton Greenstone Belt

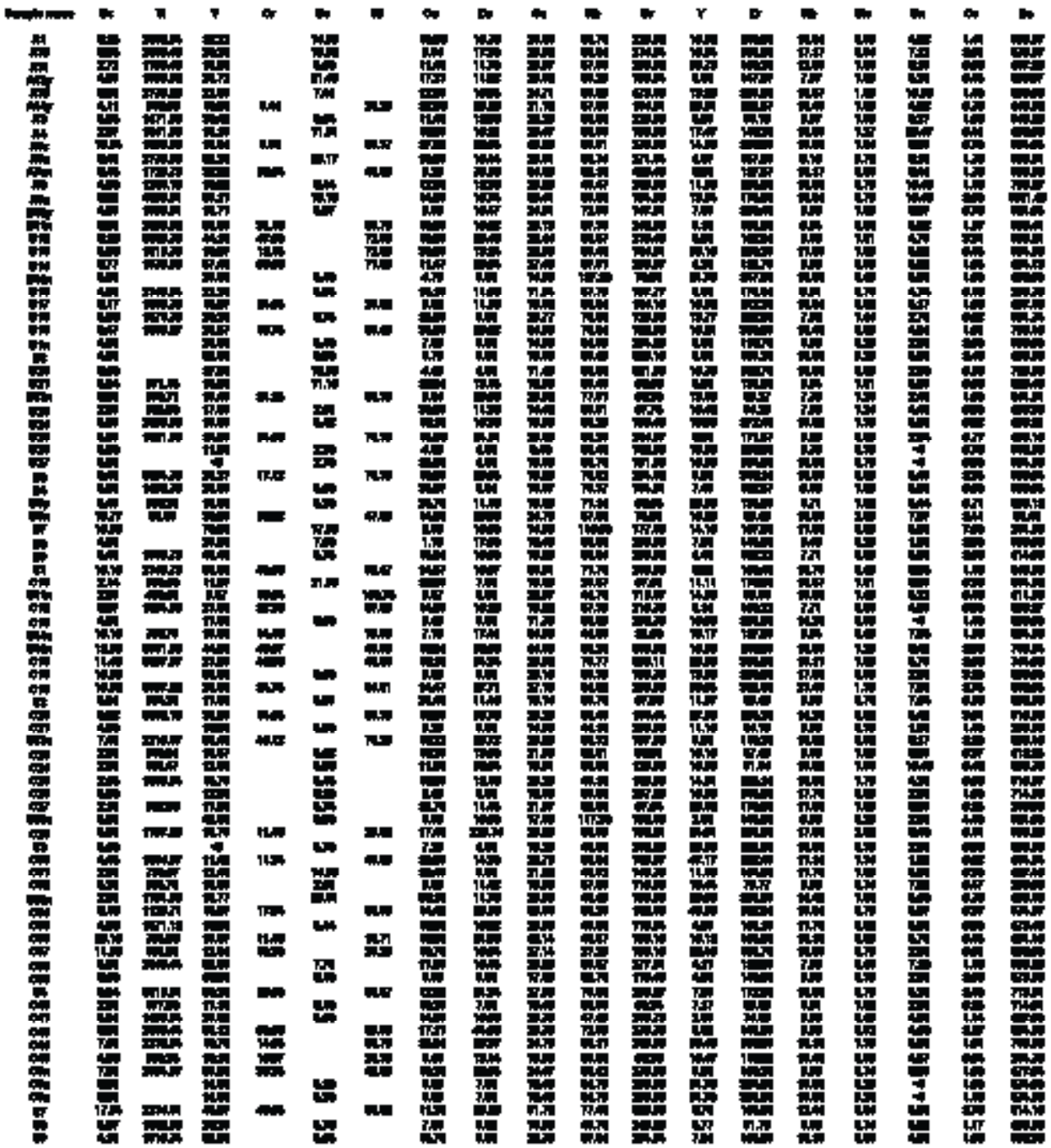

Supplementary Table 1 (continued): Geochemical data for the Moodies granitic clasts and Theespruit felsic schists associated with the Barberton Greenstone Belt

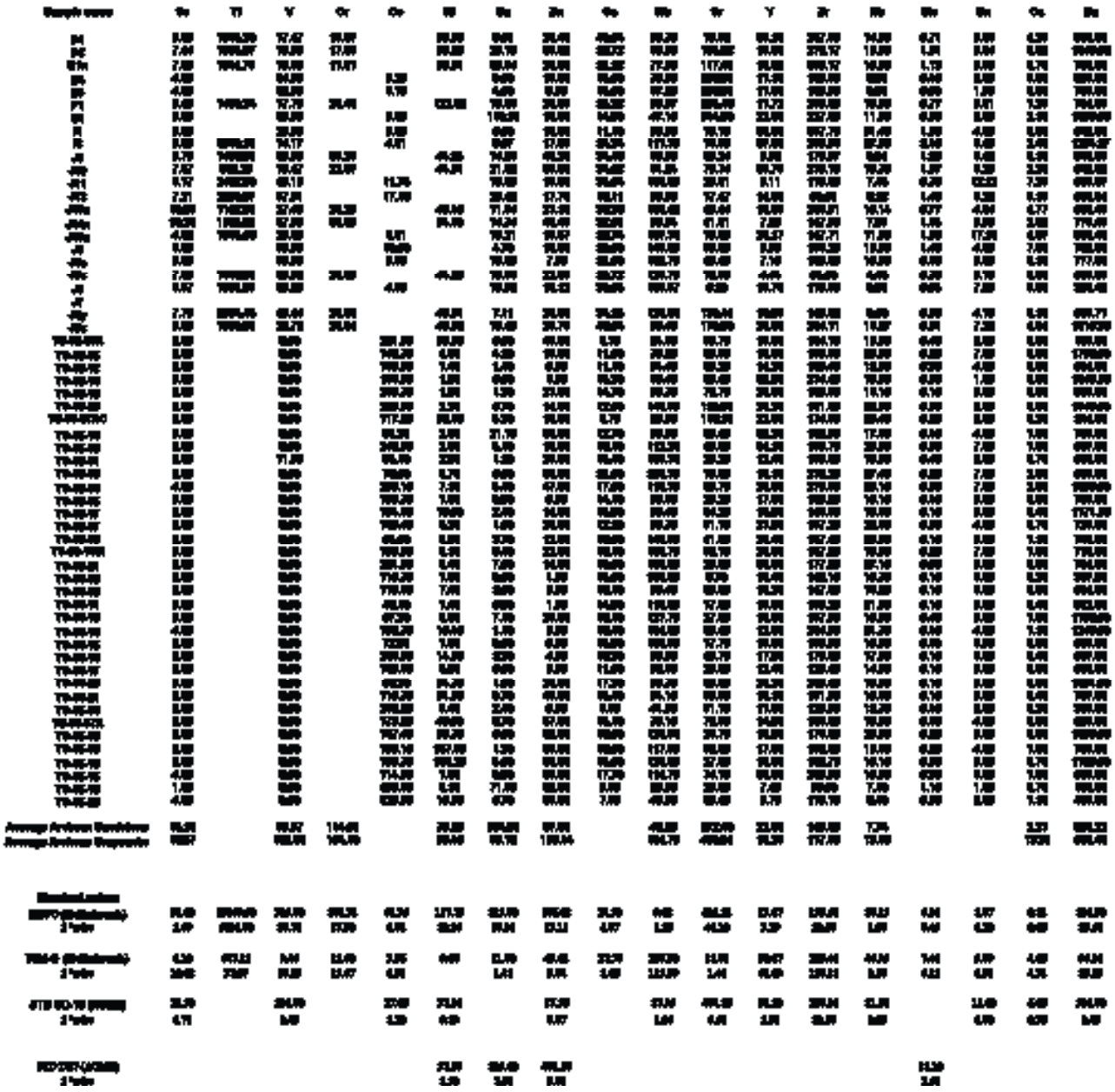

Supplementary Table 1 (continued): Geochemical data for the Moodies granitic clasts and Theespruit felsic schists associated with the Barberton Greenstone Belt

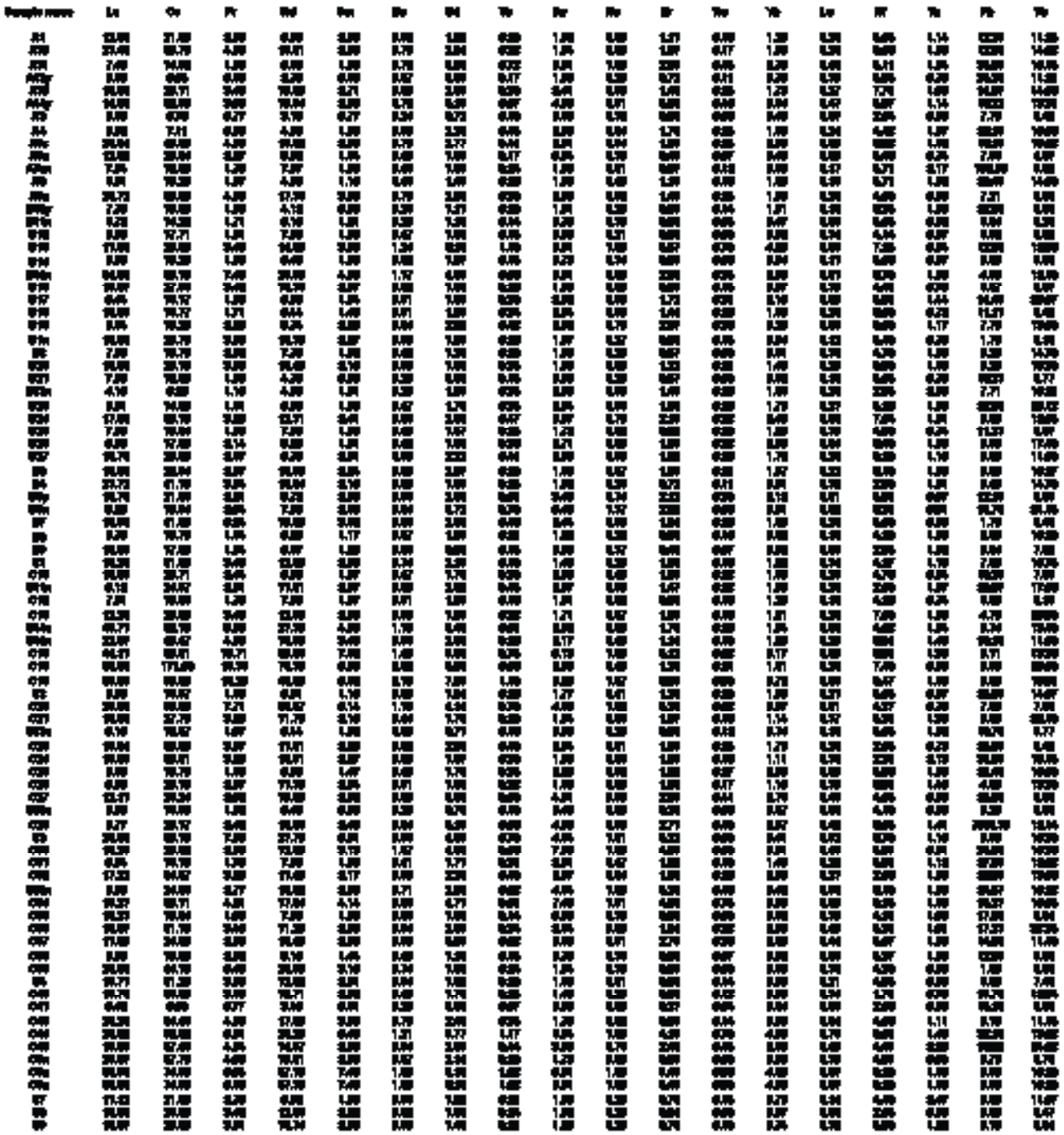

Supplementary Table 1 (continued): Geochemical data for the Moodies granitic clasts and Theespruit felsic schists associated with the Barberton Greenstone Belt

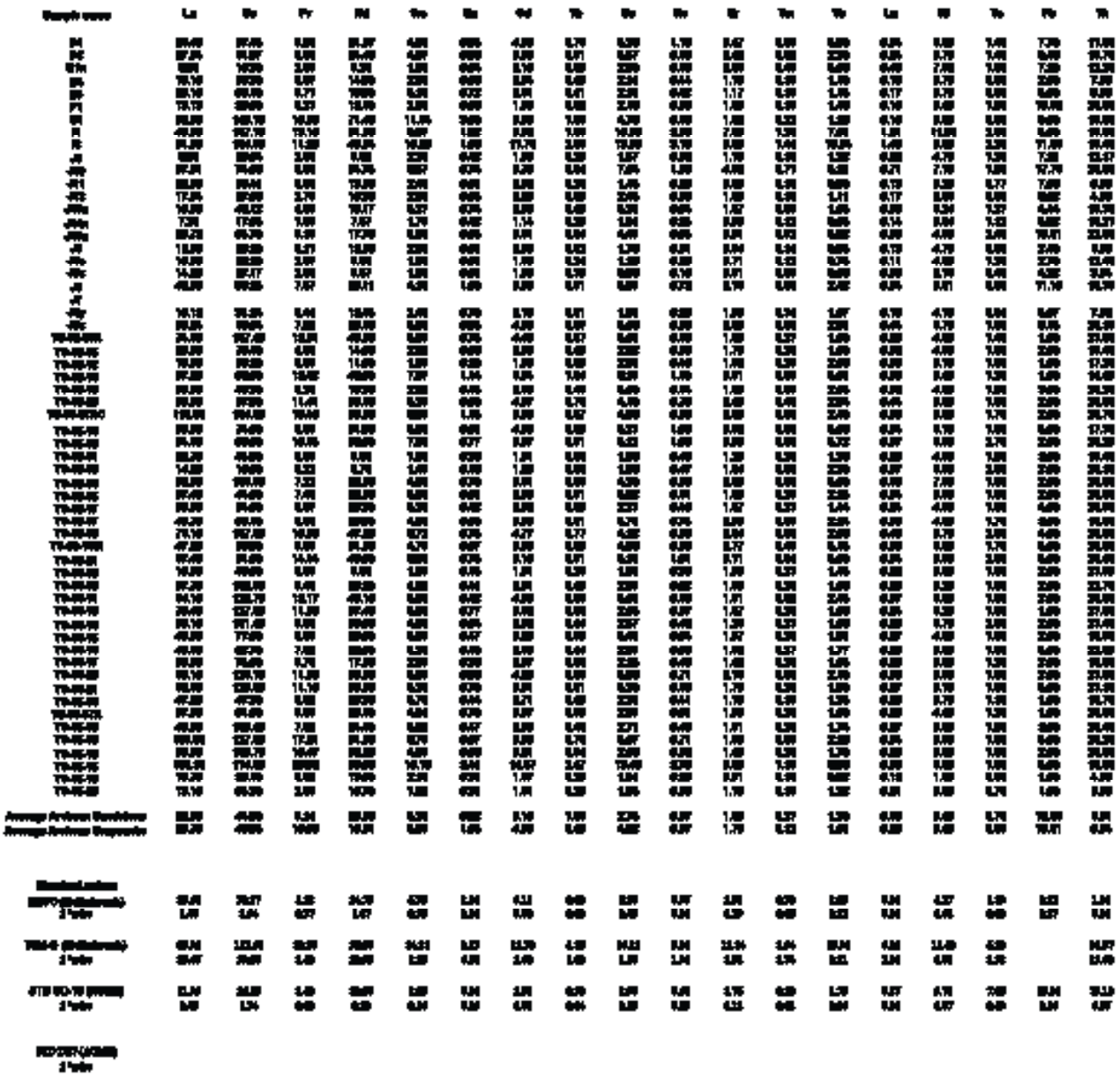

Supplementary Table 1 (continued): Geochemical data for the Moodies granitic clasts and Theespruit felsic schists associated with the Barberton Greenstone Belt

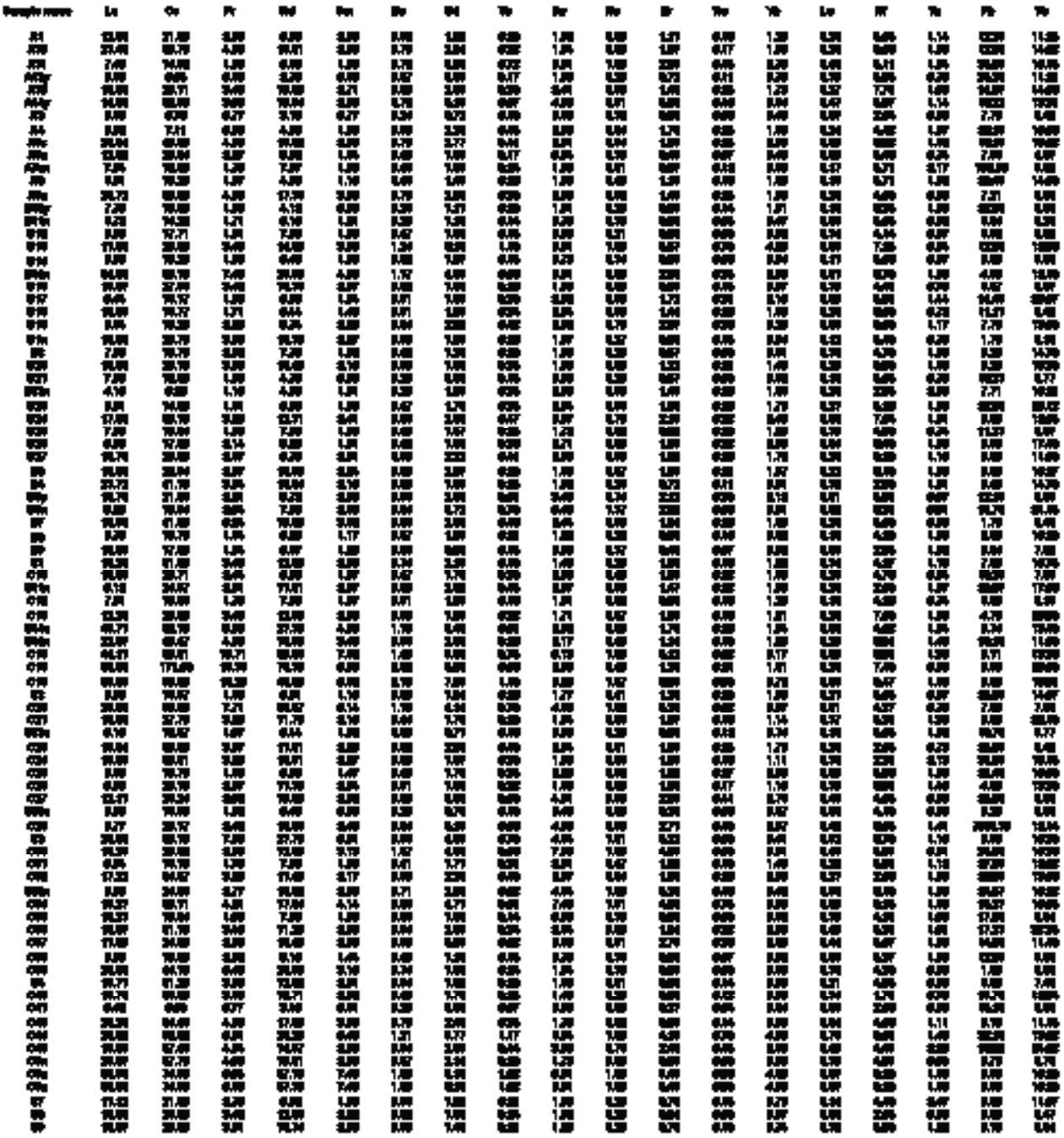

Supplementary Table 1 (continued): Geochemical data for the Moodies granitic clasts and Theespruit felsic schists associated with the Barberton Greenstone Belt

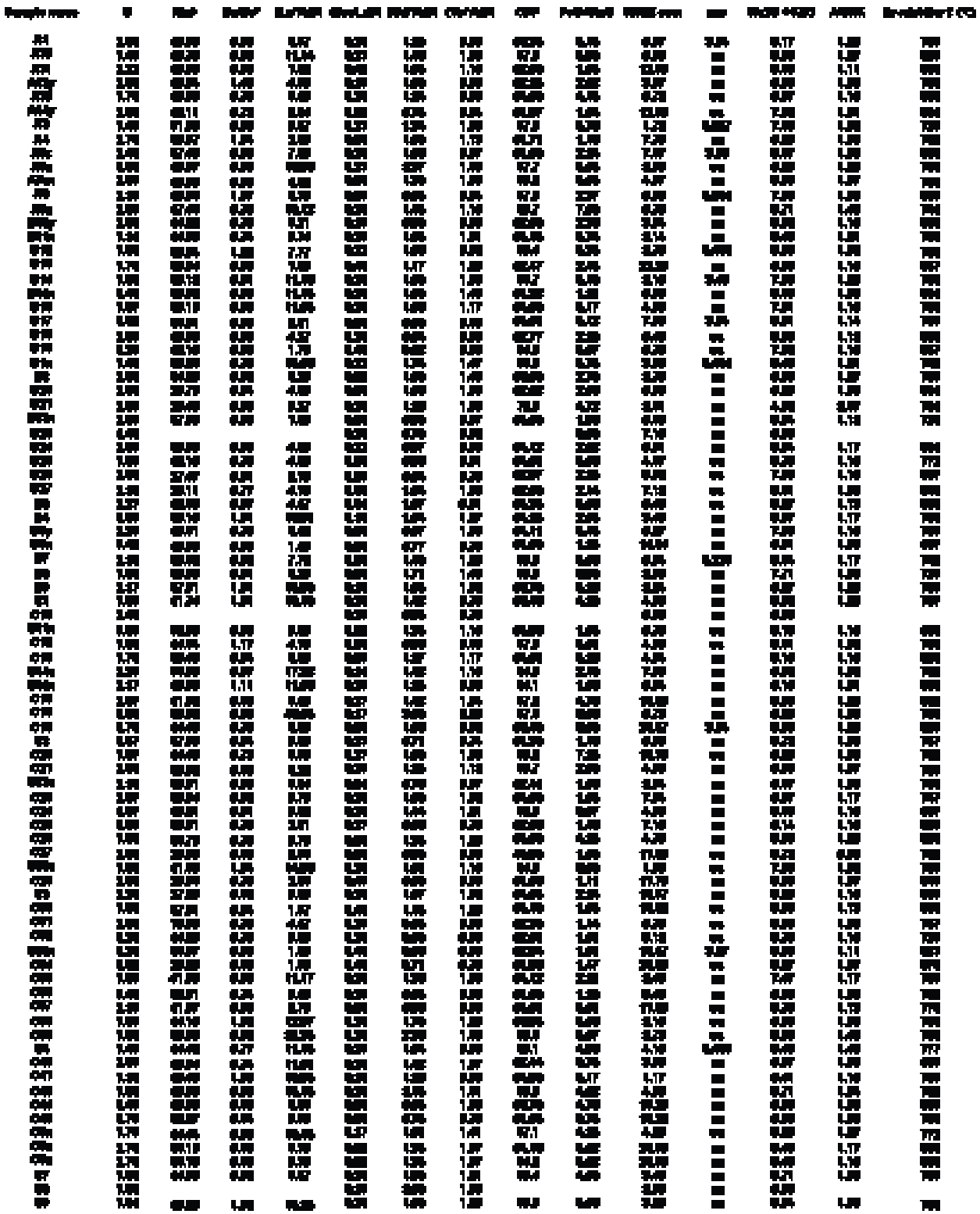

Supplementary Table 1 (continued): Geochemical data for the Moodies granitic clasts and Theespruit felsic schists associated with the Barberton Greenstone Belt

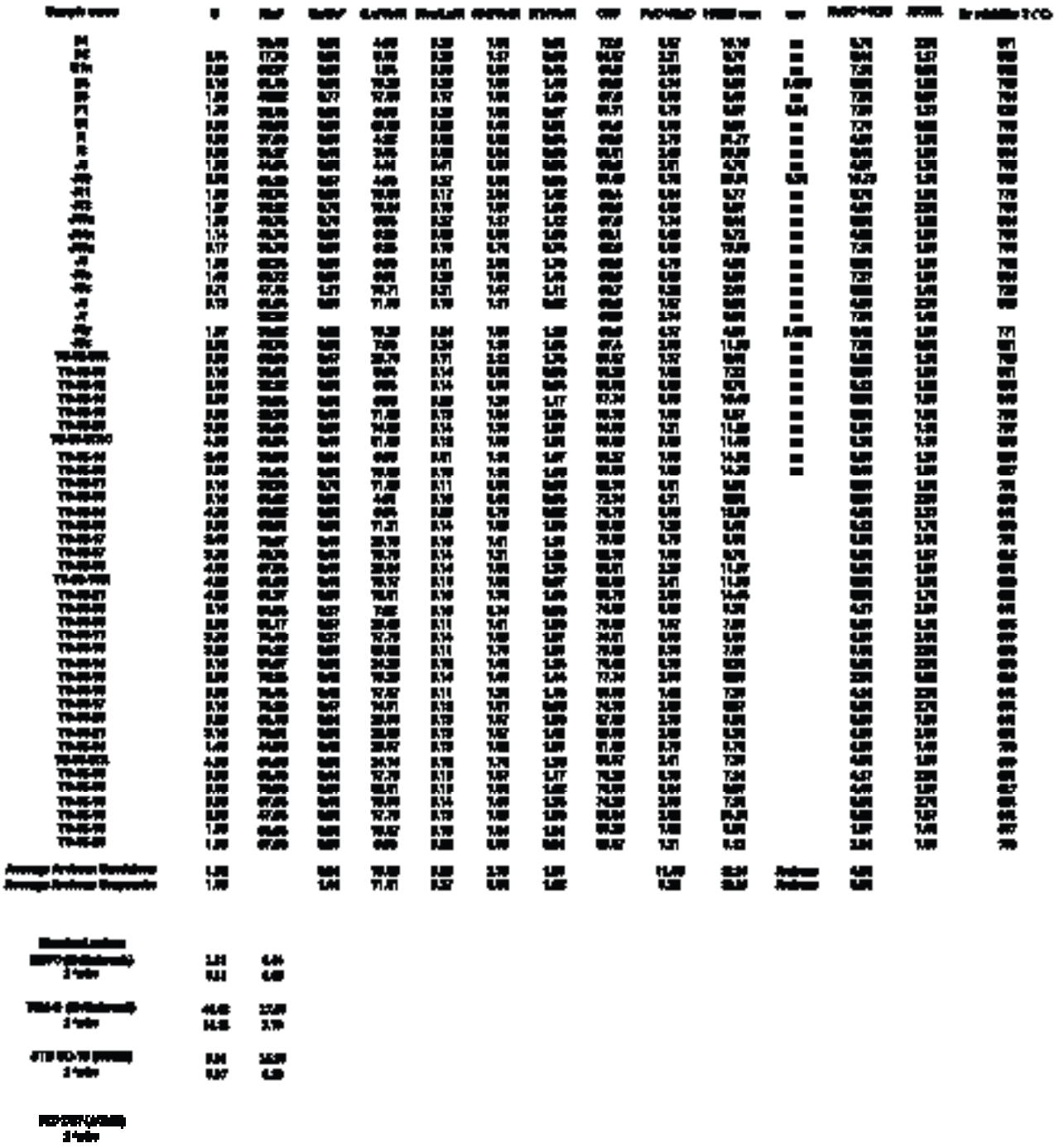

Supplementary Table 1 (continued): Geochemical data for the Moodies granitic clasts and Theespruit felsic schists associated with the Barberton Greenstone Belt

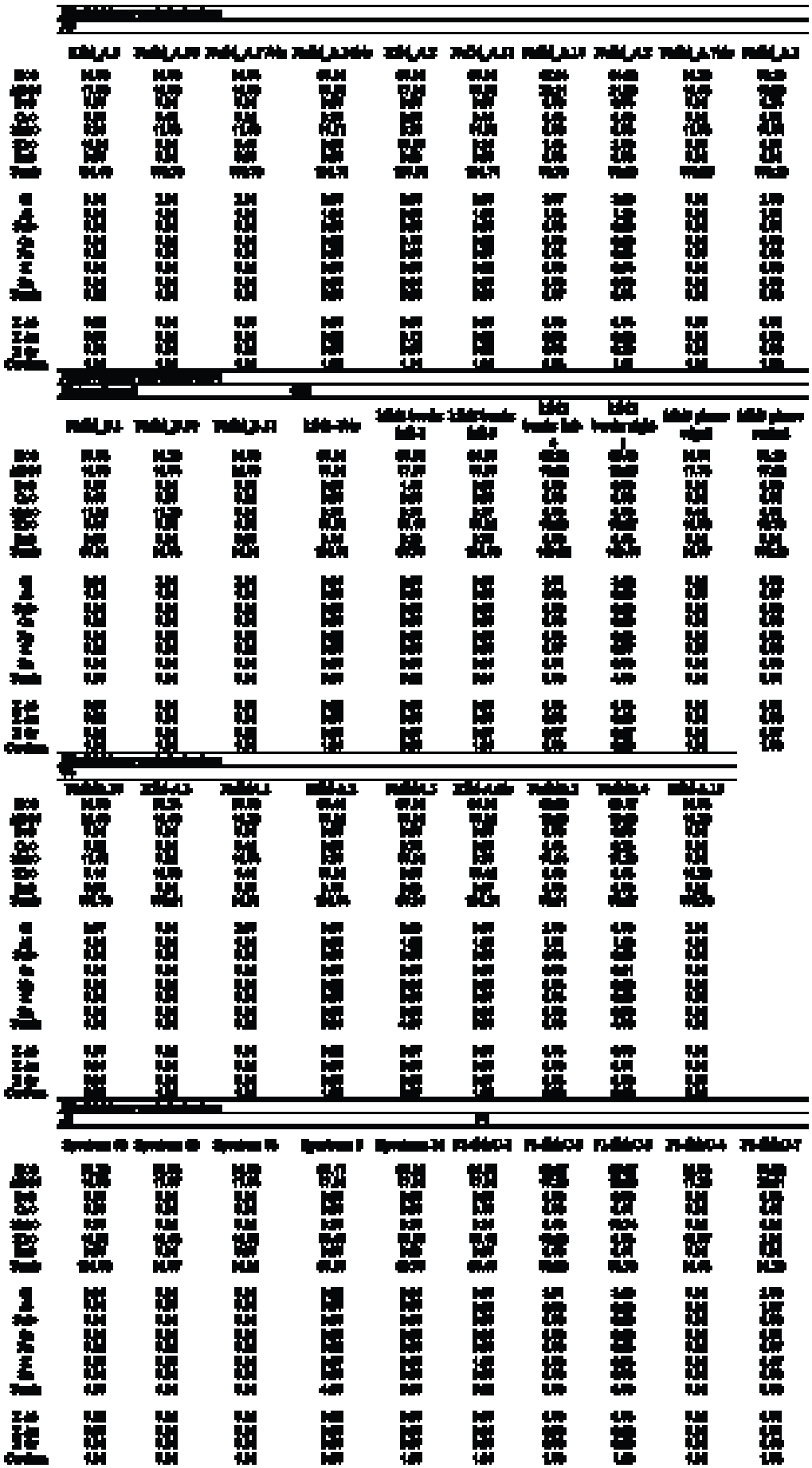

Supplementary Table 2: S.E.M mineral analysis

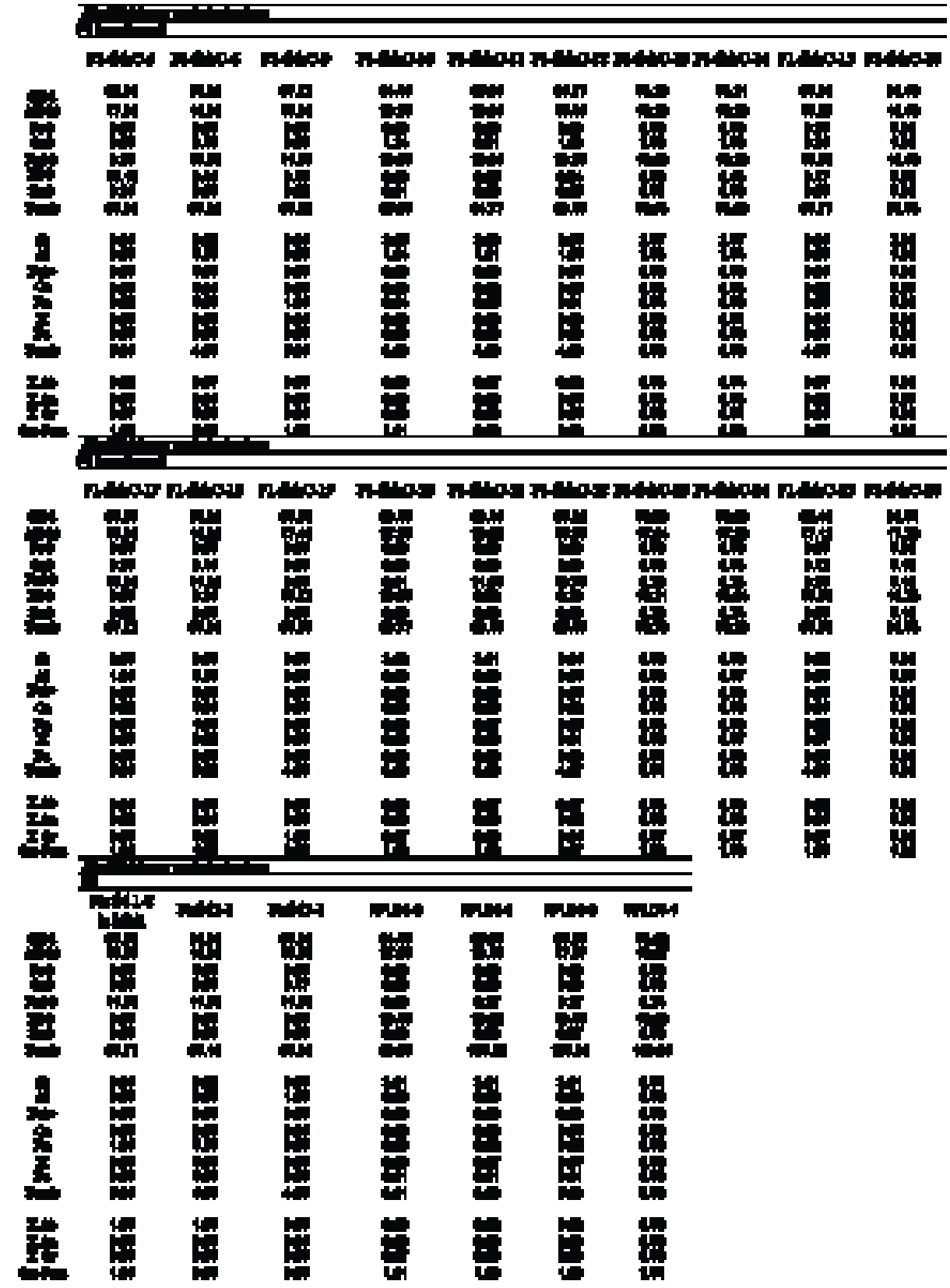

Supplementary Table 2 (continued): S.E.M mineral analysis

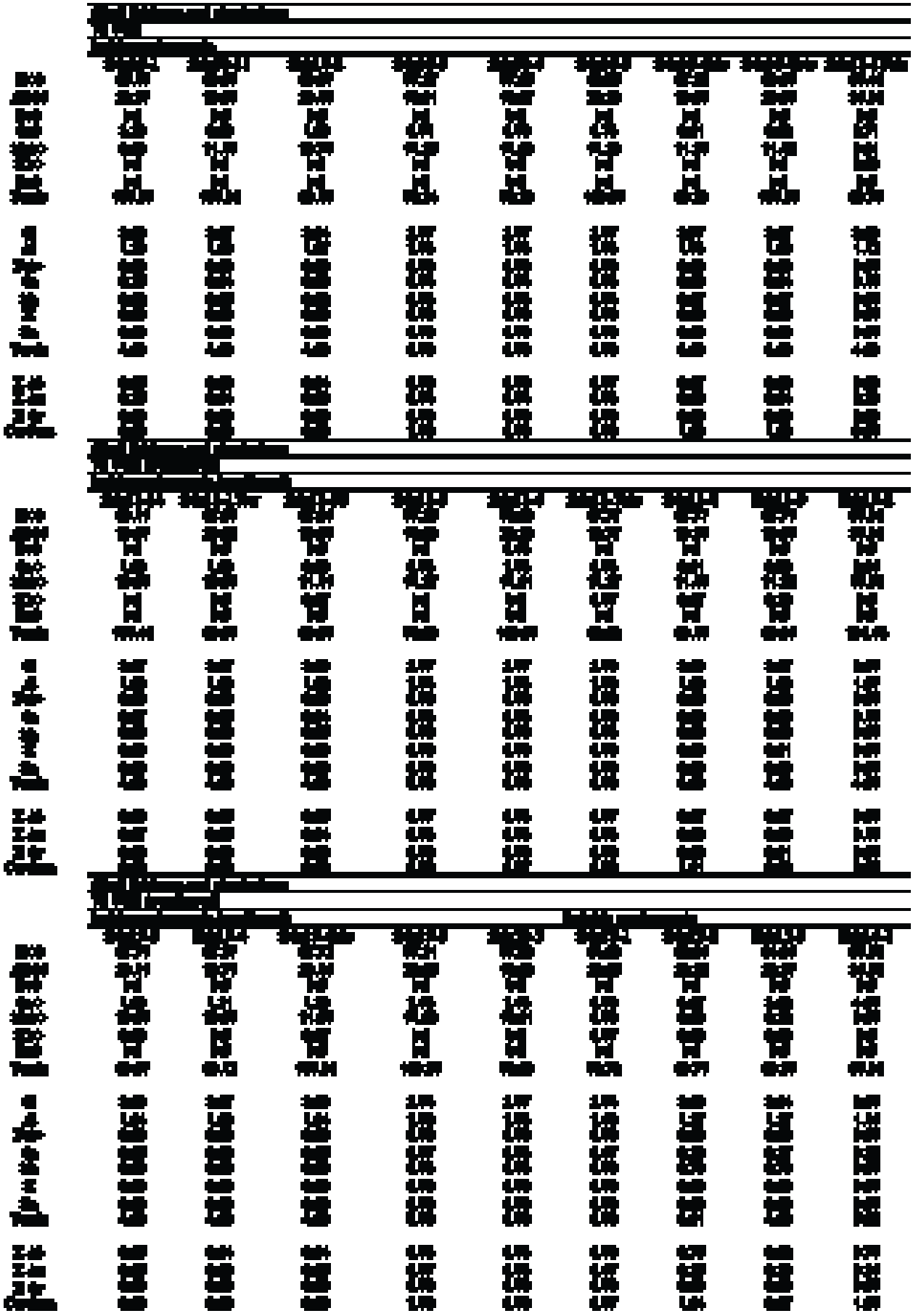

Supplementary Table 2 (continued): S.E.M mineral analysis

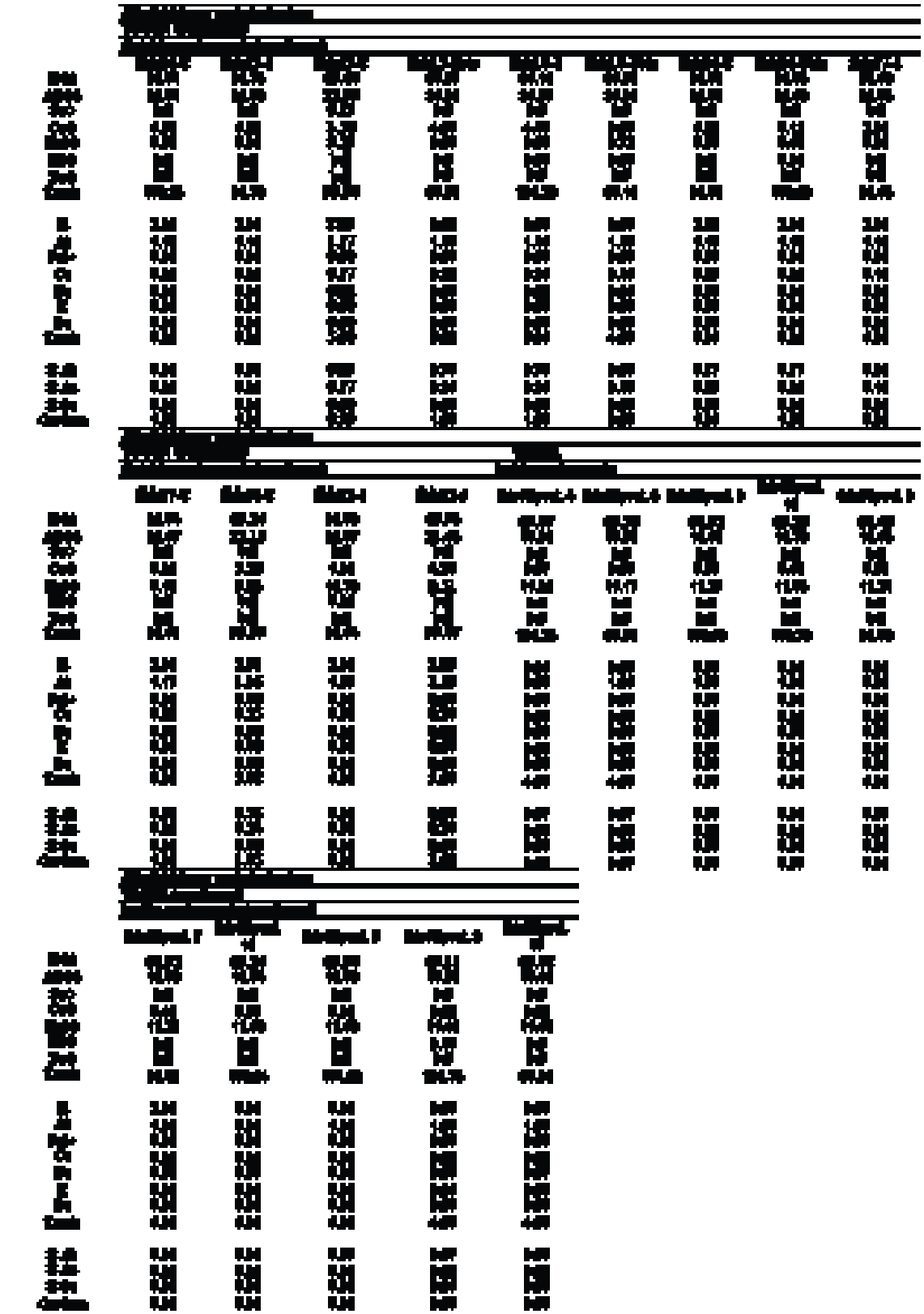

Supplementary Table 2 (continued): S.E.M mineral analysis

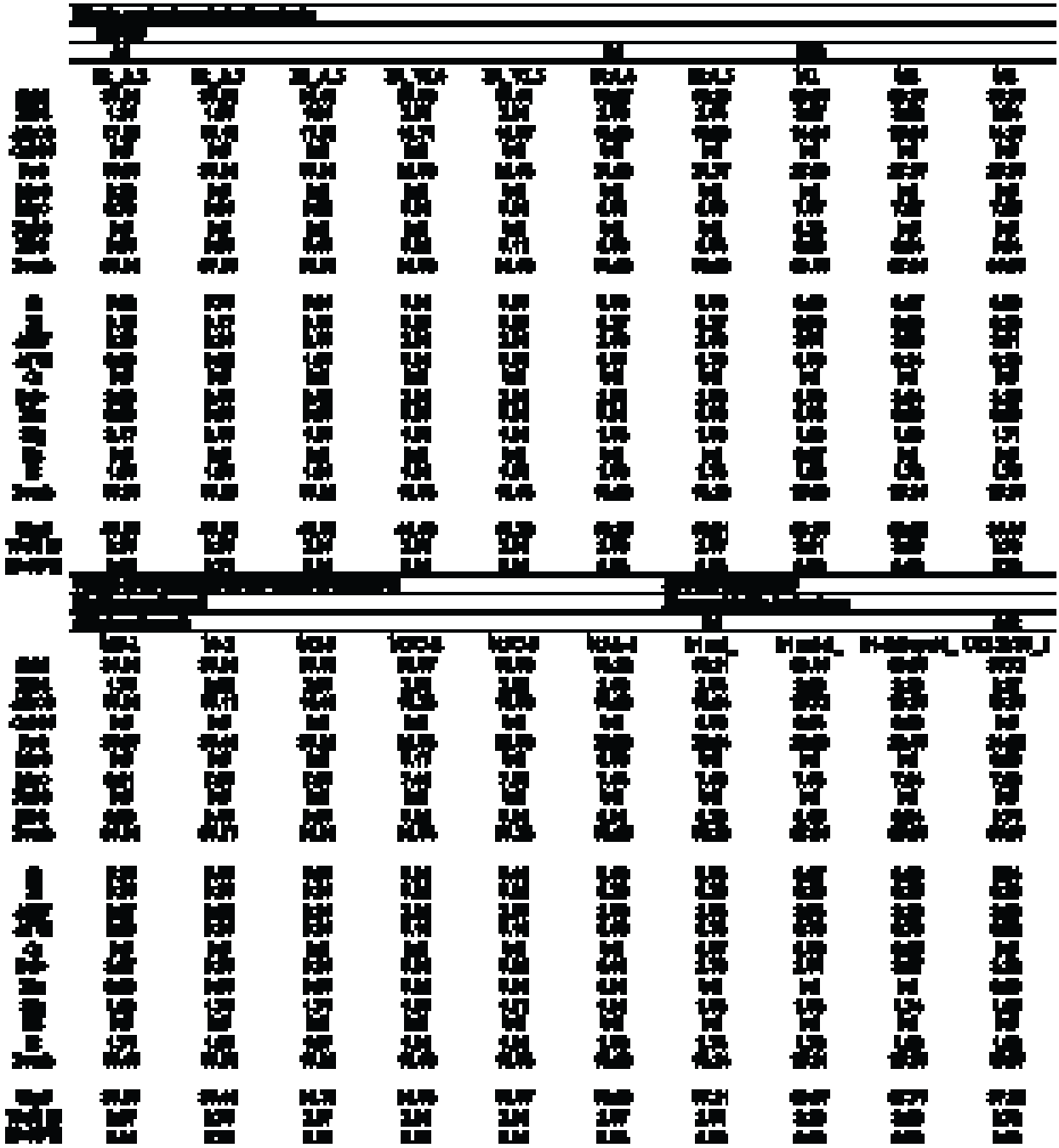

Supplementary Table 2 (continued): S.E.M mineral analysis

Supplementary Table 2 (continued): S.E.M mineral analysis

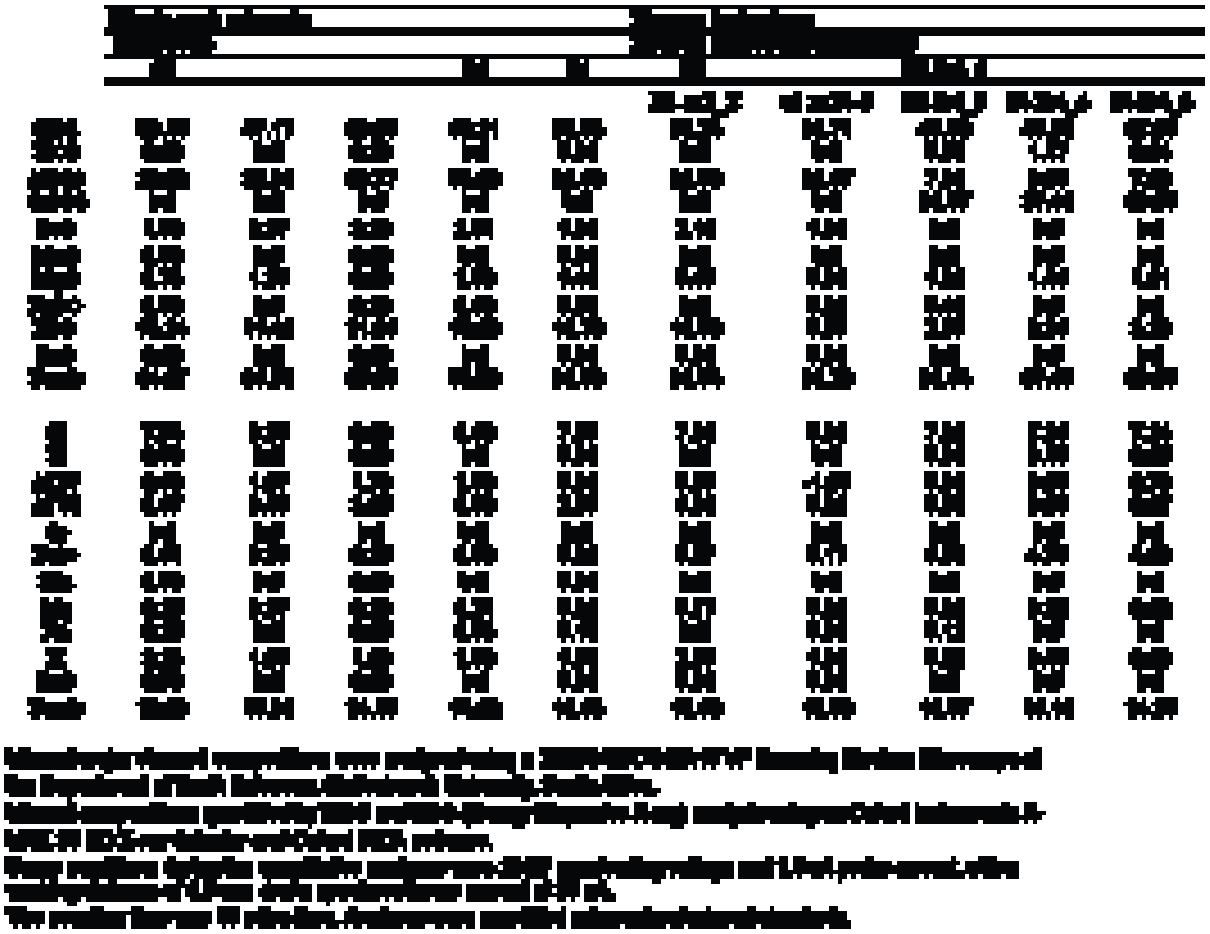

Supplementary Table 2 (continued): S.E.M mineral analysis

Supplementary Table 3: LA-ICP MS Ti in zircons analysis of the Moodies granites zircons

Sample name	$\delta^{18}O$ Quartz	$\delta^{18}O$ Quartz duplicates	$\delta^{18}O$ Feldspar	$\delta^{18}O$ Zircon	2 sr Zircons	$\delta^{18}O$ Whole Rock (measured)	$\delta^{18}O$ Whole Rock (calculated)
A1	16.39			5.05	0.3	16.02	6.98
A3	15.79						
A5	16.34	15.45	15.79				
A8	16.3						
A8b						15.95	
Average outcrop A	16.21						
stdev	0.28						
B1	12.48						
B12	11.96						
B13	12.03						
B14	12.1	11.28		5.1	0.4	10.35	7.17
B14		11.13				10.35	
B17	11.57			4.9	0.3	9.06	6.9
B2	11.97						
B25	11.6					10.57	
B7				5.91	0.64	9.53	7.42
Average outcrop B	11.96			5.3	0.45		7.16
stdev	0.31			0.58	0.17		0.35
C12	16.51						
C19	16.97						
C33	16.75		15.11				
C4	16.41		13.98				
C43	16.33						
C44	15.26						
C22b						16.31	
Average outcrop C	16.37		14.58				
stdev	0.59		0.8				
D2	12.75						
E1	13.56		13.06				
E2						13.43	
E4	13.05						
Average outcrop E	13.31						
stdev	0.36						
F1	12.51						
J10	12.5						
J5	12.19						
J9	12.61	12.58					
J8	13.08						
Average outcrop J	12.65						
stdev	0.36						

*Oxygen isotope data from quartz, K-feldspar and zircons extracts from Moodies granitic Moodies granites. Andesitic-rhyolitic = 2.5‰ - 0.06*t^2 *(wt.% SiO2 in zircon or whole-rock) (Lackey et al. 2008).*

Supplementary Table 4a: Oxygen isotope data for the Moodies granites and the matrix of the Moodies Group basal conglomerate

Sample	d18O	wt	P	umol	umol/mg	yield
Quartz					1 mg = 16.65 u	
A1 qz	16.39	1.94	9.3	27.34	14.86	89.2
A3 qz	15.79	2.22	8.2	24.11	10.86	65.2
A5 qz	15.45	1.94	4.0	11.76	6.39	38.4
A5 qz	16.34	1.65	8.5	24.99	15.15	91.0
A8 qz	16.30	1.29	8.4	18.82	14.59	87.6
B1 qz	12.48					
B12 qz	11.96	1.93	10.9	32.05	16.60	99.7
B13 qz	12.03	2.45	13.4	39.40	16.08	96.6
B14 qz	12.10	2.51	14.8	42.92	17.10	102.7
B14-1 qz	11.28	4.15	25.4	74.68	17.99	108.1
B14-2 qz	11.13	1.72	5.5	16.17	9.40	56.5
B17 qz	11.57					
B2 qz	11.97	2.42	13.7	40.28	16.64	100.0
B25 qz	11.60	2.38	11.5	33.81	14.33	86.0
C12 qz	16.51	3.12	26.8	78.79	25.25	151.7
C19 qz	16.97	1.72	8.2	24.11	14.02	84.2
C19 qz	16.48	2.14	12.8	37.93	17.72	106.4
C33 qz	16.75	2.03	12.2	35.87	17.67	106.1
C4 qz	16.41	1.68	9.0	26.46	15.75	94.6
C43 qz	16.33	1.18	6.0	17.64	15.21	91.3
C44 qz	15.26	1.22	5.3	15.58	12.77	76.7
D2 qz	12.75	1.87	10.2	29.99	16.04	96.3
E1 qz	13.56					
E4 qz	13.05	1.58	9.0	26.46	16.64	99.9
F1 qz	12.51					
J10 qz	12.50	2.90	15.9	46.75	16.12	96.8
J5 qz	12.42	1.5	3.6	10.58	7.06	42.4
J8 qz	13.08					
J9 qz	12.81	2.14	10.8	31.16	14.56	87.5
J9 qz	12.58	2.95	17.7	52.04	17.64	105.9
					ave Qz	90.5
Feldspar				orthoclase		12.65 umol/n
A5 fsp	15.79	2.68	10.3	30.28	11.38	90.0
C33 fsp	15.11	2.38	10.4	30.58	12.85	101.6
C4 fsp	13.98	2.98	10.8	31.75	10.79	84.8
C4 fsp	16.29	2.03	7.7	22.64	11.15	88.2
E1 fsp	13.06	3.05	11.5	33.81	11.09	87.6
					ave fsp	90.4

Supplementary Table 4b: Detail of the oxygen isotope data for the quartz and feldspar from the Moodies granites obtained by laser

ANALYTICAL METHODS

Supplementary Table 1: XRF Standards

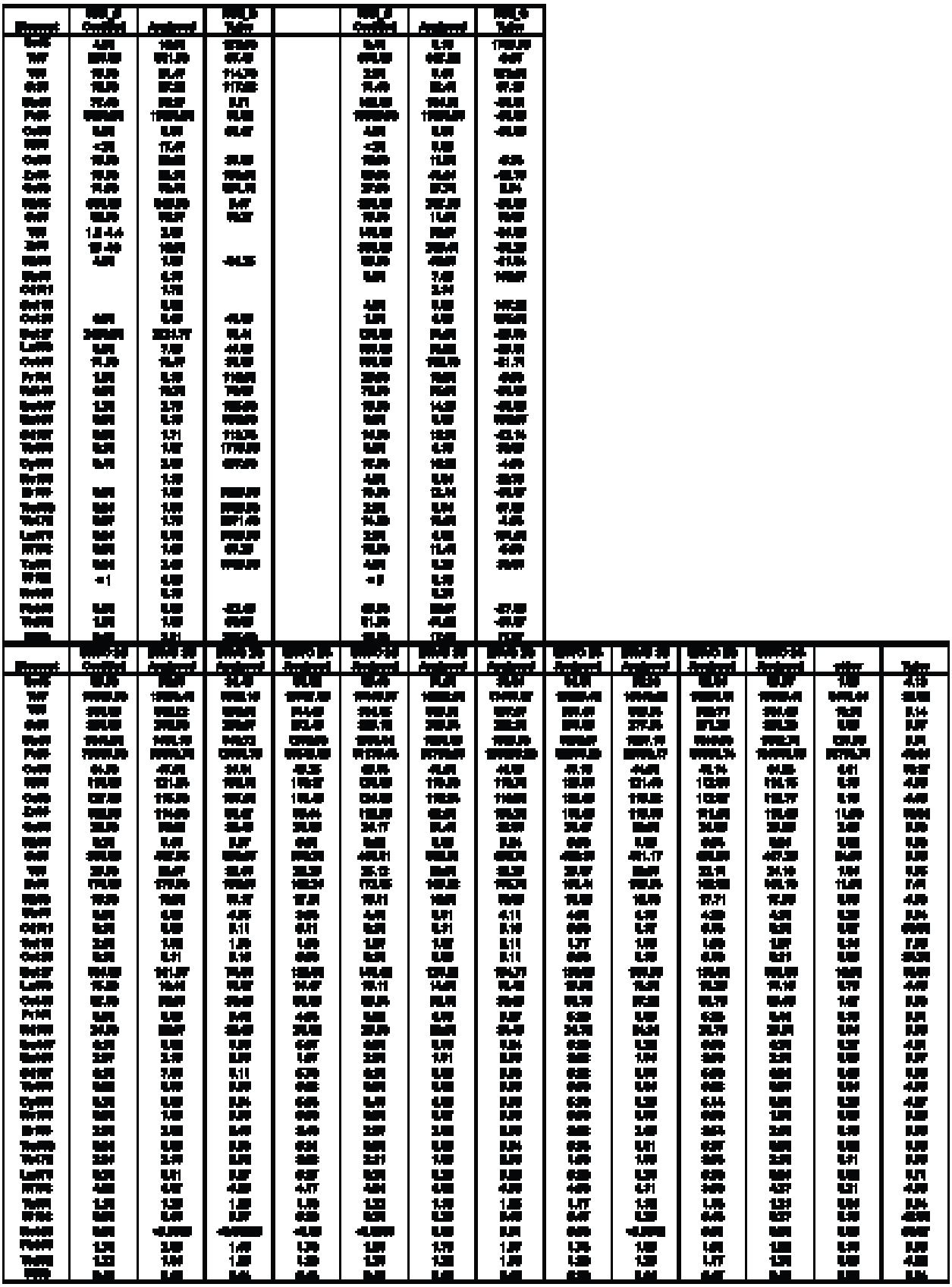

Supplementary Table 2: LA ICP MS Standards

Laboratory & Sample Preparation	
Laboratory name	Geological Survey of Denmark and Greenland (GEUS)
Sample type / mineral	Magmatic zircons
Sample preparation	Conventional mineral separation, 1 inch resin mount, 1 µm polish to finish
Imaging	CL, LEO 1430 VP, 10 nA, 15 mm working distance
Laser ablation system	
Make, Model & type	ESI/New Wave Research, UP213, Nd:YAG
Ablation cell & volume	Custom build low volume cell, volume ca.3 cm^3
Laser wavelength	213 nm
Pulse width	3 ns
Fluence	2.5 J/cm^2
Repetition rate	10 Hz
Spot size	30 µm
Sampling mode / pattern	30 µm single spot analyses
Carrier gas	100% He, Ar make-up gas combined using a T-connector close to sample cell
Pre-ablation laser warm-up (background collection)	40 seconds
Ablation duration	20 seconds
Wash-out delay	30 seconds
Cell carrier gas flow	0.3 l/min He
ICP-MS Instrument	
Make, Model & type	Thermo Finnigan Element2 single collector HR-SF-ICP-MS
Sample introduction	Via conventional tubing
RF power	1100 W
Make-up gas flow	1.0 l/min Ar
Detection system	Single collector secondary electron multiplier
Masses measured	202, 204, 206, 207, 208, 232, 233, 235, 238
Integration time per peak	4 ms
Total integration time per reading	Approx. 1 sec
Sensitivity	20000 cps/ppm Pb
Dead time	16 ns
Data Processing	
Gas blank	40 second on-peak
Calibration strategy	GJ-1 used as primary reference material, Plešovice & M127 used as secondary reference material (Quality Control)
Reference Material info	M127 (Nasdala et al. 2008 ; Matley 2010) Plešovice (Sláma et al. 2008) GJ-1 (Jackson et al. 2004)
Data processing package used / Correction for LIEF	In-house spreadsheet data processing using intercept method for LIEF correction
Mass discrimination	Standard-sample bracketing with $^{206}Pb/^{204}Pb$ and $^{206}Pb/^{238}U$ normalised to reference material GJ-1
Common-Pb correction, composition and uncertainty	204-method, Stacey & Kramers (1975) composition at the projected age of the mineral, 5% uncertainty assigned
Uncertainty level & propagation	Ages are quoted at 2 sigma absolute, propagation is by quadratic addition. Reproducibility and age uncertainty of reference material and common-Pb composition uncertainty are propagated.
Quality control / Validation	Plešovice: Wtd ave $^{206}Pb/^{238}U$ age = 338 ± 4 (2SD, MSWD = 0.2) M127: Wtd ave $^{206}Pb/^{238}U$ age = 522 ± 5 (2SD, MSWD = 0.8)
Other information	Detailed method description reported by Frei & Gerdes (2009)

Supplementary Table 3: LA-SF-ICP-MS U-Th-Pb dating methodology CAF, Stellenbosch University

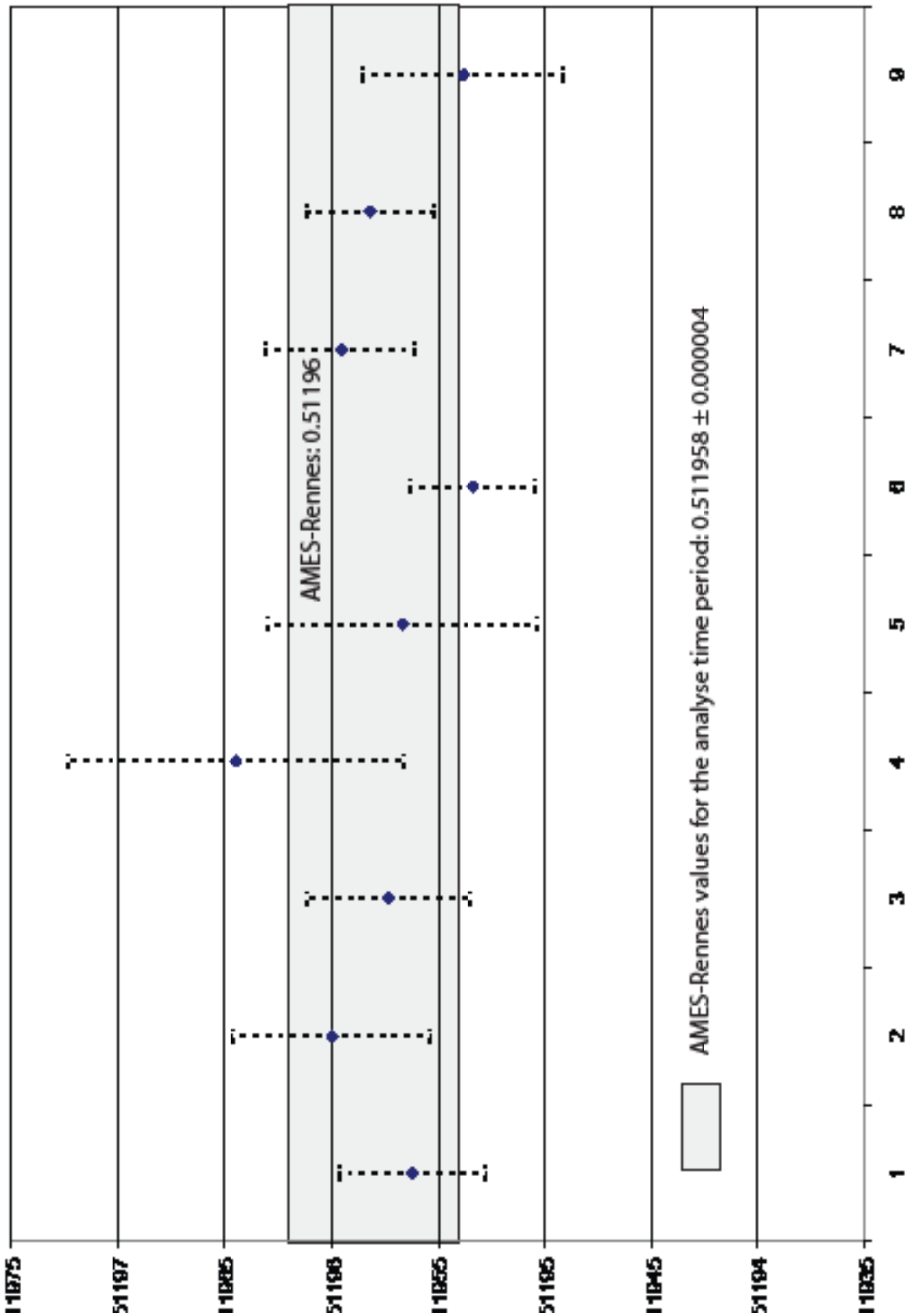

Supplementary Diagram 1a : Standards of the Sm-Nd isotopic data

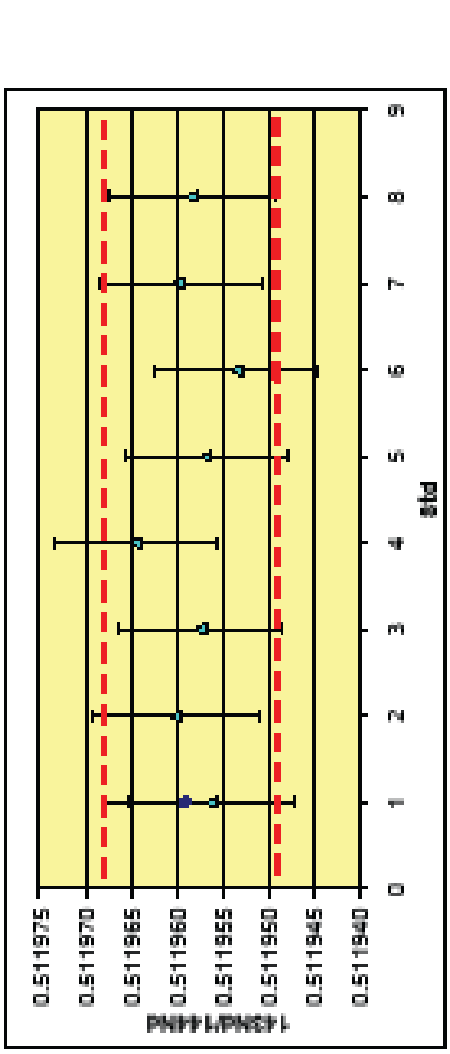

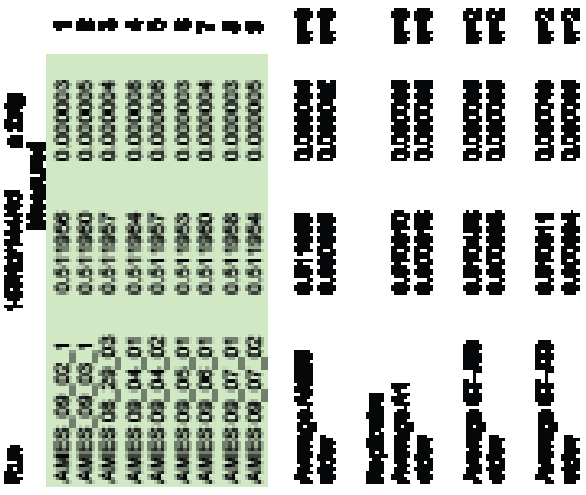

Supplementary Table 4: Standards of the Sm-Nd isotopic data

ANALYTICAL METHODS

1. XRF

Samples were crushed into a fine powder with a jaw crusher and milled in an agate mill (to prevent from trace and REE contamination) prior to the preparation of a fused disc for major element and trace analysis. Glass disks were prepared for XRF analysis using 1.5 g of high purity trace element and REE element free flux ($LiBO_2$ = 80%, Li_2B4O_7 = 20%) mixed with 0.28 g of the rock sample. Whole-rock major element compositions were determined by XRF spectrometry on a Philips 1404 Wavelength Dispersive spectrometer at the Department of Earth Sciences, Stellenbosch University, South Africa. The spectrometer is fitted with an Rh tube, analysing crystals LIF200, LIF220, LIF420, PE, TLAP and PX1. The instrument is fitted with a gas-flow proportional counter and a scintillation detector. The gas-flow proportional counter uses a 90% Argon, 10% methane gas mixture. Major elements were analyzed on a fused glass disk at 50 kV and 50 mA tube operating conditions. Matrix effects in the samples were corrected for by applying theoretical alpha factors and measured line overlap factors to the raw intensities measured with the SuperQ Philips software. Control standards that were used in the calibration procedures for major element analyses were AGV (Andesite from the United States Geological Survey, Reston), NIM-G (Granite from the Council for Mineral Technology, South Africa) and BHVO-1 (Basalt from the United States Geological Survey, Reston). A comparison of the measured and accepted major element compositions of the control standards used, as a reflection of the accuracy of the analytical technique, is presented in Supplementary Table 1.

2. SEM

Mineral major element compositions were analysed using a Leo® 1430VP Scanning Electron Microscope at the Department of Earth Sciences, Stellenbosch University, South Africa. Mineral compositions quantified by EDX (Energy Dispersive X-ray) analysis using an Oxford Instruments ® 133 keV ED X-ray detector and Oxford INCA software. Beam conditions during the quantitative analyses were 20 kV accelerating voltage and 1.5 nA probe current, with a working distance of 13 mm and a specimen beam current of −4.0 nA. X-ray counts were typically ~7000 cps (for biotite), and the counting time was 50 s live-time. Analyses were quantified using natural mineral standards.

3. Oxygen isotopes analysis of quartz, feldspars and whole rock

For oxygen isotope analyses of quartz, the laser fluorination methods described by Harris & Vogeli (2010) were used on 1-3 mg of sample. Each sample was reacted in the presence of approximately 10 kPa BrF_5, and the purified O_2 was collected onto a 5 Å molecular sieve contained in a glass storage bottle. It was not possible to analyse the feldspar by laser fluorination because significant reaction took place between the feldspar and the BrF_5 in the reaction chamber at room temperature. All alkali feldspar separates were therefore analysed using a conventional silicate line following methods described by Harris and Ashwal (2002). Approximately 10 mg of sample was reacted

with ClF_3, and the liberated O_2 converted to CO_2 using a hot platinized carbon rod.

Isotope ratios were measured off-line using a Finnigan Delta XP mass spectrometer in dual-inlet mode. All data are reported in δ notation where $\delta^{18}O = (R_{sample}/R_{standard} -1)*1000$, and R = the measured ratio of $^{18}O/^{16}O$. For the conventional analyses, duplicate splits of the quartz standard (NBS28) run with each batch of eight samples were used to convert the raw data to the SMOW scale using the $\delta^{18}O$ value of 9.64 % for NBS28 recommended by Coplen et al., (1983). During the course of this work, 8 analyses of NBS28 gave a 2σ error of 0.16. The O-isotope ratios of samples analysed using laser fluorination were measured on O_2 gas. Measured values of our internal standard MON GT (Harris et al., 2000) were used to normalise raw data and correct for drift in the reference gas. The average difference in $\delta^{18}O$ values of duplicates of MON GT analysed during this study was 0.14 ‰, and corresponds to a 2σ value of 0.19‰. MON GT was recalibrated against the UWG-2 garnet standard of Valley et al., (1995) using the current laser system, and has a revised $\delta^{18}O$ value of 5.38 ‰, assuming a $\delta^{18}O$ value of 5.80 ‰ for UWG2.

4. Lu-Hf analyses of zircons

Lutetium–hafnium–ytterbium isotopes were analysed on zircons. The lutetium–hafnium–ytterbium isotopes were measured at the Goethe University Frankfurt with a Thermo-Finnigan Neptune multicollector ICP-MS coupled to a New Wave Research UP-213 laser system with a teardrop shaped, low volume laser cell, following the procedure described by Gerdes and Zeh (2006, 2009). Data were collected in static mode (^{172}Yb, ^{173}Yb, ^{175}Lu, ^{176}Hf–Yb–Lu, ^{177}Hf, ^{178}Hf, ^{179}Hf, ^{180}Hf) during 55 seconds of laser ablation. Where possible the "Lu–Hf–Yb laser spot" of 40 µm diameter was drilled "on top" of the 20–30 µm "U–Pb laser spot" previously analysed. Care was taken to drill exactly in the same domain (core or rim), which was previously used for U–Th–Pb isotope analyses. These domains were carefully selected on the basis of CL-images. During few ablation sessions the laser position had to be re-adjusted slightly, i.e., by manually moving the laser in x–y direction. This was necessary when the signal strength for ^{180}Hf fell below the critical intensity of 1 volt (Gerdes and Zeh, 2009). Nitrogen (~0.005 l/min) was introduced via a Cetac Aridus into the Ar sample carrier gas to enhance sensitivity (~10–20%) and to reduce oxide formation.
All analyses with 180Hf signal strength <1 volt have been removed. Additional outliers were removed by using an automated outlier test that was implemented by A. Gerdes and A. Zeh. Then, all remaining ratios were used to calculate the average $^{176}Hf/^{177}Hf$ and the standard error (2 SE) for each spot analysis. All data were adjusted relative to the JMC 475 $^{176}Hf/^{177}Hf$ ratio of 0.282160. The effect of the inter-element fractionation on the Lu/Hf was estimated to be about 6 % or less based on analyses of the GJ-1 and Plesoviče zircon. Accuracy and reproducibility was checked by repeated analyses (n = 57 and 10, respectively) of reference zircon GJ-1 and Plesoviče.

5. Nd – Sm protocole

The samples were crushed using a stainless steel jaw crusher and a representative fraction was powered in an agate ball mill at the Department of Earth Sciences of the Stellenbosch University (South Africa). Clean quartz was used between two samples, in the jaw crusher and the mill for cleaning
Procedures for dissolution of whole-rock powders, Sm and Nd separation, and mass spectrometric techniques were carried out at the Laboratory "Magmas et Volcans" of the Blaise Pascal University (Clermont-Ferrand, France). Depending on the expected concentration of the samples, 100-200

mg of fine power rock was weighed and spiked with with ~200 to 450 mg of a 149Sm-150Nd tracer solution. The spiked samples were dissolved in 500 µL of HNO_3 and 2 mL of HF. The samples were kept at 75 °C in Teflon vessels for a day until dissolution was completed. The samples are then kept at 50 °C in 250 µL of percloric acid (HClO4) and 3 mL of HNO_3 and then 90 °C to dry out for two days. The conversion into chlorides is done through addition of 8 mL of HCl in 75 °C for a day. However, as the material prepared was samples of granites and TTG containing many accessory mineral carrying Sm and Nd (monazite, apatite, zircons mostly) the spiked samples were put into a centrifugor in order to identify possible un-dissolved material. If residual material was found it was then transferred into in a Teflon pillulier with HF-HNO_3, in a bomb for 30 hours at 210 °C. When taken outside the bomb the residual material was then put into chloride form and added to the main sample. Sm-Nd purification and extraction was performed using the cascade procedure (AG50X4, TRU Spec. and then Ln Spec. columns) described in Pin et al. (1994).
Nd was loaded on double W filaments with H_3PO_4 and analysed in static multicollector mode with a ^{144}Nd ion beam of ca. 2 V. Nd isotope ratios and [Nd] concentrations were determined by thermal ionization mass spectrometry (TIMS) on a TRITON Tl instrumentation. A typical run consists in at least 9 10-cycle blocks of measurements with 30s baselines to allow the full rotation of the virtual amplificatory system. Blanks for Sm and Nd were < 2 ng. $^{143}Nd/^{144}Nd$ ratios were corrected for mass-fractionation using a power-law and $^{144}Nd/^{146}Nd=1.385233$; they were also normalized to the AMES-Rennes standard using $^{143}Nd/^{144}Nd=0.511959 \pm 0.000009$ (accepted value). Measurements of the AMES-Rennes Nd standard gave $^{143}Nd/^{144}Nd= 0.511958 \pm 0.000004$ (n=9) during the period of data acquisition (Supplementary Table 4).
Samarium was loaded on triple W filaments with H_3PO_4 and analysed in static multicollector mode with a ^{152}Sm ion beam of 0.5 V (high voltage of the multicollector = 8 kV). Sm concentrations were determined using a VG Sector 54 multicollector thermal ionisation mass spectrometer (TIMS). The Sm data were normalised to $^{152}Sm/^{147}Sm = 1.783$.
The standards values are a measure of the external reproducibility of the standards and provide a reasonable estimate of the analytical precision of the reported ratios. The 2s errors given for the 143Nd/144Nd ratios are in-run errors and show the relative quality of the analyses. The ratios obtained for both standards were within analytical error of the accepted values, but however reported ratios have been bias-corrected. Two replicate samples were also run an the measured ratios were in within errors of each others. As outlined above, the standards analysed with the samples are within error of their expected values, and so the overall analytical procedure was reliable. In addition, two samples were replicated, some in separate dissolutions, to determine the sample variability. Replicate differences for $^{147}Sm/^{144}Nd$ are generally less than 1 %.

6. U-Pb SHRIMP

SHRIMP U/Pb dating of zircons was undertaken at the ANU. No inherited cores were identified in CL images of the zircons. The SHRIMP analytical procedures followed the methods described in Comptson et al (1984) and Williams (1998). The standard zircon SL13 (Claoue-Long et al., 1995) was used to measure U concentration whereas the U–Pb ratios were referenced to the zircon standard FC1 (1100 Ma old) (Paces and Miller, 1993). Errors are 1-sigma; Pbc and Pb* indicate the common and radiogenic portions, respectively. Error in Standard calibration was 0.36% (not included in above errors but required when comparing data from different mounts). Common Pb corrected using measured ^{204}Pb. The age calculations and the concordia plots were done using Isoplot/Ex software (Ludwig, 2003; Ludwig, 2004).

7. U-Pb LA-ICP MS

All U–Pb age data obtained at the Geological Survey of Denmark and Greenland in Copenhagen were acquired by laser ablation - single collector - magnetic sectorfield - inductively coupled plasma - mass spectrometry (LA-SF-ICP-MS) employing a Thermo Finnigan Element2 mass spectrometer coupled to a NewWave UP213 laser ablation system. All age data presented here were obtained by single spot analyses with a spot diameter of 30 µm and a crater depth of approximately 15–20 µm. The methods employed for analysis and data processing are described in detail by Gerdes and Zeh (2006) and Frei and Gerdes (2009). For quality control, the Plešovice (Sláma et al. 2008) and M127 (Nasdala et al. 2008; Mattey 2010) zircon reference materials were analyzed, and the results were consistently in excellent agreement with the published ID-TIMS ages. Full analytical details and the results for all quality control materials analysed are reported in Table Y in the electronic supplementary material. The calculation of concordia ages and plotting of concordia diagrams were performed using Isoplot/Ex 3.0 (Ludwig 2003).

8. Trace and rare Earth element LA-ICP MS

Fusion disks used for XRF analysis were coarsely crushed and a chip of sample mounted along with 9 other samples in a 2.4 cm round resin disk. The mount was mapped, and then polished for analysis. Trace elements were quantified using NIST 612 for calibration and 29Si as internal standard, using standard – sample bracketing. Three replicate measurements were made on each sample. The calibration standard was run every 12 samples. A quality control standard was run in the beginning of the sequence as well as with the calibration standards throughout. BHVO 2G, a basaltic glass certified reference standard produced by USGS (Dr Steve Wilson, Denver, CO 80225), was used for this purpose. Data was processed using Glitter software, distributed by Access Macquarie Ltd., Macquarie University NSW 2109. A comparison of the measured and accepted major element compositions of the control standards used, as a reflection of the accuracy of the analytical technique, is presented in Supplementary Table 2.

Instrumental Set-up:

A New Wave 213nm laser ablation system connected to an Agilent 7500ce ICP-MS was used in the analysis fusion disks. Ablation was performed in He gas and mixed with argon after exiting the ablation cell, then passed through a mixing chamber before introduction into the ICP.

Analysis Parameters:

Laser Ablation:
Wavelength: 213 nm
Energy density on the sample: ~ 10.5 J/cm3
Pulse duration: 3.9 ns
Repetition rate: 10 Hz
Spot size: 110 µm
Laser warm-up (blank counting): 20 sec
Data acquisition: 50 sec spot analysis

ICP-MS parameters:

RF Power: 1450 kW
Plasma gas flow: 15 L/min
Auxiliary gas flow: 0.9 L/min
Carrier gas flow: 0.98 L/min Ar
Option gas flow (He – used for ablation): 0.95 L/min
Acquisition mode: Time Resolved Analysis
Integration time: 0.01 sec / isotope
Optimized for oxide levels < 0.6%

9. Oxygen isotope SHRIMP

SHRIMP II oxygen isotope analysis followed the methods described by Ickert et al. (2008). The internal standard used was the Temora II zircon with a $\delta^{18}O$ value of 8.2‰ (Black et al., 2004). Oxygen isotope compositions were recalculated relative to Vienna Standard Mean Ocean Water and expressed as $\delta^{18}O$ (Craig, 1961).

References:

Black, L.P., Kamo, S.L., Allen, C.M., Davis, D.W., Aleinikoff, J.N., Valley, J.W., Mundil, R., Campbell, I.H., Korsch, R.J., Williams, I.S., Foudoulis, C., 2004. Improved Pb-206/U-238 microprobe geochronology by the monitoring of a trace-element-related matrix effect; SHRIMP, IDTIMS, ELA-ICP-MS and oxygen isotope documentation for a series of zircon standards. Chemical Geology 205, 115–140.

Claoue-Long, J.C., Compston W.,Roberts J. and Fanning C. M., 1995. Two Carboniferous ages: a comparison of SHRIMP zircon dating with conventional zircon ages and 40Ar/39Ar analysis, in Geochronology, Time Scale and Global Stratigraphic Correlation, W.A. Berggren, et al., Eds p. 3-21.

Compston, W., Williams, I.S. and Meyer,C., 1984. U-Pb geochronology of zircons from lunar breccia 73217 using a sensitive high-resolution ion-microprobe. Journal of Geophysic Research, B 98, p. 525-534.

Coplen, T.B., Kendall, C. and Hopple, J., 1983. Comparison of stable isotope reference samples. Nature 302, 236–238.

Craig, H., 1961. Isotopic variations in meteoric waters. Science, v.133, p.1833–1834.

Frei, D. and Gerdes, A., 2009. Precise and accurate in situ U–Pb dating of zircon with high sample throughput by automated LA-SF-ICPMS. Chemical Geology 261, 261–270.

Gerdes, A. and Zeh, A., 2009. Zircon formation versus zircon alteration — New insights from combined U–Pb and Lu–Hf in-situ LA-ICP-MS analyses, and consequences for the interpretation of Archean zircon from the Central Zone of the Limpopo Belt. Chemical Geology 261, 203-243.

Gerdes. A. and Zeh, A., (2006). Combined U–Pb and Hf isotope LA-(MC)-ICP-MS analyses of

detrital zircons: comparison with SHRIMP and new constraints for the provenance and age of an Armorican metasediment in Central Germany. Earth and Planetary Science Letters 249, 47–61.

Harris, C. and Ashwal, L.D., 2002, The origin of low d18O granites and related rocks from the Seychelles. Contributions to Mineralogy and Petrology 143, 366-376.

Harris, C. and Vogeli, J., 2010. Oxygen isotope composition of garnet in the peninsula granite, Cape Granite suite, South Africa: constraints on melting and emplacement mechanisms. South African Journal of Geology 113, 401-412.

Harris, C., Smith, H.S. and le Roex, A.P., 2000. Oxygen isotope composition of phenocrysts from Tristan da Cunha and Gough Island lavas: variation with fractional crystallization and evidence for assimilation. Contributions to Mineralogy and Petrology 138, 164-175.

Ickert, R.B., Hiess, J., Williams, I.S., Holden, P., Ireland, T.R., Lanc, P., Schram, N. and Foster, 2008. a SHRIMP II: Analyses of MPI-DING silicate-glass reference materials and zircon from contrasting granites. Chemical Geology 257, 114–128.

Jackson S, Pearson NJ, Griffin WL, Belousova, E.A., 2004. The application of laser ablation – inductively coupled plasma – mass spectrometry to in situ U–Pb zircon geochronology. Chemical Geology 211, 47–69.

Ludwig, K., 2003. Isoplot/Ex version 3: a Geochronological toolkit for Microsoft Excel. Geochronology Center, Berkeley.

Ludwig, K.R., 2004. User's Manual for Isoplot/Ex version 3.00-A Geochronology Toolkit for Microsoft Excel. Berkeley Geochronological Center Special publication of the Geological Society of South Africa 4, p 70.

Mattey, J.M., 2010. Analysis of the relative decay constants of 235U and 238U by multi-step CA-TIMS measurements of closed-system natural zircon samples. Chem Geol 275: 186–198.

Nasdala, L., Hofmeister, W., Norberg, N., Mattinson, J.M., Corfu, F., Dörr, W., Kamo, S.L., Kennedy, A.K., Kronz, A., Reiners, P.W., Frei, D., Košler, J., Wan, Y., Götze, J., Häger, T., Kröner, A., Valley, J.W., 2008. Zircon M257–a homogeneous natural reference material for the ion microprobe U-Pb analysis of zircon. Geostand Geoanal Res 32: 247–265.

Paces, J.B. and Miller, J.D., 1993. Precise U-Pb ages of Duluth Complex and related mafic intrusions, northeastern Minnesota: geochronological insights into physical, petrogenetic, paleomagnetic and tectonomagmatic process associated with the 11 Ga midcontinental system. Journal of Geophysics research 98, 13997-14013.

Pin, C., Briot, D., Bassin, C. and Poitrasson, F., 1994. Concomitant separation of strontium and samarium-neodymium for isotopic analysis in silicate samples, based on specific extraction chromatography. Analytica Chimica Acta 298:,209-217.

Sláma, J., Košler, J., Condon, D.J., Crowley, J.L., Gerdes, A., Hanchar, J.M., Horstwood, M.S.A., Morris, G.A., Nasdala, L., Norberg, N., Schaltegger, U., Schoene, B., Tubrett, M.N., Whitehouse, M.J., 2008. Plešovice zircon—a new natural reference material for U–Pb and Hf isotopic microanalysis. Chemical Geology 249:1–35.

Stacey, J.S. and Kramers, J.D., 1975. Approximation of terrestrial lead isotope evolution by a two-stage model. Earth and Planetary Science Letters 26, 207-221.

Valley, J.W., Kitchen, N., Kohn, M.J., Niendorf, C.R., Spicuzza, M.J., 1995. UWG-2, a garnet standard for oxygen isotope ratios: strategies for high precision and accuracy with laser heating. Geochimica and Cosmochimica Acta 59, 5223-5231.

Williams, I.S., 1998. U-Th-Pb geochronology by ion microprobe, in Applications of Microanalytical Techniques to Understanding Mineralizing Processes, M.A. McKibben, W.C. Shanks III, and W.I. Rydley, Eds p. 1-35.